Lanthanide architectures, rotaxanes and responsive d-f assemblies

Manuel Tropiano

Wadham College
University of Oxford

A thesis submitted in partial fulfilment of the requirements for the degree of *Doctor of Philosophy*

Hilary Term 2013

Table of Contents

Abstract v

Publications vi

Acknowledgements vii

Abbreviations ix

1 **Introduction 1**

1.1 General aspects of the lanthanide series 1

1.2 Lanthanide luminescence 1

1.2.1 Sensitised luminescence 2

1.3 Magnetic properties 5

1.3.1 Structural aspects derived from NMR spectroscopy 7

1.4 Luminescent lanthanide-containing compounds 9

1.4.1 Anion sensing 10

1.4.2 Sensing of other analytes 14

1.5 Stability of lanthanide complexes 15

1.5.1 Thermodynamic stability 16

1.5.2 Kinetic stability 17

1.6 The Cu(I) click chemistry reaction 19

1.7 Project aims 23

1.8 References 24

2 **Luminescent lanthanide complexes containing a redox active chromophore 27**

2.1 Introduction 27

2.2 An alkyne appended lanthanide complex 29

2.2.1 Crystal structure 30

2.3 A self-assembled lanthanide-ferrocene complex 32

2.3.1 Self-assembly of Eu.P-DO3A 2.6 with ferrocene carboxylic acid 32

2.3.2 Spectroelectrochemistry 33

2.4 Kinetically stable lanthanide-ferrocene complexes 36

2.4.1 Introduction 36

2.4.2 Synthesis 36
2.4.3 NMR spectroscopy characterisation 38
2.4.4 Photophysical characterisation 40
2.4.5 Spectroelectrochemistry 46
2.4.6 Discussion of the mechanism of electrochemical quenching 48
2.5 Alternative redox active chromophores 52
2.5.1 Introduction 52
2.5.2 Synthesis of lanthanide complexes containing an anthraquinone chromophore 53
2.5.3 NMR spectroscopy characterisation 55
2.5.4 Photophysical characterisation 57
2.5.5 Towards the synthesis of benzoquinone derivatives of Ln.DO3A complexes 60
2.5.6 NMR spectroscopy characterisation 62
2.5.7 Photophysical characterisation 64
2.6 Conclusions 67
2.7 References 68
3 **Synthesis and study of a lanthanide appended rotaxane 69**
3.1 Introduction 69
3.2 Strategies for the synthesis of the lanthanide appended rotaxane 71
3.3 Synthesis of the azide functionalised rotaxane 73
3.4 Synthesis of the lanthanide appended rotaxane 74
3.5 NMR spectroscopy characterisation 77
3.7 Photophysical characterisation 78
3.8 Anion sensing 79
3.8.1 Binding of chloride in dichloromethane 79
3.8.2 Binding of oxyanions in dichloromethane 84
3.8.3 Binding in dichloromethane:methanol mixture 86
3.9 Binding of anions to a model compound 88
3.10 Conclusions 92
3.11 References 94

4 **Synthesis and study of macrocyclic structures containing lanthanide complexes 95**

4.1 Introduction 95

4.2 Preparation of the lanthanide complexes 99

4.2.1 Synthesis 99

4.2.2 NMR spectroscopy characterisation 103

4.2.3 Photophysical characterisation 105

4.3 Preparation of organic synthons containing azide functional groups 107

4.3.1 Synthesis 107

4.4 Attempted synthesis of the macrocycle 110

4.5 Conclusions 111

4.7 References 112

5 **Synthesis and study of heterobimetallic f-f' arrays 113**

5.1 Introduction 113

5.2 Synthesis and characterisation of azido-appended complexes 119

5.2.1 Introduction 119

5.2.2 Synthesis 120

5.2.3 NMR spectroscopy characterisation 123

5.2.4 Photophysical Studies 125

5.3 Preparation and study of f-f' heterobimetallic complexes 130

5.3.1 Introduction 130

5.3.2 Synthesis 131

5.3.3 NMR spectroscopy characterisation 133

5.3.5 Photophysical characterisation 137

5.4 Conclusions 141

5.5 References 142

6 **Synthesis and study of lanthanide bioconjugates 143**

6.1 Introduction 143

6.2 Aldehyde appended lanthanide complexes 145

6.2.1 Synthesis 145

6.2.2 NMR spectroscopy characterisation 146

6.2.3 Photophysical characterisation 148

6.3 Lanthanide bioconjugates containing a dopamine group 149
6.3.1 Synthesis 149
6.3.2 NMR spectroscopy characterisation 150
6.3.3 Photophysical characterisation 152
6.3.4 Uptake experiments 154
6.4 Lanthanide bioconjugates containing an L-DOPA group 156
6.4.1 Introduction 156
6.4.2 Synthesis 157
6.4.3 NMR spectroscopy characterisation 158
6.4.4 Photophysical characterisation 158
6.5 Conclusions 161
6.6 References 162

7 **Conclusion and Future Perspective 163**
7.1 Redox Mediated Switching of Lanthanide luminescence 163
7.2 Anion modulated luminescence in lanthanide appended rotaxanes 163
7.3 Multi-macrocyclic structures containing lanthanide complexes 164
7.4 Behaviour of heterobimetallic *f-f'* lanthanide arrays 165
7.5 Synthesis and study of lanthanide bioconjugates 165

8 **Experimental 167**
8.1 General procedures 167
8.2 Synthesis 171
8.4 X-ray crystallographic data 209
8.5 References 210

Abstract

"Lanthanide architectures, rotaxanes and responsive d-f assemblies"

Manuel Tropiano, Wadham College, University of Oxford.
DPhil. Thesis, Hilary Term 2013.

This work describes the use of copper catalysed "Click" chemistry in the synthesis of lanthanide containing compounds and outlines the application of the products in modulation of luminescence, anion sensing, bioconjugation and multiemissive probes.

Chapter one discusses the fundamental properties of lanthanides with a focus on luminescence and magnetism. A brief literature review on the use of emissive lanthanide probes for sensing application is given. The chapter concludes with an overview on "click" chemistry and its use in the design of lanthanide containing architectures.

A redox switchable luminescent lanthanide complex using a ferrocene group as antenna is described in chapter 2. Insights into the mechanism of modulation of the luminescence signal are given. Other complexes containing redox active aryl chromophores were prepared and their luminescence properties elucidated.

In chapter three, a lanthanide complex is coupled with a rotaxane by Cu(I) "click" reaction. A detailed study of the anion sensing ability of this supramolecular structure follows.

Chapter 4 describes the synthesis of orthogonally functionalised synthons containing azide and alkyne groups that are amenable to form macrocyclic structures upon Cu(I) "click" reaction.

Chapter 5 describes the preparation and study of a novel class of lanthanide complexes containing an appended azide group, and their luminescence properties are studied. The chapter continues with the description of heterobimetallic f-f' complexes prepared using Cu(I) "click" chemistry.

Chapter six describes the synthesis of lanthanide bioconjugates able to target the dopamine transporter (DAT) protein.

Chapter seven delineates the overarching conclusions from the thesis and possible future work in the field, while chapter eight provides experimental procedures.

Publications

1. M. Tropiano, N. L. Kilah, M. Morten, H. Rahman, J. J. Davis, P. D. Beer and S. Faulkner, *J. Am. Chem. Soc.*, 2011, **133**, 11847-11849.
2. E. J. Shiells, L. S. Natrajan, D. Sykes, M. Tropiano, P. Cooper, A. M. Kenwright and S. Faulkner, *Dalton Trans.*, 2011, **40**, 11451-11457.
3. H. L. C. Feltham, F. Klower, S. A. Cameron, D. S. Larsen, Y. H. Lan, M. Tropiano, S. Faulkner, A. K. Powell and S. Brooker, *Dalton Trans.*, 2011, **40**, 11425-11432.
4. T. J. Sørensen, O. A. Blackburn, M. Tropiano and S. Faulkner, *Chem. Phys. Lett.*, 2012, **541**, 16-20.
5. M. Tropiano, C. J. Record, E. Morris, H. S. Rai, C. Allain and S. Faulkner, *Organometallics*, 2012, **31**, 5673-5676.
6. O. A. Blackburn, M. Tropiano, T. J. Sorensen, J. Thom, A. Beeby, L. M. Bushby, D. Parker, L. S. Natrajan and S. Faulkner, *Phys. Chem. Chem. Phys.*, 2012, **14**, 13378-13384.
7. C. Allain, P. D. Beer, S. Faulkner, M. W. Jones, A. M. Kenwright, N. L. Kilah, R. C. Knighton, T. J. Sorensen and M. Tropiano, *Chemical Science*, 2013, **4**, 489-493.
8. T. J. Sorensen, M. Tropiano, O. A. Blackburn, J. A. Tilney, A. M. Kenwright and S. Faulkner, *Chem. Commun.*, 2013, **49**, 783-785.
9. J. Lehr, J. Bennett, M. Tropiano, T. J. S√∏rensen, S. Faulkner, P. D. Beer and J. J. Davis, *Langmuir*, 2013, **29**, 1475-1482.
10. L. J. Charbonniere, S. Faulkner, C. Platas-Iglesias, M. Regueiro-Figueroa, A. Nonat, T. Rodriguez-Blas, A. de Blas, W. S. Perry and M. Tropiano, *Dalton Trans.*, 2013, **42**, 3667-3681.

Acknowledgements

First of all, I would like to thank my supervisor Stephen Faulkner for the opportunity he has given me to be part of his research group. During these years he has been a source of constant help and inspiration, helping me enjoy every aspect of research during my PhD. I could not have had a better mentor.

Thanks to Paul Beer for being a great co-supervisor and for introducing me to the world of supramolecular chemistry. Thanks for the support during these years and for the time spent discussing chemistry with me.

I am grateful to all the staff at the Chemistry Research Laboratory for the analytical service provided and the support. In particular I would like to thank Dr Nick Rees for help with the NMR facilities. Thanks to the EPSRC mass spectrometry service in Swansea for recording some of the MALDI spectra. Thanks to Dr. Alan Kenwright for measuring some of the paramagnetic NMR spectra and for useful discussion about paramagnetic NMR. Thanks to Richard Knighton for the synthesis of the rotaxane used in this work and in general thanks to the Beer group for the help during my time in their lab.

During my time in Oxford I have met some great people and I must thank past and present members of the Faulkner group. Thanks to Cleménce Allain who introduced me to the chemistry of lanthanide complexes during the first months of my project. A special mention goes to all the Part II students during my first year for the support shown with my endless language-related questions and with whom I had a great time: Chris, Freddie, Hannah and James. Thanks to Dr. Michael Jones for measuring and solving crystallographic data and for the patience in trying to teach me. I am always going to be grateful to you for being there to help at any time with absolutely everything. Thanks for the chats and laughs in the lab on every possible topic and for the gems you have left me with, such as the “Flight of the Conchords” and Mr Gormsby. Thanks for introducing me to cricket and squash; while I still do not

understand the first, I am really enjoying the second. Thanks to Dr. Thomas Sørensen for being a friend rather than just a colleague and for the scientific advice during the last almost two years. A special thanks goes to Dr. Octavia Blackburn for being such a great friend and constant source of advice. Thanks for time spent in the lab, working with the “big laser”, going to conferences and drinking espressochocs together. Thanks to all the present members of the Faulkner group for making the lab a great place to work and for the support you have shown while I was writing this thesis.

I would like to thank my family for always being there for me, for the encouragement shown and the support given. Thanks to mum and dad for going through hard times to give me the opportunity for an education and for always being proud of me, for this I love you.

Finally thanks to Anna Rita, who has always been on my side and with whom I have spent the best days of my life. Thanks for making me happy.

Abbreviations

a.u.	arbitrary units
AADC	aromatic acid decarboxylase enzyme
ATR	attenuated total reflectance
BeT	back electron transfer
br	broad
CA	contrast agent
CAN	cerium ammonium nitrate
Cbz	benzylchloroformate
CT	charge transfer
CuAAC	copper azide-alkyne cycloaddition
Cyclen	1,4,7,10-tetraazacyclododecane
d	days
d	doublet
DAT	dopamine trasporter
DCM	dichloromethane
dd	doublet of doublets
DMF	dimethylformamide
DMSO	dimethylsulfoxide
DO2A	1,4,7,10-tetraazacyclododecane-1,7-diacetic acid
DO3A	1,4,7,10-tetraazacyclododecane-1,4,7-triacetic acid
DOSY	diffusion-ordered spectroscopy
DOTA	1,4,7,10-tetraazacyclododecane-1,4,7,10-tetraacetic acid
DOTAM	1,4,7,10-tetraazacyclododecane-1,4,7,10-tetraacetamide
DTBZ	[^{11}C]dihydrotetrabenazine
DTPA	diethylene triamine pentaacetic acid
DTPAA	DTPA anhydride
ESMS	electrospray mass spectrometry
eT	electron transfer

ET	energy transfer
$E_T(30)$	Dimroth–Reichardt parameter of solvent polarity
EtOAc	ethyl acetate
Fc	ferrocene
h	hours
HRMS	high-resolution mass spectrometry
I	ionic strength
IC	internal conversion
ILCT	intra-ligand charge transfer
IR	infrared
ISC	inter-system crossing
L-DOPA	L-3,4-dihydroxyphenylalanine
LMCT	ligand to metal charge transfer
Ln	lanthanide
LRMS	low-resolution mass spectrometry
m	multiplet
MALDI	matrix-assisted laser desorption ionisation
Me	methyl
MeOH	methanol
MLCT	metal to ligand charge transfer
MRI	magnetic resonance imaging
MsCl	methanesulfonyl chloride
MWCO	molecular weight cut-off
NHE	normal hydrogen electrode
NIR	near infrared
NMR	nuclear magnetic resonance
OAc	acetate
ORTEP	Oak Ridge thermal ellipsoid plot
PARACEST	paramagnetic chemical exchange saturation transfer
PD	Parkinson' disease

PET	positron emission tomography
Ph	phenyl
Phen	phenanthridine
PPh_3	triphenylphosphine
RT	room temperature
s	singlet
S	singlet state
SAP	square anti-prism
SPECT	single-photon emission computed tomography
t	triplet
T	triplet state
t-BuONO	*tert*-butyl nitrite
TBA	tetrabutylammonium
TBTA	Tris[(1-benzyl-1*H*-1,2,3-triazol-4-yl)methyl]amine
TFA	trifluoroacetic acid
TLC	thin layer chromatography
$TMSN_3$	trimethylsilyl azide
TOF	time of flight
TRES	time resolved emission spectrum
TSAP	twisted square anti-prism
VMAT2	vesicular monoamine transporter 2

1 Introduction

1.1 General aspects of the lanthanide series

The similarities in chemical properties of lanthanide complexes derive from the electronic properties of these metal ions. Since f orbitals penetrate the xenon core, shielded by 5s and 5p electrons, there is almost no overlap with orbitals of the ligands. This results in a low participation of f orbitals in bonding and hence negligible crystal field effects. As a consequence, the bonding in lanthanide complexes is predominantly determined by electrostatic interactions between the ligand and the trivalent metal ion with coordination number from eight to ten in water, depending on the size of the metal. Coordination geometries are mainly governed by the steric requirements of the ligands while the 3+ oxidation state, the most common for lanthanide complexes in aqueous solutions, renders them hard metal ions that preferentially bind O and N donor atoms.

1.2 Lanthanide luminescence

The wealth of electronic configurations means that the emission properties of each lanthanide are greatly different throughout the series. Lanthanide luminescence can span the UV, visible and near IR wavelengths, with each emission spectrum characterised by sharp emission bands, whose shape and position are minimally perturbed by the local environment of the Ln(III) ion. This is once more a consequence of the minimal crystal field effect on f orbitals, both in the ground and in the excited states, so that the internuclear distances in the excited state remain the same, thus generating a very small Stokes shift upon direct excitation.

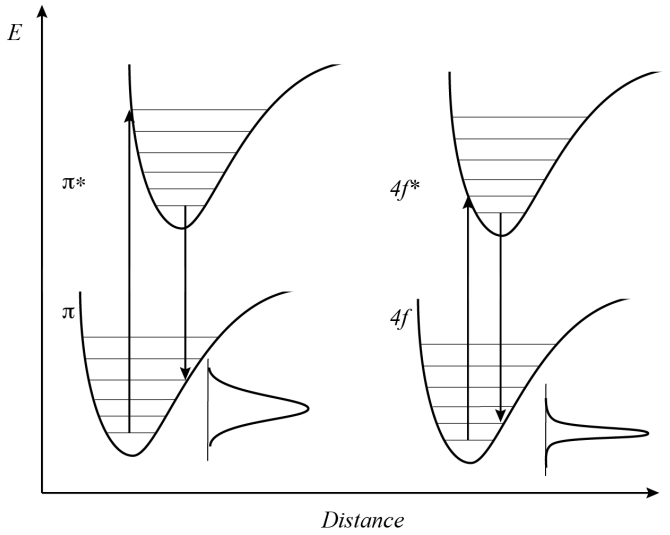


Figure 1-1. Ground and excited states of an organic chromophore (left) and of a lanthanide complex (right) highlighting the respectively broad and sharp emission spectra.

1.2.1 Sensitised luminescence

Direct excitation of a lanthanide ion will only result in weak emission since f-f electric dipole transitions are Laporte forbidden. Magnetic dipole and quadrupolar transitions, although allowed, are very weak, resulting in overall molar absorption coefficients close to unity. Nonetheless, population of the emissive excited state of a lanthanide ion can be achieved through the excitation of a nearby chromophore. This energy transfer process is often referred to as the "antenna effect", where a light harvesting group, the antenna, is used to generate the otherwise difficult to populate lanthanide excited states. Once these excited states are populated, the transition to the ground state will be characterised by a long lifetime of luminescence, given the forbidden nature of the f-f transition, and large apparent Stokes shift, given the excitation at higher energies into the chromophore manifold.

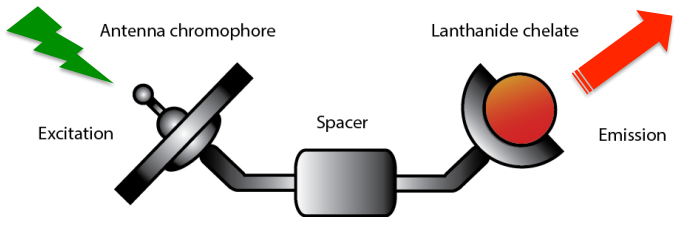


Figure 1-2. . Schematic of a lanthanide chelate-antenna assembly with energy transfer taking place through the spacer group.

Figure 1-3 depicts the possible energy transfer pathways that can lead to lanthanide-centred luminescence upon excitation of an antenna chromophore in a lanthanide-antenna assembly. In a classical energy transfer cascade, the singlet excited state, S_1, of the organic chromophore is populated by a single or multiphoton excitation process. Upon population of the chromophore-centred triplet state, T_1, through intersystem crossing (ISC) from S_1, energy transfer (ET) to the lanthanide excited states can take place by either a Förster of Dexter mechanism, depending on the donor-acceptor energy overlap and chemical structure. Multiphoton excitation of lanthanide complexes in solution has been recently demonstrated both via sensitisation, hence through multiphoton absorption of the antenna, or via direct excitation into the lanthanide manifold.[1-4] It has been shown that efficient energy transfer occurs when the donor triplet state lies above the acceptor state by at least 2000 cm^{-1}, where back energy transfer is minimised while maintaining a good donor-acceptor energy overlap.[5]

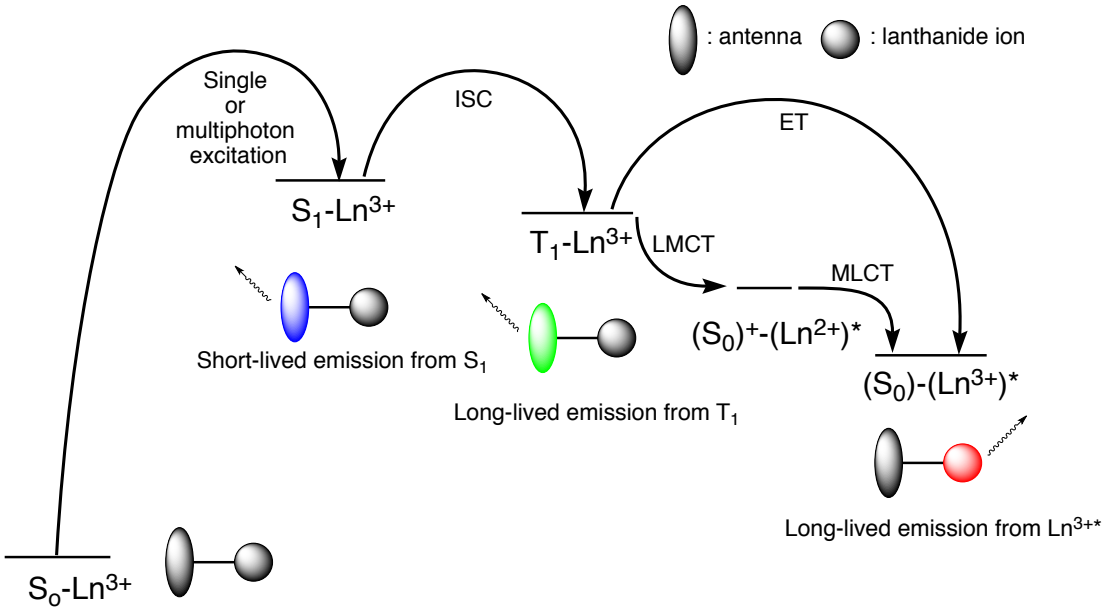


Figure 1-3. Simplified Jablonski diagram representing the main energy transfer pathways leading to emission from a lanthanide ion.

While organic chromophores are widely exploited for the sensitisation of high energy emitting lanthanides such as terbium and europium, the inherent complexity of chromophore synthesis has meant that transition metal containing chromophores have

become increasingly employed as antennae for the sensitisation of near IR emitting lanthanides since the first report of a d-f hybrid more than ten years ago.[6, 7] They offer higher photostability when compared to organic counterparts and a wide range of absorptions: from visible to near IR wavelengths. The near unity yield of formation of the triplet metal-to-ligand charge-transfer (^{3}MLCT) state in such systems ensures an efficient energy transfer process, while their usually long lifetimes of emission have been used for the study of the mechanism of energy transfer in this class of complexes.[8, 9] Indeed, it has been shown that the energy transfer in this class of dyads is mainly governed by a Dexter mechanism where the donor chromophore is either linked directly to the lanthanide, or where superexchange can mediate a Dexter-like process, with efficient lanthanide sensitisation at distances of up to 20 Å for totally conjugated systems.[10]

In the case of electron-rich chromophores, a double electron transfer mechanism between chromophore and Yb(III) can take place when thermodynamically favourable. A ligand-to-metal charge transfer (LMCT) state is formed that in turn is able to populate the emissive excited state of the lanthanide ion (Figure 1-3). This mechanism explains why sensitisation of ytterbium still occurs even when the spectral overlap between donor and acceptor states is negligible. Indeed, a double electron transfer mechanism is responsible for the population of the emissive $^2F_{5/2}$ state, as postulated for the first time by Horrocks and co-workers.[11] This mechanism is only thermodynamically feasible for ytterbium, since in the case of other lanthanide ions, even where the formation of the LMCT state is thermodynamically possible, it would be lower in energy than the lanthanide emissive state, as is the case for terbium and europium.

Finally, sensitisation directly from the chromophore singlet excited state is not to be excluded. This pathway certainly contributes to the overall energy transfer cascade in most lanthanide complexes, and dominates when intra-ligand charge-transfer (ILCT) states are present in the system.[12-14]

1.3 Magnetic properties

In a paramagnetic system, the interaction of an NMR active nucleus with the surrounding electrons in a molecule can be thought of as the interaction between magnetic moments arising from the nuclear and the unpaired electron spins. This is normally averaged to zero given the degeneracy of the electron spin states, but adopts a non-zero value when the molecule is immersed in a magnetic field and the degeneracy of spin states is removed. This induced electron magnetic moment gives rise to changes to the nuclear chemical shift, known as the hyperfine shift. This is defined as the difference in chemical shift of the nucleus between the paramagnetic and the corresponding diamagnetic system. There are two factors that contribute to the experimental hyperfine shift, both derive from the presence of one or more unpaired electrons and can be classified as *(i)* effects taking place directly at the resonating nucleus and *(ii)* contributions deriving from a through space dipole-dipole interaction between two magnetic moments (namely the electronic and the nuclear magnetic moments). The former is called contact or Fermi coupling and contributes to the contact shift (Δ_c), while the latter is known as the pseudocontact contribution to the hyperfine shift or pseudocontact shift (Δ_p). The resulting paramagnetic induced shift is then given by the sum of these contributions and the diamagnetic shift (Δ_d).

$$\Delta = \Delta_d + \Delta_c + \Delta_p \qquad (1)$$

Contact shift contributions to the hyperfine shift derive from the spin polarisability at the nucleus of interest, and are a consequence of through bond spin coupling between the orbital of the unpaired electron spin and the orbital centred on the resonating nucleus. For complexes containing a paramagnetic lanthanide ion its contribution can be expressed as follows:

$$\Delta_c = -\frac{A \cdot \langle S_z \rangle_J}{h \cdot \gamma_I \cdot B_0} \qquad (2)$$

where A/h is the hyperfine coupling constant, B_0 is the strength of the magnetic field, γ_I is the gyromagnetic ratio of the resonating nucleus and $\langle S_z \rangle_J$ is the spin expectation value of the paramagnetic centre in the general case of $S > 1/2$ and presence of spin orbit coupling. For lanthanide complexes this contribution can often be neglected as the orbital overlap of the observed nucleus and the paramagnetic metal is usually negligible, unless there is direct nucleus-metal bond.

The pseudocontact shift contribution derives instead from a through space interaction between magnetic dipoles and thus depends on the mutual orientation of the magnetic dipole vectors. The expression of the pseudocontact shift for lanthanide-containing complexes was first derived by Bleaney.[15] It is expressed as follows:

$$\Delta_p = \frac{2\beta^2 D}{60k^2T^2}\left(\frac{\langle r^2\rangle A_2^0(3cos^2\theta - 1) + \langle r^2\rangle A_2^2(sin^2\theta cos2\phi)}{r^3}\right) \qquad (3)$$

In this equation r, θ, ϕ are the spherical coordinates of the resonating nucleus with reference to a paramagnetic centre at the origin of the reference system (Figure 1-4), β is the Bohr magneton, k is the Boltzmann constant, $\langle r^2\rangle A_2^0$ and $\langle r^2\rangle A_2^2$ are two crystal field coefficients and D is a coefficient containing magnetic susceptibility factors. The latter is specific for each lanthanide ion and is responsible for the change of sign of the chemical shift in NMR spectra of analogous lanthanide compounds, e.g. Eu(III) and Tb(III). For systems with axial symmetry this expression simplifies to:

$$\Delta_p = \frac{2\beta^2 D}{60k^2T^2}\left(\frac{\langle r^2\rangle A_2^0(3cos^2\theta - 1)}{r^3}\right) \qquad (4)$$

It is important to notice that the geometric information is contained only in the expression of the pseudo-contact shift and that it depends on the distance between the observed nucleus and the lanthanide, taken as the origin of the spherical coordinates, and the angle θ between the nucleus and the z-axis.

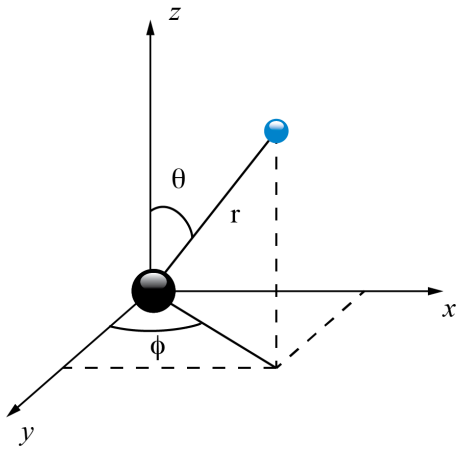
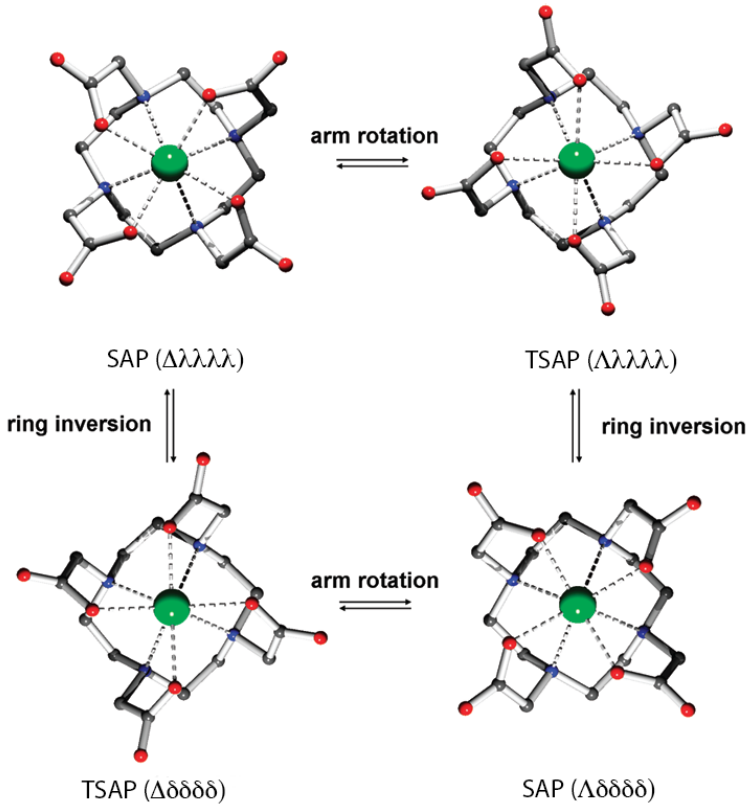


Figure 1-4. Reference system used to describe the effect of a paramagnetic centre, at the origin of the axes (black sphere), on the observed nucleus (blue sphere) with spherical coordinates ϕ, θ and r and z-axis aligned along the direction of the external magnetic field.

Desreux, Aime and coworkers have shown that the paramagnetic effects of lanthanide ions on the ^{1}H-NMR of complexes related to those described in this thesis can be ascribed entirely to pseudocontact contributions.[16, 17]

1.3.1 Structural aspects derived from NMR spectroscopy

The interpretation of ^{1}H and ^{13}C NMR spectra of lanthanide complexes can be carried out using the pseudocontact shift expression above, at least for a complex with axial symmetry. By considering such spectra together with structural data obtained by single crystal X-ray diffraction, the behaviour in solution of the series of lanthanide complexes having a DOTA-like structure can be rationalised.[17] Figure 1-5 depicts the possible conformations that can be adopted by a lanthanide DOTA complex in solution. Rotation of the arms changes the helicity of the complex, as does the rotation of the ethylene groups of the macrocycle, giving rise to two enantiomeric pairs of diastereoisomers that can interconvert.


arm rotation
SAP (Δλλλ

to the need to use polar coordinates relative to a defined magnetic axis, it is still a simple task to discriminate between SAP and TSAP structures on the basis of analogy with axially symmetric systems.

1.4 Luminescent lanthanide-containing compounds

The luminescence properties arising from lanthanide-containing compounds have been greatly exploited over the years. Using time-gated luminescence techniques, any short-lived fluorescence signal originating from the background can be completely removed, acquiring only the long-lived signal displayed by the lanthanide probe. The use of this technique improves the signal-to-noise ratio to the extent that concentrations as low as femtomolar can still be detected. Figure 1-6 gives a graphical depiction of how the employment of a delay time can facilitate the detection of lanthanide luminescence in a complex biological matrix.

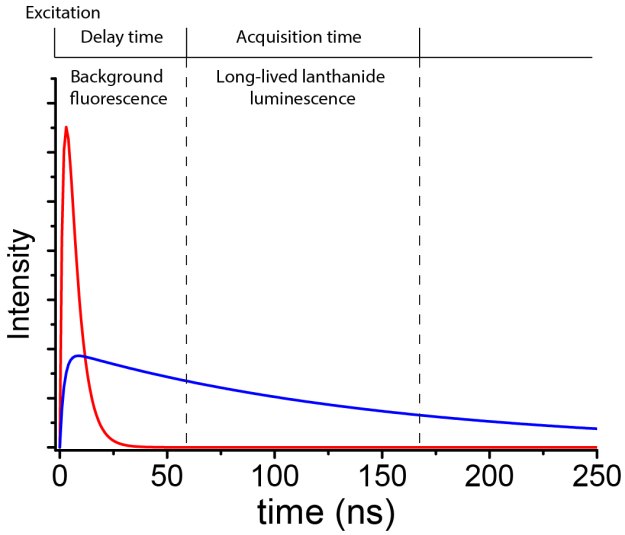


Figure 1-6. Time gated detection of a luminescent signal. A delay time is applied after the excitation pulse during which the detector is switched off. This allows the decay of all short-lived processes and the detection of only long-lived luminescence during the acquisition time.

The well-separated and sharp emission bands allow the use of multiple lanthanides in the same system, which can be exploited as multi-emissive luminescent probes and for ratiometric detection. The deconvolution of the signals is further simplified by the

different luminescence lifetimes, ranging from milliseconds for Eu(III) and Tb(III) to nanoseconds for Nd(III) and Sm(III).[21-24]

Given that lanthanide luminescence is a result of a complex energy transfer cascade, the perturbation of each of the steps leading to the final luminescence can result in the modulation of the luminescence signal. Indeed, each of the energy transfer steps has been exploited in order to obtain lanthanide complexes capable of responding to changes of pH, as well as concentration of anions, cations and neutral analytes. Several lanthanide based luminescent receptors have been reported in the literature. However, in order to be of widespread use for biomedical application, it is important that they fulfil certain requirements such as a long wavelength of excitation (in the visible range), good water solubility, and most importantly high kinetic and thermodynamic stability. While complexes based on the DO3A structure are in most cases kinetically inert and water soluble, the choice of the chromophore is restricted to those having their lowest energy excited state lying at least 2000 cm^{-1} above the emissive state of the lanthanide. This is not easily achieved, especially for lanthanides such as terbium and europium whose high energy emissive states somewhat limit the choice of chromophore that can be employed. Long wavelength excitation of Eu(III) and Tb(III) therefore requires the use of chromophores with small singlet-triplet energy gaps in order for lanthanide sensitisation to occur upon excitation in the visible range, while precluding back energy transfer from the lanthanide to the chromophore triplet state. Examples include the use of phenanthridine, acridones, azaxanthones and acetophenone derivatives.[25-28]

1.4.1 Anion sensing

The anion sensing ability of lanthanide complexes can be exploited both by direct interaction of the anion with the metal centre or with the antenna chromophore, built upon the structure of an anion receptor. Direct interaction with the metal ion often induces an increase in luminescence intensity due to displacement of solvent molecules containing O-H oscillators that readily quench the lanthanide

luminescence. The coordination number of the metal complex can also have an effect on the selectivity of anion recognition. Eight coordinate complexes will prefer coordination to small monodentate anions, while seven coordinate complexes will preferentially bind to bidentate chelating anions, provided that the steric requirements are met. The anion binding abilities of lanthanide-based luminescent receptors have recently been reviewed by Butler and Parker,[29] and the discussion here is limited only to concepts essential to the subsequent chapters. Examples of emissive probes whose luminescence can be modulated via such a mechanism are presented in Figure 1-7.

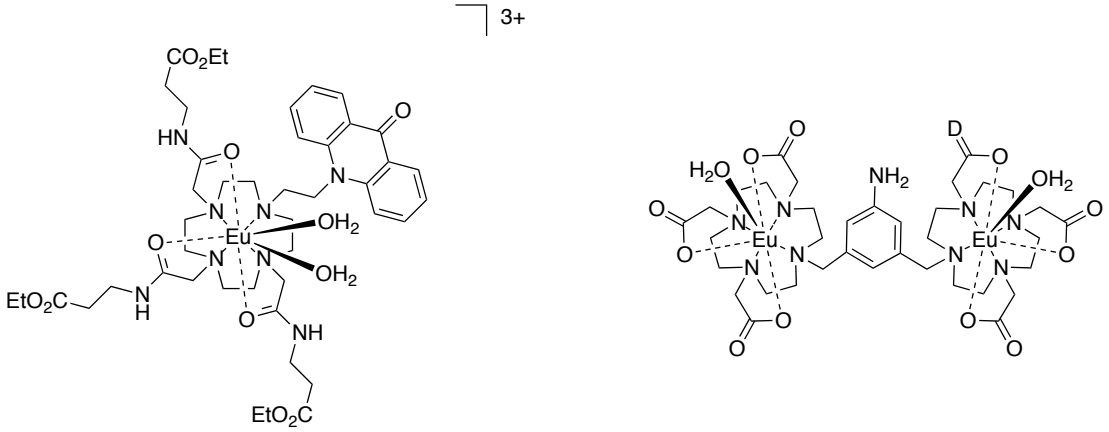


Figure 1-7. Molecular structures of lanthanide-containing receptors employed for anion recognition exploiting unsaturated metal ion coordination.

Complex **1.1** is able to interact with hydrogencarbonate in water. The unsaturated nature of the metal ion plays a central role in the anion recognition process. The positive charge of the complex improves the binding ability compared to neutral or anionic complexes with equivalent chemical structures, highlighting the prevalent ionic nature of the interaction between anion and receptor.[30] The bimetallic complex **1.2** is also able to interact with carboxylate anions; in this case the interplay between the anion-metal coordination and the pre-organised structure renders this complex particularly suitable to interact with rigid phthalates.[31] In both cases the antenna chromophore does not participate in the anion recognition event, but acts only as a long wavelength sensitiser in compound **1.1** and as a rigid bridging unit in complex

1.2. Furthermore, the introduction of an aryl-containing anion can also contribute to the enhancement of the luminescence, with the anion providing an additional sensitising unit whereby the energy transfer can only take place when anion and lanthanide are in close proximity. This approach is particularly important when it can exploit the hypersensitive transitions in the lanthanide emission spectrum. For instance, the electric-dipole ΔJ_2 band in Eu(III), at ca. 615 nm, is sensitive to the ligand environment and hence undergoes a greater change upon binding to the anionic guest than the magnetic-dipole allowed ΔJ_1 transition, which is not affected by any change in the metal coordination sphere.

Interaction of the anionic species with the sensitising group can also result in modulation of luminescence. This can involve the interaction of the ground or excited states of the antenna group. The former mechanism can be easily detected by a change in the absorption or excitation spectrum of the receptor. In this case an enhancement or a quenching of the luminescence signal can be observed depending on the chemical change that the chromophore undergoes, becoming a more or less effective antenna for lanthanide sensitisation. In the second mechanism the chromophore singlet excited state forms an exciplex with the anionic species, usually resulting in quenching due to electron transfer. This is generally a dynamic process and follows the general Stern-Volmer relationship. Deviations from a purely dynamic mechanism are often observed and are the consequence of a long-lived encounter complex between anion and chromophore. Studies of the dependence of intensity and lifetime of luminescence upon quencher concentration and temperature are often necessary to unequivocally assign the type of quenching for each system under study.[32]

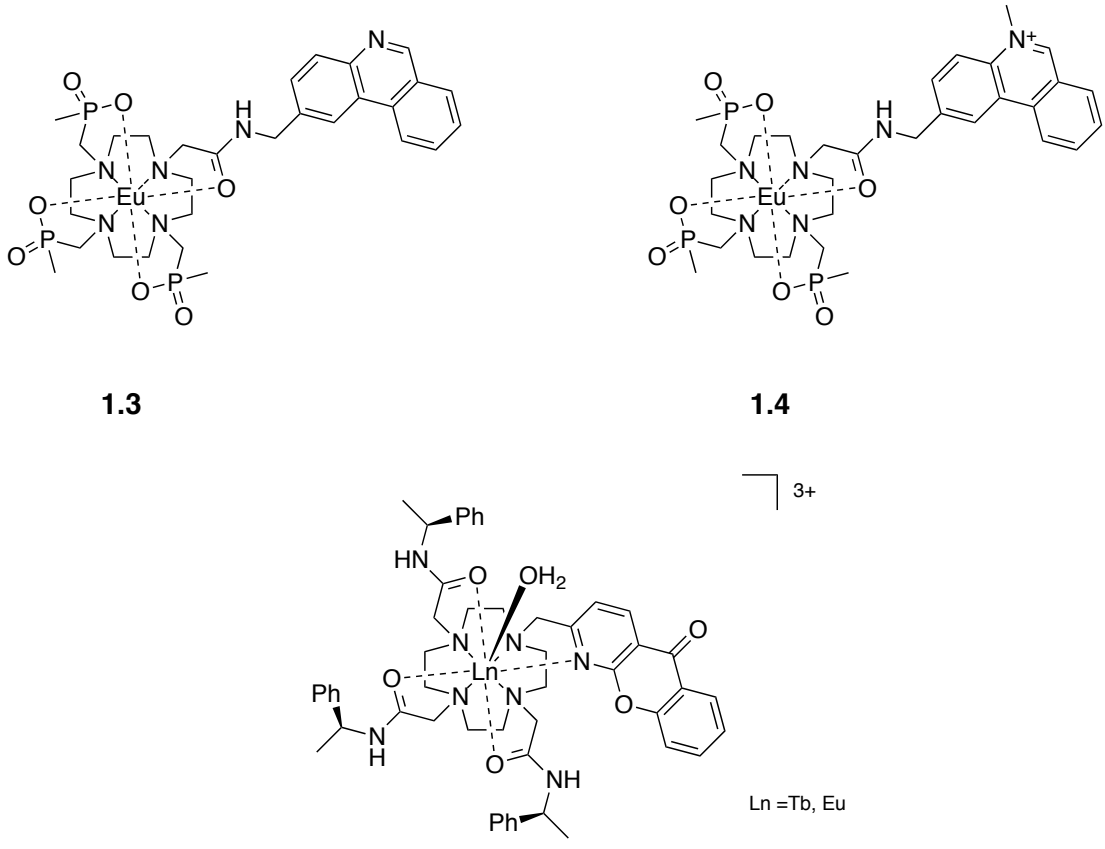


Figure 1-8. Representative chemical structures of lanthanide complexes capable of sensing anions through interaction with the sensitising moiety.

Complex **1.3,** containing a phenanthridine chromophore, can be used as a luminescent probe to detect changes in pH. The mechanism of quenching in this case is due to a change in the ground state of the chromophore upon protonation of the nitrogen atom; leading to an improved energy overlap with the lanthanide ion and resulting in a "switching on" of the luminescence. The analogous methylated complex **1.4** can instead be used as a receptor for halide ions; in this case the mechanism of quenching most likely involves the singlet excited state of the chromophore and the formation of an encounter complex with the anion.[26, 33] Deviation from the linear Stern-Volmer plot was instead observed for complex **1.6** where the electron poor chromophore forms a long-lived exciplex with anions such as urate and ascorbate as demonstrated by a negative dependence of the quenching efficiency with temperature.[32]

1.4.2 Sensing of other analytes

Lanthanide luminescence has also been exploited for the detection of biologically and environmentally relevant cationic and neutral species. The detection can use the geometric requirements of targeted transition metal ions to induce conformational changes in the complex and hence directly affect the coordination sphere of the lanthanide ion. Complex **1.7** provides one example of such an approach, where the presence of Zn(II) triggers a rearrangement of the chelating unit together with a change in the solvation of the lanthanide ion, which is reflected in a decrease of luminescence intensity and lifetime.[34] Compound **1.8** applies the same principle to the detection of Cu(II) using a rigid chelating group. In this case the fluorescence response is enhanced given that complexation of each Cu(II) ion is reported by two luminescent lanthanide complexes.[35]

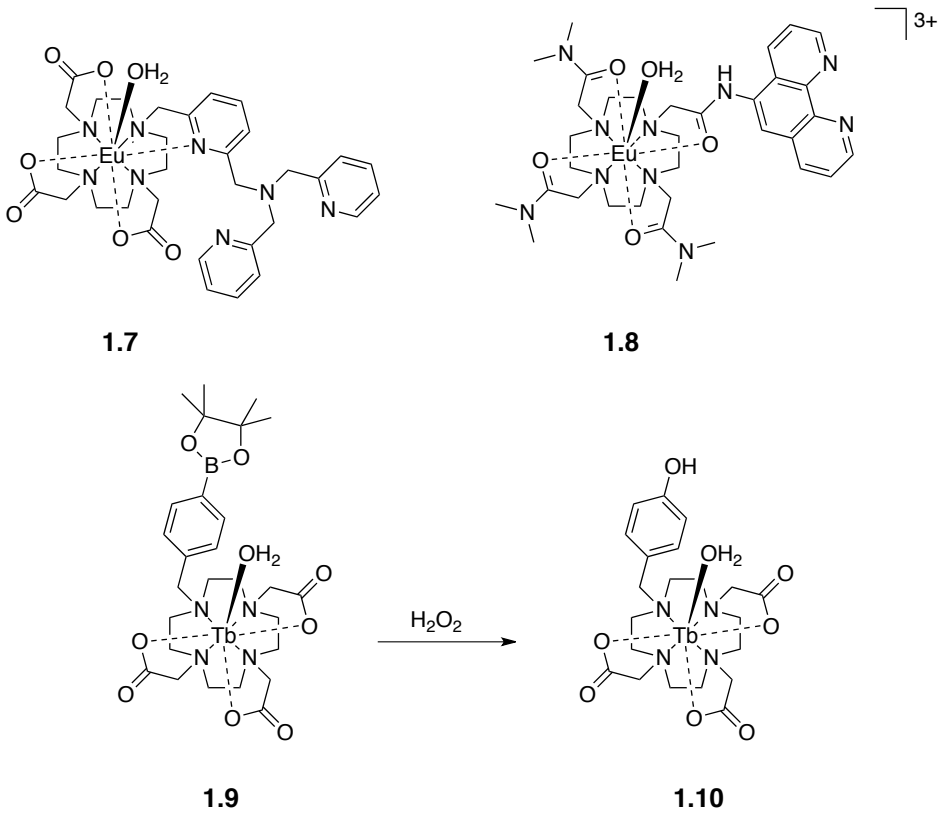


Figure 1-9. Representative lanthanide complexes able to detect cationic, anionic and neutral species through structural and chemical modifications.

The Tb(III) complex **1.9** was developed for the detection of hydrogen peroxide. The mechanism of sensing is based on the same principle as the phenanthridine containing complex **1.3** in that the analyte changes the ground state of the antenna chromophore. Reaction with hydrogen peroxide yields complex **1.10.** The formation of a phenolic ring, renders the chromophore a good sensitising group for Tb(III), in contrast to the electron poor boronate precursor. The result is a "switch on" luminescent receptor that selectively detects hydrogen peroxide over other biologically important reactive oxygen species (ROS).[36] This reaction-based sensing approach is very promising and has received increasing attention in recent years.[37-40] This approach is distinct from those previously discussed in that, upon reaction with the target analyte, the chemical structure of the receptor is changed irreversibly. This is an advantage when devising luminescent probes with a very low detection limit since the latter is directly related to the concentration of the receptor itself. Also, assuming a good quantum yield of luminescence of the receptor in its "on" state, a linear response can be obtained over a wide range of concentrations. However, possible drawbacks include the reaction kinetics and, most importantly the formation of by-products that can themselves interact with the probe or greatly affect the sample under study. Furthermore, the chemical properties of the probe upon reaction can change to the point of affecting its localisation in the cell or even increase its toxicity. Indeed, these systems are not strictly sensors as they lack reversibility and cannot easily be calibrated.

1.5 Stability of lanthanide complexes

The use of lanthanide-containing complexes relies on their stability during the course of the experiment they are employed in. Thermodynamic and kinetic stabilities are therefore of primary importance and are crucial properties to be kept in mind for the design of ligands amenable to lanthanide complexation. The thermodynamics are usually favourable if using an appropriate number of hard donor atoms suitably arranged for coordination, given the purely ionic nature of the metal-ligand interaction. Contrastingly, the intrinsic lability of lanthanide ions can only be overcome using ligands containing multiple chelating arms arranged around the

lanthanide which are capable of rendering the demetallation process highly unfavourable. Mono- and bidentate ligands containing rigid donor groups are usually not suitable for this purpose as is clearly the case with the family of β-diketonates. Indeed, their lanthanide complexes are known to be kinetically labile to the point that different species are present in solution as a consequence of fast ligand exchange.[41] Lanthanide chelates formed with macrocyclic polyaminocarboxylate ligands are frequently not only thermodynamically stable but also kinetically inert. The rest of the discussion on complex stability is focused on this class of compounds.

1.5.1 Thermodynamic stability

Linear and macrocyclic ligands based on polyaminocarboxylates offer unsurpassed thermodynamic stability thanks to the hard nature of the donors and the flexibility of their chemical structures that can wrap around the metal ion without steric constraints. The thermodynamic stability constants of some representative lanthanide complexes are tabulated in Table 1. The data for EDTA and DTPA ligands show a dependence upon the charge density on the lanthanide ion. The linear increase of stability along the lanthanide series for EDTA is indeed due to an increase in charge density on the metal ion and hence to a stronger electrostatic interaction with the ligand.

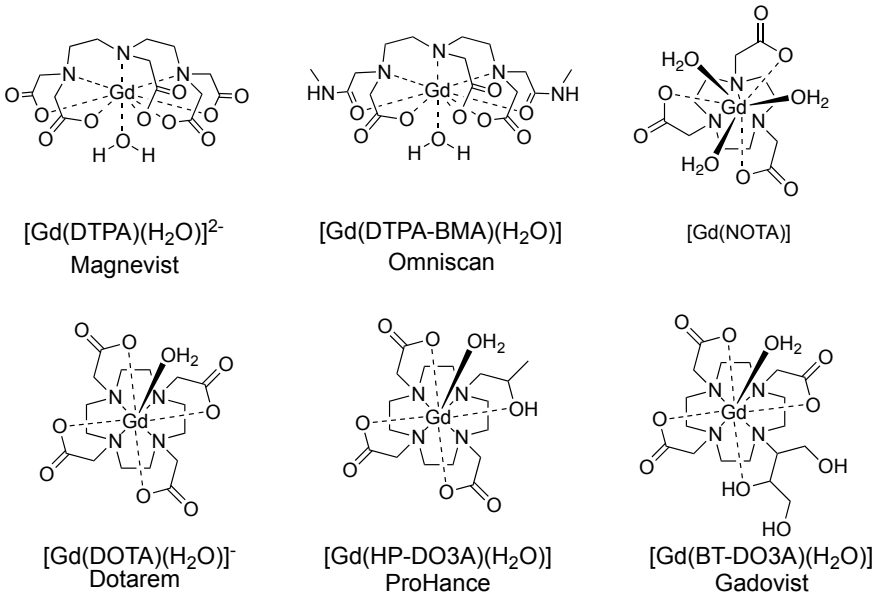


Figure 1-10. Chemical structures of lanthanide complexes discussed in this paragraph.

A different behaviour is observed for the complexes formed with DTPA, where a plateau in stability is reached with Tb(III) and Ho(III). The differences in structure between these two ligands account for the contrasting behaviours. The more flexible EDTA is able to wrap around even the smaller lanthanide without steric constraints whereas for the more rigid DTPA structure, the increase in the electrostatic interaction is counterbalanced by the steric effects of donor groups getting closer together. The overall higher stability of the latter is simply due to its higher denticity. Complexes formed with DOTA are at least two orders of magnitude more stable than the corresponding DTPA complexes. The preorganised macrocyclic structure and the higher basicity of donor groups have both been shown to play important roles in the overall thermodynamic stability of DOTA complexes along the lanthanide series.[42, 43]

Table 1. Thermodynamic stability constants for representative linear and macrocyclic polyaminocarboxylate complexes of lanthanide ions.

	Log K_a (H_2O, I=0.1 M, 25˚C)		
	EDTA[44]	DTPA[44]	DOTA[42]
La^{3+}	15.5	19.5	22.9
Eu^{3+}	17.3	22.5	23.5
Gd^{3+}	17.4	22.5	24.7
Tb^{3+}	17.9	22.7	24.2
Lu^{3+}	19.9	22.4	25.4

1.5.2 Kinetic stability

The kinetic stability of the lanthanide complexes with polyaminocarboxylate ligands has been extensively studied, mainly for gadolinium complexes given their use as MRI contrast agents. In this case a clear relationship between the rigidity of the ligand and the kinetics of formation and dissociation of the metal complexes can be noted. Due to their flexible structure, the complexation of lanthanide ions by EDTA and DTPA is a fast process. In the case of DTPA and its derivatives, the kinetics of complexation are characterised by a saturation behaviour, indicating rapid formation of an intermediate and its slow rearrangement to give the final product.[45] This is not the case for lanthanide complexes of DOTA. The formation of a lanthanide-DOTA

complex has been postulated to occur via a three-step mechanism using potentiometric techniques. The metal ion is firstly coordinated by the acetate arms outside the cavity in a fast process to form $LnH_2DOTA(H_2O)_5$. Coordination to two nitrogen atoms and concerted proton transfer to two carboxylate arms follow in the first slow rate determining step forming $LnH_2DOTA(H_2O)_3$. After fast deprotonation of the carboxylate arms the remaining nitrogen atoms coordinate to the lanthanide ion to give the final complex $LnDOTA^-$ in the second rate-determining step.[46] Such processes are clearly influenced by the local pH, the rate of lanthanide complexation being optimal in the pH range just below 7, which maximises the chance of deprotonating intermediate species while avoiding the prospect of forming lanthanide hydroxide precipitates and colloids.

Table 2. Dissociation kinetics of some gadolinium complexes discussed in this chapter ($k_{obs} = k_0 + k_1[H^+]$).

Compound	k_0 (s^{-1})	k_1 ($M^{-1}s^{-1}$)[b]	Ref.
$[Gd(DOTA)]^-$	$<5 \times 10^{-8}$	5×10^{-6}	47
$[Gd(DTPA)]^{2-}$	-[a]	$\sim 1.2 \times 10^{-3}$	48
[Gd(HP-DO3A)]	$-7(\pm 20) \times 10^{-10}$	2.6×10^{-4}	49
[Gd(BT-DO3A)]	2×10^{-10}	2.8×10^{-5}	49
[Gd(DTPA-BMA)]	-[a]	$>2 \times 10^{-3}$	48
[Gd(NOTA)]	8.3×10^{-6}	2.3×10^{-2}	50

[a] No study of pH dependent and independent rates of lanthanide exchange has been reported for DTPA or DTPA-BMA. [b] The values for k_1 are estimates, based on the assumption that the pH dependent pathway will dominate at pH = 1.

When considering the kinetic stability of a lanthanide chelate, dissociation and transmetallation reactions are the main processes that must be taken into account. For complexes formed with EDTA, the proton-assisted dissociation dominates over direct attack by another metal ion. Indeed, the structure does not leave space for direct attack, because none of the acetate arms remains exposed.[51] This can be contrasted with the DTPA case where the two residual negative charges on $Ln(DTPA)^{2-}$ make direct attack more likely. A study by Brücher et al. demonstrated that at physiological pH the transmetallation mechanism dominates and that the kinetics of the process

largely depend on the attacking metal, with Cu^{2+} and Zn^{2+} possessing much larger kinetic constants than Eu^{3+} for the transmetallation process.[52]

The dissociation of $Ln(DOTA)^-$ complexes is a proton assisted process, although even at low pH the kinetics of dissociation remain much slower than DTPA analogues (see Table 2). At pH 7 the acid catalysed dissociation of $Ln(DOTA)^-$ makes a negligible contribution to the rate of gadolinium exchange.[47] The transmetallation kinetics of Zn^{2+} for DOTA and DOTA-like lanthanide complexes has been studied and a qualitative comparison with open chain polyaminocarboxylates, such as DTPA, show higher kinetic stabilities for complexes derived from macrocyclic structures. For $Gd(DOTA)^-$, no reaction was observed even after 4 days in the presence of 2.5 mM $ZnCl_2$.[53] A thorough study on the comparison of kinetic stabilities of DTPA, DTPA-BMA, DOTA and HP-DO3A complexes of Gd(III) has recently been published by Baranyai et al.[54] The effect of endogenous ligands such as citrate, phosphate, carbonate and histidinate on the exchange reaction of the Gd(III) complexes with Cu(II), have been studied. The open chain complexes, Gd(DTPA) and Gd(DTPA-BMA) show dissociation kinetics that are assisted by the presence of any of the endogenous ligands. A pH dependence was also found, but this was related to the speciation of the ligand in solution, with the carbonate being the most likely cause of dissociation at physiological pH. By contrast, Gd(III) complexes based on macrocyclic ligands such as $Gd(DOTA)^-$ and Gd(HP-DO3A), showed no dependence of the transmetallation reaction kinetics on the concentration of Cu(II) or endogenous ligands. With these complexes, dissociation reactions only occur through a proton assisted mechanism which is however extremely slow even at physiological pH.

1.6 The Cu(I) click chemistry reaction

In 2002 Kolb, Finn and Sharpless introduced the concept of "click chemistry" to describe their approach towards chemical transformations. This term was intended to include all those chemical methods that could be applied reliably both in small and large scale reactions and whose starting building blocks showed excellent selectivity

for each other.[55] The authors also outlined some criteria that these transformations should meet in order to be classified as "click chemistry" reactions. These can be summarised as follows:

- Modular
- High yielding
- Wide in scope
- Afford only inoffensive by-products that can be easily removed
- Stereospecific
- Simple to perform requiring only benign and easy to remove solvents

A number of reactions that meet these requirements have since been identified and include nucleophilic ring opening reactions, non-aldol carbonyl chemistry, addition to carbon-carbon multiple bonds and cycloaddition reactions. In particular, the most widespread and hence most famous reaction among these is the Cu(I) catalysed Huisgen 1,3-dipolar cycloaddition of alkynes with azides to form 1,2,3-triazoles, that since its discovery by Sharpless, Folkin and Meldal has been known as the "click" reaction.[56, 57]

This Cu(I) catalysed azide-alkyne cycloaddition (CuAAC) reaction has demonstrated great versatility over the years and has been successfully applied in bioconjugation, materials science and drug discovery.[58] The advantages in the use of this reaction are indeed exceptional, in that most common organic groups do not interact with the azide or alkyne in mild conditions and hence no protecting groups are usually required. Also, together with the excellent yields of product formation, this transformation is compatible with water and most of the solvents used in organic chemistry.

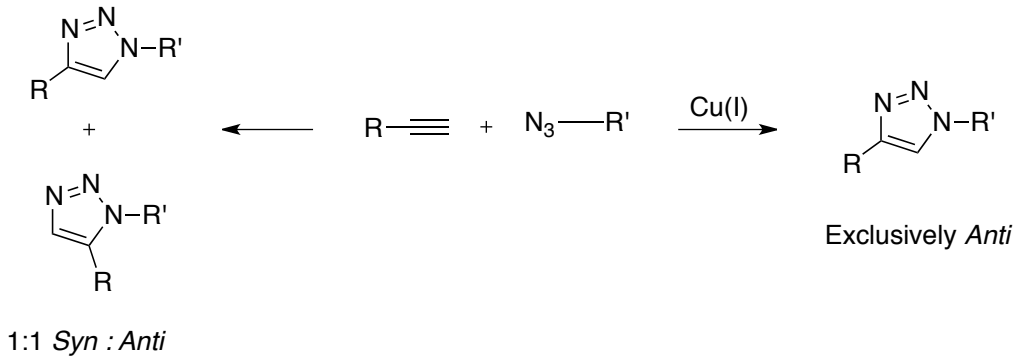


Figure 1-11. Stereoselectivity of the Cu(I) catalysed alkyne-azide cycloaddition over the non-catalysed transformation.

In addition this reaction has been extensively employed in the formation of supramolecular structures with the triazole groups often acting as anion receptor moieties in these architectures.[59]

This transformation opens up numerous possibilities also in the field of lanthanide-containing complexes, for the formation of bioconjugates and selective preparation of multimetallic arrays and hence the development of multimodal imaging agents. Indeed, in 2006, Hulme reported the first example of a Cu(I) catalysed click reaction on a Eu(III) DOTA-like complex.[60] The presence of micromolar amounts of Cu(I) was detected via the conjugation of an azide containing sensitising chromophore with the alkyne containing complex by "click" reaction, resulting in a strong enhancement of Eu(III) centred luminescence. In that instance, the authors cleverly used the fast reaction kinetics of the CuAAC reaction to selectively detect Cu(I) in real time.

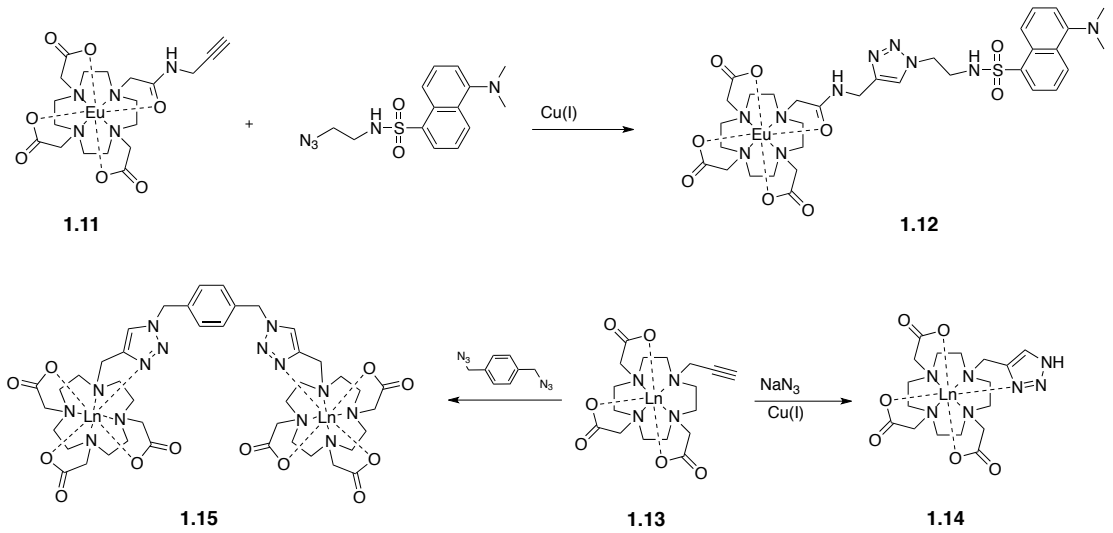


Figure 1-12. Illustration of some early examples of the CuAAC click chemistry reaction applied to lanthanide chelates.

The use of seven coordinate complexes containing an alkyne group was exploited by Lowe and Faulkner to directly change the coordination environment of the metal ion upon "click" reaction.[61, 62] In this case, the formation of the triazole ring upon reaction of the complex with an azide derivative was accompanied by a dramatic changes in the NMR and luminescence spectra, with the triazole directly participating in coordination to the lanthanide metal. Since then, Cu(I) click chemistry has been widely exploited with DOTA-like complexes for the formation of multiplexed Gd(III) MRI contrast agents, bioconjugates, multimetallic complexes and, among others, multimodal imaging agents.[63-69]

The field has also been expanded with the development of the copper-free click chemistry reaction, that exploits the highly reactive cyclooctyne groups and allows this transformation to be used *in vivo* where the presence of Cu(I) would be toxic to the biological environment.[70, 71]

1.7 Project aims

This works aims to prepare kinetically stable lanthanide complexes based on the DO3A moiety and employ such units as building blocks for the construction of supramolecular architectures, responsive luminescent compounds and multiemissive probes. In particular these building blocks must be amenable to functionalisation using mild reaction conditions with high conversion yields. The following chapters discuss the synthesis of alkyne and azide containing lanthanide complexes and their use as substrates in 'click' chemistry reactions. The characterisation of the properties of the products and their photophysical behaviour in electrochemically active d-f hybrid systems, supramolecular architectures, heterobimetallic complexes and bioconjugates are discussed in detail.

1.8 References

1. L.-M. Fu, X.-F. Wen, X.-C. Ai, Y. Sun, Y.-S. Wu, J.-P. Zhang and Y. Wang, *Angew. Chem. Int. Ed.*, 2005, **44**, 747-750.
2. L.-O. Palsson, R. Pal, B. S. Murray, D. Parker and A. Beeby, *Dalton Trans.*, 2007, 5726-5734.
3. A. Picot, A. D'Aléo, P. L. Baldeck, A. Grichine, A. Duperray, C. Andraud and O. Maury, *J. Am. Chem. Soc.*, 2008, **130**, 1532-1533.
4. T. J. Sørensen, O. A. Blackburn, M. Tropiano and S. Faulkner, *Chem. Phys. Lett.*, 2012, **541**, 16-20.
5. M. Latva, H. Takalo, V.-M. Mukkala, C. Matachescu, J. C. Rodríguez-Ubis and J. Kankare, *J. Lumin.*, 1997, **75**, 149-169.
6. S. I. Klink, H. Keizer and F. C. J. M. van Veggel, *Angew. Chem. Int. Ed.*, 2000, **39**, 4319-4321.
7. A. Beeby, R. S. Dickins, S. FitzGerald, L. J. Govenlock, C. L. Maupin, D. Parker, J. P. Riehl, G. Siligardi and J. A. G. Williams, *Chem. Commun.*, 2000, 1183-1184.
8. S. Faulkner, L. S. Natrajan, W. S. Perry and D. Sykes, *Dalton Trans.*, 2009, 3890-3899.
9. W. S. Perry, S. J. A. Pope, C. Allain, B. J. Coe, A. M. Kenwright and S. Faulkner, *Dalton Trans.*, 2010, **39**, 10974-10983.
10. T. Lazarides, D. Sykes, S. Faulkner, A. Barbieri and M. D. Ward, *Chem. Eur. J.*, 2008, **14**, 9389-9399.
11. W. D. Horrocks Jr, J. P. Bolender, W. D. Smith and R. M. Supkowski, *J. Am. Chem. Soc.*, 1997, **119**, 5972-5973.
12. M. Kleinerman, *J. Chem. Phys.*, 1969, **51**, 2370-2381.
13. A. D'Aléo, F. Pointillart, L. Ouahab, C. Andraud and O. Maury, *Coord. Chem. Rev.*, 2012, **256**, 1604-1620.
14. C. Yang, L.-M. Fu, Y. Wang, J.-P. Zhang, W.-T. Wong, X.-C. Ai, Y.-F. Qiao, B.-S. Zou and L.-L. Gui, *Angew. Chem. Int. Ed.*, 2004, **43**, 5010-5013.
15. B. Bleaney, *J. Magn. Reson.*, 1972, **8**, 91-100.
16. C. C. Bryden, C. N. Reilley and J. F. Desreux, *Anal. Chem.*, 1981, **53**, 1418-1425.
17. S. Aime, M. Botta and G. Ermondi, *Inorg. Chem.*, 1992, **31**, 4291-4299.
18. M. Polâšek, J. Kotek, P. Hermann, I. Cisarová, K. Binnemans and I. Lukeš, *Inorg. Chem.*, 2008, **48**, 466-475.
19. S. Aime, M. Botta, M. Fasano, M. P. M. Marques, C. F. G. C. Geraldes, D. Pubanz and A. E. Merbach, *Inorg. Chem.*, 1997, **36**, 2059-2068.
20. S. Aime, A. Barge, M. Botta, A. S. De Sousa and D. Parker, *Angew. Chem. Int. Ed.*, 1998, **37**, 2673-2675.
21. D. G. Smith, G.-l. Law, B. S. Murray, R. Pal, D. Parker and K.-L. Wong, *Chem. Commun.*, 2011, **47**, 7347-7349.
22. M. P. Placidi, A. J. L. Villaraza, L. S. Natrajan, D. Sykes, A. M. Kenwright and S. Faulkner, *J. Am. Chem. Soc*, 2009, **131**, 9916-9917.
23. T. J. Sorensen, M. Tropiano, O. A. Blackburn, J. A. Tilney, A. M. Kenwright and S. Faulkner, *Chem. Commun.*, 2013, **49**, 783-785.

24. C. Song, Z. Ye, G. Wang, J. Yuan and Y. Guan, *Chem. Eur. J.*, 2010, **16**, 6464-6472.
25. A. Dadabhoy, S. Faulkner and P. G. Sammes, *J. Chem. Soc. Perkin Trans. 2*, 2000, 2359-2360.
26. D. Parker, K. Senanayake and J. A. G. Williams, *Chem. Commun.*, 1997, 1777-1778.
27. P. Atkinson, K. S. Findlay, F. Kielar, R. Pal, D. Parker, R. A. Poole, H. Puschmann, S. L. Richardson, P. A. Stenson, A. L. Thompson and J. Yu, *Org. Biomol. Chem.*, 2006, **4**, 1707-1722.
28. A. Beeby, L. M. Bushby, D. Maffeo and J. A. G. Williams, *J. Chem. Soc. Perkin Trans. 2*, 2000, 1281-1283.
29. S. J. Butler and D. Parker, *Chem. Soc. Rev.*, 2013, **42**, 1652-1666.
30. Y. Bretonniere, M. J. Cann, D. Parker and R. Slater, *Chem. Commun.*, 2002, 1930-1931.
31. J. A. Tilney, T. J. Sørensen, B. P. Burton-Pye and S. Faulkner, *Dalton Trans.*, 2011, **40**, 12063-12066.
32. F. Kielar, C. P. Montgomery, E. J. New, D. Parker, R. A. Poole, S. L. Richardson and P. A. Stenson, *Org. Biomol. Chem.*, 2007, **5**, 2975-2982.
33. D. Parker, P. Senanayake and J. A. G. Williams, *J. Chem. Soc. Perkin Trans. 2*, 1998, 2129-2140.
34. S. J. A. Pope and R. H. Laye, *Dalton Trans.*, 2006, 3108-3113.
35. T. Gunnlaugsson, J. P. Leonard, K. Senechal and A. J. Harte, *Chem. Commun.*, 2004, 782-783.
36. A. R. Lippert, T. Gschneidtner and C. J. Chang, *Chem. Commun.*, 2010, **46**, 7510-7512.
37. B. K. McMahon and T. Gunnlaugsson, *J. Am. Chem. Soc.*, 2012, **134**, 10725-10728.
38. E. Pershagen, J. Nordholm and K. E. Borbas, *J. Am. Chem. Soc.*, 2012, **134**, 9832-9835.
39. T. Terai, K. Kikuchi, Y. Urano, H. Kojima and T. Nagano, *Chem. Commun.*, 2012, **48**, 2234-2236.
40. T. Terai, H. Ito, K. Kikuchi and T. Nagano, *Chem. Eur. J.*, 2012, **18**, 7377-7381.
41. K. Binnemans, in *Handbook on the Physics and Chemistry of Rare Earths*, eds. J. C. B. K.A. Gschneidner and V. K. Pecharsky, Elsevier, 2005, vol. 35, pp. 107-272.
42. W. P. Cacheris, S. K. Nickle and A. D. Sherry, *Inorg. Chem.*, 1987, **26**, 958-960.
43. K. Kumar, C. A. Chang and M. F. Tweedle, *Inorg. Chem.*, 1993, **32**, 587-593.
44. R. M. Smith and A. E. Martell, *Sci. Total Environ.*, 1987, **64**, 125-147.
45. E. Balogh, R. Tripier, P. Fouskova, F. Reviriego, H. Handel and E. Toth, *Dalton Trans.*, 2007, 3572-3581.
46. J. Moreau, E. Guillon, J.-C. Pierrard, J. Rimbault, M. Port and M. Aplincourt, *Chem. Eur. J.*, 2004, **10**, 5218-5232.
47. E. Tóth, E. Brücher, I. Lazar and I. Tóth, *Inorg. Chem.*, 1994, **33**, 4070-4076.
48. P. Wedeking, K. Kumar and M. F. Tweedle, *Magn. Reson. Imaging*, 1992, **10**, 641-648.
49. É. Tóth, R. Király, J. Platzek, B. Radüchell and E. Brücher, *Inorg. Chim. Acta*, 1996, **249**, 191-199.
50. G. Tircsó, Z. Kovács and A. D. Sherry, *Inorg. Chem.*, 2006, **45**, 9269-9280.

51. E. Brücher and P. Szarvas, *Inorg. Chim. Acta*, 1970, **4**, 632-636.
52. L. Sarka, L. Burai and E. Brücher, *Chem. Eur. J.*, 2000, **6**, 719-724.
53. S. Laurent, L. V. Elst and R. N. Muller, *Contrast Media Mol. Imaging*, 2006, **1**, 128-137.
54. Z. Baranyai, Z. Pálinkás, F. Uggeri, A. Maiocchi, S. Aime and E. Brücher, *Chem. Eur. J.*, 2012, **18**, 16426-16435.
55. H. C. Kolb, M. G. Finn and K. B. Sharpless, *Angew. Chem. Int. Ed.*, 2001, **40**, 2004-2021.
56. V. V. Rostovtsev, L. G. Green, V. V. Fokin and K. B. Sharpless, *Angew. Chem. Int. Ed. Engl.*, 2002, **41**, 2596-2599.
57. C. W. Tornøe, C. Christensen and M. Meldal, *J. Org. Chem.*, 2002, **67**, 3057-3064.
58. J. E. Moses and A. D. Moorhouse, *Chem. Soc. Rev.*, 2007, **36**, 1249-1262.
59. K. D. Hänni and D. A. Leigh, *Chem. Soc. Rev.*, 2010, **39**, 1240-1251.
60. R. F. Viguier and A. N. Hulme, *J. Am. Chem. Soc.*, 2006, **128**, 11370-11371.
61. G. J. Stasiuk and M. P. Lowe, *Dalton Trans.*, 2009, 9725-9727.
62. M. Jauregui, W. S. Perry, C. Allain, L. R. Vidler, M. C. Willis, A. M. Kenwright, J. S. Snaith, G. J. Stasiuk, M. P. Lowe and S. Faulkner, *Dalton Trans.*, 2009, 6283-6285.
63. T. L. Mindt, C. Müller, F. Stuker, J.-F. Salazar, A. Hohn, T. Mueggler, M. Rudin and R. Schibli, *Bioconjugate Chem.*, 2009, **20**, 1940-1949.
64. D. J. Mastarone, V. S. R. Harrison, A. L. Eckermann, G. Parigi, C. Luchinat and T. J. Meade, *J. Am. Chem. Soc.*, 2011, **133**, 5329-5337.
65. L. Frullano, C. Catana, T. Benner, A. D. Sherry and P. Caravan, *Angew. Chem., Int. Ed.*, 2010, **49**, 2382-2384.
66. J. K. Molloy, O. Kotova, R. D. Peacock and T. Gunnlaugsson, *Org. Biomol. Chem.*, 2012, **10**, 314-322.
67. C. Szijjarto, E. Pershagen and K. E. Borbas, *Dalton Trans.*, 2012, **41**, 7660-7669.
68. M. Tropiano, C. J. Record, E. Morris, H. S. Rai, C. Allain and S. Faulkner, *Organometallics*, 2012, **31**, 5673-5676.
69. P. A. Sukerkar, K. W. MacRenaris, T. R. Townsend, R. A. Ahmed, J. E. Burdette and T. J. Meade, *Bioconjugate Chem.*, 2011, **22**, 2304-2316.
70. P. V. Chang, J. A. Prescher, E. M. Sletten, J. M. Baskin, I. A. Miller, N. J. Agard, A. Lo and C. R. Bertozzi, *Proc. Natl. Acad. Sci. USA*, 2010, **107**, 1821-1826.
71. M. E. Martin, S. G. Parameswarappa, M. S. O' Dorisio, F. C. Pigge and M. K. Schultz, *Bioorg. Med. Chem. Lett.*, 2010, **20**, 4805-4807.

2 Luminescent lanthanide complexes containing a redox active chromophore[1]

2.1 Introduction

The energy transfer mechanism involved in the population of a lanthanide ion excited states, the antenna effect, has been thoroughly studied over the past thirty years. The exploitation of these pathways has led to the development of several compounds whose lanthanide luminescence is modulated by the presence of a particular ion or, generally speaking, analyte. More recently, transition metal complexes have been used as light harvesting chromophores for transferring energy to NIR emitting lanthanides. The advantages of this strategy include the higher photostability of transition metal complexes compared to organic chromophores and the kinetic inertness they offer, should one envisage biological use of the heterometallic probe.[1] On the other hand, the scope of such chromophores is often limited by their low-lying excited energy states, that render them particularly useful only for sensitisation of lanthanides with lower energy states, namely ytterbium, erbium and neodymium. While the energy transfer to neodymium and erbium can be explained by a Förster or Dexter mechanism, in the case of ytterbium, which possesses a single excited state, the overlap between donor and acceptor states is often negligible. A double electron transfer mechanism, where the electron is first donated to the Yb(III) centre by the chromophore and then transferred back to the chromophore leaving the lanthanide ion in its excited state, must be invoked where it is thermodynamically feasible.[2] The validity of this mechanism has been demonstrated with a phenanthridine antenna in the molecule shown in Figure 2-1. Indeed, this two-step electron transfer mechanism

[1] Part of this work has already been published as a communication in *J. Am. Chem. Soc. 2011, 133, 11847–11849.*

is observed only when the phenanthridine moiety is deprotonated, while the energy transfer step from the antenna to the lanthanide ion becomes the rate determining step upon protonation of the phenanthridine group.[3]

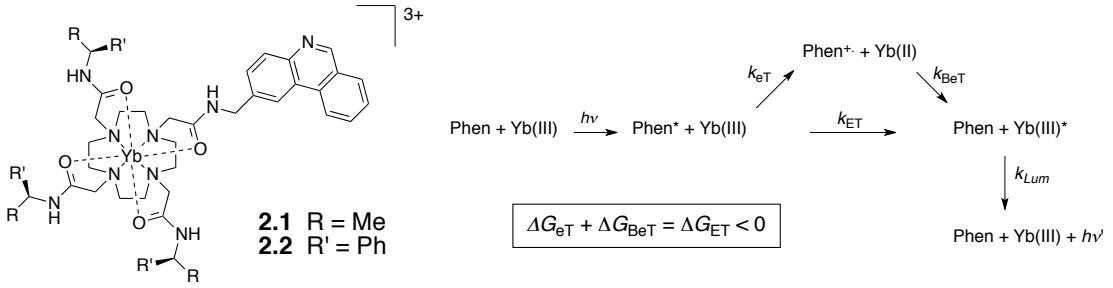


Figure 2-1. An ytterbium complex containing a phenanthridine chromophore capable of a double electron transfer mechanism for lanthanide sensitisation.

In this chapter, a family of alkyne DO3A complexes are prepared and employed as a robust and versatile starting material for the synthesis of ferrocene appended lanthanide complexes. It will be demonstrated that a transition metal chromophore such as ferrocene can be a useful sensitiser not only for NIR emitting lanthanides but also for a visible emitter such as europium. The redox activity of the transition metal will be exploited in the modulation of lanthanide luminescence and other redox active chromophores will be sought for the preparation of luminescent complexes that respond to a change of redox potential.

2.2 An alkyne appended lanthanide complex

In 2009 Lowe, Faulkner et al. showed for the first time that a seven coordinate lanthanide complex based on the DO3A structure could be used as a versatile platform for the CuAAC "click" reaction with substrates containing an azide functionality.[4, 5] The authors demonstrated that this complex (**2.6**) was reactive enough to form a triazolyl ring even upon reaction with sodium azide, yielding a complex whose ^{1}H-NMR spectrum was not only that of an eight coordinate species (characterised by sharp resonances typical of four different axial ring proton environments), but was also pH dependent, due to the presence of an acidic proton on the triazolyl ring, clearly demonstrating that the reaction effectively took place. The same strategy was used to couple organic azides as a way to extend the chromophore group and also as bridging unit to form bimetallic complexes. The versatility of this alkyne substrate has since then been exploited for the formation of, among others, bioconjugates, multimetallic contrast agents for MRI applications and for the preparation of d-f hybrid complexes.[6, 7]

It was reasoned that the same platform could give scope for further exploitation especially given its versatility and the ease of formation of the corresponding "click" product. The preparation of this class of lanthanide complexes followed the synthesis reported in the literature. Firstly, the triester **2.3** was obtained from cyclen by alkylation with *tert*-butyl bromoacetate in acetonitrile under basic conditions. Alkylation of the fourth nitrogen atom was achieved using propargyl bromide in very high yield and in no need of purification as judged by the ^{1}H-NMR of **2.4**. Deprotection of the carboxylic acid moieties upon reaction with TFA in dichloromethane afforded the ligand **2.5** in quantitative yield. Complexation was carried out in methanol using an excess of lanthanide to ensure complete reaction of the ligand. Excess of metal could be readily precipitated as the insoluble hydroxide by raising the pH of the solution (see Figure 2-2 for the synthesis scheme).

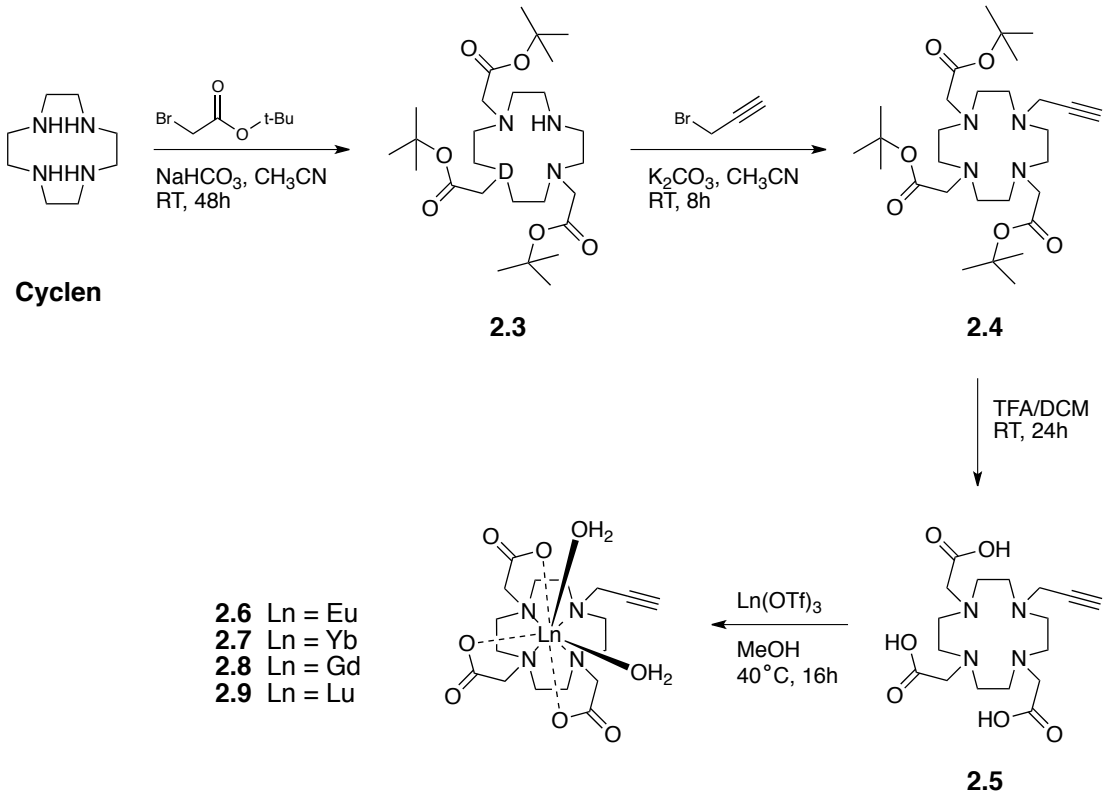


Figure 2-2. Synthesis followed for the preparation of a series of lanthanide containing complexes that could be used as substrates for the CuAAC "click" reaction.

2.2.1 Crystal structure

Crystals suitable for X-ray analysis of the Lu(III) complex **2.9** were grown by vapour diffusion of acetone into a concentrated solution of the complex in water. This is one of the very few crystal structures of a seven coordinate lanthanide complex based on the DO3A structure, probably given the difficulty of packing of the molecule in a crystal while still satisfying the coordination requirements of a complex with broken symmetry. The structure of **2.9**, solved and analysed by Dr. Michael Jones, is unusual in that two complexes are bridged by a carbonate, while the structure is stabilised by two sodium ions in the asymmetric unit and multiple water molecules in an extensive, complex 3-dimensional hydrogen-bonding network. The crystal was found to be a non- merohedral twin by rotation about the c-axis with a twin ratio of ca. 70 : 30. Similarly, in the crystal structure of [Gd(DO3A)] reported by Chang et al. the asymmetric unit is formed by three complexes linked together by a carbonate species encapsulated within the cavity formed by the [Gd(DO3A)] complexes.[8]

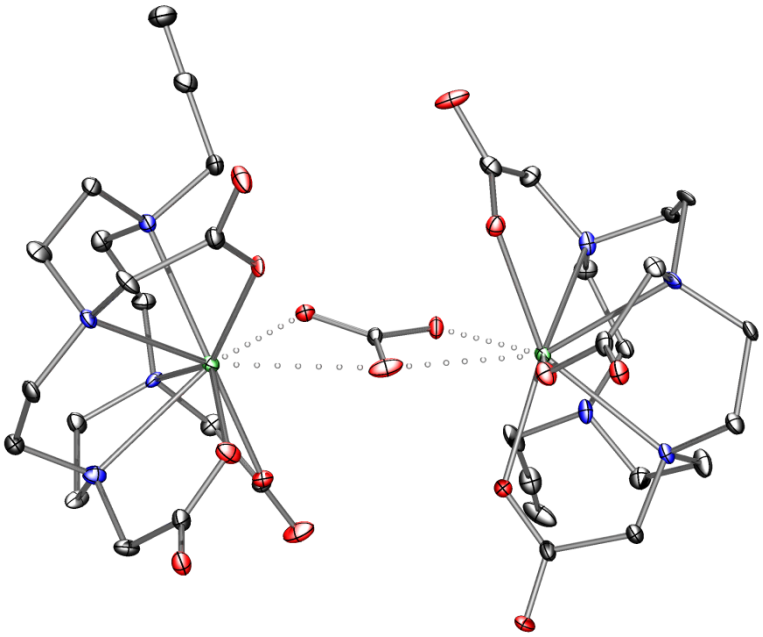


Figure 2-3. Representation of the solid state structure of **2.9** as ORTEP depiction with thermal ellipsoid displayed at 30% probability and the water molecules, sodium and hydrogen atoms omitted for clarity. Black, blue, red, green are carbon, nitrogen, oxygen and lutetium atoms respectively.

This supramolecular interaction between the complex and a carbonate anion causes the complex to form dimers in the solid state. In principle, this supramolecular interaction could also take place in solution. Indeed, the dependence of the paramagnetic ^{1}H-NMR spectra and of the hydration number "q" of the Eu(III) complex upon changes of pH of the solution, may support this hypothesis. A strong dependence of the shape of ^{1}H-NMR the spectrum upon changing the pH can be noticed. Indeed, it is known that a change in pH affects the predominance of one isomer over the other, with the SAP present at pH<5 and a predominant TSAP conformation at pH>7. Nonetheless the change observed was not only of chemical shift but also of overall peak width, suggesting a more rigid structure in solution at basic pH conditions. If it is also considered that the hydration of the Eu(III) complex **2.6** (determined from luminescence measurements in H_2O and D_2O) changes with pH, with a q value of 2.3 at pH<5 and and of 0.7 at pH>8, it is quite clear that the basification of the solution is having a direct effect on the coordination sphere of the lanthanide ion and indirectly on the overall structure of the complex. It seems then reasonable to conclude that at high pH values the concentration of OH^- anions is such

that an interaction with the unsaturated metal takes place, occupying the eighth coordination site, hence rigidifying the complex structure. Association of lanthanide complexes at high pH has been observed before.[9] It is clear that the behaviour observed in this system follows similar trends. Indeed, the Lewis acidity of the lanthanide centre would favour the formation of oxo or hydroxo dimers.

Diffusion ^{1}H-NMR measurement would in theory provide a direct answer on the size of the species in solution at different pH values, especially if a dimer forms, in which case the diffusion coefficient should have a twofold increase. Unfortunately this hypothesis could not be proved by a DOSY experiment, since the spectrum of the diamagnetic Lu(III) derivative **2.9** was too broad, thus not permitting monitoring of a specific resonance.

2.3 A self-assembled lanthanide-ferrocene complex

2.3.1 Self-assembly of Eu.P-DO3A 2.6 with ferrocene carboxylic acid

Initially, a self-assembly approach was undertaken where the supramolecular interactions between a lanthanide complex and a ferrocene-containing moiety could be exploited to form a heterobimetallic d-f hybrid directly from the metal components.

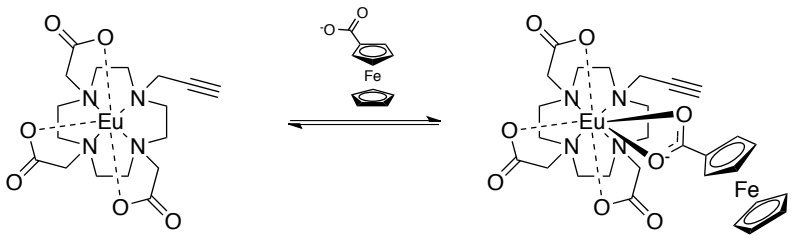


Figure 2-4. Supramolecular interaction between the seven coordinate Eu.P-DO3A **2.6** and ferrocene carboxylic acid.

The interaction of ferrocene carboxylic acid with the coordinatively unsaturated propargyl Eu-DO3A (**2.6**) complex was followed by luminescence spectroscopy,

monitoring the emission spectrum of europium upon addition of the ferrocene group. Upon titration of a solution of propargyl Eu-DO3A with ferrocene carboxylic acid in water, the emission intensity was gradually quenched as a consequence of the interaction between the two metal moieties (see Figure 2-5). Indeed, luminescence quenching of europium by ferrocene is known, where the quenching mechanism has been shown to take place by electron transfer from the ferrocene to the europium excited state.[10] This titration served as a qualitative indication of the interaction between the carboxylate and the seven coordinate europium complex. Indeed, although a thorough binding study was not performed in this case, the interaction of carboxylates with coordinatively unsaturated lanthanide complexes in solution has been well demonstrated and widely exploited in the literature.[11-14]

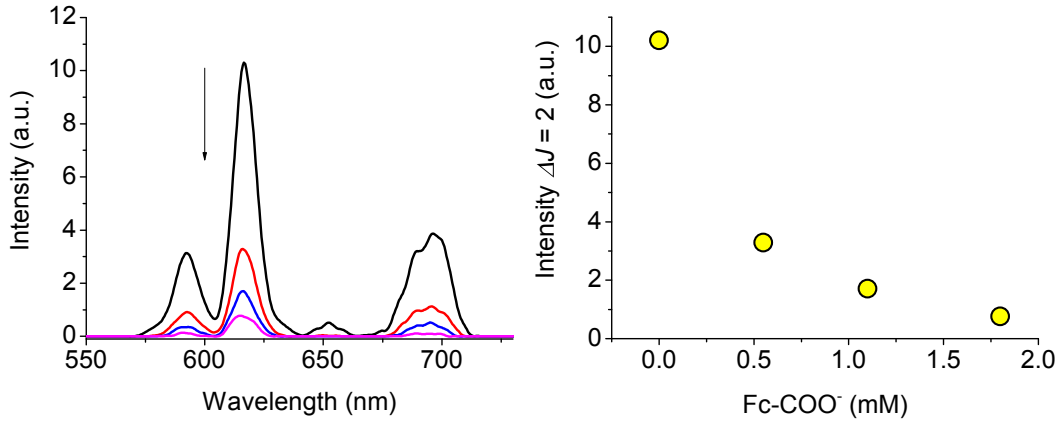


Figure 2-5. Europium emission spectrum upon titration with ferrocene carboxylic acid and corresponding intensity of the $\Delta J = 2$ band vs. concentration of added guest in water at pH 9. $\lambda_{ex} = 285$ nm, delay time: 0.1 ms, gate time: 0.1 ms.

Despite the overall decrease of luminescence, the residual emission of the supramolecular assembly could be used to probe the effect of the oxidation state of ferrocene to the luminescence properties originating from the europium centre.

2.3.2 Spectroelectrochemistry

Figure 2-6 describes the setup used for spectro-electrochemical experiments. The electrochemical redox processes were carried out in a micro-cuvette containing ca.

140 μL of sample placed directly into a spectrofluorimeter sample holder. The three electrodes used consisted of a platinum mesh as a working electrode, a platinum wire as the counter electrode and a Ag/AgCl wire as the reference electrode. These were positioned outside the optical path of the incident light as to minimise scattered light while the oxidation and reduction processes were performed by chronoamperometry using a potentiostat. Oxidation and reduction were monitored using UV-Vis absorption and synchronised luminescence measurements were taken *in situ*.

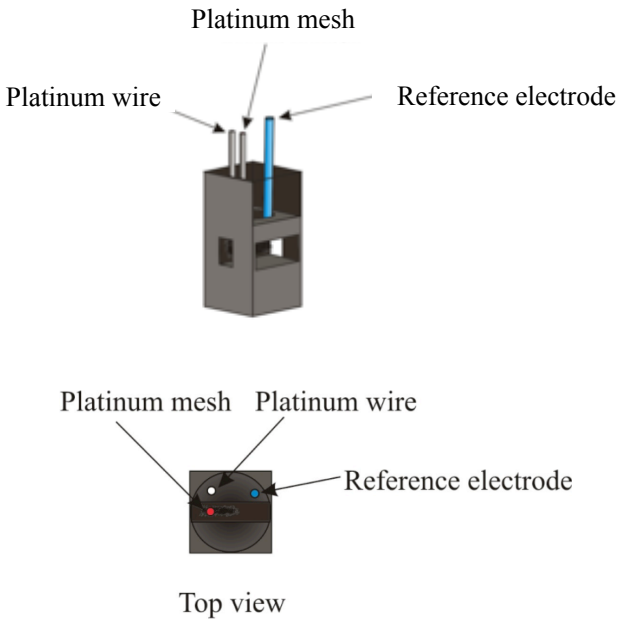


Figure 2-6. Drawing of the setup used for the spectroelectrochemical measurements.

The emission arising from europium in the supramolecular assembly was monitored upon consecutive oxidation-reduction cycles of the ferrocene moiety. Figure 2-7 shows the behaviour of lanthanide emission while the ferrocene moiety is being electrochemically oxidised to ferrocenium. *In situ* oxidation resulted in diminishing europium luminescence, while subsequent reduction of the ferrocenium group back to ferrocene fully restored the luminescence of the self-assembled dyad (Figure 2-7). The lifetime of the excited state followed the same trend, decreasing from 0.45 ms in the reduced form to 0.10 ms in the oxidised form.

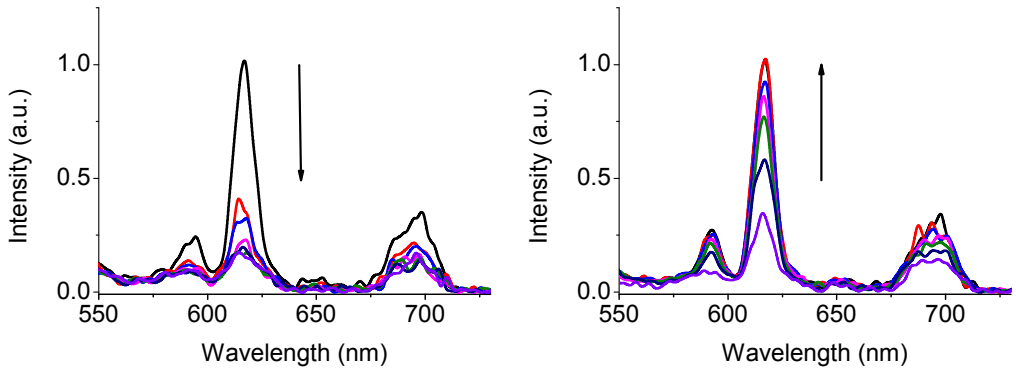


Figure 2-7. Europium emission upon oxidation (left) and consecutive reduction of the ferrocene carboxylic acid (right) in water at pH 9. λ_{ex}= 285 nm, delay time: 0.1 ms, gate time: 0.1 ms.

This proof of principle experiment seemed to suggest that the quenching behaviour of ferrocene is dependent upon its oxidation state. This hinted at the possibility to exploit redox active species to modulate the luminescence of a lanthanide centre in close proximity. Indeed, the nature of this preliminary experiment does not rule out other aspects of the self-assembly, such as a different binding affinity towards the europium complex of the oxidised ferrocene species. In particular, a much lower binding affinity of the oxidised ferrocenium species could induce a disassembly of the supramolecular adduct and hence not allow a direct comparison with the reduced analogue.

If a system as such is to be used in a complex chemical environment containing several species, these are likely to interfere with the self-assembly process. The overall stability of this molecular assembly could then be affected and its photophysical properties interfered with. Hence, an alternative complex was pursued in which the electrochemically active group and the luminescent unit are covalently linked, thus ensuring stability. Accordingly it was resolved to prepare a kinetically stable system in which the ferrocene moiety was covalently linked to the lanthanide binding pocket.

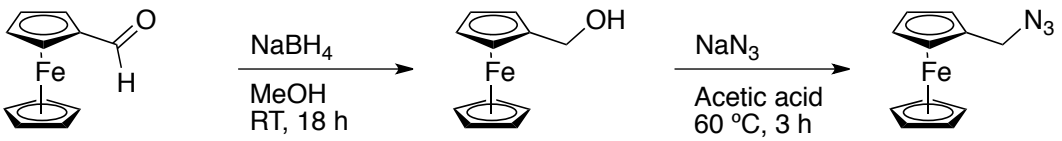
2.4 Kinetically stable lanthanide-ferrocene complexes

2.4.1 Introduction

Starting from the alkyne containing lanthanide complexes, it was decided to exploit the versatility and ease of the CuAAC "click" chemistry reaction to build a dyad wherein a ferrocene and a lanthanide unit are in close proximity and covalently linked together. Furthermore, the formation of the triazole ring upon reaction would not only enhance the kinetic stability of the complex, providing an eighth donor, but also improve the luminescence through the antenna effect. The choice of ferrocene as the electrochemically active unit is justified by its chemical stability and electrochemical robustness and compatibility with the electrochemical window of a solvent such as water, where the target complex is most likely to dissolve.

2.4.2 Synthesis

Azidomethyl ferrocene was obtained from ferrocene aldehyde (**2.10**) as shown in Figure 2-8. Upon reaction with $NaBH_4$, **2.10** was reduced to hydroxymethyl ferrocene that could be then converted to azidomethyl ferrocene (**2.12**) using an excess of sodium azide in acetic acid.

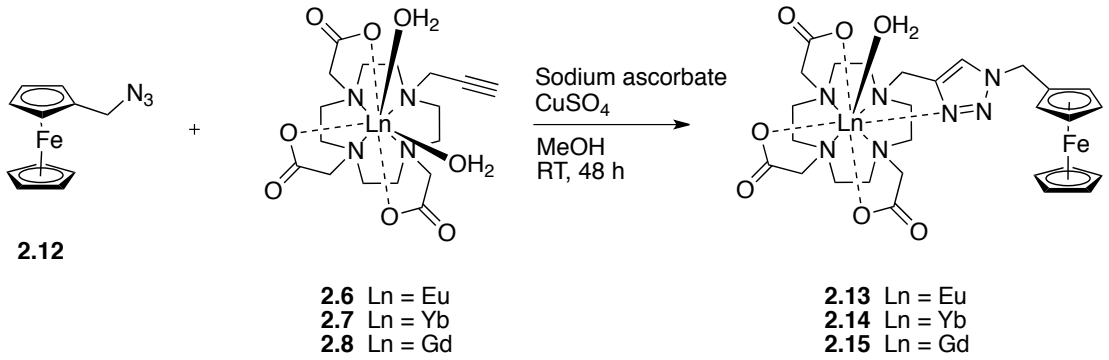


2.10 **2.11** **2.12**

Figure 2-8. Synthesis of azidomethyl ferrocene.

The reaction of the alkyne containing lanthanide DO3A complex with **2.12** was performed under classical Cu(I) click chemistry conditions, with a mixture of water and *tert*-butanol as solvent system and Cu(I) generated *in situ* from Cu(II) and sodium ascorbate. The solubility of ferrocene azide in *tert*-butanol was enough to carry out the reaction. Another suitable solvent for this reaction was found to be methanol, in

which both starting materials were readily soluble. In this particular case, it was found that the choice of the solvent was not a real issue, as the reaction could be conducted even in water, where initially a biphasic system would form between the aqueous phase, containing the lanthanide complex, and the oily azidomethyl ferrocene, that would turn into a clear solution upon formation of the final product, soluble in water.



2.12

2.6 Ln = Eu
2.7 Ln = Yb
2.8 Ln = Gd

2.13 Ln = Eu
2.14 Ln = Yb
2.15 Ln = Gd

Figure 2-9. Synthetic scheme of the formation of the lanthanide complex-ferrocene dyad under Cu(I) "click" chemistry conditions.

The reaction was followed by TLC chromatography, where azidomethyl ferrocene gave a spot at R_f = 0.7 (2:1 EtOAc:Hexane) and instead remained on the baseline when reacted and hence anchored to the polar DO3A core. The product could be purified by extraction of any unreacted ferrocene starting material into DCM and by dialysis of the water-soluble product using a 500 MWCO membrane. The synthesised complexes were characterised by mass spectrometry, paramagnetic NMR and luminescence spectroscopy. Accurate electrospray mass spectra were also obtained. Figure 2-10 shows a representative example of the characteristic isotopic distributions for the Eu-Fc (**2.13**) and Yb-Fc (**2.14**) dyads.

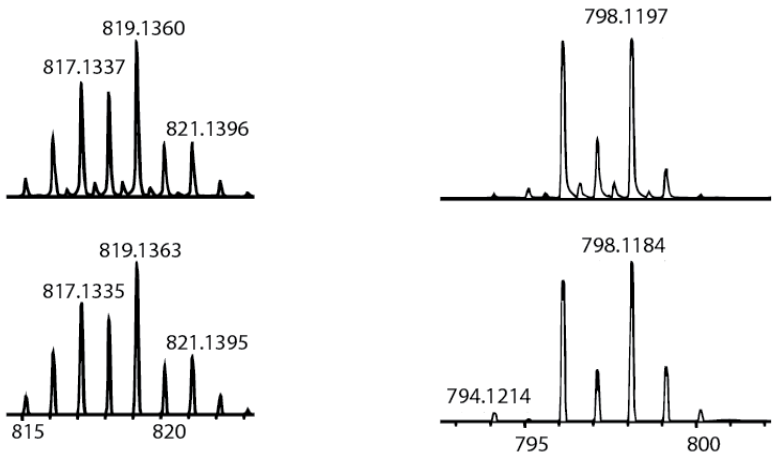


Figure 2-10. Experimental (top) and theoretical (bottom) high resolution mass spectra of **2.14** (left) and **2.13** (right) as their $[M+Na]^+$ adducts.

2.4.3 NMR spectroscopy characterisation

Paramagnetic ^{1}H-NMR spectroscopy proved to be an excellent tool for the characterisation of the click products. The alkyne DO3A complex is in fast exchange between TSAP and SAP isomers, giving broad spectra at pH 7 and sharp spectra only at pH 10. Upon formation of the triazole group, the NMR spectra of the click products display sharp and highly shifted resonances, indicating an overall rigidification of the structure in solution, giving an octadentate ligand and predominant SAP geometry around the metal (as opposed to an open TSAP conformation displayed by seven-coordinate lanthanide DO3A complexes).

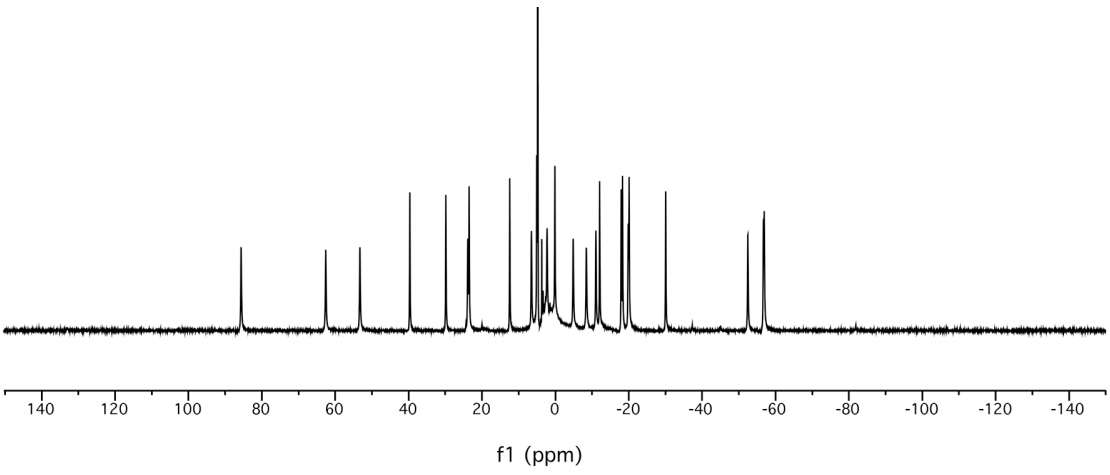


Figure 2-11. Paramagnetic ^{1}H-NMR spectrum of complex **2.7** at pD 10 in D_2O.

This is clear evidence of coordination of the nitrogen on the triazole to the lanthanide ion, leading to an eight-coordinate complex with only one isomer dominating in solution, although close inspection of the paramagnetic NMR in Figure 2-12 reveals that the TSAP conformer is present as the minor isomer in less than 5% abundance.

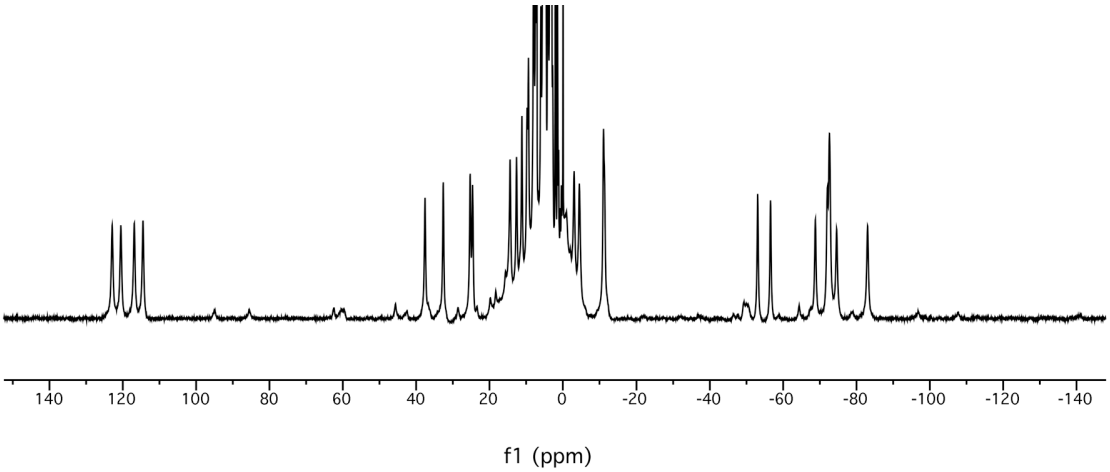


Figure 2-12. Paramagnetic ^{1}H-NMR spectrum of **2.14** registered at pD 7 in D_2O.

The spectrum shown in Figure 2-12 highlights the presence of highly shifted resonances representing the axial ring protons of the complex in its broken symmetry SAP conformation. While in the alkyne complex the speciation in solution is pH dependent, the clicked product NMR appears to give identical spectra between pH 2 and 10, confirming the kinetic stability of the complex and its locked structure.

2.4.4 Photophysical characterisation

Figure 2-13 shows a comparison between the absorption spectrum of the alkyne and of the ferrocene appended click product.

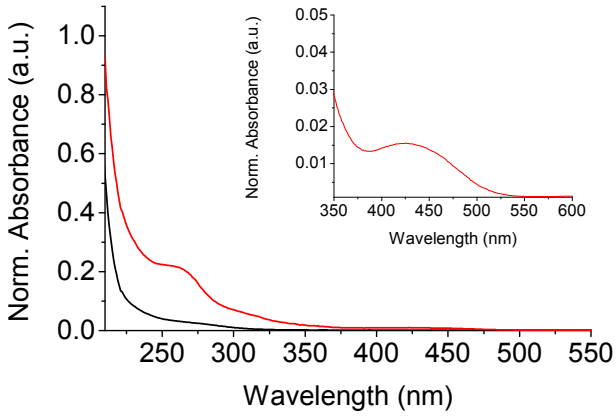


Figure 2-13. Comparison of the UV-Vis spectra of **2.6** (black line) and **2.13** (red line) in H_2O at pH 7 with the insert showing a zoom in the **2.13** spectrum.

The presence of an organic chromophore is clearly noticeable and the weak absorption band in the visible part of the spectrum can be ascribed to a metal centred d-d transition.

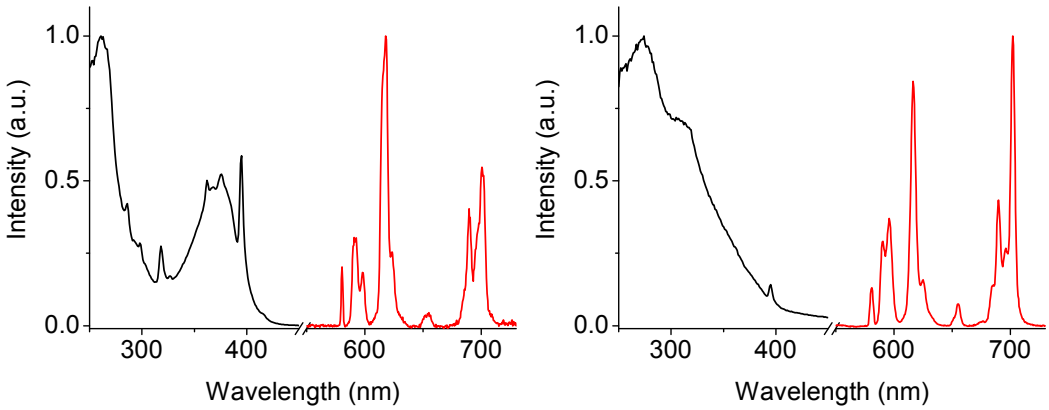


Figure 2-14. Comparison of the excitation and emission spectra of the Eu(III) complexes **2.6** (left) and **2.13** (right) in H_2O at pH 7.

From the luminescence spectra it can be noticed that, in the case of complex **2.6**, the excitation spectrum is dominated by sharp peaks characteristic of the direct excitation into the lanthanide ion manifold. This is indeed to be expected, given the absence of a

chromophore other than the alkyne, whose excited state can be populated only at higher energies (hence the tail at energy higher than 30,000 cm^{-1} in the excitation spectrum). By contrast, in the clicked product (**2.13**) the direct excitation peak relative to the $^7F_0 \rightarrow {}^5L_6$ transition, is subsumed by the much stronger indirect excitation band, attributable to the presence of the triazole chromophore and the ferrocene excited states acting as antennas.

Indirect excitation resulted in the characteristic europium emission, characterised by a significantly different fine structure in the emission profile compared to **2.6**. In particular, the intensity of the hypersensitive $\Delta J = 2$ transition changes drastically compared to the rest of the bands, indicating a change in the local environment around the lanthanide ion, as it would be expected upon coordination of the triazole to the metal centre, also observed in the literature.[5]

In the case of the ytterbium complex **2.14**, excitation with a nitrogen laser at 337 nm resulted in long-lived ytterbium centred near IR emission at 980 nm. A long pass filter was used between the sample and the detector to reject all stray light from the laser source, and the emission wavelength was selected using a monochromator. In this case, given the only excited state of ytterbium, namely the $^2F_{5/2}$, and hence the wide energy gap with the excited states of other chromophore present in the molecule, sensitised emission via the ferrocene antenna would be expected. Indeed, upon excitation at 425 nm, emission from ytterbium was also observed, indicating that the ferrocene group is directly acting as an antenna chromophore.

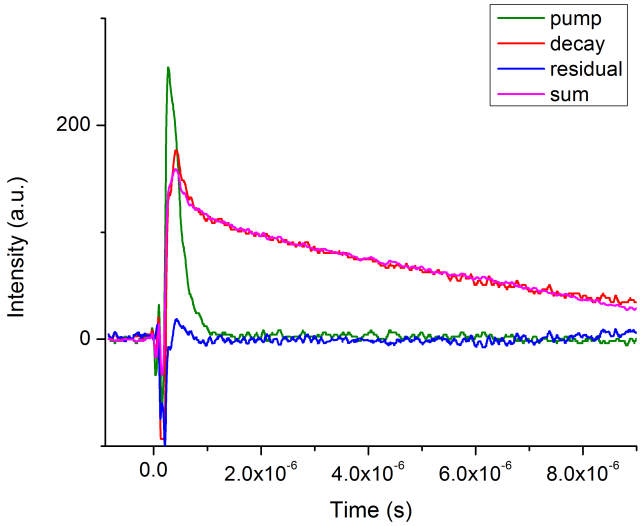


Figure 2-15. Emission decay profile of **2.14** following excitation at 337 nm and monitoring at 980 nm, in D_2O. Pump: detector response; decay: excited state emission decay; residual: difference between decay and sum; sum: fitted decay.

Indeed, the ability to sensitise Yb(III) upon excitation at 425 nm is not surprising given that the lowest excited state for ferrocene has been estimated to be ca. 15,000 ± 1,000 cm^{-1}.[15] Together with this energy transfer pathway, a sequential double electron transfer mechanism can also take place in the case of Yb(III), wherein an electron is first transferred from the chromophore to the lanthanide ion and then back to the chromophore, leaving the lanthanide in its excited state.

In order for this sequential electron transfer to happen, the energy transfer pathway must be thermodynamically feasible. Applying the Rehm-Weller equation, an estimate of the free energy change resulting from this double electron transfer mechanism can be expressed, in eV, by the following equation[16]:

$$\Delta G_{ET} = (E_{ox} - E_{red}) - E_S - \frac{e_0^2}{\varepsilon_a} \qquad (2.1)$$

Here, E_{ox} is the reduction potential of the donor (the oxidiser), E_{red} is the reduction potential of the electron acceptor (the Ln^{3+}/Ln^{2+} couple), E_s is the energy of the excited state of the donor and e_0^2/ε_a takes into account the energy of interaction

between the radical couple resulting in the process. For an exciplex, a value of $e_0^2/\varepsilon_a \approx$ 0.15 eV is usually assumed, but in this particular case it can be assumed to be much smaller as the separation between donor and acceptor is much greater than in an exciplex case to which this expression was originally applied.

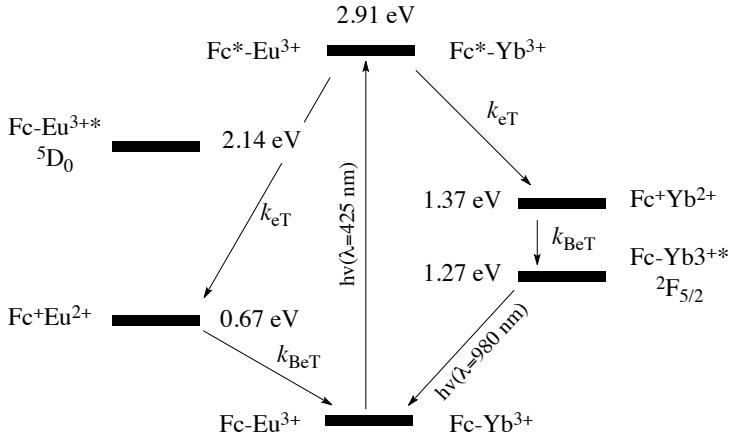


Figure 2-16. Schematic of the energy states implicated in the double electron transfer mechanism taking place between lanthanide and antenna.

In the case of ytterbium, the reduction potential associated with the Yb^{3+}/Yb^{2+} couple is -1.05 V vs. the NHE, while the ferrocene redox couple measured in the complex was determined to be -0.32 V vs. the NHE.[17] Considering these values, an energy of the singlet state of 23,500 cm^{-1}, corresponding to the energy of the d-d transition at 425 nm, or higher, would be enough to drive the double electron transfer process, resulting in a negative ΔG_{ET} according to equation 2.1. The value of -1.05 V for the Yb^{3+}/Yb^{2+} couple should be considered as the lowest limit given that it refers to the aqua ion, while the true reduction potential will be somewhat higher in a complex. It should also be noticed that the Rehm-Weller equation gives an estimate of the energy required for the first electron transfer and does not specify if that energy will be enough for the population of the luminescent state under investigation. This is usually the case for ytterbium, having only one excited state at low energy. The same is not true for europium, where the lowest lying emissive state, $^5D_0$, is lower in energy than the intermediate charge transfer state. Indeed, even though the electron transfer could

take place, this would not lead to the population of the europium centred emissive state, as can be seen in Figure 2-16.

It can be concluded that for Yb(III) in complex **2.14**, sensitisation of its excited state can take place both via a conventional energy transfer from low-lying states on the chromophore or via a double electron transfer process. In the case of the Eu(III) complex **2.13** instead, the excitation spectrum in Figure 2-14 suggests that sensitisation of the metal centre is taking place via the antenna chromophore, while the values of lifetime (listed in Table 2-1) do not show a particularly efficient quenching due to the low lying LMCT state, although these are lower than the values of lifetime of other Eu(III) complexes based on the DO3A structure and containing a triazolyl donor.[5]

Time-resolved luminescence spectroscopy was employed in order to obtain an estimate of the number of water molecules coordinated to the metal ion using the modified Horrocks' equation[18].

$$q = A_{Ln} \cdot (k_H - k_D - B_{Ln}) \qquad (2.2)$$

In this equation A and B are parameters specific for each lanthanide (A_{Eu} = 1.2 ms, B_{Eu} = 0.25 ms^{-1} and A_{Yb} = 1 μs , B_{Yb} = 0.1 μs^{-1}) and take into account the degree of non-radiative quenching associated with the presence of O-H oscillators in solvent molecules coordinated to the lanthanide ion (the need to apply a correction for exchangeable N-H oscillators, expressed by the parameter B, can be ignored in our system, as there are none). The values obtained (tabulated in Table 2-1) confirm the observation made based on the NMR spectra and on the analysis of the emission profile. The observed hydration number of 1.4 for the europium complex is consistent with the presence of an octadentate species in solution, where only one water molecule can coordinate to the predominant isomer. In the ytterbium case, the value of 0.7 obtained is consistent with the contraction of the lanthanide radius along the

series and the predominance of the monocapped square-anitprismatic geometry observed for the late lanthanide ions.[19-21]

Table 2-1. Lifetime values of the excited states of the luminescent lanthanide-ferrocene dyads discussed in this chapter.

Compound	λ_{ex}/nm	λ_{em}/nm	τ_{H2O}/μs	τ_{D2O}/μs	q
2.13	300	615	380	820	1.4
2.14	337	980	1.0	5.9	0.7

Unlike other transition metal complexes that have been used to prepare d-f hybrids, ferrocene is not strongly luminescent, thus meaning that information regarding the efficiency of the energy transfer step cannot be obtained by intensity or time-resolved luminescence based on the antenna. Indeed, ferrocene is regarded as being an efficient quencher for triplet and singlet excited states.[15] This is likely to be true at close intermetallic distances in a ferrocene-lanthanide compound but the presence of the triazole bridge between the two avoids marked quenching of luminescence. A time-resolved emission spectrum (TRES) was recorded for the Yb(III) complex **2.14** showing that there is indeed no residual fluorescence arising from the organic chromophore, thus indicating an efficient energy transfer step.

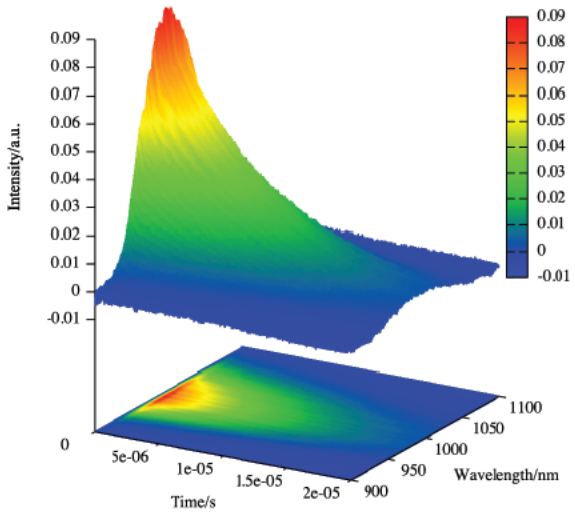


Figure 2-17. Time-resolved emission spectrum (TRES) of the near-IR emitting complex **2.14** registered upon 337 nm excitation in D_2O.

2.4.5 Spectroelectrochemistry

Having prepared a kinetically stable lanthanide complex comprising an electrochemically active group such as ferrocene, the fluorescence originating from Yb(III) in **2.14** was monitored while varying the oxidation state of the ferrocene group. Chronoamperometry was employed to cycle a Pt working electrode between oxidative (0.6 V) and reductive (0 V) potentials. The oxidation and reduction processes could be followed by UV-Vis absorption (Figure 2-18) where the oxidation dependent LMCT transition shifted to higher wavelength, from 420 to 660 nm, as it would be expected from the oxidation of ferrocene to form the ferrocenium ion.

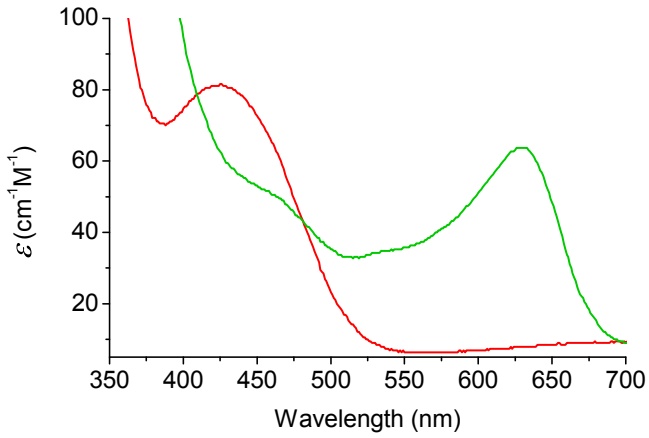


Figure 2-18. UV-Vis absorption spectrum of **2.14** in H_2O before (red) and after (green) electrochemical oxidation.

Figure 2-19 represents the emission spectrum related to complex **2.14** in its reduced and oxidised state. A decrease in emission intensity was observed, accompanied by a decrease in the ytterbium excited state lifetime upon oxidation.

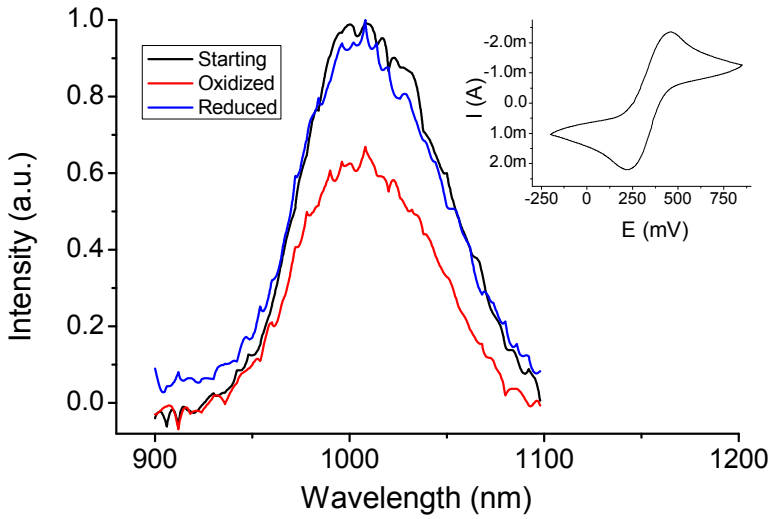


Figure 2-19. Yb(III)-centred emission profile of complex **2.14** upon 337 nm excitation before and after one redox cycle. Inset: diffusive cyclic voltammogram (2 mM in 0.1 M NaClO4, 100 mV s^{-1}, Pt gauze working electrode).

Considering the reduced form of the complex as the unquenched species, the efficiency of quenching can be derived from the values of lifetime applying the following equation:

$$\phi_{quench} = 1 - \frac{\tau_{ox}}{\tau_{red}} \qquad (2.3)$$

Using the lifetimes in Table 2-2, ϕ_{quench}= 0.25 for the ytterbium complex **2.14**. This is in agreement with the ratio of the observed intensity in the corresponding emission spectra (Figure 2-19).

Table 2-2. Lifetime values of the excited states of the luminescent lanthanide-ferrocene dyads before and after electrochemical oxidation with the corresponding quenching efficiency. Lifetimes registered in H_2O for **2.13** and in D_2O for **2.14**.

Compound	**λ_{ex}/nm**	**λ_{em}/nm**	Reduced **τ/μs**	Oxidised **τ/μs**	**ϕ_{quench}**
2.13	300	615	380	250	0.34
2.14	337	980	5.9	4.4	0.25

Once formed, the oxidised species could be reversed electrochemically giving the reduced form and restoring the luminescence signal to its initial intensity and lifetime.

Similarly, *in situ* spectroelectrochemical experiments were carried out on the europium complex **2.13**. The sample was cycled between oxidative and reductive potentials while registering the emission spectrum originating from the europium centre. The intensity of the signal could be quenched up to 40% and restored completely for several cycles while the value of lifetime of 0.25 ms of the oxidised species in water is in good agreement with the quenching displayed in the emission spectra (see Figure 2-20 and Table 2-2).

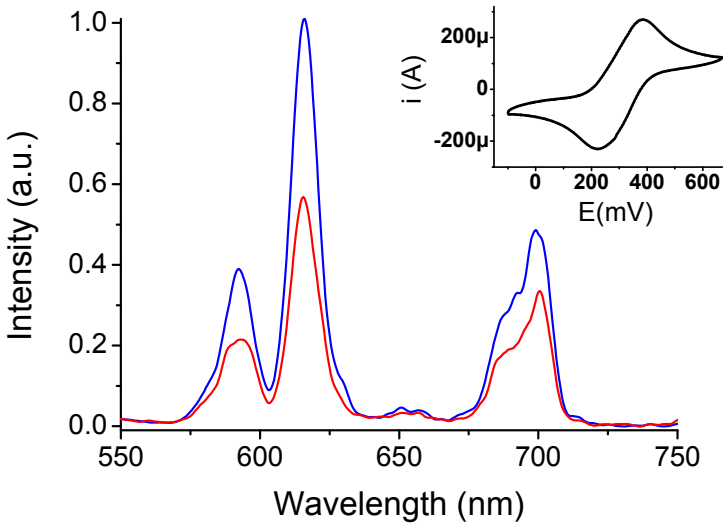


Figure 2-20. Emission profile of complex **2.13** upon 320 nm excitation before and after one redox cycle. Inset: diffusive cyclic voltammogram (2 mM in 0.1 M NaClO4, 100 mV s^{-1}, Pt gauze working electrode).

2.4.6 Discussion of the mechanism of electrochemical quenching

As mentioned earlier, sensitisation of ytterbium may imply the population of an intermediate chromophore-to-lanthanide charge transfer state where this is thermodynamically feasible. It was reasoned that this double electron transfer mechanism could be amenable to manipulation if a redox active group such as ferrocene were to be included in the molecule. It was then expected that oxidation of ferrocene would render the first electron transfer step energetically disfavoured hence

resulting in an overall quenching of ytterbium luminescence. Indeed, the partial quenching of luminescence observed upon oxidation of the ferrocene group has to be ascribed to this mechanism. On the other hand, the fact that ytterbium can still be sensitised even in the oxidised species,, is suggestive of a parallel energy transfer process. This is not surprising given that many energy levels higher in energy than the ferrocene centred LMCT state are present in the molecule from which the energy transfer could take place through the same pathway. Furthermore, ferrocenium has been reported to have low energy excited states lying at ca. 14,800 cm^{-1} that can be responsible for the sensitisation of the Yb(III) even when the ferrocene group is in its oxidised state.[15]

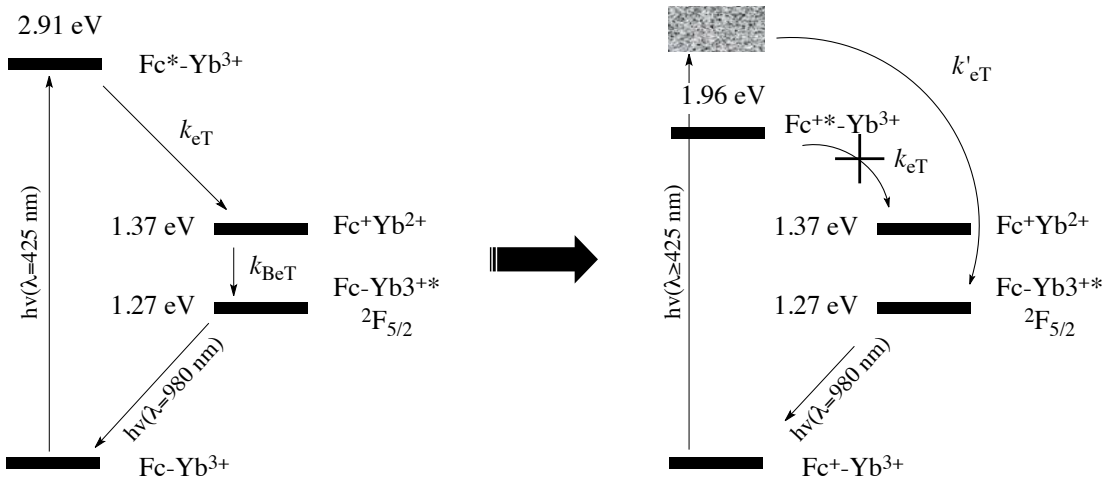


Figure 2-21. Possible sensitisation mechanism in the reduced (left) and oxidised (right) form of the Yb(III) complex **2.14**.

While this mechanism is valid for ytterbium, the same is not true for europium, where the chromophore-to-lanthanide charge transfer state would be lower in energy than the Eu(III) $^5D_0$ emissive state. The quenching observed in this case must then be related to the formation of ferrocenium and the presence of a low-lying energy state contributing to the lanthanide non-radiative quenching. This is to be expected, given the very good overlap between the absorption spectrum of the acceptor (the ferrocenium group) and the emission spectrum of europium, as displayed in Figure 2-22.

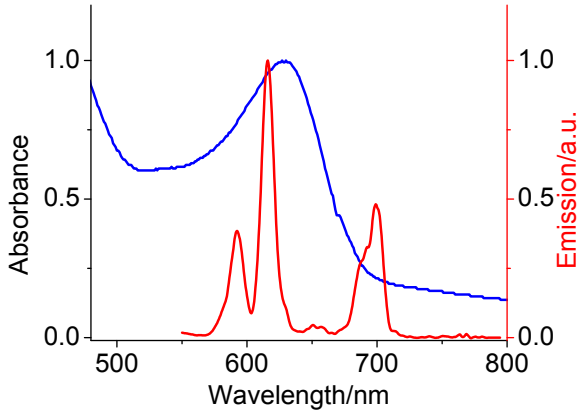


Figure 2-22. Comparison of the emission profile of the europium complex **2.13** and part of the absorption profile of its oxidised form showing the energy overlap between donor and acceptor.

In the case of europium, the increased ability of ferrocenium to quench luminescence is related to the formation of a ferrocene-centred excited state at low energy and its good overlap with the emission from Eu(III). The mechanism of quenching of ytterbium luminescence is instead more likely due to the disruption of the double electron transfer mechanism due to the presence of the ferrocenium group acting as a strong electron acceptor. Despite ferrocenium being known for its ability to act as a quencher of singlet and triplet states both via energy and electron transfer, it is clear that Yb(III) sensitisation via the triazole chromophore is still taking place, meaning that energy transfer to the lanthanide excited state is faster than non radiative depopulation. Furthermore, triplet excited state determination carried out on the gadolinium analogue **2.15** showed a triplet state dominated by the organic chromophore and no sign of the ferrocene or ferrocenium triplet state could be observed. This is not surprising given that the measurement of phosphorescence from ferrocene has proved to be elusive so far and it is generally accepted that, unlike other metallocenes, ferrocene is not phosphorescent.[15]

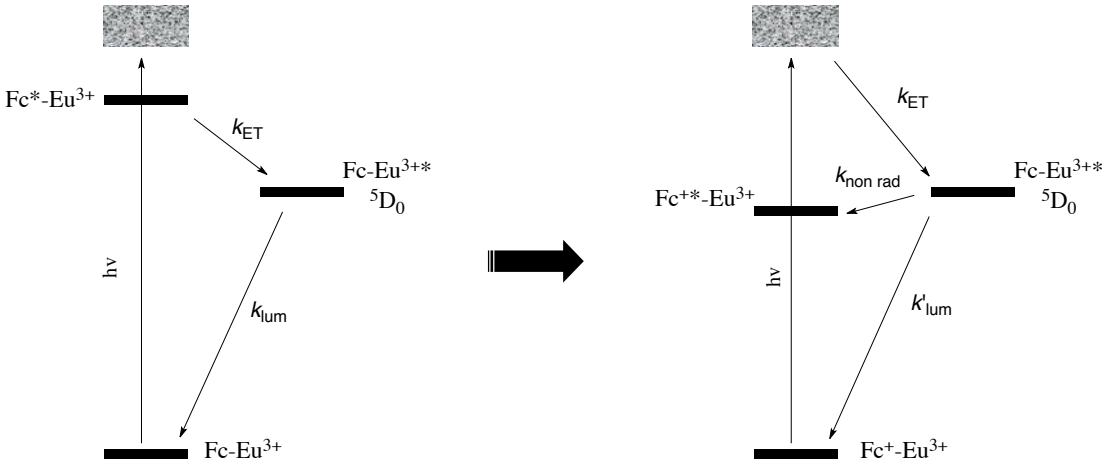


Figure 2-23. Proposed mechanism of sensitisation (left) and of quenching (right) of the europium complex **2.13** in its reduced and oxidised state respectively.

2.5 Alternative redox active chromophores

2.5.1 Introduction

In the previous sections it has been shown that the derivatisation of a lanthanide complex with a redox active group such as ferrocene provides a novel way of modulating lanthanide luminescence. The electrochemical oxidation of the redox active group is able to disrupt the chromophore-to-lanthanide energy transfer resulting in the non-radiative deactivation of the luminescent excited state. Even though the lanthanide luminescence can be modulated electrochemically, the quenching of the signal is still incomplete, indicating a still efficient energy transfer step towards the population of the lanthanide excited states. Indeed, the relatively low quenching efficiency of luminescence has to be ascribed to the presence of an additional chromophore, the triazole, whose electronic properties are unchanged upon electrochemical oxidation (at least not in the electrochemical window studied). It was then reasoned that the use of an electroactive chromophore as the only antenna in the molecule could provide a way to improve the quenching efficiency, wherein the electronic properties of the chromophore would change with its redox state.

The quinones are a well-known class of compounds that exhibit interesting spectroscopic and electrochemical properties. The energies of the electronic excited states are widespread in the UV and visible range, with yields of triplet state formation close to unity.[22] These properties make them suitable candidates for the sensitisation of visible and near-IR emitting lanthanides. Indeed, reports of lanthanide complexes with chromophores based of 9,10-anthraquinone have been published in the literature, showing that this group acts as an antenna for near-IR luminescence.[23] Furthermore the electronic properties of unsubstituted anthraquinones show distinct differences between the oxidised and reduced species resulting in significantly different absorption spectra.[24] This is a desirable property for the design of luminescent lanthanide complexes whose emission is amenable to modulation upon a change of the redox potential in solution.

The target complexes chosen are illustrated in Figure 2-24. The common lanthanide-chelating motif is further functionalised using a 9,10-anthraquinone group and a benzoquinone derivative. Aside from their photophysical properties, the electrochemical redox potential of these group would allow their exploitation in aqueous solvents.

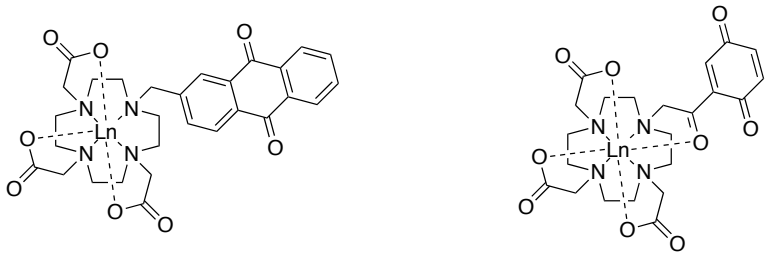


Figure 2-24. Target compounds containing redox active chromophores that could be exploited for the modulation of lanthanide luminescence through a change of redox potential.

2.5.2 Synthesis of lanthanide complexes containing an anthraquinone chromophore

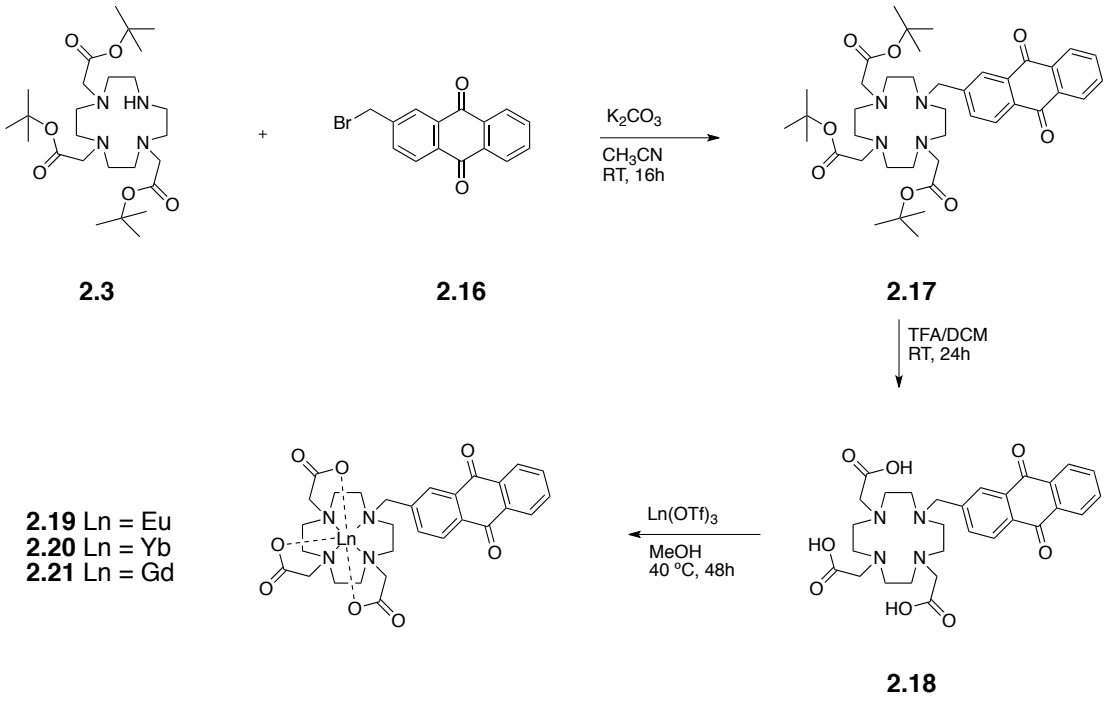


Figure 2-25. Synthetic scheme for the preparation of lanthanide complexes containing an anthraquinone chromophore.

Figure 2-25 shows the synthesis followed for the preparation of lanthanide complexes containing an anthraquinone chromophore. The triester (**2.3**) was alkylated under standard conditions using commercially available 2-Bromomethyl-anthraquinone (**2.16**). Purification by silica flash column chromatography afforded the protected ligand that could be further recrystallised from dichloromethane using hexane. X-ray quality crystals could be obtained by slow diffusion of hexane in a solution of **2.17** in dichloromethane. The crystal structure, resolved by Dr Michael Jones, shows the compound crystallised as the potassium complex, with a bromide as a counter ion and an additional water molecule in the coordination sphere. The K^+ ion, encapsulated into the macrocycle cavity by interactions with nitrogen atoms of the macrocycle and oxygen atoms of the carbonyl groups, is disordered over two sites by coordination to a partially occupied water molecule which also causes the bromide counterion to be disordered. The packing of the molecule in the crystal shows a strong pi-stacking interaction between the anthraquinone groups of adjacent molecules, with a distance of 3.4 Å between the centroids of the aromatic rings.

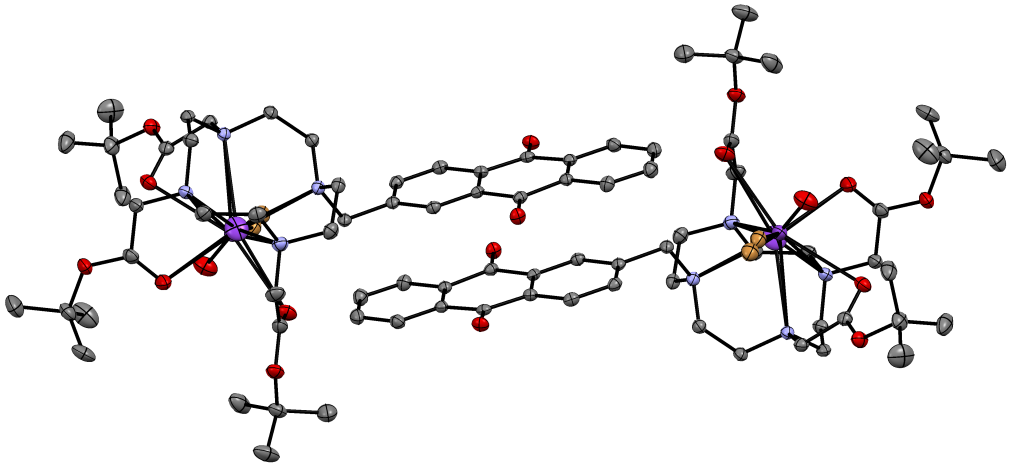


Figure 2-26. Crystal structure of **2.17** highlighting the packing of molecules by pi-stacking interactions, 50 % ORTEP depiction created in Mercury.

Cleavage of the *tert*-butyl groups was performed using TFA in dichloromethane, obtaining the ligand quantitatively. The complexes were obtained simply by stirring the ligand and the corresponding lanthanide triflate salt in methanol at 40 ºC, using a small excess of lanthanide salt and adjusting the pH to 5 for optimal complexation

conditions. Any excess of lanthanide was removed at the end of the reaction by raising the pH and precipitating it as the insoluble hydroxide. Figure 2-27 shows the high-resolution ES-MS of the europium and ytterbium derivatives in comparison with the corresponding theoretical isotopic pattern.

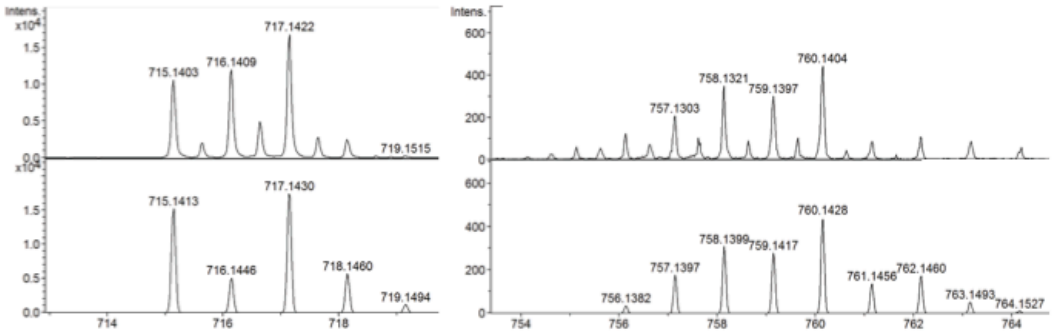


Figure 2-27. Experimental (top) and theoretical (bottom) high resolution mass spectra of **2.19** (left) and **2.20** (right) as their $[M+H]^+$ and [M+Na] adducts respectively.

2.5.3 NMR spectroscopy characterisation

The presence of the anthraquinone group reduced the solubility of the complexes and became somewhat problematic, especially when trying to obtain the concentration of the complex in solution necessary for NMR characterisation. The compounds were only sparingly soluble in protic solvents such as methanol or water, and totally insoluble in DMF, acetonitrile or chloroform. NMR spectra were hence registered in d_6-DMSO.

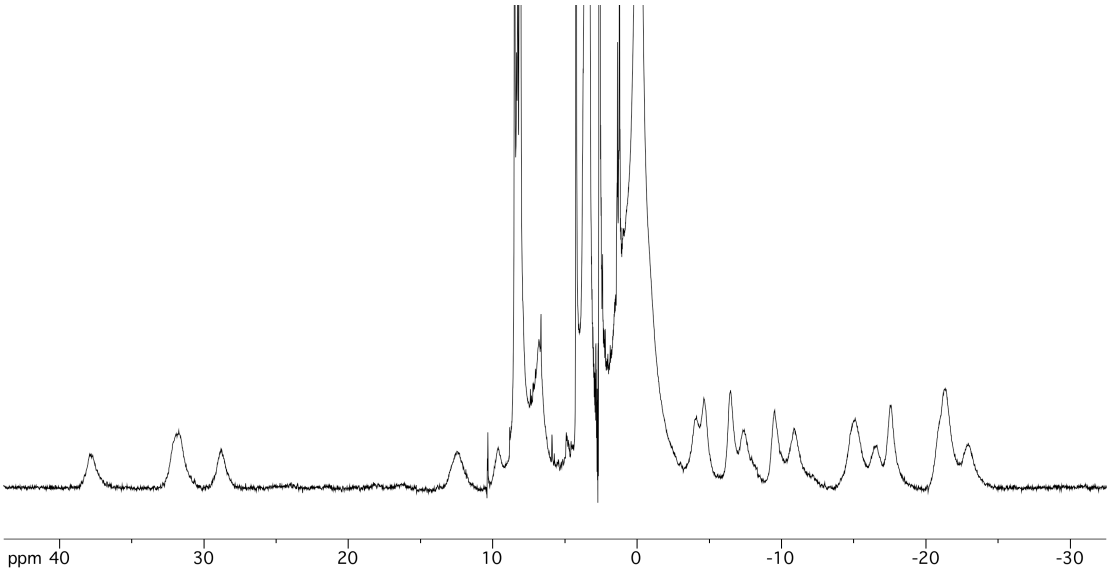


Figure 2-28. Paramagnetic ^{1}H-NMR spectrum of **2.19** registered in d_6-DMSO.

The ^{1}H-NMR spectrum of **2.19** shows shifted broad peaks as expected from a seven-coordinate lanthanide complex. The predominance of only the SAP isomer could be due to the presence of the bulky anthraquinone group preventing free rotation of the carboxylate arms in solution and hence locking the complex in one isomeric structure. The ^{1}H-NMR spectrum of the ytterbium analogue **2.20** also shows that the predominant isomer in solution has the SAP geometry, although the presence of the TSAP isomer is more pronounced in this case as can be judged by low shifted resonances in the spectrum in Figure 2-29 (less than 10% by integration of the NMR signals).

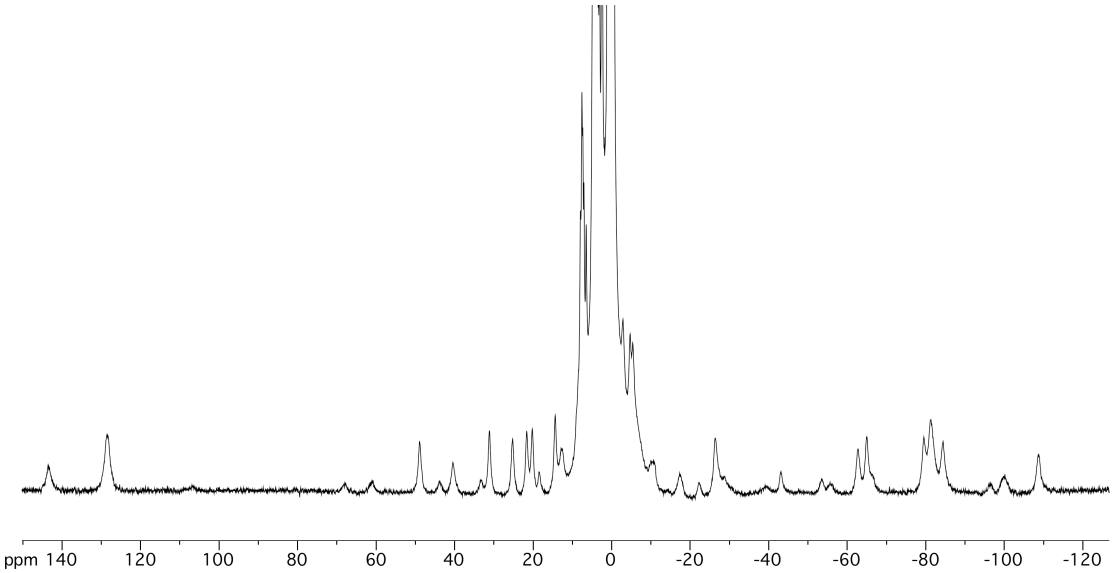


Figure 2-29. Paramagnetic ^{1}H-NMR spectrum of **2.20** registered in d_6-DMSO.

2.5.4 Photophysical characterisation

The luminescence spectrum exhibited by the Eu(III) complex **2.19** is shown in Figure 2-30. From the excitation and absorption spectra, it can be observed that sensitisation is occurring via the anthraquinone group, although the still visible peak of the direct excitation of europium at 396 nm indicates a poor efficiency of the sensitisation mechanism.

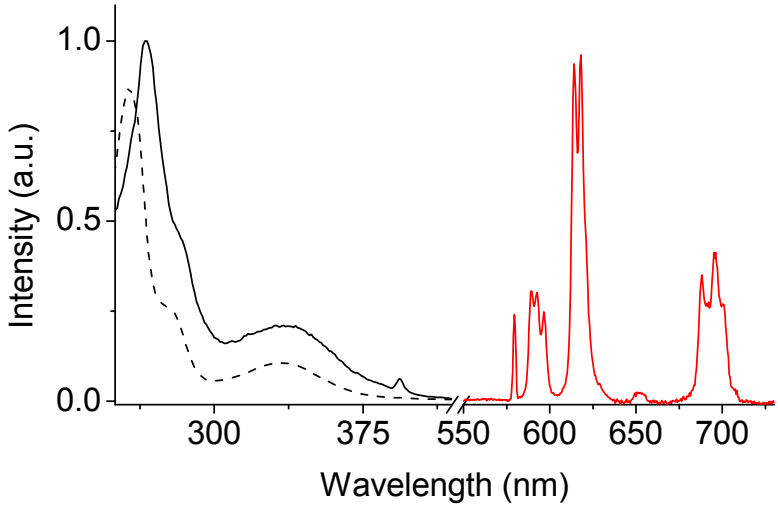


Figure 2-30. Absorption (dashed line), excitation (black line) and emission spectra (red line) of **2.19** registered in H_2O.

In order to understand the photophysical properties of the system better, the energy of the triplet state was determined using the gadolinium analogue **2.21**. Gadolinium excited states are higher in energy than the excited state of the ligand, thus ensuring the ligand centred nature of the triplet measured. From Figure 2-31 the 0-0 transition is estimated to be around 25,000 cm^{-1}. It is then reasonable to exclude a back energy transfer mechanism from the europium to the chromophore, since the emissive $^5D_0$ state lies at ca. 17,200 cm^{-1}, hence thermal repopulation of a high energy triplet state can be ruled out entirely. Lifetime measurements in water and deuterium oxide were used to determine the hydration number of europium using the equation mentioned before.

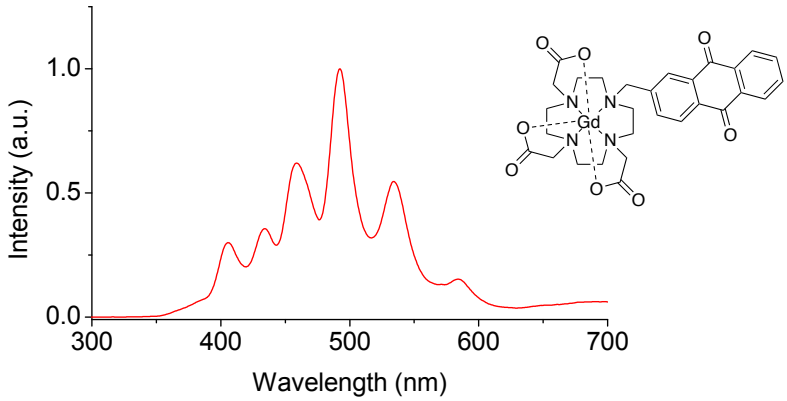


Figure 2-31. Phosphorescence spectrum of **2.21** measured at 77 K.

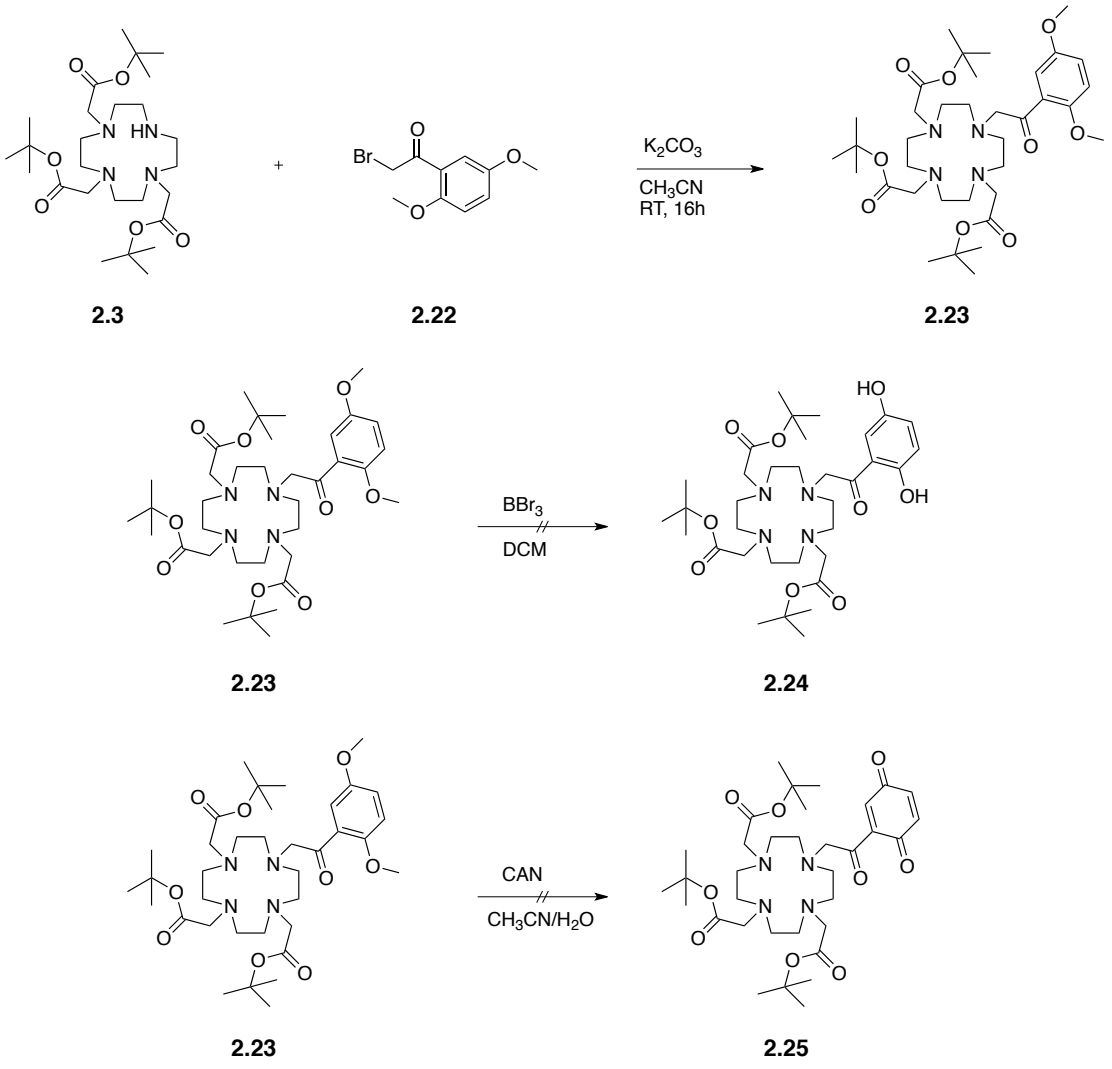
With an emission lifetime of 0.39 ms and 1.28 ms in water and deuterium oxide respectively, the calculated q value accounted to 1.8. Indeed, this is to be expected given the structure of the complex and the lack of an eighth donor group. Furthermore, the lifetime values are in agreement with other seven coordinate complexes based on the DO3A structure, thus excluding a direct quenching mechanism of the lanthanide excited state by low lying energy states.

Interestingly, the ytterbium complex **2.20** did not show any sensitised luminescence upon laser excitation at 337 nm. This is likely to be a consequence of the poor spectral

overlap between chromophore and lanthanide and also the unfavourable thermodynamics for an alternative double electron transfer mechanism.

2.5.5 Towards the synthesis of benzoquinone derivatives of Ln.DO3A complexes

The starting point for the synthesis of the benzoquinone-containing complex in Figure 2-24 was the alkylation of the triester **2.3** with the commercially available 2-Bromo-2′,5′-dimethoxyacetophenone (**2.22**). Flash column chromatography was used to purify the product, which was obtained in 50 to 60 % yield. Heating of the reaction did not prove necessary, probably as a result of the good nucleophilicity of the bromo-derivative enhanced by the electron donating methoxy groups on the aromatic ring.



2.3 **2.22** **2.23**

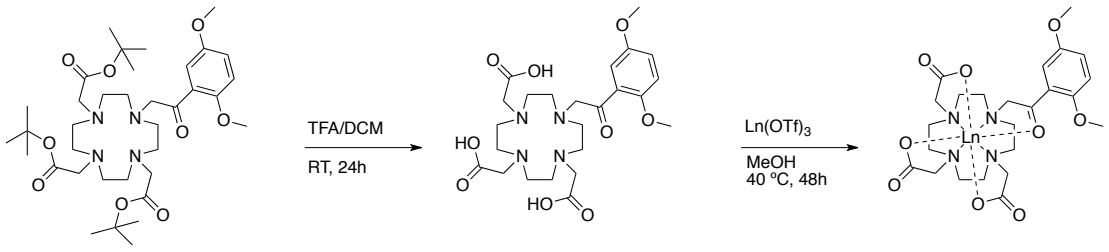
2.23 **2.24**

2.23 **2.25**

Figure 2-32. Synthetic strategy followed for the preparation of protected ligand containing a benzoquinone or hydroquinone group.

Unfortunately, the reduction of the dimethoxy- derivative could not be accomplished. This reaction was attempted using cerium ammonium nitrate (CAN) to directly yield the benzoquinone or by using BBr_3 to give the related hydroquinone. Reaction with CAN on the precursor **2.23** resulted in only partial conversion to the oxidised product, which could not be then separated from the starting material. Furthermore, reaction of **2.23** with BBr_3 resulted in the formation of a mixture of several components that could not be separated and identified.

It was nonetheless decided to proceed to the formation of complexes containing the 2',5'-dimethoxyacetophenone moiety, as these could constitute a class of molecules with appealing photophysical properties due to the presence of a chromophore absorbing in the visible range. It was envisaged that this could be exploited for the formation of europium complexes amenable to long wavelength sensitisation.



2.23 **2.26** **2.27** Ln = Eu **2.28** Ln = Yb

Figure 2-33. Reaction scheme for the preparation of the lanthanide complexes containing a dimethoxyacetophenone chromophore.

Cleavage of the protecting *tert*-butyl groups using TFA in dichloromethane and complexation in methanol using the triflate salt of the corresponding lanthanide ion afforded the desired complexes (**2.27** and **2.28** in Figure 2-33). Any excess of lanthanide was eliminated by precipitation of its insoluble hydroxide at basic pH values. Characterisation of the complexes included paramagnetic ^{1}H-NMR, luminescence and UV-Vis spectroscopy, and high-resolution ES-MS (see Figure 2-34).

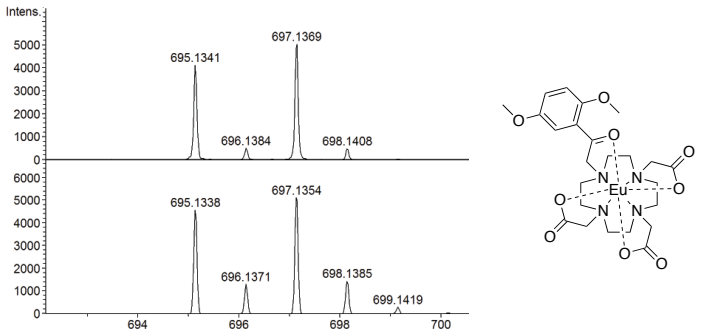


Figure 2-34. Experimental (top) and theoretical (bottom) high resolution mass spectra of **2.27** as the $[M+Na]^+$ adduct.

2.5.6 NMR spectroscopy characterisation

By contrast with the seven-coordinate anthraquinone-appended derivative, it was expected that the carbonyl group situated on the fourth arm would act as donor to form an eight coordinate complex. This was indeed the case, as indicated by the sharp peaks in the ^{1}H-NMR spectra displayed by both the europium and ytterbium analogues (Figure 2-35 and Figure 2-36).

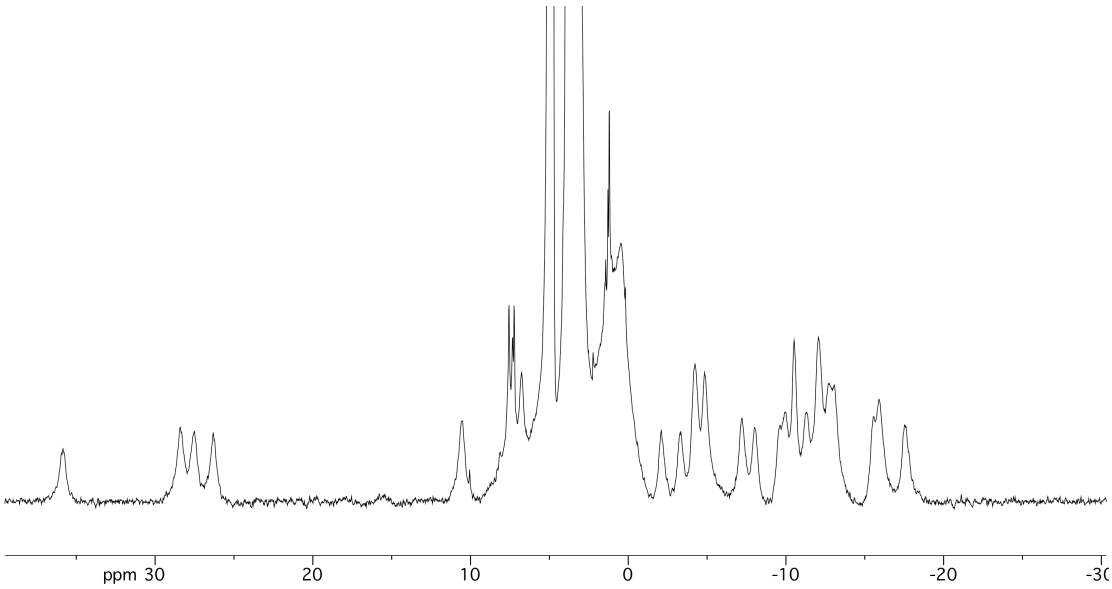


Figure 2-35. Paramagnetic ^{1}H-NMR spectrum of **2.27** registered in D_2O at pD 7.

The closed structure of the SAP isomer predominates, reasonably because of the strong ligand field formed by four oxygen donors. This structure was retained in

solution at different pH values, with the NMR spectrum displaying an identical profile between pH 2 and 10, suggesting that the compound does not undergo significant structural change or aggregation upon changing the pH.

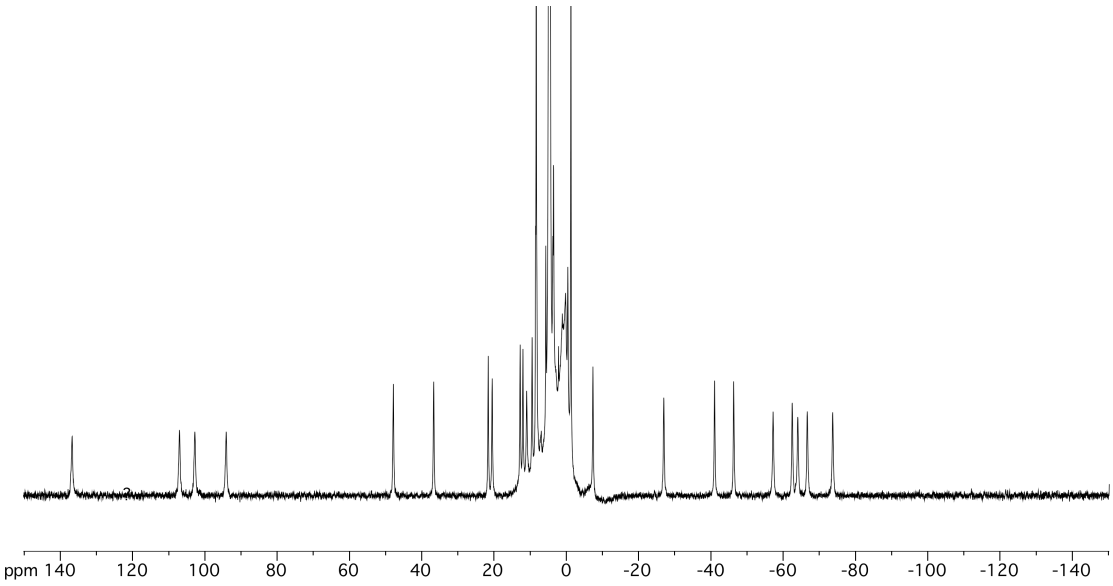


Figure 2-36. Paramagnetic ^{1}H-NMR spectrum of **2.28** registered in D_2O at pD 7.

2.5.7 Photophysical characterisation

The luminescence properties of the europium and ytterbium complexes were investigated by UV-Visible absorption, steady state and time resolved luminescence spectroscopy. Figure 2-37 shows the emission, excitation and UV-Vis absorption spectra of the complex **2.27**. The good overlap between absorption and excitation spectrum indicates that energy transfer from the chromophore is indeed taking place. Interestingly, the properties of this chromophore are such that europium emission can be sensitised with long-wavelength light, with an excitation spectrum tailing up to 420 nm.

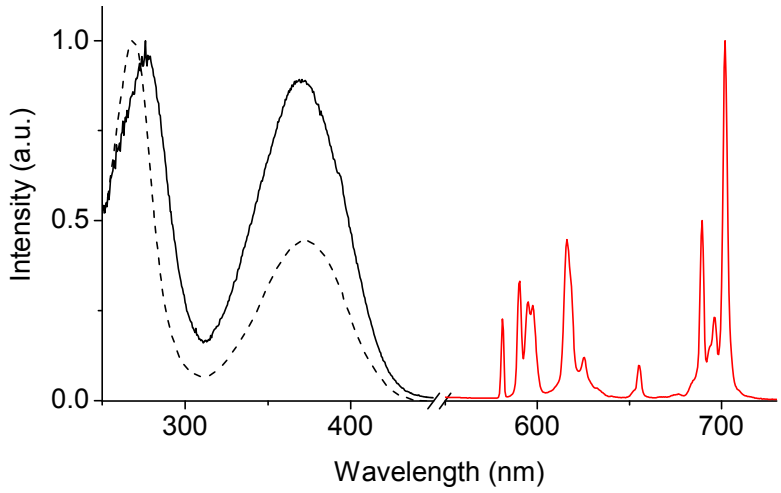


Figure 2-37. Emission (red line) excitation (black line) and absorption spectra (dashed line) of the Eu(III) complex **2.27** in H_2O.

This is likely to be due to the presence of a low energy ILCT state centred on the chromophore, where the methoxy- groups can act as electron donors and the carbonyl has an increased ability to act as electron acceptor upon interaction with the trivalent lanthanide ion.

Table 2-3. Lifetime values of the lanthanide complexes presented in this paragraph

Compound	λ_{ex}/nm	λ_{em}/nm	τ_{H2O}/μs	τ_{D2O}/μs	q
2.27	395	616	270	490	1.7
2.28	337	980	0.720	8.09	1.2

The Yb(III) complex **2.28** showed long lifetimes values with a determined q value of 1.2. This hydration number indicates that the carbonyl oxygen of the chromophore is indeed coordinating the lanthanide ion affording an eight-coordinate complex as inferred from NMR spectroscopy.

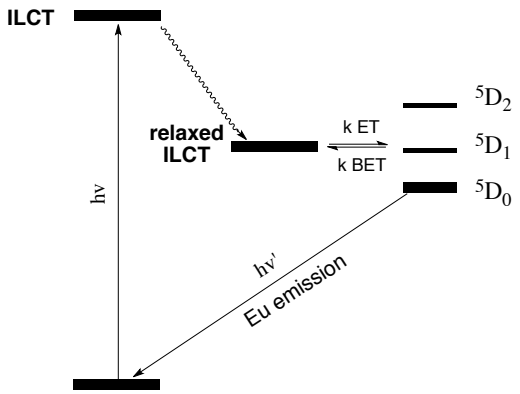


Figure 2-38. Simplified energy transfer diagram of the proposed mechanism of quenching of the Eu(III) luminescence in **2.27**.

The Eu(III) analogue instead shows unusually short luminescence lifetimes in comparison with other values obtained in this work and in the literature using europium complexes based on the DO3A structure. It is clear that the emissive $^5D_0$ state is being quenched, most likely this is due to the short energy separation between the Eu(III) emissive state and the lowest lying excited state centred on the chromophore, as would be expected from the study of the UV-Vis absorption spectrum of **2.27** (see Figure 2-38).

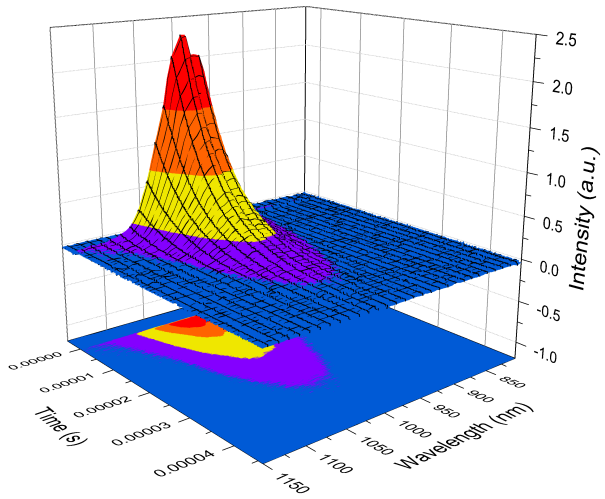


Figure 2-39. TRES spectrum of **2.28** registered upon excitation at 337 nm, in D_2O.

In order to investigate the possibility of quenching of the chromopohore centred triplet state, a sample of **2.27** in deuterium oxide was degassed by five freeze-pump-thaw cycles. The intensity of the emission spectra, and especially the lifetimes, did not show any discernible difference between the aerated and degassed samples. This rules out quenching of the triplet state by oxygen.

Another alternative mechanism of quenching could simply be the formation of an excited state lower in energy than the emissive $^5D_0$, reasonably as a consequence of an electron transfer from the chromophore to the lanthanide itself. This is likely to be feasible, especially in this case, with a strongly electron donor chromophore in close proximity to the lanthanide centre. Indeed, while the predominance of this mechanism would cause a quenching in the case of Eu(III) emissive state resulting in short lifetimes for **2.27**, this would not be so for **2.28**, where an electron transfer mechanism would be favourable for the population of the emissive $^2F_{5/2}$ state, as indeed indicated by its long luminescence lifetimes. As a consequence of this quenching, the hydration number for the europium complex **2.27** is not reliable, with a 'real' q value closer to one and an eight coordinate complex in solution, as also indicated by the sharp resonances in the ^{1}H-NMR spectrum.

2.6 Conclusions

In this chapter it has been demonstrated that lanthanide luminescence can be modulated electrochemically. A robust redox centre such as ferrocene has been incorporated in a luminescent lanthanide complex to form a kinetically stable d-f hybrid. A change in the oxidation state of the ferrocene has been shown to perturb the emission intensity and lifetimes of the emitting lanthanide ions. An analysis of the energy transfer in the europium and ytterbium complexes has been attempted with a proposed quenching mechanism that could in principle be applied to all lanthanides.

In search of a novel class of chromophores that could be exploited for both their electrochemistry and as antenna groups, the synthesis of complexes containing a quinone and an anthraquinone group was attempted. Unfortunately none of these classes lead to a successful candidate for the electrochemical modulation of luminescence. Despite their ease of formation, the complexes containing the anthraquinone group revealed to be remarkably insoluble, thus precluding any further electrochemical study. Furthermore, the formation of complexes containing a benzoquinone or hydroquinone group proved to be synthetically difficult, preventing the formation of the desired products. Nonetheless, the complexes containing the dimethoxyacetophenone group revealed to have very interesting photophysical properties, leading to the formation of a europium complex that could be excited using visible light, suggesting that these chromophores could be good candidates for long wavelength Eu(III) sensitisation.

2.7 References

1. V. Fernandez-Moreira, F. L. Thorp-Greenwood and M. P. Coogan, *Chem. Commun.*, 2010, **46**, 186-202.
2. W. D. Horrocks Jr, J. P. Bolender, W. D. Smith and R. M. Supkowski, *J. Am. Chem. Soc.*, 1997, **119**, 5972-5973.
3. A. Beeby, S. Faulkner and J. A. G. Williams, *J. Chem. Soc. Dalton Trans.*, 2002, 1918-1922.
4. G. J. Stasiuk and M. P. Lowe, *Dalton Trans.*, 2009, 9725-9727.
5. M. Jauregui, W. S. Perry, C. Allain, L. R. Vidler, M. C. Willis, A. M. Kenwright, J. S. Snaith, G. J. Stasiuk, M. P. Lowe and S. Faulkner, *Dalton Trans.*, 2009, 6283-6285.
6. P. A. Sukerkar, K. W. MacRenaris, T. R. Townsend, R. A. Ahmed, J. E. Burdette and T. J. Meade, *Bioconjugate Chem.*, 2011, **22**, 2304-2316.
7. M. Tropiano, C. J. Record, E. Morris, H. S. Rai, C. Allain and S. Faulkner, *Organometallics*, 2012, **31**, 5673-5676.
8. C. A. Chang, L. C. Francesconi, M. F. Malley, K. Kumar, J. Z. Gougoutas, M. F. Tweedle, D. W. Lee and L. J. Wilson, *Inorg. Chem.*, 1993, **32**, 3501-3508.
9. J. Hall, R. Haner, S. Aime, M. Botta, S. Faulkner, D. Parker and A. S. de Sousa, *New J. Chem.*, 1998, **22**, 627-631.
10. K. M. Christensen, A. Bakac and J. H. Espenson, *Chem. Phys.*, 1993, **176**, 359-365.
11. S. Faulkner, B. P. Burton-Pye, T. Khan, L. R. Martin, S. D. Wray and P. J. Skabara, *Chem. Commun.*, 2002, 1668-1669.
12. S. J. A. Pope, B. J. Coe, S. Faulkner and R. H. Laye, *Dalton Trans.*, 2005, 1482-1490.
13. S. Faulkner and B. P. Burton-Pye, *Chem. Commun.*, 2005, 259-261.
14. S. Pope, B. Burton-Pye, R. Berridge, T. Khan, P. Skabara and S. Faulkner, *Dalton Trans.*, 2006, 2907.
15. S. Fery-Forgues and B. Delavaux-Nicot, *J. Photochem. Photobiol. A*, 2000, **132**, 137-159.
16. A. Weller, *Pure Appl. Chem*, 1968, **16**, 115-123.
17. A. J. Bard, R. Parsons and J. Jordan, *Standard potentials in aqueous solution*, Dekker, New York, 1985.
18. A. Beeby, I. M. Clarkson, R. S. Dickins, S. Faulkner, D. Parker, L. Royle, A. S. de Sousa, J. A. G. Williams and M. Woods, *J. Chem. Soc.-Perkin Trans. 2*, 1999, 493-503.
19. A. Beeby and S. Faulkner, *Chem. Phys. Lett.*, 1997, **266**, 116-122.
20. S. Faulkner, A. Beeby, R. Dickins, D. Parker and J. A. G. Williams, *J. Fluoresc.*, 1999, **9**, 45-49.
21. E. J. Shiells, L. S. Natrajan, D. Sykes, M. Tropiano, P. Cooper, A. M. Kenwright and S. Faulkner, *Dalton Trans.*, 2011, **40**, 11451-11457.
22. S. L. Murov, *Handbook of photochemistry*, Dekker, New York, 1973.
23. J. E. Jones and S. J. A. Pope, *Dalton Trans.*, 2009, 8421-8425.
24. E. H. van Dijk, D. J. T. Myles, M. H. van der Veen and J. C. Hummelen, *Org. Lett.*, 2006, **8**, 2333-2336.

3 Synthesis and study of a lanthanide appended rotaxane[2]

3.1 Introduction

Supramolecular structures that are able to sense anions are becoming increasingly important due to the degree of selectivity that can be achieved by judicious chemical modifications of the anion binding site. Interlocked systems such as rotaxanes or catenanes constitute an important family of supramolecular assemblies where the topology of the cavity dictates the steric requirements for the interacting guest.[1] Indeed, the formation of such systems can be achieved by anion templation, where two or more components assemble around the anion and the final mechanically interlocked structure is formed by ring closure.[2, 3] Such supramolecular scaffolds can be exploited in anion recognition and their structures tuned to be selective towards a specific species by varying the size of the cavity and directionality of the possible interactions within. For most of these systems the association equilibrium has been studied by NMR; the inclusion of a luminescent reporter group is then undoubtedly advantageous, as it lowers the limits of detection of the target analyte.

In an earlier work, inclusion of an emissive lanthanide complex on the axle of a pseudorotaxane yielded a supramolecular structure in which the interpenetration between axle and macrocycle upon addition of chloride was signalled by rhenium sensitised neodymium luminescence.[4] Although this study hinted on the possibility to include lanthanide-based luminescent reporters into interlocked supramolecular assemblies, the lability of the system did not permit the study of the anion binding ability of this potential receptor.

[2] Part of this work has already been published as an Edge Article in *Chem Sci., 2013, 4, 489-493*.

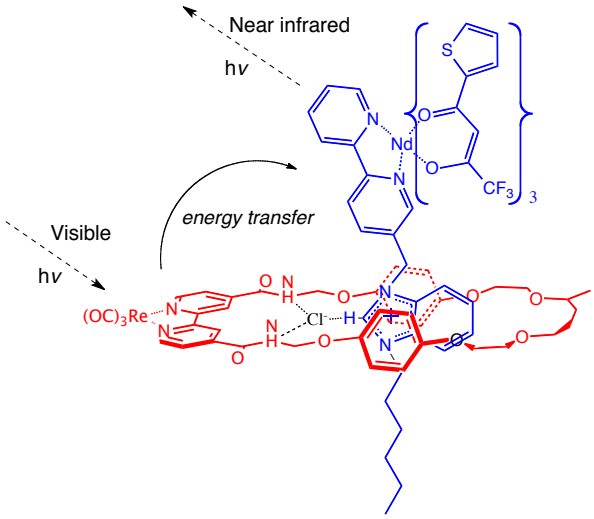


Figure 3-1. A lanthanide-containing pseudorotaxane whose formation was signaled by sensitisation of lanthanide luminescence by the Re(I) complex in close proximity. Redrawn from Ref.[4]

In this chapter the preparation of a lanthanide containing rotaxane is described. This is followed by a discussion of the binding of anions and the spectral changes induced to the lanthanide luminescence.

3.2 Strategies for the synthesis of the lanthanide appended rotaxane

The possible synthetic approaches leading to the formation of a lanthanide functionalised rotaxane are illustrated in Figure 3-2:

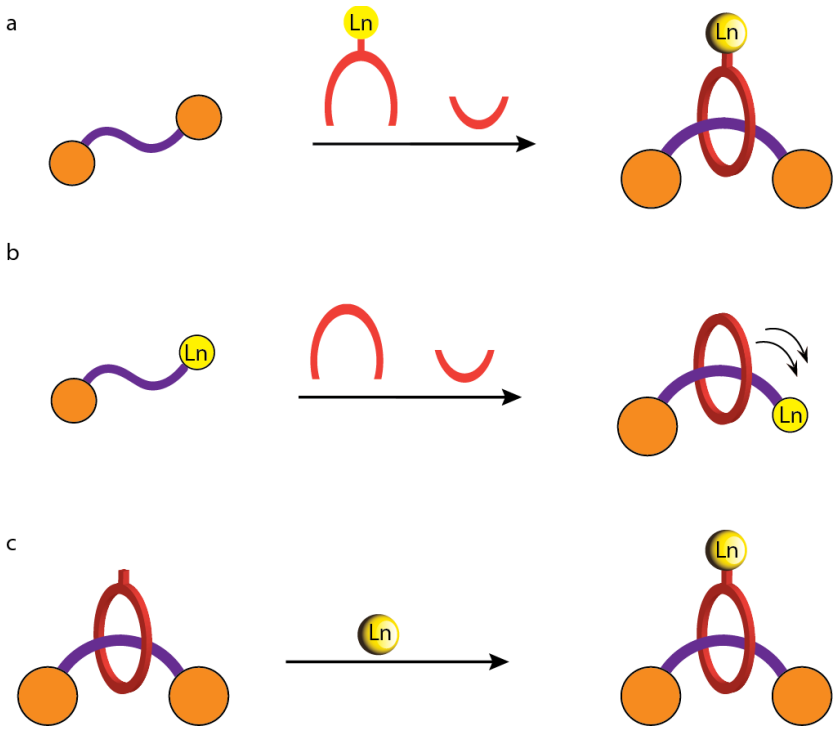


Figure 3-2. Possible synthetic strategies for the formation of a rotaxane containing a lanthanide complex as part of the macrocycle (a) or thread (b) before the assembly of the rotaxane or as part of the macrocycle to be incorporated after the assembly of the rotaxane (c).

The direct incorporation of the DO3A ligand onto the axle by a stoppering reaction with a preassembled pseudorotaxane (Figure 3-2b) would in principle be a valid option for the formation of the target compound. However, it was reasoned that the DO3A ligand would be too small in size to act as an effective stopper, especially after the cleavage of the *tert*-butyl groups and complexation. Furthermore, such stoppering reactions can be unpredictable, owing to the difference in reaction rate between the stopper and the thread when the latter is in its "free" form or when it is already part of a pseudorotaxane structure. On the other hand, the incorporation of the lanthanide binding ligand onto the macrocycle, followed by the anion templated synthesis of the rotaxane (Figure 3-2a), would impart markedly different chemical properties to the

macrocycle, hence leading to a more difficult synthesis and isolation of the structure. Instead, the approach taken for the synthesis of the supramolecular architecture involved the initial assembly of the rotaxane scaffold and subsequent functionalisation with a kinetically stable lanthanide complex. Adopting this synthetic strategy, the formation of the rotaxane assembly could be achieved using the standard anion templated procedure to obtain an already assembled mechanically interlocked structure with the possibility to be further functionalised with a lanthanide complex. Having estabilished the reliability of lanthanide complexes of propargyl-DO3A as a substrate in the CuAAC ”click’” reaction, the presence of an azido group on the rotaxane would then provide an ideal site for the subsequent direct functionalisation.

3.3 Synthesis of the azide functionalised rotaxane

The synthesis of the rotaxane was accomplished by Richard Knighton, a member of the Beer group in Oxford. This involved the chloride templated condensation clipping reaction between a pyridinium chloride axle (**3.1**), a diamine macrocycle precursor (**3.2**) and 5-azidoisophthaloyl chloride (**3.3**) to afford the azide functionalised rotaxane **3.4** as shown in Figure 3-3. The interlocked nature of the structure was confirmed by ^{1}H-NMR spectroscopy and by X-ray crystallography, showing the templating chloride anion located in the rotaxane cavity.

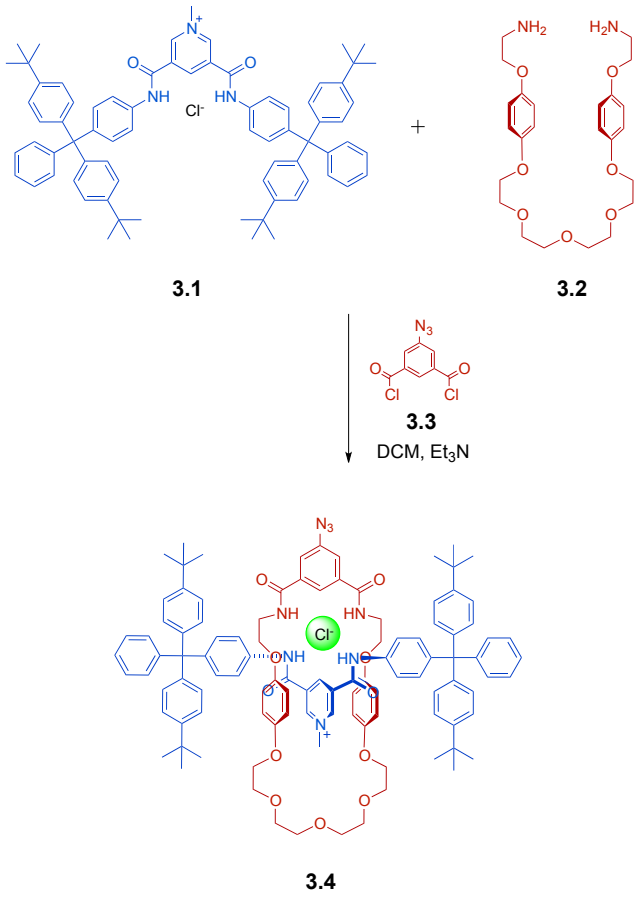


Figure 3-3. Synthesis scheme of the azide functionalised rotaxane.

3.4 Synthesis of the lanthanide appended rotaxane

The very different physical properties of the alkyne and azide-containing molecules made it rather difficult to find the appropriate reaction conditions for the CuCAAC "click" reaction. Due to the insolubility of the rotaxane in polar solvents such as water or methanol, the reaction conditions used for the coupling of the propargyl-DO3A complexes with other systems could not be replicated. Attempts to carry out the reaction in acetonitrile did not show any appreciable consumption of the starting materials, most likely due to the poor solvation of the lanthanide complex. A variety of other conditions were tried without success, including the use of biphasic solvent mixtures.

Other reaction conditions that were explored include:

- The use of DMF in which both the rotaxane and the lanthanide complex proved to be soluble.
- Use of a large excess of Cu(I) from the *in situ* reduction of Cu(II) with sodium ascorbate to account for a possible sequestration of the catalyst by the rotaxane cavity.
- Use of a different Cu(I) source instead of *in situ* reduction of $CuSO_4$, such as the complex $Cu(I)(MeCN)_4PF_6$ in the presence of TBTA in DMF.

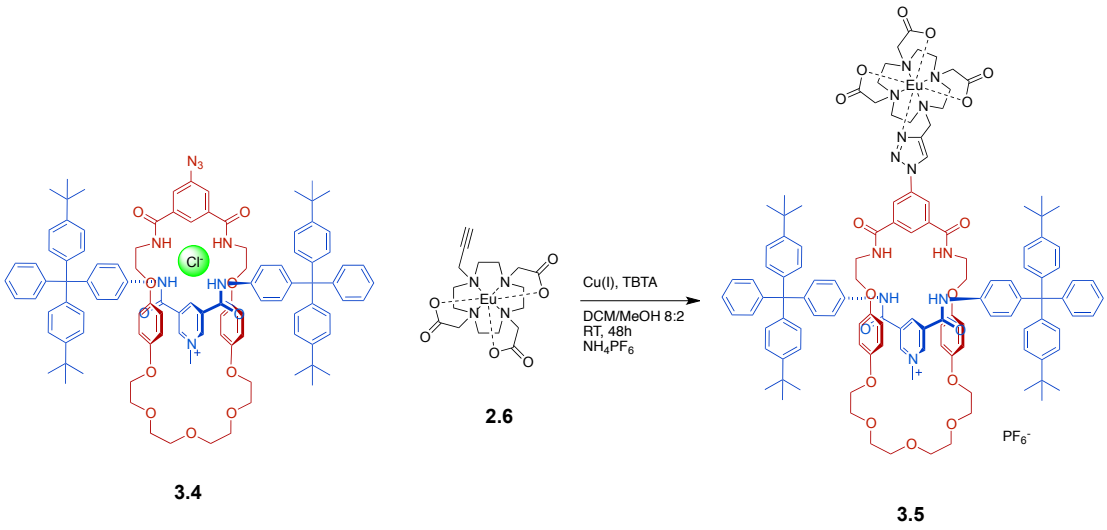


Figure 3-4. Synthetic method used for the preparation of the lanthanide appended rotaxane **3.5**.

Finally, reaction in a methanol:dichloromethane solvent mixture, using $[Cu(I)(MeCN)_4][PF_6]$ in the presence of TBTA, afforded the target compound in high yield (80%). The reaction was easily monitored by silica TLC and by ESMS (Figure 3-5 and Figure 3-6), which clearly showed the formation of the product with the concomitant disappearance of the peak corresponding to the starting rotaxane.

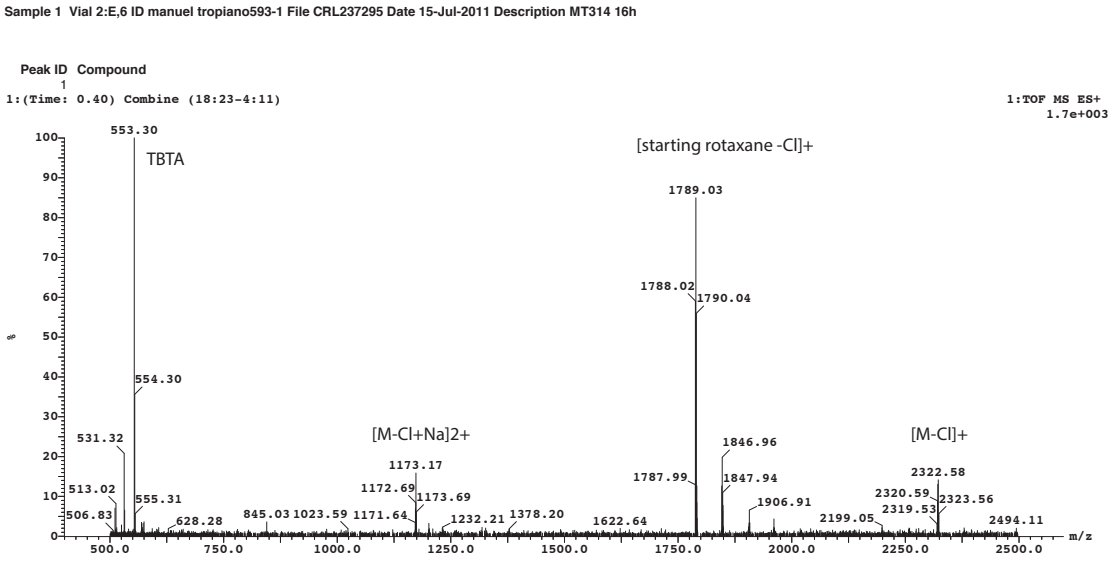


Figure 3-5. ESMS of the ongoing reaction mixture showing both the presence of the starting unreacted rotaxane and the ion corresponding to the product that starts to form.

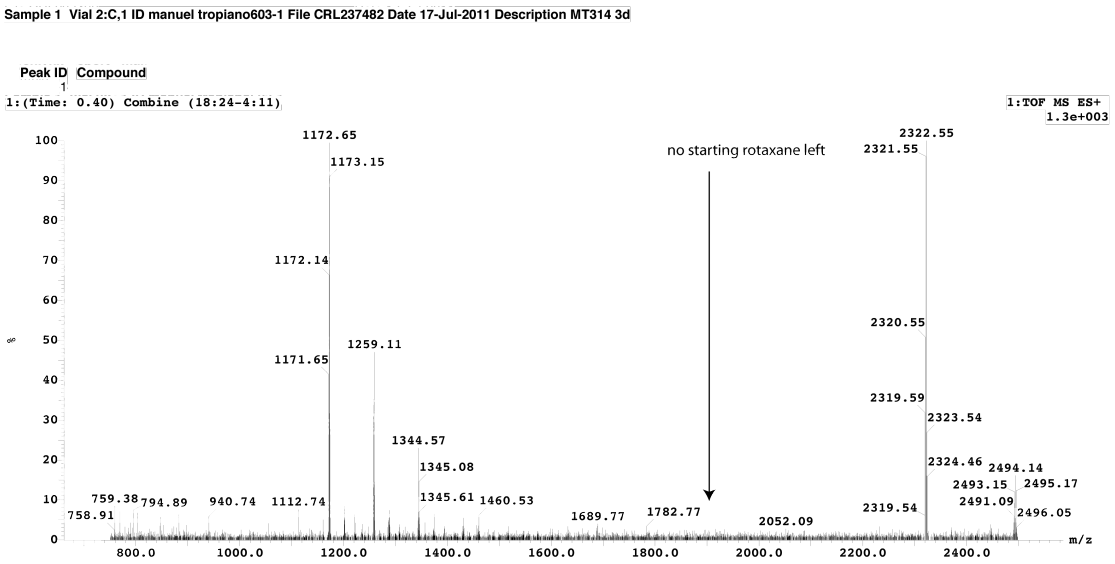


Figure 3-6. ESMS of the reaction mixture once all the starting azide rotaxane has been consumed and the only species now visible is the product.

The crude rotaxane proved to be soluble in organic solvents such as dichloromethane although the polar nature of the appended lanthanide complex prevented the use of silica gel chromatography for purification due to its high affinity with the polar stationary phase. Instead, the final product was purified by size exclusion chromatography. The accurate mass spectrum of the europium-containing product is shown in Figure 3-7.

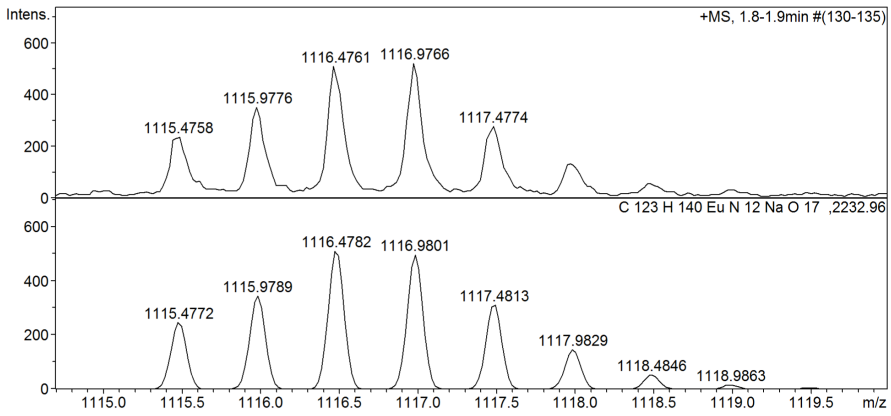


Figure 3-7. High resolution ESMS of **3.5**, showing the experimental (top) and theoretical isotope pattern.

3.5 NMR spectroscopy characterisation

The ^{1}H-NMR spectrum of **3.5** is shown in Figure 3-8. It is clearly indicative of the successful formation of the triazole moiety and its concomitant coordination to the lanthanide ion. Indeed, comparison with related systems (*vide supra*) confirms the octadentate nature of the ligand binding to the metal ion, and the predominance of square antiprismatic (SAP) geometry at the lanthanide centre.

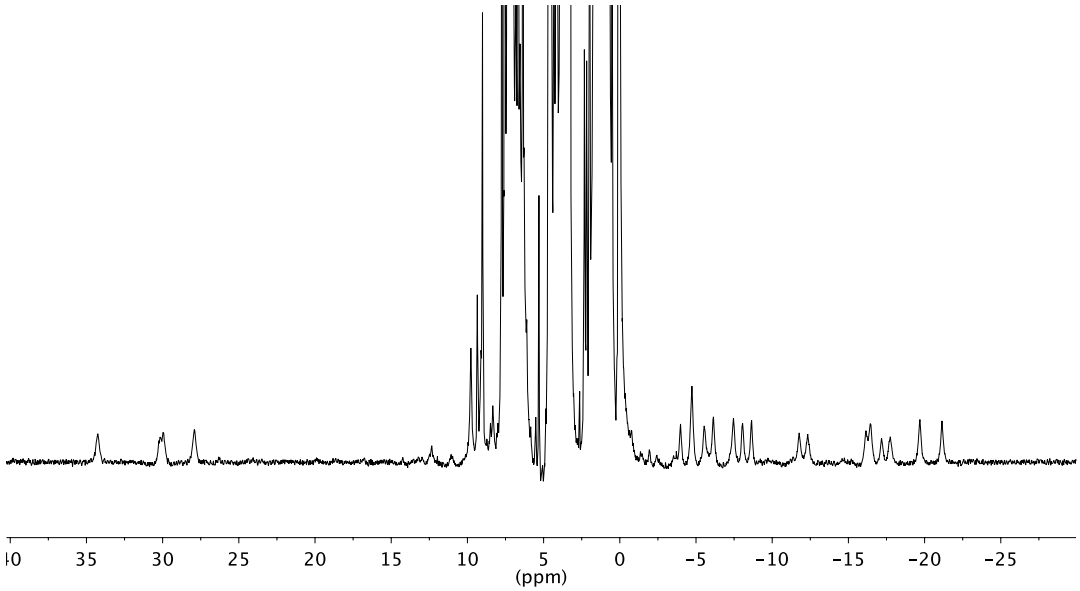


Figure 3-8. ^{1}H-NMR of **3.5** registered in 1:1 CD_3OD/CD_2Cl_2.

While the spectrum shown in Figure 3-8 could be obtained in a 1:1 (*v:v*) mixture of $CDCl_3$:CD_3OD, the spectra in pure $CDCl_3$ or CD_2Cl_2 were greatly broadened and very hard to interpret: this may be a consequence of surfactant-like behaviour of the molecule and the consequent likelihood of aggregation processes taking place in more apolar solvents. Such behaviour seems reasonable given the hydrophilic lanthanide binding domain and the hydrophobic nature of the rotaxane.

3.7 Photophysical characterisation

The emission spectrum of the **3.5** is shown in Figure 3-9. As can be noticed, luminescence from the lanthanide ion could be sensitised via the chromophores present in the structure and mainly by the proximate triazole group. The overall shape of the spectrum is indeed very similar to the emission profile shown by the triazolyl-Eu(III)-DO3A complex **2.13** where the lower $\Delta J_2/\Delta J_1$ ratio indicates a change in the crystal field as it would be expected from the formation of the triazolyl ring and hence presence of a further donor atom.[5]

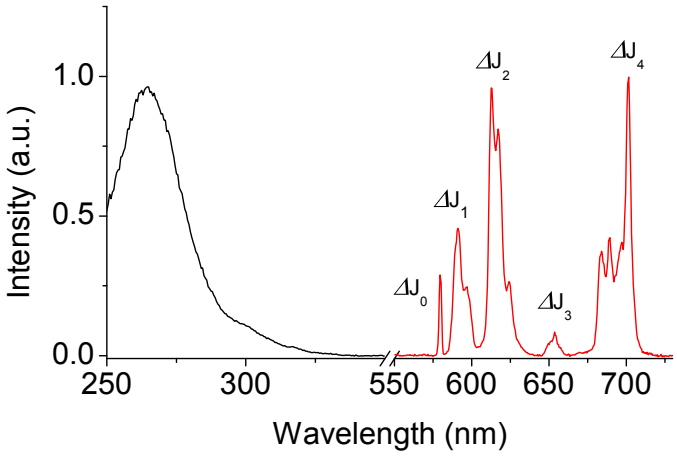


Figure 3-9. Excitation and emission spectrum of **3.5** obtained in dichloromethane.

The high-resolution spectrum in Figure 3-9 allows for close inspection of the emission bands. The splitting of the ΔJ_1 transition is indicative of the degree of symmetry and the size of the B_0^2 parameter. Three equally spaced components are usually observed in case of low symmetry of the local coordination sphere. Furthermore, the presence of strong satellite peaks characterising the ΔJ_2 transition could give an indication on the strength of the bond between the lanthanide ion and ligand. Clearly, these site symmetry considerations only constitute a qualitative indication of the structure that could be adopted by this molecule in solution. A scrupulous analysis could only be applied if measurements could be made on single crystal samples with extensive use of Judd-Ofelt theory.[6, 7]

Measurements of the excited state lifetimes were performed in solution of dichloromethane and binary mixture of 1:1 methanol:dichloromethane (*v:v*). The insolubility of the molecule in water or even methanol did not allow the calculation of the hydration number through the measurement in H_2O (or CH_3OH) and D_2O (or CD_3OD) and the use of the modified Horrocks' equation. The value of 0.85 ms obtained in dichloromethane is nonetheless wholly consistent with an octadentate ligand binding to the metal centre. While the solvation of even simple molecules in binary solvent mixtures is complicated, it is reasonable to suppose that the methanol molecules will coordinate in the vacant site of the lanthanide coordination sphere.

3.8 Anion sensing

The ability of the synthesised lanthanide rotaxane to bind anions could then be studied by fluorescence thanks to the presence of the europium ion included in the supramolecular structure. The cavity formed between the macrocycle and axle of the rotaxane would serve as a binding pocket with a unique topology, able to show selectivity for small anions such as chloride. At the same time the ninth axial coordination site of the lanthanide complex could also act as a binding site for anions. With this in mind we set out to study the anion binding behaviour of the europium rotaxane.

3.8.1 Binding of chloride in dichloromethane

Addition of chloride to the europium rotaxane in dichloromethane resulted in a marked decrease in luminescence intensity upon addition of one equivalent of anion. Increase of anion concentration caused an increase in luminescence intensity to a total recovery of the starting luminescence signal (Figure 3-10). This behaviour suggests that the chloride is participating in two chemical events in solution. These were ascribed to interactions with the rotaxane cavity and the lanthanide centre.

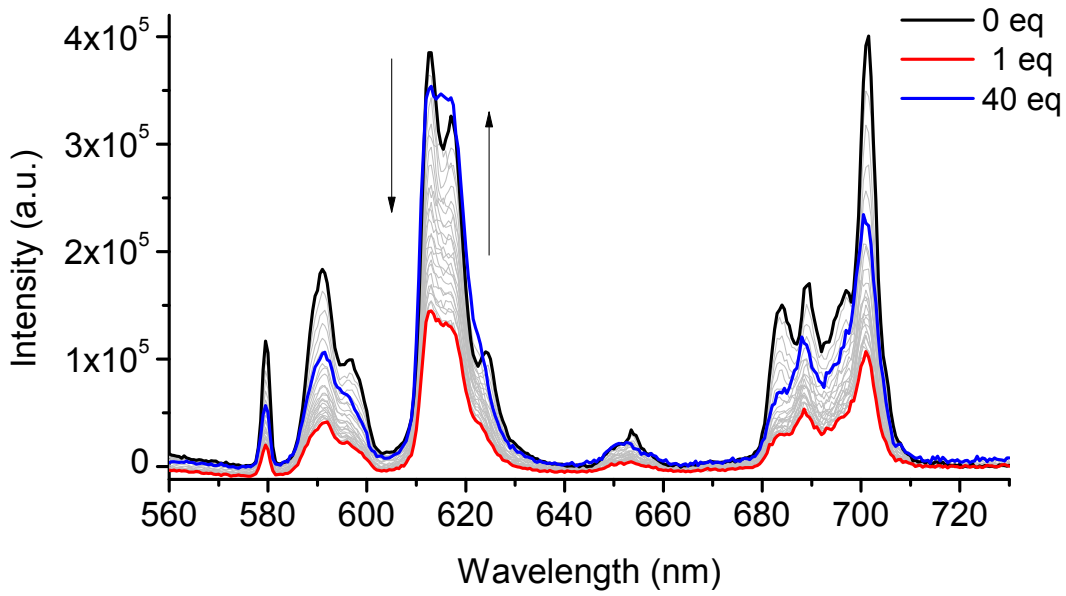


Figure 3-10. Luminescence behaviour of the Eu(III) rotaxane **3.5** (10^{-5}M) upon addition of increasing amounts of TBACl in dichloromethane, λ_{ex} = 270 nm.

A close inspection of the general band structure of the europium emission allows for a better understanding of the solution behaviour of the system upon addition of the anion. Upon initial addition of chloride the emission spectrum shows a more marked change in the hypersensitive ΔJ_2 transition and, as a consequence, a change in the $\Delta J_2/\Delta J_1$ ratio. Upon further increase of chloride concentration, the intensity of all transitions increases with consequently no change in the $\Delta J_2/\Delta J_1$ ratio (see Figure 3-11).

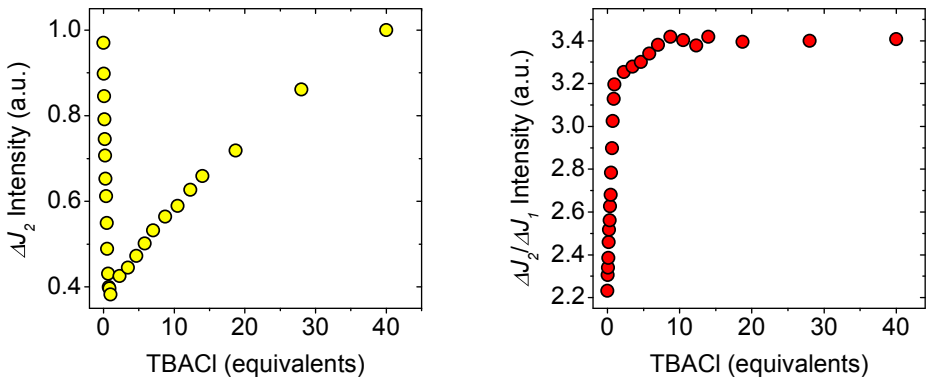


Figure 3-11. Changes in the emission profile of **3.5** upon addition of TBACl as signaled by the changes in the ΔJ_2 band (left) and $\Delta J_2/\Delta J_1$ ratio (right).

It is then clear that in the first event the chloride is interacting with the lanthanide centre at the ninth axial coordination site, hence triggering a change in the local crystal field environment. Indeed, this would cause a change in the shape and intensity of the hypersensitive ΔJ_2 transition. Upon further increase in chloride concentration, the anion is able to bind to the rotaxane cavity inducing a rigidification of the structure and hence an overall increase in luminescence without triggering a change solely to the intensity of the hypersensitive transition.

To gain further insight into the anion binding behaviour of the system in solution, the interaction with chloride was also studied by time-resolved spectroscopy, measuring the excited-state lifetime of the Eu(III). The lifetime data mirror the behaviour observed for the steady state luminescence measurements. This confirms the presence of two distinct binding events during the course of the titration that can be monitored by a change in luminescence. Initially, the luminescence lifetime of the europium centred emission decreases rapidly as a consequence of non-radiative quenching of the lanthanide excited state by the bound chloride (presumably through a photo-electron transfer process).[8] When the concentration of chloride is further increased, the rigidification of the structure, upon binding of chloride into the rotaxane cavity, decreases the probability of non-radiative vibrational quenching of the lower excited states on the antenna, hence increasing the probability of energy transfer from the antenna to the lanthanide.

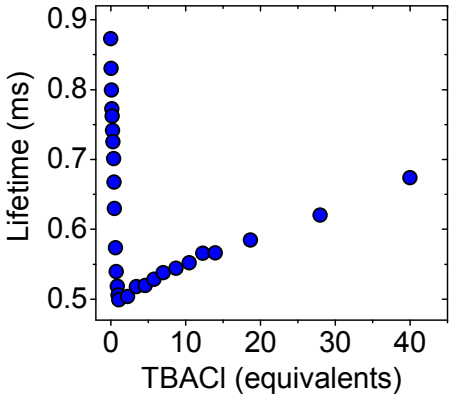


Figure 3-12. Behaviour of the Eu(III)-centred luminescence lifetime of **3.5** upon increasing concentration of chloride in dichloromethane. λ_{ex} = 270 nm, λ_{em} = 616 nm.

The analysis of the binding events could be performed by considering either an independent or a sequential binding mechanism. The latter approach would require the chloride to interact first only with the lanthanide centre and then with the rotaxane cavity in a stepwise fashion (see Figure 3-13). This is obviously a highly unlikely event and it would require some degree of cooperativity within the system.

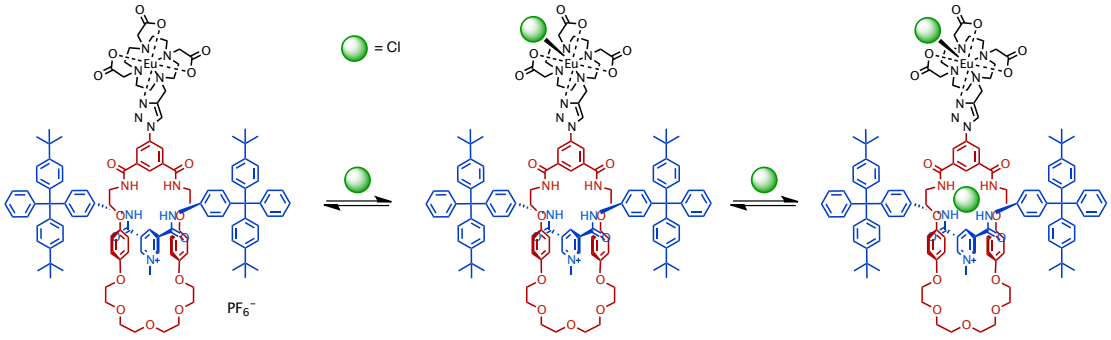


Figure 3-13. Schematic diagram of a sequential binding mechanism, in which the chloride first interacts with the lanthanide centre and then with the cavity formed within the rotaxane structure.

In the independent binding mechanism, chloride is instead involved in two independent binding events and the system can be described with two independent association constants. This picture could also be influenced by the presence of kinetically trapped species, but it is assumed that the system can explore the entire potential energy surface and hence be under thermodynamic control.

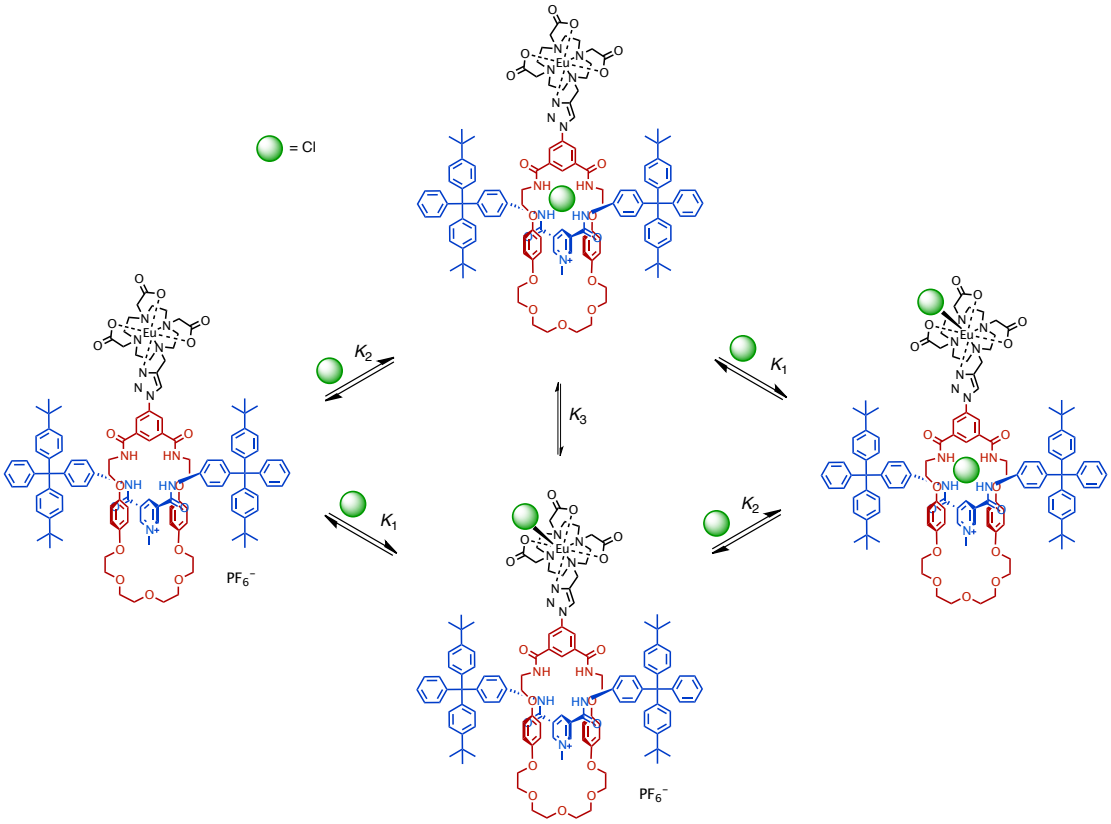


Figure 3-14. Independent binding mechanism, in which the chloride can bind independently to the two possible binding sites present in the supramolecular structure.

Table 3-1 outlines the binding constants obtained in this work. Modelling of the obtained data was performed using Dynafit software.[9] Figure 3-15 shows the correlation between experimental data and each of these models. It is immediately clear that an independent model gave a significantly better agreement between experimental and modelled data. In the model, two binding constants of 1360 M^{-1} and 750,000 M^{-1} were used for the binding of the anion to the rotaxane cavity and the ninth axial coordination site of Eu(III). Furthermore, by plotting the $\Delta J_2/\ \Delta J_1$ ratio, the data allowed the study of only the interaction of chloride with the lanthanide centre. In this case the observed data could be fitted using Dynafit to obtain an association constant of 504,000 M^{-1}.

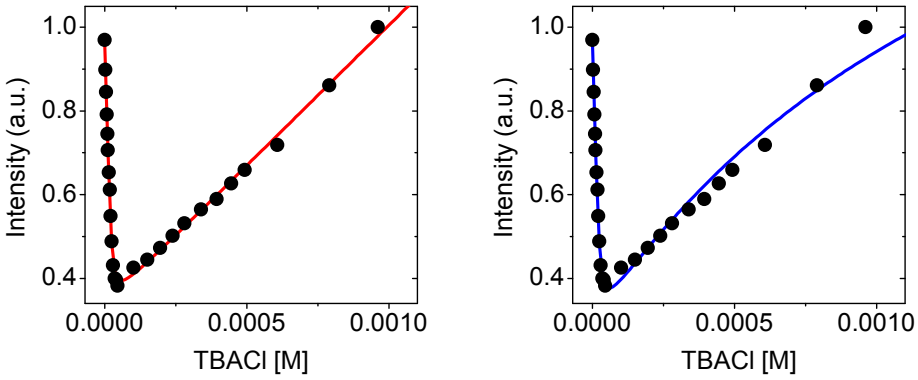


Figure 3-15. Comparison of the experimental and modelled data for the independent (left) and sequential (right) binding models.

3.8.2 Binding of oxyanions in dichloromethane

As mentioned earlier, rotaxane systems such as the one studied in this work have shown great selectivity of response to chloride over other oxyanions of larger sizes.[2, 10-13] This is merely a consequence of the topology of the cavity formed between the axle and the macrocycle. Indeed, upon titration with dihydrogenphosphate and acetate anions, the europium rotaxane system showed only a monotone response, indicating that only one binding event was occurring. The distinct change in the ΔJ_2 transition once more suggested that the anion is binding to the lanthanide centre, without inducing structural changes to the rotaxane scaffold. Binding to the metal ion was completely predominant and the data could be fitted to a 1 to 1 binding model obtaining association constants of 58,000 M^{-1} and 304,000 M^{-1} for acetate and dihydrogenphosphate respectively.

In the case of dihydrogenphosphate, the effect on lanthanide luminescence affects all Eu(III) transitions, indicating that the interaction is not site-selective and most likely involves a dynamic quenching of the lanthanide excited state. Furthermore, the sigmoidal shape of the binding isotherm at the beginning of the titration suggests that the speciation of the hydrogenphosphate anion in this solvent is not dominated only by its diprotonated form and that it is likely to change during the course of the titration upon interaction with the Eu(III) centre (Figure 3-16).

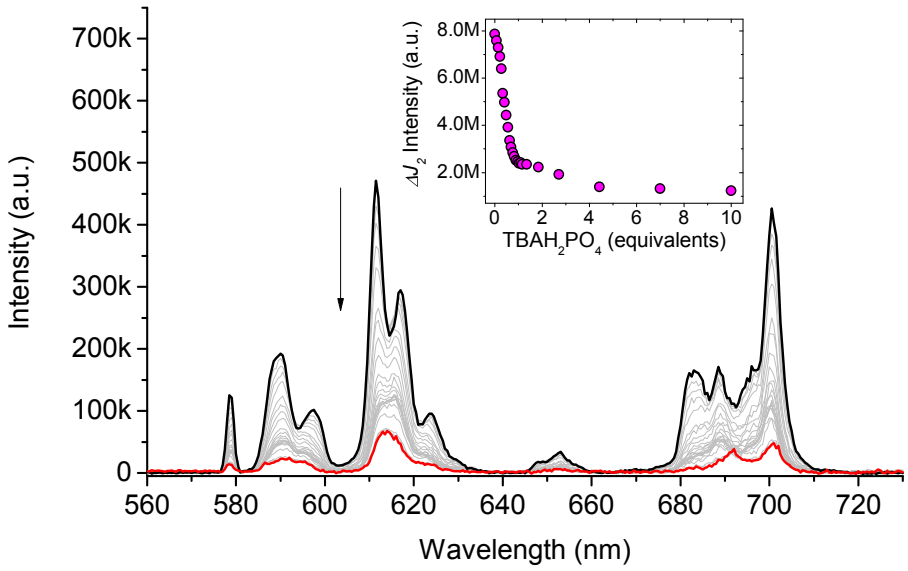


Figure 3-16. Modulation of Eu(III) luminescence in **3.5** (10^{-5} M) upon addition of $TBAH_2PO_4$ in dichloromethane. λ_{ex} = 270 nm.

Acetate shows a somewhat different behaviour, with the decrease in intensity in the luminescence spectrum of the receptor accentuated for the ΔJ_2 hypersensitive transition (Figure 3-17).

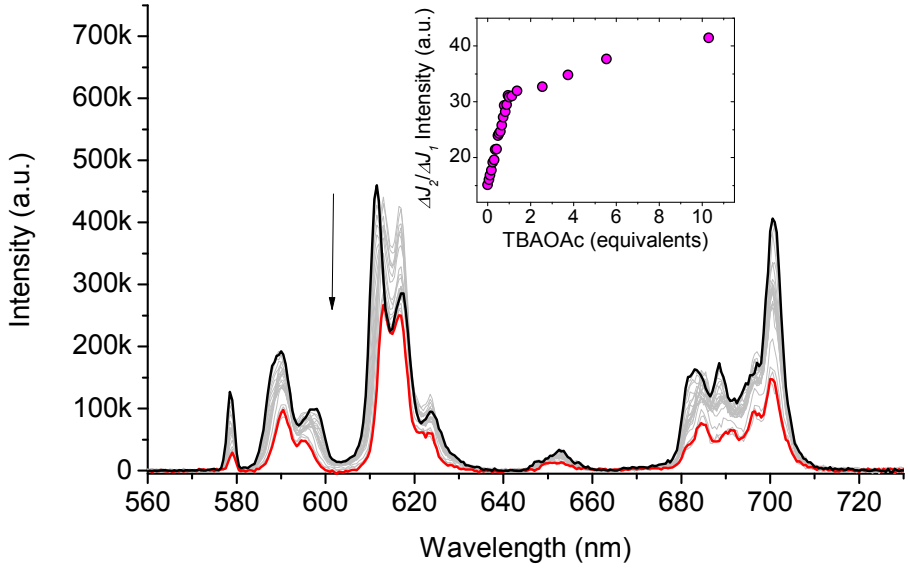


Figure 3-17. Modulation of Eu(III) luminescence in **3.5** (10^{-5} M) upon addition of TBAOAc in dichloromethane. λ_{ex} = 270 nm.

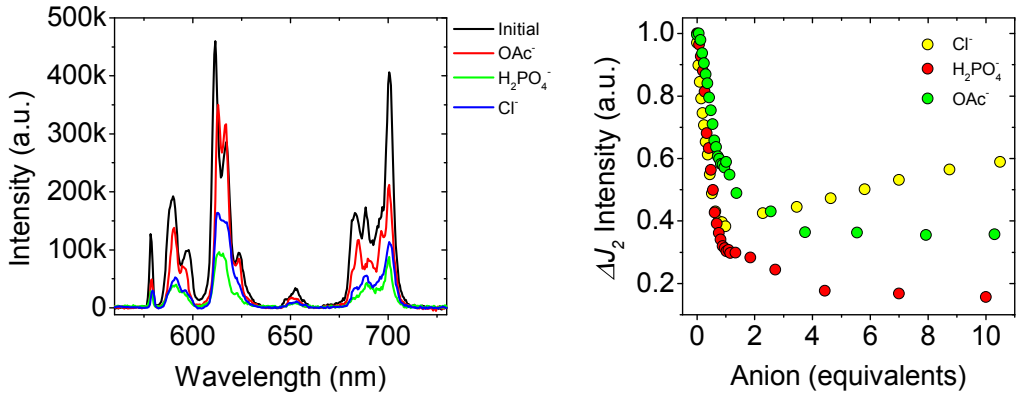


Figure 3-18. Comparison of the changes in the emission spectrum of **3.5** upon addition of the three anions discussed in this work (left). Corresponding binding curves (right).

3.8.3 Binding in dichloromethane:methanol mixture

Having studied the system in a non-competitive solvent such as dichloromethane, the ability of this supramolecular receptor system to bind chloride in a more competitive solvent was explored. Due to the poor solubility in more polar mixtures, the study was limited to a 1:1 (*v:v*) dichloromethane-methanol solvent system. In this case, the ability to bind anions was significantly decreased, to the point that only binding to the lanthanide centre could be observed. This is not surprising, giving the already low value of the association constant between chloride and the rotaxane cavity found in dichloromethane.

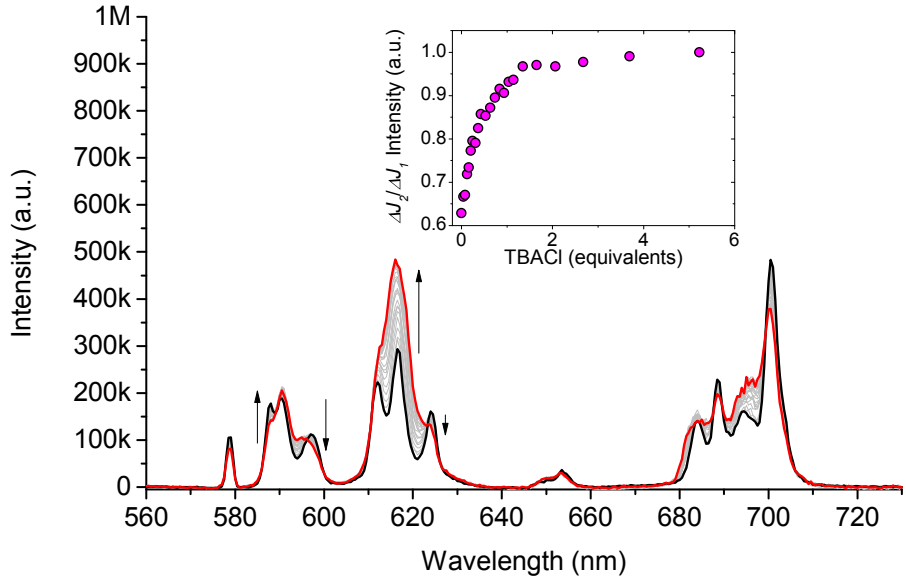


Figure 3-19. Modulation of Eu(III) luminescence in **3.5** (C=10^{-5} M) upon addition of TBACl in dichloromethane/methanol 1:1. λ_{ex} = 270 nm.

Binding to the lanthanide centre was signalled by marked changes in the emission spectra for chloride and acetate while the emission spectrum showed only minimal changes upon addition of dihydrogenphosphate, although the binding could be observed and an association constant could be obtained nonetheless. In the case of chloride and acetate, the most affected transition was the ΔJ_2, indicating that these anions are undoubtedly interacting with the Eu(III) centre. This was further confirmed by the overall enhancement of luminescence. Displacement of bound methanol leads to removal of O-H oscillators in close proximity to the lanthanide ion and hence to an overall increase in emission.

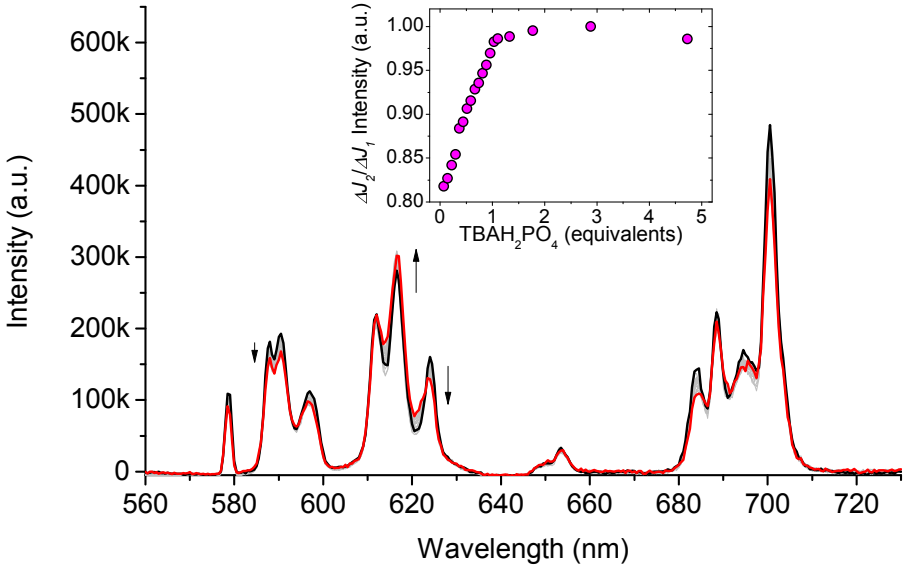


Figure 3-20. Modulation of Eu(III) luminescence in **3.5** ($C=10^{-5}$ M) upon addition of $TBAH_2PO_4$ in dichloromethane/methanol 1:1. λ_{ex} = 270 nm.

An increase in observed lifetime, although small, was also observed through the course of the titration (from 0.87 ms to 0.90 for chloride and dihydrogenphosphate and to 1.0 ms for acetate) confirming that the enhancement of luminescence is indeed due to a process directly affecting the coordination sphere of the lanthanide and possibly due to a displacement of a coordinated methanol molecule. The small change in the emission spectrum accompanied by addition of dihydrogenphosphate is indicative of an interaction that, although as strong as the acetate case, is not greatly disrupting the metal coordination environment, whereas the more pronounced change

upon addition of acetate may be due to a displacement of the coordinating triazole donor with the anion coordinating in a bidentate fashion.

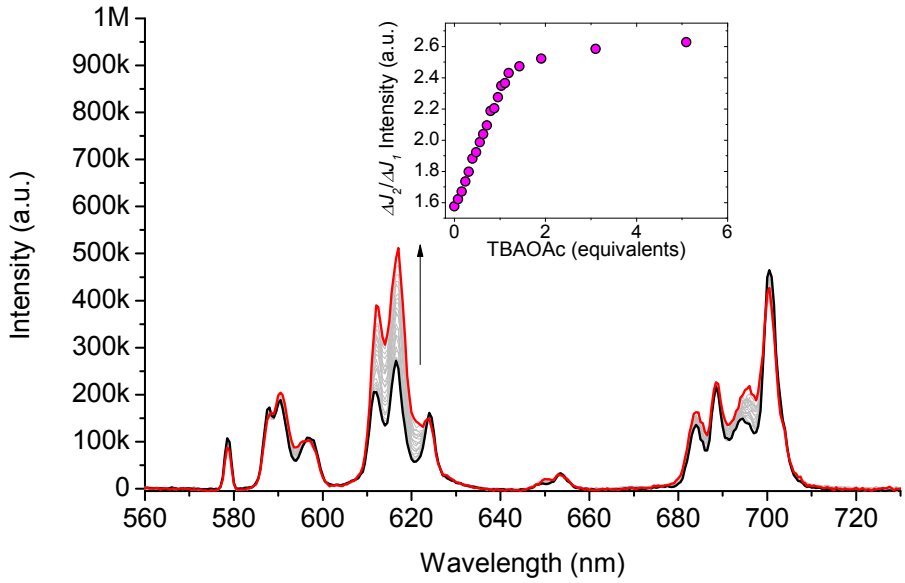
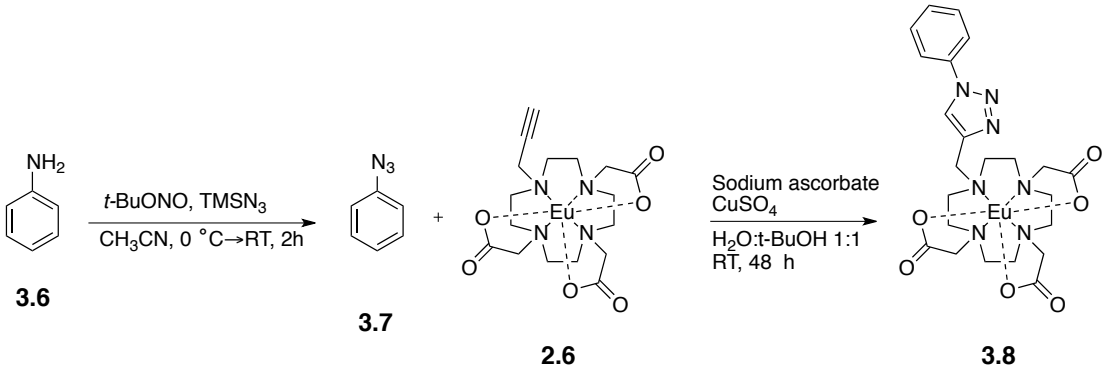


Figure 3-21. Modulation of Eu(III) luminescence in **3.5** ($C=10^{-5}$ M) upon addition of TBAOAc in dichloromethane/methanol 1:1. λ_{ex} = 270 nm.

3.9 Binding of anions to a model compound

The assignment of the binding sites in the lanthanide rotaxane assembly was further supported by the study of a model compound.



3.6 **3.7** **2.6** **3.8**

Figure 3-22. Description of the synthesis of the model compound **3.8**.

The Eu(III) complex **3.8**, shown in Figure 3-22, was then synthesised. The structure resembles the lanthanide site in the rotaxane assembly, but omits the rotaxane. It was

reasoned that the presence of the emissive metal in the same binding environment would give a direct comparison of the photophysical behaviour upon addition of anions. The synthesis involved the reaction between the Eu(III) complex **2.6** with azido benzene (**3.7**), obtained from aniline (**3.6**) upon reaction with trimethylsilyl azide in the presence of *tert*-butyl nitrite.

Table 3-1. Summary of the binding constant obtained for the Eu(III) rotaxane **3.5** and the model compound **3.8** with the corresponding anion and solvent indicated

Compound	**Solvent**	**Anion**	K **(M^{-1})[a]**
Eu rotaxane (**3.5**)	DCM	Cl^-	5.04×10^5
	DCM	AcO^-	5.8×10^4
	DCM	$H_2PO_4^-$	3.04×10^5
Eu.rotaxane (**3.5**)	DCM-MeOH 1:1	Cl^-	9.5×10^4
	DCM-MeOH 1:1	AcO^-	2.3×10^4
	DCM-MeOH 1:1	$H_2PO_4^-$	7.0×10^4
Eu model (**3.8**)	DCM-MeOH 1:1	Cl^-	6.5×10^4
	DCM-MeOH 1:1	AcO^-	2.3×10^4
	DCM-MeOH 1:1	$H_2PO_4^-$	2.8×10^4

[a]Obtained from ΔJ ratios binding plots.

Due to the polarity of the model compound, the anion binding studies could only be performed in 1:1 (*v:v*) dichloromethane/methanol mixtures. In this solvent only binding to the lanthanide was observed for the europium rotaxane, hence it was expected that the model compound would behave in the same way as the lanthanide rotaxane, assuming the assignments of the binding sites made were correct.

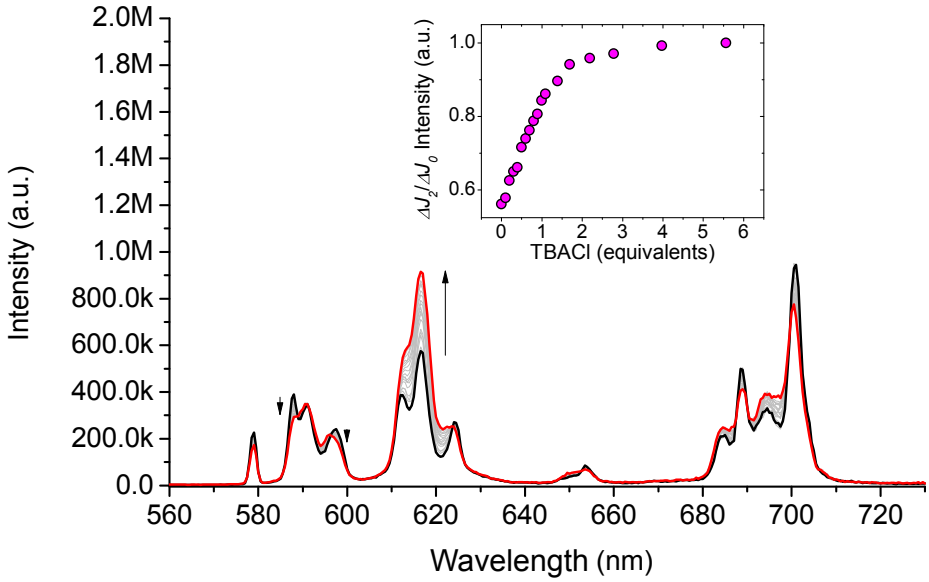


Figure 3-23. Modulation of the emission of **3.8** (10^{-5} M) upon addition of TBACl in 1:1 dichloromethane/methanol. λ_{ex} = 265 nm.

Table 3-1 shows the value of association constants obtained for the model compound upon titration with the three different anions used in this study. The luminescence spectra distinctly changed upon addition of anions and the increase in luminescence hints to a solvent displacement mechanism, as also confirmed by the increase in the excited state lifetime (from 0.92 ms to 1.00 ms for acetate and from 0.92 to 0.95 ms for chloride and dihydrogenphosphate). As can be noted, the values for each anion are remarkably similar in both the model system and the Eu(III)-containing rotaxane. This confirms the assignment of the binding sites made earlier based on steady state and time resolved luminescence.

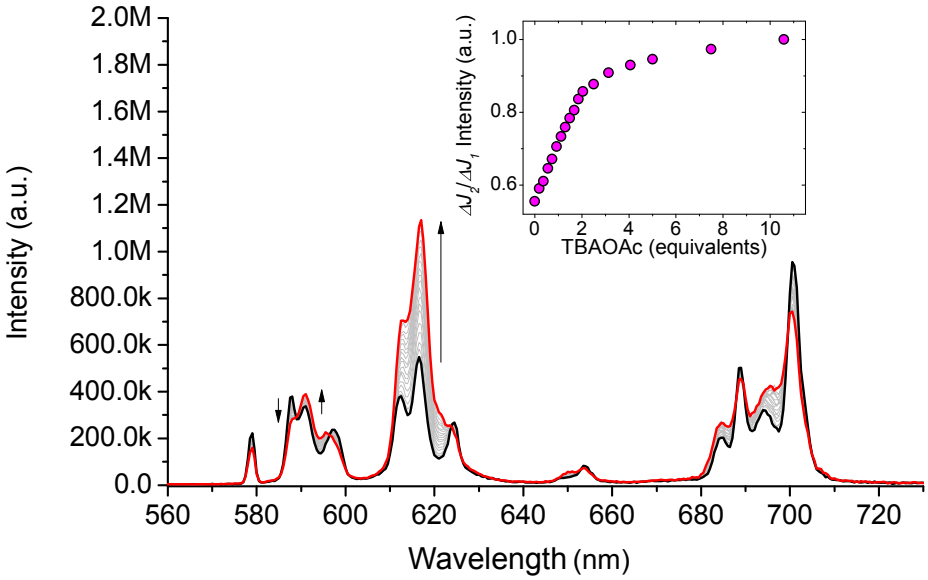


Figure 3-24. Modulation of the emission of **3.8** ($C=10^{-5}$ M) upon addition of TBOAc in 1:1 dichloromethane/methanol. λ_{ex}=265 nm.

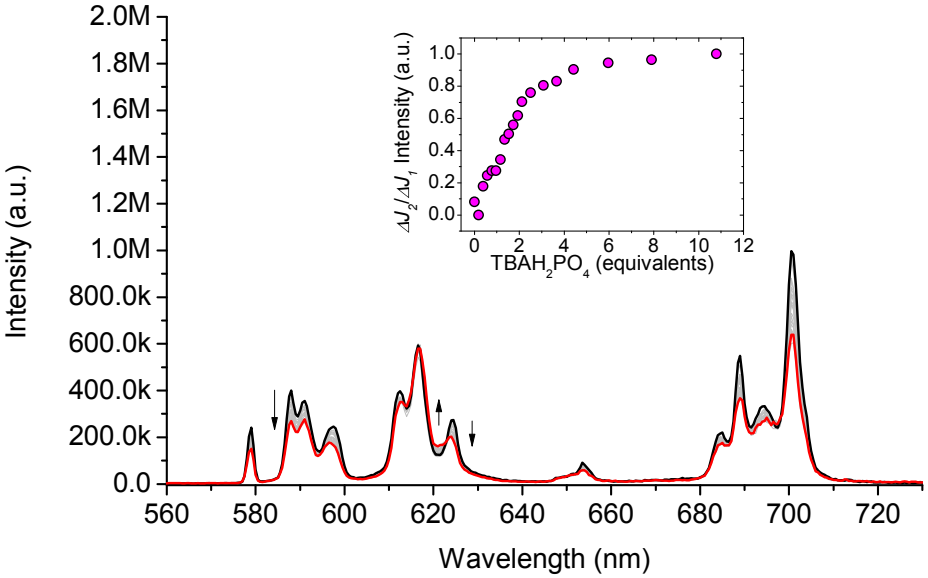


Figure 3-25. Modulation of the emission of **3.8** ($C=10^{-5}$ M) upon addition of $TBAH_2PO_4$ in 1:1 dichloromethane/methanol. λ_{ex}=265 nm.

3.10 Conclusions

A lanthanide-appended rotaxane has been synthesised for the first time. CuAAC "click" chemistry proved to be a powerful synthetic tool to link molecular structures with very different chemical properties, although, as shown here, it doesn't always translate into immediate reactions and favourable reaction conditions had to be found in this case.

The combination of a luminescent tag coupled with the anion binding ability of the rotaxane has lead to a probe with enhanced sensitivity towards chloride detection. This, together with the high signal to noise ratio that characterises fluorescence techniques, gives an improved detection limit of this class of compounds, when coupled with a fluorescent tag. Indeed, these anion binding studies have been performed using micromolar concentrations of sensor as opposed to millimolar concentrations for the more commonly used NMR technique. Furthermore, the use of a long-lived fluorescence signal, given by the lanthanide ion, can potentially be applied in time-gated detection, greatly decreasing interference from the background.

The rotaxane so formed showed dual response to chloride in dichloromethane due to the binding of this anion also to the lanthanide centre. The two binding events were shown to be independent and both could be deconvoluted from the Eu(III) fluorescence signal. This demonstrates that binding events at a relatively long distance from the signalling unit can still be sensed due to an overall rigidification of the molecular structure and hence to changes in the energy transfer cascade for europium sensitisation. The size requirements for the rotaxane cavity showed selectivity towards small anions with no noticeable binding to acetate and dihydrogenphosphate in dichloromethane. Nonetheless, the strength of the interaction between the anion and the metal centre was such that this dominated the fluorescence behaviour in more competitive solvent mixtures where no binding of the anion to the cavity within the rotaxane domain could be observed. Indeed, although the cavity present in the rotaxane makes use of directional hydrogen bonding and pre-organisation, this is

clearly not as strong as the purely electrostatic interaction between lanthanides and a negatively charged species.

3.11 References

1. J.-P. Sauvage and C. Dietrich-Buchecker, *Molecular catenanes, rotaxanes and knots : a journey through the world of molecular topology*, Wiley-VCH, Weinheim; Chichester, 1999.
2. M. D. Lankshear and P. D. Beer, *Acc. Chem. Res.*, 2007, **40**, 657-668.
3. M. S. Vickers and P. D. Beer, *Chem. Soc. Rev.*, 2007, **36**, 211-225.
4. M. R. Sambrook, D. Curiel, E. J. Hayes, P. D. Beer, S. J. A. Pope and S. Faulkner, *New J. Chem.*, 2006, **30**, 1133-1136.
5. M. Jauregui, W. S. Perry, C. Allain, L. R. Vidler, M. C. Willis, A. M. Kenwright, J. S. Snaith, G. J. Stasiuk, M. P. Lowe and S. Faulkner, *Dalton Trans.*, 2009, 6283-6285.
6. C. Görller-Walrand and K. Binnemans, in *Handbook on the Physics and Chemistry of Rare Earths*, eds. Karl A. Gschneidner, Jr. and E. LeRoy, Elsevier, 1998, vol. Volume 25, pp. 101-264.
7. B. M. Walsh, in *Advances in Spectroscopy for Lasers and Sensing*, eds. B. Bartolo and O. Forte, Springer Netherlands, 2006, pp. 403-433.
8. A. Weller, *Pure Appl. Chem*, 1968, **16**, 115-123.
9. P. Kuzmic, *Anal. Biochem.*, 1996, **237**, 260-273.
10. L. M. Hancock and P. D. Beer, *Chem. Eur. J.*, 2009, **15**, 42-44.
11. L. M. Hancock, L. C. Gilday, S. Carvalho, P. J. Costa, V. Félix, C. J. Serpell, N. L. Kilah and P. D. Beer, *Chem. Eur. J.*, 2010, **16**, 13082-13094.
12. L. M. Hancock, L. C. Gilday, N. L. Kilah, C. J. Serpell and P. D. Beer, *Chem. Commun.*, 2011, **47**, 1725-1727.
13. N. H. Evans, C. J. Serpell and P. D. Beer, *Chem. Commun.*, 2011, **47**, 8775-8777.

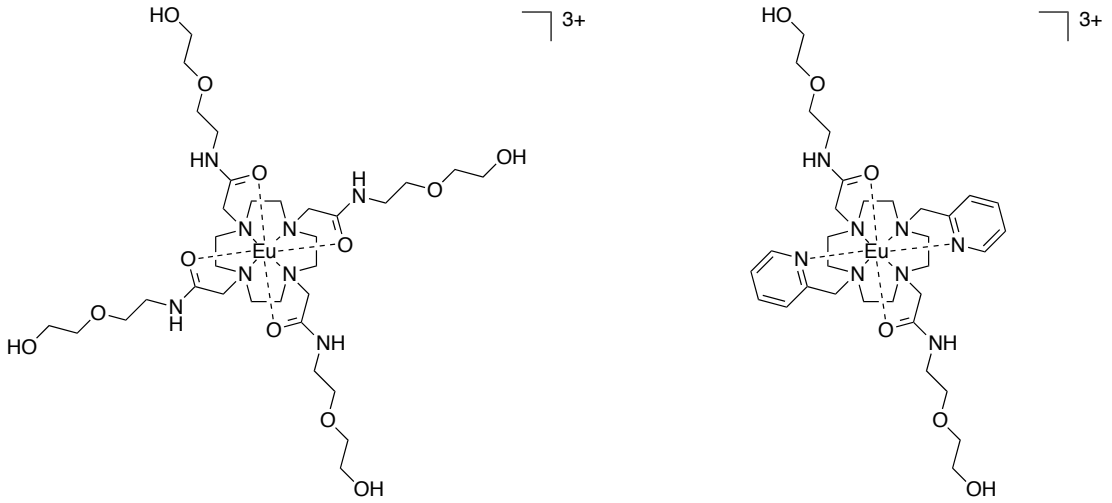
4 Synthesis and study of macrocyclic structures containing lanthanide complexes

4.1 Introduction

The anion sensing ability of lanthanide complexes is well documented in the literature, with lanthanide containing compounds being widely exploited for the detection of several anionic species. The advantages of the use of lanthanide probes have already been outlined in the introduction and include the line-like emission of the metal and the high sensitivity that can be achieved thanks to time-gated detection. The strategies used to improve the sensitivity and the selectivity of this class of luminescent probes include the use of a chromophore whose photophysical properties are disrupted by the presence of the target analyte and the direct exploitation of the metal-anion interaction, with the consequent displacement of solvent molecules and hence an increase in the intensity of fluorescence. In particular, in the case of receptors capable of binding halides, the receptor-anion interaction must overcome the strength of the hydrogen bond network formed around the anion in solution, especially in aqueous solvents.

The exploitation of a photoelectron transfer mechanism between the electron rich anion and the antenna present on the lanthanide receptor, although giving good detection limits, does not show selectivity towards a specific halide given that all are able to quench a chromophore through this mechanism. By contrast, the direct interaction of the anion with the metal centre is usually weak and requires the chemical modification of the complex backbone to include groups that are able to hydrogen bond and give some degree of directionality to the interactions involved. Lima et al. have reported a positively charged Eu(III) complex capable of binding

fluoride, although no comments were made about the selectivity over other halides.[1] In the same work, the authors clearly showed the importance of the pendant arms on the cyclen core in the anion binding event with complex **4.2** showing a stronger interaction over **4.1**. This was attributed to the additional hydrogen bond interaction with fluoride involving the C-H groups of the pyridyl moieties.



4.1 **4.2**

Figure 4-1. Structures of the complexes studied by Lima et al. as lanthanide receptors for the detection of fluoride.

While the interaction between halide anions and receptor has been shown to be improved by incorporation of hydrogen bond donor groups on the pendant arms of the lanthanide complex (the receptor), the problem of selectivity still holds. It is then expected that the size of the anion remains the only discriminating factor. With this in mind it was reasoned that a lanthanide probe with improved selectivity towards halide should not only have hydrogen bond donor groups on the pendant arms, but also contain a cavity that could wrap around the anion situated on the ninth axial coordination site of the lanthanide itself.

In the previous chapter it was observed that the strength of the interaction between lanthanide and anions eclipsed the much weaker interaction displayed by supramolecular structures such as rotaxanes. In the light of these findings, it was

reasoned that the metal ion could indeed be exploited directly for the anion binding site. The combination of size requirements, pre-organisation and directionality, displayed by supramolecular structures could be coupled with the strength of the interaction of the anionic guest with a lanthanide ion encapsulated into a chelate based on the DOTA structure.

With this in mind we set out to prepare a complex that could serve as a platform for the formation of size selective macrocyclic cavities that, in combination with the free ninth axial coordination site of the lanthanide metal, would enhance the strength and selectivity of the interaction with the anionic guest. Furthermore, the same platform could be used for the formation of other supramolecular structures such as catenanes and rotaxane, where, in this case, the lanthanide complex would be present directly in the anion binding site and could participate in the anion template formation of the supramolecular architecture (see Figure 4-2).

Given the versatility demonstrated by the CuAAC "click" chemistry reaction, it was decided to synthesise synthons containing alkyne and azide functionalities. These molecules could be eventually coupled to form macrocyclic structures while offering a versatile platform to be used as a possible starting point for the preparation of other more complex chemical architectures. In order to try to preserve the thermodynamic and kinetic stability of the lanthanide complex, it was chosen to maintain the DOTA-like structure of the ligand, and to functionalise it with alkyne containing arms in trans- position on the cyclen scaffold. This would form a cavity upon formation of the final macrocycle that could be exploited for host-guest binding studies. Similarly, the azide-functionalised organic synthons would have the ability to form supramolecular structures through host-guest interactions. Figure 4-2 shows a sketch of the possible molecular architectures obtainable from such synthons.

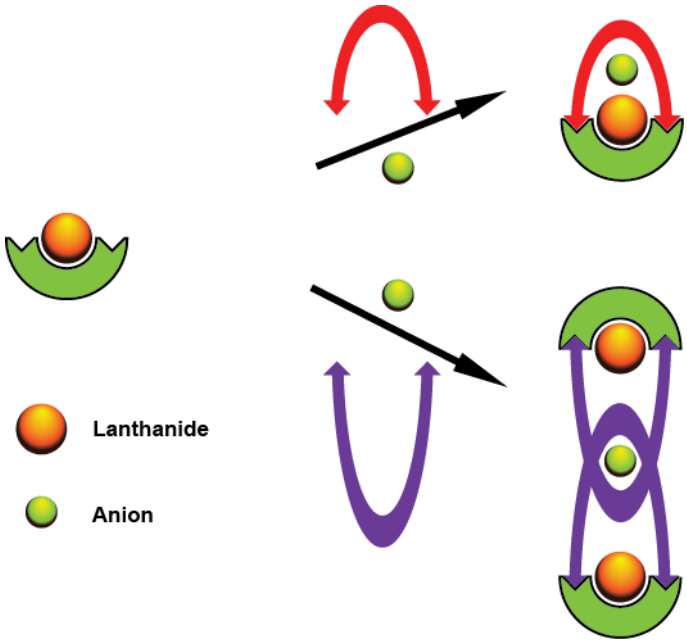


Figure 4-2. Sketch of the possible structures that can potentially be obtained starting from alkyne and azide functionalised synthons.

4.2 Preparation of the lanthanide complexes

4.2.1 Synthesis

Figure 4-3 shows the synthesis adopted for the formation of a C_2 symmetric lanthanide complex. Initially, cyclen was selectively protected in *trans*- positions using benzylchloroformate following a literature procedure.[2] Alkylation with *tert*-butylbromoacetate was achieved using standard nucleophilic substitution conditions. The product **4.4** was obtained in high yield upon recrystallization or purified by silica gel chromatography. The carbamate protecting groups were then cleaved by hydrogenation using Pd/C as catalyst yielding the *tert*-butyl DO2A quantitatively. The use of benzylchloroformate allowed for mild deprotection conditions so that the *tert*-butyl protecting groups were preserved upon hydrogenation.

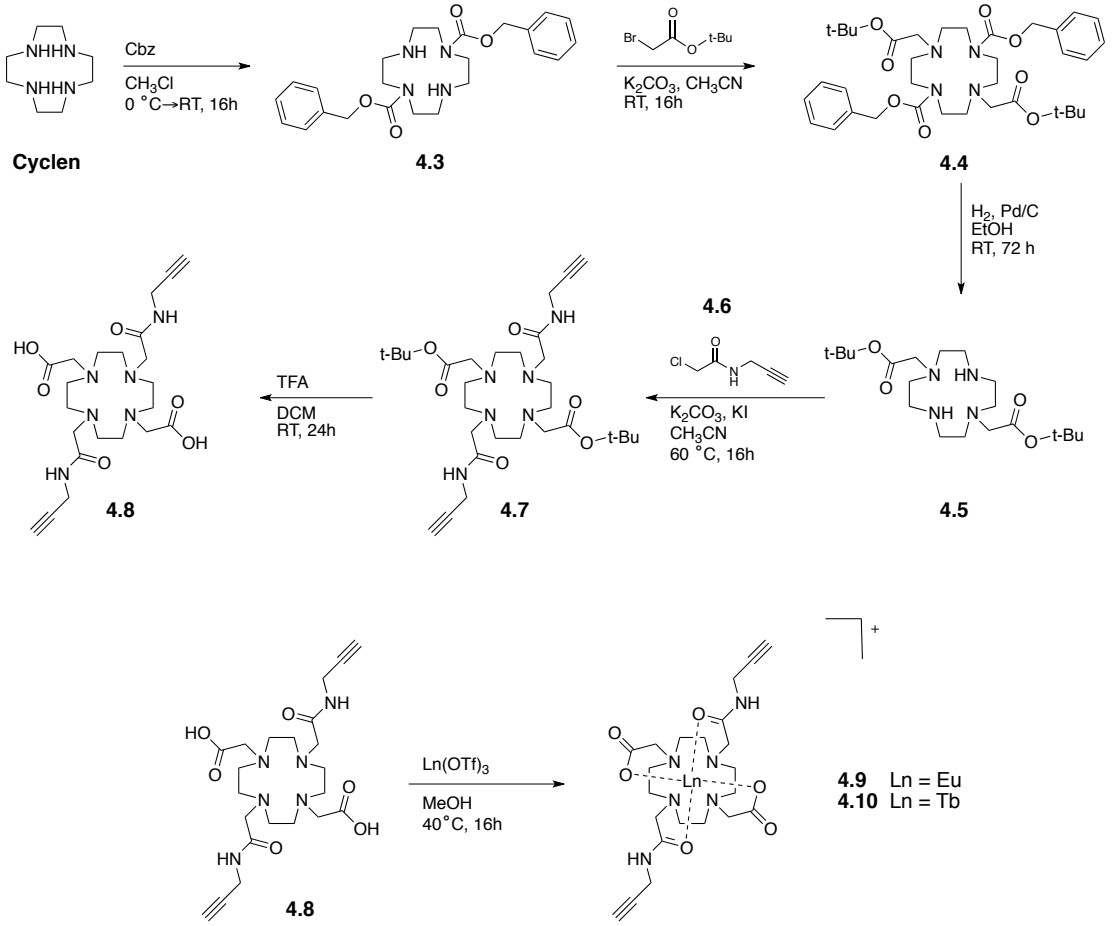


Figure 4-3. Synthetic procedure followed for the preparation of the lanthanide complexes in this chapter.

Reaction of chloroacetyl chloride with propargylamine afforded the alkyne-containing acetamide **4.6** that was used to alkylate the two free positions on the cyclen macrocycle. Heating and addition of a catalytic amount of potassium iodide were necessary in this case, as the reaction seemed to proceed otherwise slowly or not to reach completion. Column chromatography could be used to purify the crude mixture although the yield of the purified product was unsatisfactory. Instead, purification was achieved by recrystallization from chloroform and hexane resulting in reasonable yield (40 to 50 %). This method also resulted in formation of crystals suitable for X-ray analysis.

The crystal structure, solved by Dr Michael Jones, shows a high degree of symmetry and multiple intra- and inter- molecular interactions. A hydrogen bond is present between the N-H on the acetamide arm and the nitrogen atom on the cyclen backbone (2.220 Å). Also, another hydrogen bond interaction is observed in the crystal structure, between the terminal acetylide proton and the oxygen atom of the amide group of an adjacent molecule (2.237 Å).

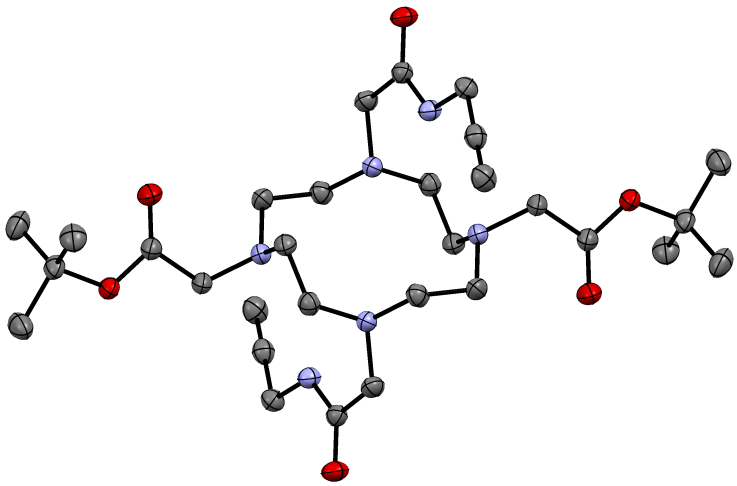


Figure 4-4. Representation of the solid state structure of **4.7** as ORTEP depiction with thermal ellipsoid displayed at 50% probability and the hydrogen atoms and solvent molecules omitted for clarity

The symmetry of the structure is also reflected in solution, giving rise to sharp and well resolved peaks in the ^{1}H-NMR spectrum even at ambient temperature, in contrast

to the often broad peaks observed for chemically similar systems with broken symmetry structures (see previous chapters).

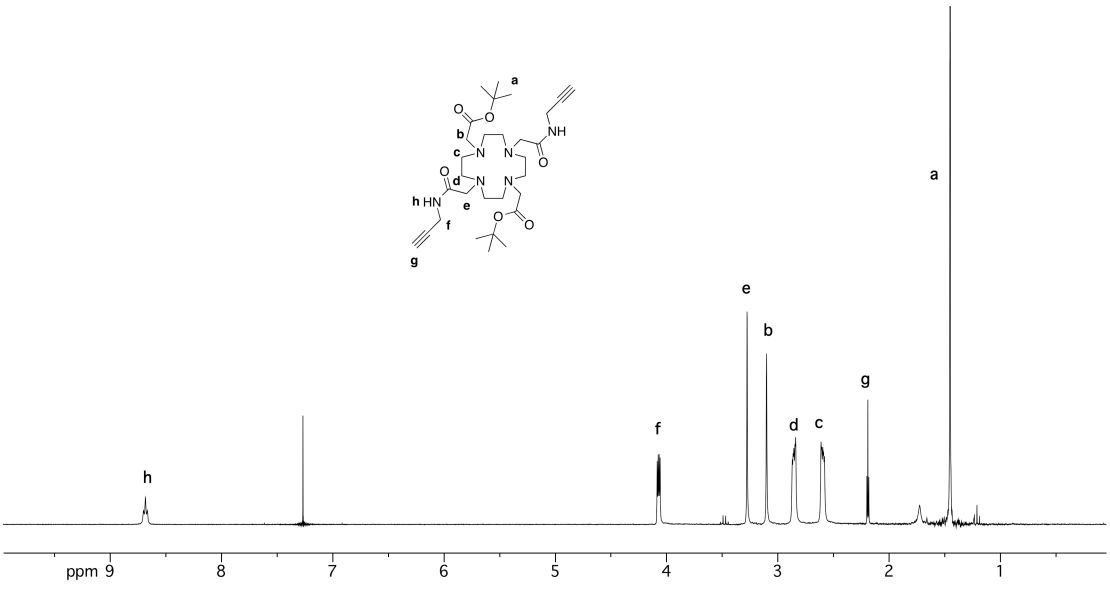


Figure 4-5. ^{1}H-NMR spectrum and peak assignments of the protected ligand **4.7** registered in $CDCl_3$ at RT.

The final cleavage of the *tert*-butyl groups was achieved by treatment with trifluoroacetic acid in dichloromethane to afford the ligand **4.8** quantitatively. In this case, the broad peaks related to the macrocycle protons observed in the ^{1}H-NMR suggest a higher degree of freedom of the structure upon deprotection, while the absence of the –NH triplet is a consequence of proton-exchange with the solvent (see Figure 4-6).

Lanthanide complexes were obtained upon mixing of the free ligand **4.8** with the corresponding lanthanide ions as their triflate salts in methanol upon gentle heating. A slight excess of lanthanide salt was used to ensure complete complexation, followed by basification and removal of the uncomplexed lanthanide in excess, precipitated as its insoluble hydroxide. Care was taken during this step not to adjust the pH higher than 10 (where hydrolysis of the amide groups could take place).[3]

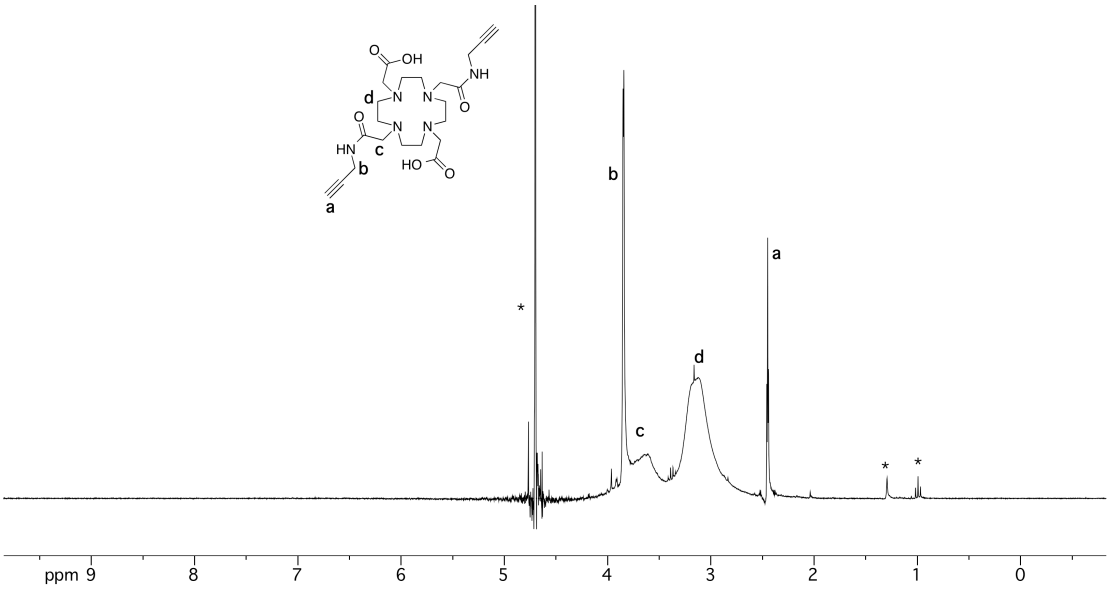


Figure 4-6. ^{1}H-NMR spectrum and peak assignments of the ligand **4.8** registered in D_2O at RT. All cyclen protons although inequivalent, give rise to the broad peak denoted with "d". * indicates residual solvent peaks.

The complexes were characterised by paramagnetic ^{1}H-NMR, mass spectrometry and luminescence spectroscopy. The accurate electrospray mass spectra are in very good agreement with the calculated isotope model, as can be seen from Figure 4-7, and show the characteristic isotope distribution of the corresponding lanthanide.

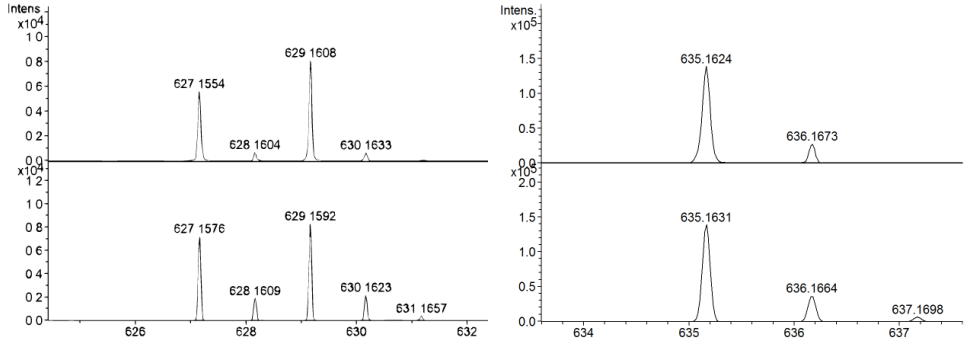


Figure 4-7. Experimental (top) and theoretical (bottom) isotopic pattern for complexes **4.9** (left) and **4.10** (right).

4.2.2 NMR spectroscopy characterisation

From the analysis of the paramagnetic ^{1}H-NMR it can be clearly observed that the effect of the presence of the metal ion is that of structure rigidification, where the macrocycle is "blocked" in only one conformation, namely the SAP, as confirmed by the highly shifted signal in the region of 30 ppm for the europium complex. Resonances indicating the presence of TSAP can also be observed in the spectrum around 10 ppm and account for less than 5% by peak integration compared to the predominant SAP species.

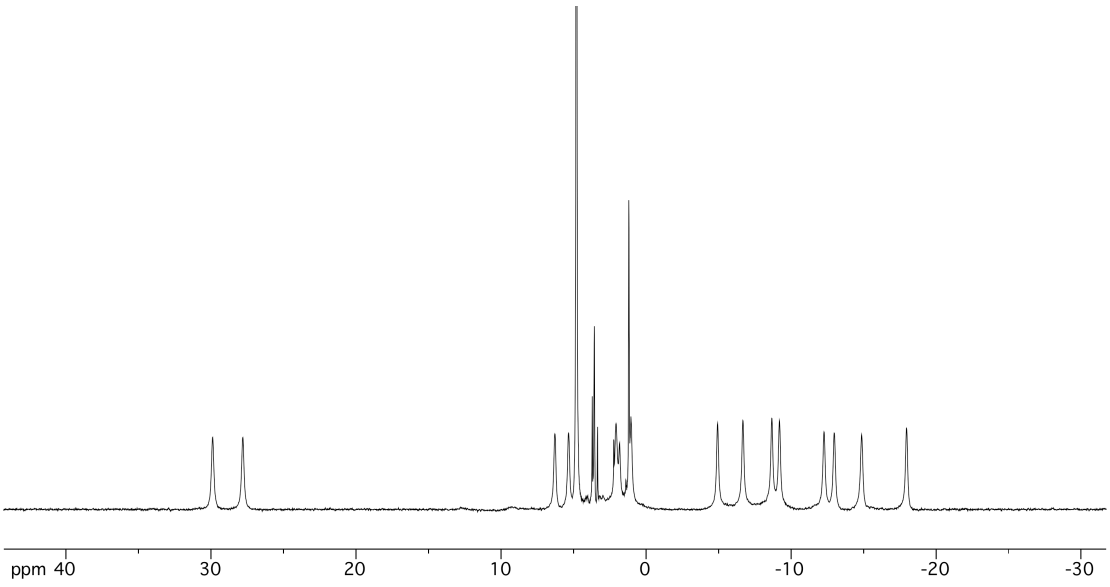


Figure 4-8. ^{1}H-NMR spectrum of the Eu(III) complex **4.9** registered in D_2O at RT.

Similarly, the Tb(III) complex **4.10** shows the same behaviour in solution as indicated by the ^{1}H-NMR spectrum, where the SAP isomer is the predominant species and the TSAP accounts for less than 10 %. From the two spectra it can be noticed the resonances corresponding to the axial ring protons have opposite sign (ca. +30 ppm for **4.9** and ca. -350 ppm for **4.10**) This derives from the overall opposite sign of the pseudocontact shift contribution for these ions in Bleaney's equation. The overall symmetry of the complexes is reflected in the much simpler spectrum when compared to ^{1}H-NMR profiles of previously presented complexes based on a DO3A ligand.

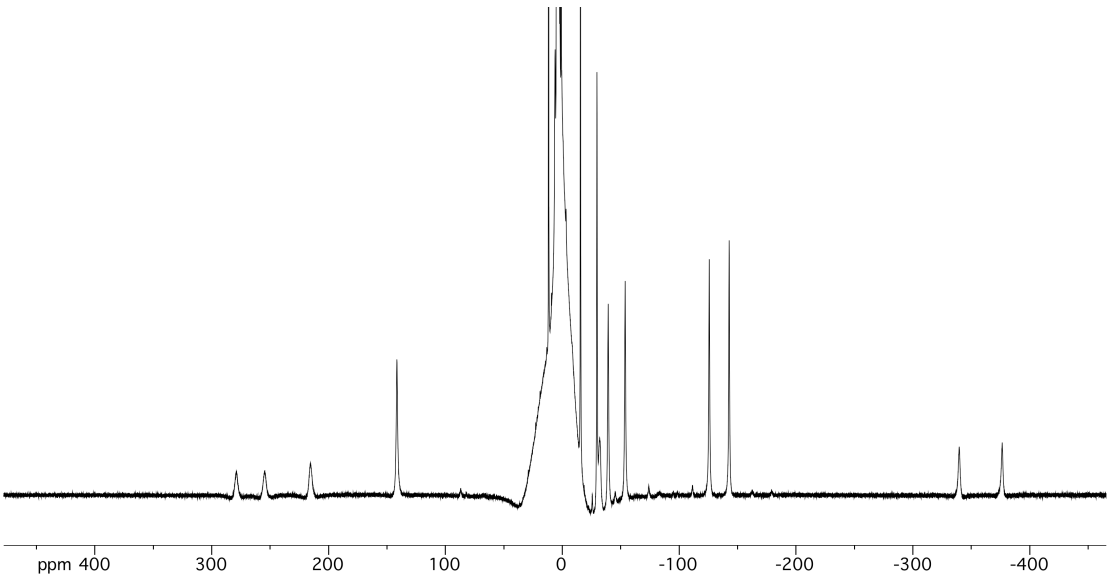


Figure 4-9. ^{1}H-NMR spectrum of the Tb(III) complex **4.10** registered in D_2O at RT.

4.2.3 Photophysical characterisation

The Eu(III) and Tb(III) complexes **4.9** and **4.10** were also characterised by steady state and time-dependent fluorescence spectroscopy. Given the absence of an organic group that could be used as a sensitising chromophore, excitation was directly into the lanthanide ion manifold. From analysis of the steady state fluorescence spectrum of the europium analogue, as shown in Figure 4-10, further details about the structure adopted by this class of complexes in solution can be deduced. In particular, the overall shape and splitting of the ΔJ_1 transition is diagnostic of a low symmetry around the lanthanide centre for the Eu(III) analogue **4.9**, while the ΔJ_2 transition is in this case determined by ligand donor polarisability.

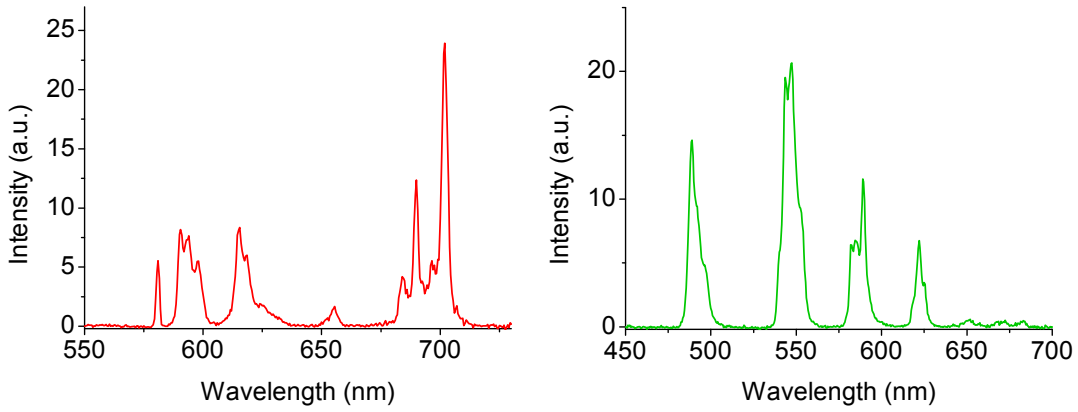


Figure 4-10. Emission spectra of **4.9** (left) and **4.10** (right) obtained upon direct excitation at 396 nm and 355 nm respectively.

Measurements of the excited state lifetimes in H_2O and in D_2O were performed in order to assess the hydration number of the complexes in solution using the modified Horrocks' equation:[4, 5]

$$q_{Eu} = 1.2 \cdot (k_H - k_D - 0.25 - 0.075 \cdot n_{NH}) \qquad (4.1)$$

$$q_{Tb} = 5 \cdot (k_H - k_D - 0.06) \qquad (4.2)$$

In this equation, n_{NH} is the number of NH oscillators in close proximity to the lanthanide ion, they are included in the equation in order to take into account their effect in the non-radiative quenching of the metal centred excited state; k is the inverse of the lifetime. Table 4-1 reports the hydration number obtained applying this equation. There is only one residual water molecule saturating the coordination sphere of the lanthanide ion, confirming that all four arms are coordinating to the metal. Indeed, as expected, the ligand provides an octadentate "cage" in which the lanthanide is encapsulated and one solvent molecule saturates the ninth axial coordination site.

Table 4-1. Excited state lifetime values of the Eu(III) and Tb(III) ion in complexes **4.9** and **4.10**, in H_2O and D_2O with the corresponding hydration number "q" associated. The complexes were excited at different wavelengths corresponding to the maxima found in the excitation spectra.

Compound	λ_{ex}/nm	λ_{em}/nm	τ_{H2O}/μs	τ_{D2O}/μs	**q**
4.9	395	616	530	2130	1.2
	318	616	480	1560	1.3
4.10	355	545	1570	2800	1.1
	380	545	1550	3020	1.3
	488	545	1720	3180	1.0

The values of lifetimes of both europium and terbium are in line with the ones reported in the literature for complexes based on DOTA and DOTAM structures.[6-11] Furthermore, from the analysis of the emission profile of the excited state as a function of time, a mono-exponential behaviour is observed, indicating the presence of only one species in solution (see Figure 4-11).

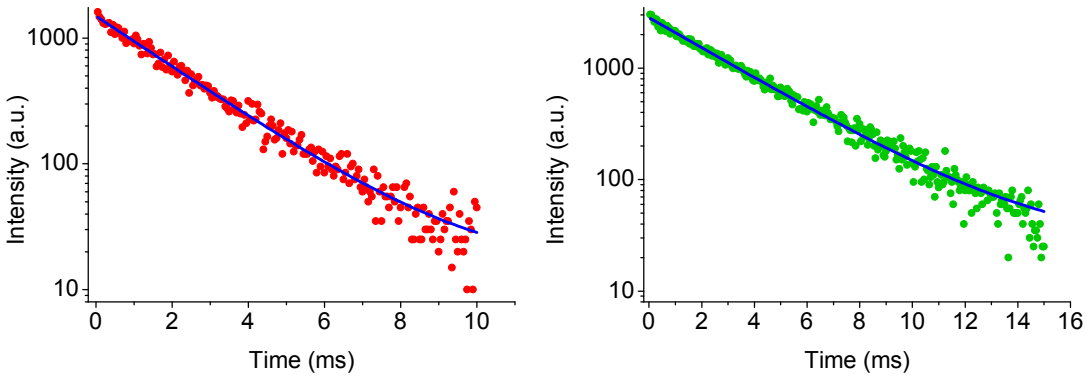


Figure 4-11. Time-resolved emission profile of complexes **4.9** (left) and **4.10** (right) in D_2O represented on a logarithmic scale of the intensity.

4.3 Preparation of organic synthons containing azide functional groups

4.3.1 Synthesis

In order to obtain the macrocyclic structure as described earlier, it was reasoned that the organic based synthon should have a fluxional structure in solution; this would facilitate its organisation around the lanthanide-containing core. It has been demonstrated that structures based on the isophthalamide group fulfill this criterion, and are also amenable to preorganisation through interaction with ions such as chloride in the isophthalamide cavity.[12-15] Indeed, by the exploitation of this anion templation effect, several macrocyclic structures have been reported in the literature, with improved yield over the non-templated synthesis and minimisation of polymeric byproducts.[16, 17] Compound **4.17** was then chosen as the target molecule, where the presence of the N-oxide would enhance the interaction of the isophthalamide N-H donors with anions through inductive effect.

The synthetic strategy adopted is shown in Figure 4-12. The hydroxyl groups of the hydroquinone derivative **4.11** were first activated by reaction with methanesulfonyl chloride. The latter was preferred to the toluensulfonyl derivative since excess of reagent could easily be removed, given its low boiling point, although the reaction

required dry solvent and inert atmosphere conditions. Reaction with sodium azide under standard S_N2 conditions yielded the bis-azide product in high yield (>90%).

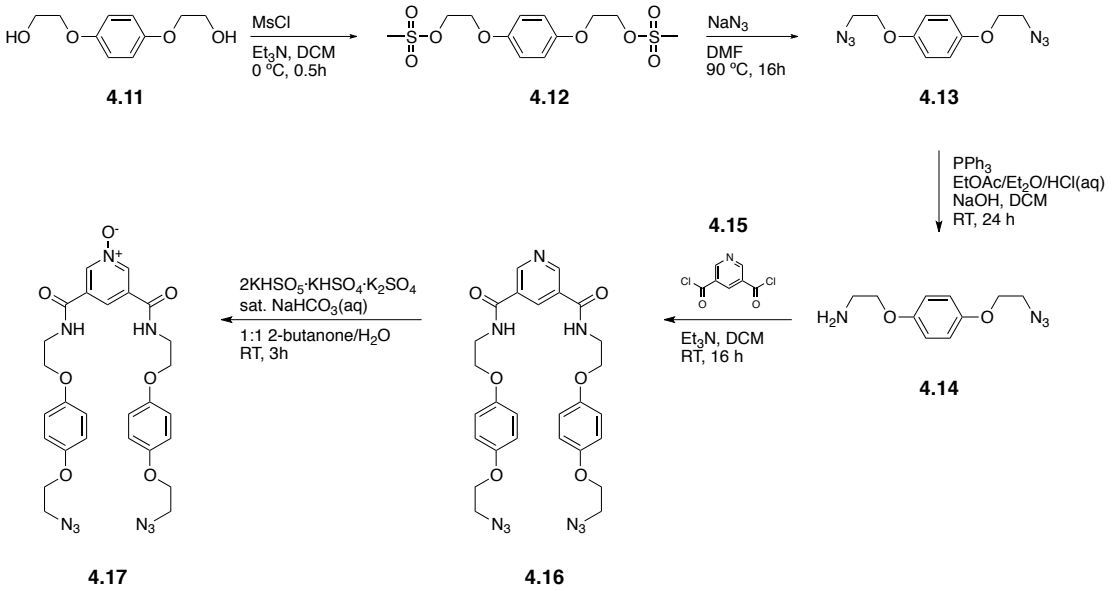


Figure 4-12. Schematic description of the synthesis of the azide-containing synthon.

This was converted to its partially reduced azido amine analogue by the Staudinger reaction with triphenylphosphine in a biphasic mixture. In this reaction, once the first amino group forms, it is protonated by the HCl present in the reaction mixture rendering the monoreduced form (**4.14**) soluble in the aqueous phase. This strategy minimises further reduction to the unwanted bis amino species, since the target compound is sequestered into the aqueous phase as soon as it forms. The water phase could then be neutralised with base and extracted in DCM. Comparison of the ^{1}H-NMR clearly shows the formation of the product with the appearance of two new sets of resonances characteristic of the broken symmetry system (Figure 4-13).

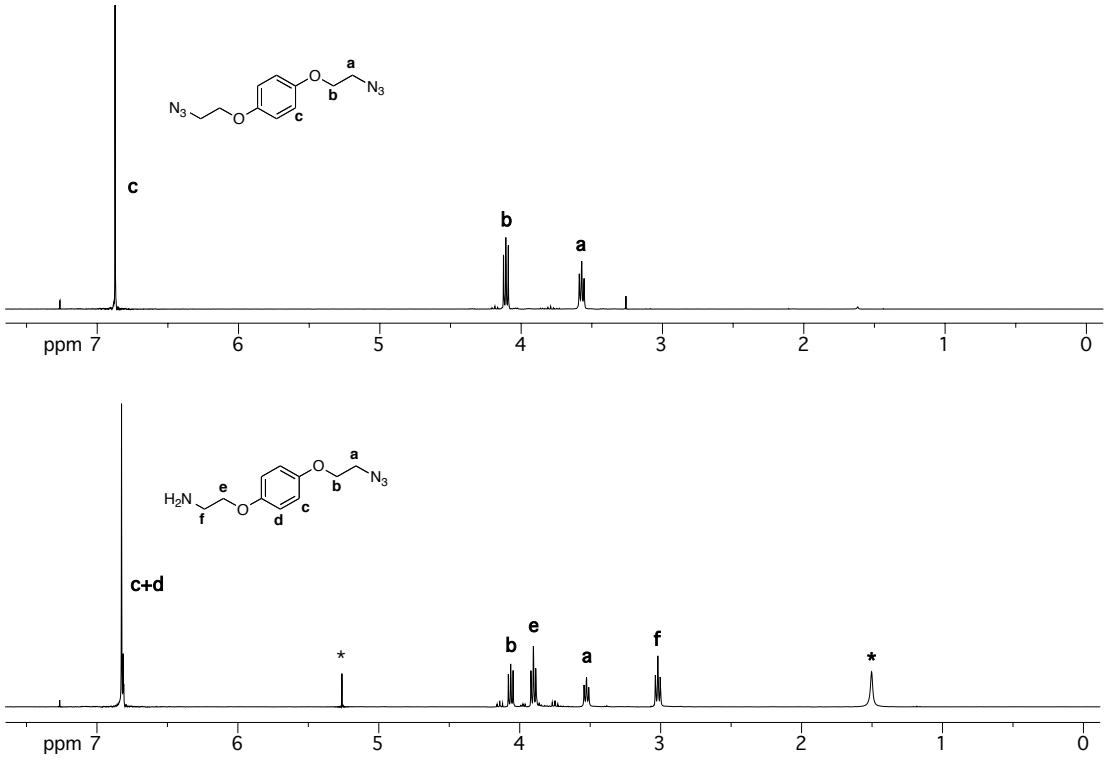
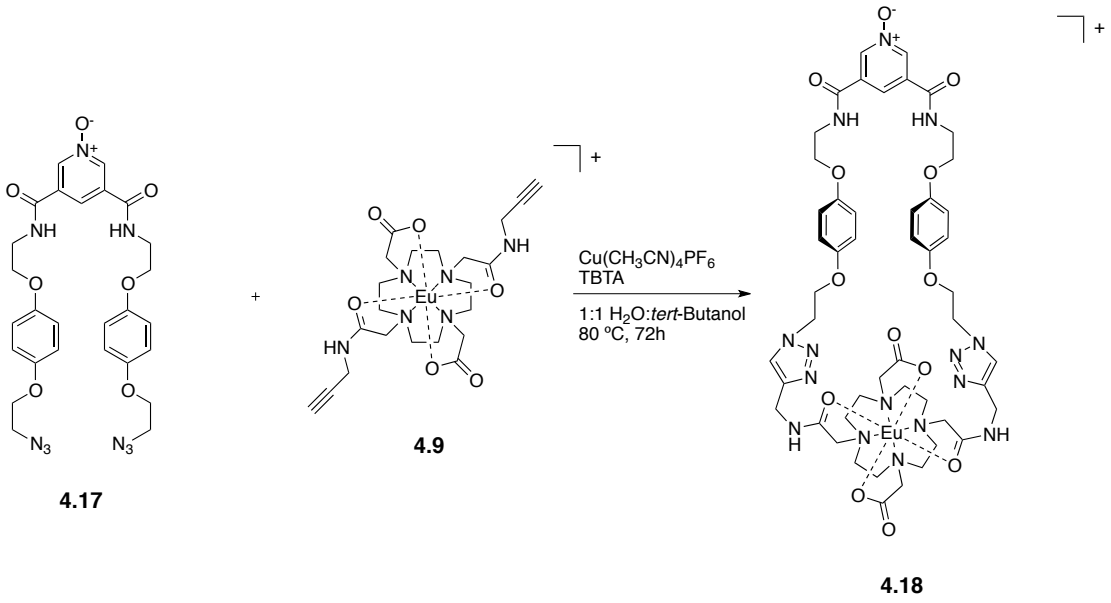


Figure 4-13. Comparison of the ^{1}H-NMR of **4.13** and **4.14** registered in $CDCl_3$ at RT. * denotes a residual solvent peak.

Reaction of **4.14** with the acid chloride (**4.15**), derived from 3,5-pyridine dicarboxylic acid, afforded **4.16,** which was itself then converted to its N-oxide derivative (**4.17**) in very high yield (~90%) by reaction with Oxone®.

4.4 Attempted synthesis of the macrocycle



4.17 4.9 4.18

Figure 4-14. Description of the attempted synthesis of the macrocyclic structure containing a lanthanide chelate.

Figure 4-14 presents the synthetic procedure used for the synthesis of the macrocyclic structure containing a lanthanide complex. The reaction was carried out using high dilution conditions, keeping the concentration of each solute below 1 mM in order to minimise the formation of polymeric by-products. In this case, the solvent mixture used was the original reported by Sharpless and co-workers, as it gave good solubility of all components.[18] $Cu(MeCN)_4PF_6$ was used as source of Cu(I), given the positive outcome for the lanthanide-rotaxane coupling reaction, together with catalytic amount of TBTA. The reaction proceeded somewhat slowly and heating was necessary to render everything soluble. The reaction was monitored by ES-MS and, though formation of the product could be observed after 12 hours, no quantitative estimate of the yield of the reaction could be made by this technique. The molecular ion at 1220 m/z was observed together with the adduct with one water molecule and a double ionised species with detected at a value of 906 m/z that might correspond to the macrocycle with an additional thread as depicted in Figure 4-15. Attempts to purify the product by chromatography or recrystallisation were ultimately unsuccessful.

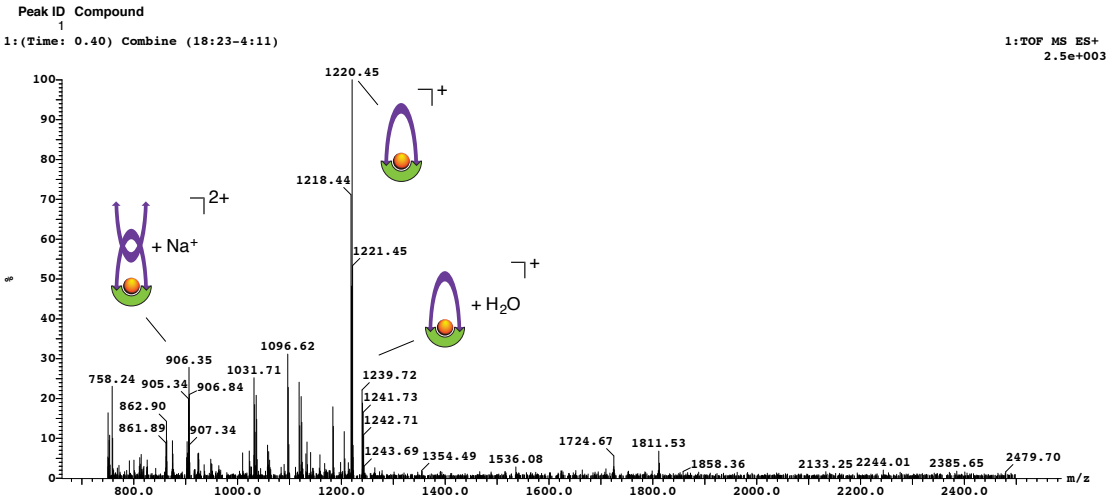


Figure 4-15. Qualitative ESMS spectrum of the ongoing reaction mixture to form **4.18**.

4.5 Conclusions

A family of kinetically stable lanthanide complexes containing two alkyne units has been prepared and their behaviour in solution has been studied by NMR and fluorescence spectroscopy. These can serve as platform for the formation of potential anion binding receptor where the binding ability is improved exploiting the strength of the anion-lanthanide interaction and the selectivity given by a size specific cavity. Steps towards the preparation of this class of compounds have been taken, with the synthesis of azide functionalised organic synthons that have the potential to form the aforementioned anion binding cavities and that are amenable to be exploited also for the formation of supramolecular structures such as catenanes, in which the lanthanide complex is directly exploited in the binding process. A preliminary reaction to form a prototype of this class of molecules was attempted and, although the product could not be isolated, the observation of molecular ions consistent with a successful "clicking" constitutes a promising preliminary result upon which to build with future experiments.

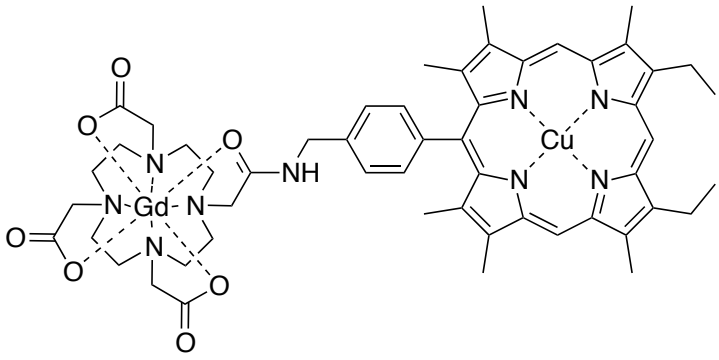
4.7 References

1. L. M. P. Lima, A. Lecointre, J.-F. Morfin, A. de Blas, D. Visvikis, L. J. Charbonnière, C. Platas-Iglesias and R. Tripier, *Inorg. Chem.*, 2011, **50**, 12508-12521.
2. L. M. De León-Rodríguez, Z. Kovacs, A. C. Esqueda-Oliva and A. D. Miranda-Olvera, *Tetrahedron Lett.*, 2006, **47**, 6937-6940.
3. L. S. Natrajan, A. J. L. Villaraza, A. M. Kenwright and S. Faulkner, *Chem. Commun.*, 2009, 6020-6022.
4. A. Beeby, I. M. Clarkson, R. S. Dickins, S. Faulkner, D. Parker, L. Royle, A. S. de Sousa, J. A. G. Williams and M. Woods, *J. Chem. Soc.-Perkin Trans. 2*, 1999, 493-503.
5. W. Horrocks Jr and D. Sudnick, *J. Am. Chem. Soc.*, 1979, **101**, 334-340.
6. A. Beeby, S. Faulkner, D. Parker and J. A. G. Williams, *J. Chem. Soc. Perkin Trans. 2*, 2001, 1268-1273.
7. R. A. Poole, C. P. Montgomery, E. J. New, A. Congreve, D. Parker and M. Botta, *Org. Biomol. Chem.*, 2007, **5**, 2055-2062.
8. B. S. Murray, E. J. New, R. Pal and D. Parker, *Org. Biomol. Chem.*, 2008, **6**, 2085-2094.
9. D. Parker, J. W. Walton, L. Lamarque and J. M. Zwier, *Eur. J. Inorg. Chem.*, 2010, **2010**, 3961-3966.
10. E. J. Shiells, L. S. Natrajan, D. Sykes, M. Tropiano, P. Cooper, A. M. Kenwright and S. Faulkner, *Dalton Trans.*, 2011, **40**, 11451-11457.
11. J. K. Molloy, O. Kotova, R. D. Peacock and T. Gunnlaugsson, *Org. Biomol. Chem.*, 2012, **10**, 314-322.
12. M. J. Chmielewski, J. J. Davis and P. D. Beer, *Org. Biomol. Chem.*, 2009, **7**, 415-424.
13. L. M. Hancock and P. D. Beer, *Chem. Eur. J.*, 2009, **15**, 42-44.
14. L. M. Hancock, L. C. Gilday, N. L. Kilah, C. J. Serpell and P. D. Beer, *Chem. Commun.*, 2011, **47**, 1725-1727.
15. N. H. Evans, C. J. Serpell and P. Beer, *Angew. Chem. Int. Ed.*, 2011, **50**, 2507-2510.
16. M. Lankshear and P. Beer, *Acc. Chem. Res.*, 2007, **40**, 657-668.
17. M. D. Lankshear and P. D. Beer, *Coord. Chem. Rev.*, 2006, **250**, 3142-3160.
18. V. V. Rostovtsev, L. G. Green, V. V. Fokin and K. B. Sharpless, *Angew. Chem. Int. Ed. Engl.*, 2002, **41**, 2596-2599.

5 Synthesis and study of heterobimetallic f-f' arrays

5.1 Introduction

The wide choice of luminescence and magnetic properties offered by lanthanide ions constitute a great potential for the engineering of molecular architectures with multiple properties. The encapsulation of two or more lanthanide ions, and in general metal ions, in the same molecular architecture offers a route to multiplexed molecular probes that can benefit from the unique features of each metal. The class of "d-f hybrids" is one example. In such systems, a Gd(III) ion can function as a contrast agent, while a transition metal can be exploited for its bright and long-lived luminescence. One of the early examples of the potential application of this class of compounds was shown by Faulkner et al. where the long-lived luminescence from Re(I) was exploited for time-gated fluorescence while offering the possibility for MRI imaging via the gadolinium centre.[1] Since then, the class of bimodal imaging agents has been enriched with many other examples, including probes exploiting ruthenium and radioisotopes for simultaneous MRI and PET imaging, when in combination with a Gd(III) chelate.[2, 3] The simultaneous detection of MRI and PET signals has been exploited by Gros and co-workers using the compound shown in Figure 5-1. Here a Gd-DO3A-AM motif is linked to a ^{64}Cu-containing porphyrin core in order to yield a probe that can be potentially used for simultaneous PET and MRI imaging.[4] Other authors have made use of two or more metal ions to confer MRI and PET or SPECT capabilities to the final contrast agent and several examples are indeed present in the literature.



5.1

Figure 5-1. A molecular probe as a potential contrast agent for bimodal imaging.

The different coordination requirements of d and f block ions, and the kinetic stability of low spin d^6 transition metal complexes have ensured that the field of heterometallic complexes containing lanthanides has been dominated by d-f hybrids, where different metal ions served as the discriminating factor for two or more different organic binding domains. By contrast, the selective formation of hetero-multimetallic lanthanide complexes is still very challenging. Indeed, the lack of steric requirements and the binding similarity among the lanthanides renders the synthesis of purely lanthanide containing multimetallic arrays a daunting task. This is especially the case with pre-organised organic scaffolds, where selectivity can only be achieved based on the difference in the ionic radii. By exploiting this principle and using an unsymmetrical ditopic ligand consisting of two different binding units, Bünzli and co-workers reported a heterobimetallic helicate where up to 90% yield was achieved for the formation of the purely heterobimetallic complex containing the La-Lu couple, while adjacent lanthanide ions such as Eu(III) and Tb(III) simply gave a statistical mixture (see Figure 5-2).[5]

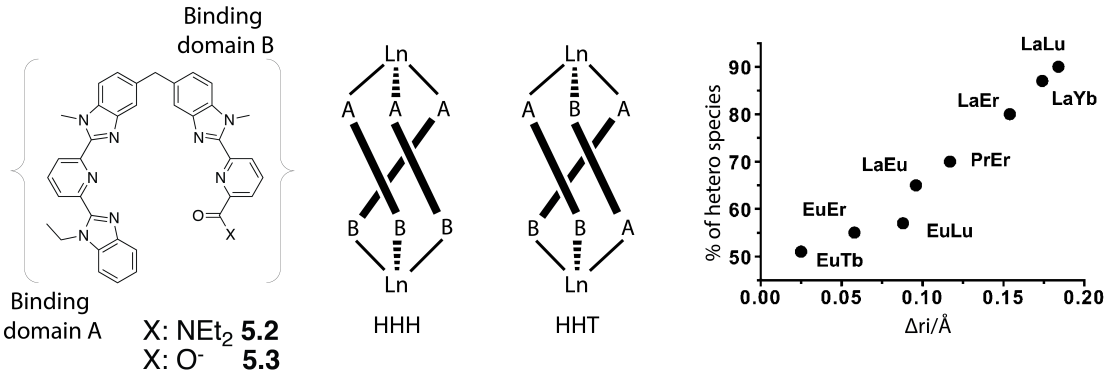


Figure 5-2. Molecular structure of the ditopic ligand used by Bünzli et al. for the formation of heterobimetallic lanthanide complexes. Adapted from Ref. 5.

Although effective in this particular case, this method is solely based on differences in the ionic radii of the metals, and cannot be used for neighbouring lanthanides such as Eu(III), Gd(III) or Tb(III), possibly the most useful among them for the preparation of heteromultimetallic probes.

It is then clear that, in order to obtain a heteromultimetallic lanthanide complex, different synthetic strategies must be employed. These rely on the use of lanthanide complexes as chemical building blocks that are stable under the reaction conditions employed. This approach was first used by Faulkner et al. exploiting kinetically stable 4-aminobenzylDO3A complexes as building blocks (Figure 5-3). Reaction with DTPA anhydride, followed by addition of a second lanthanide ion, which binds in the DTPA diamide pocket, afforded a pure f-f' heterobimetallic system.[6]

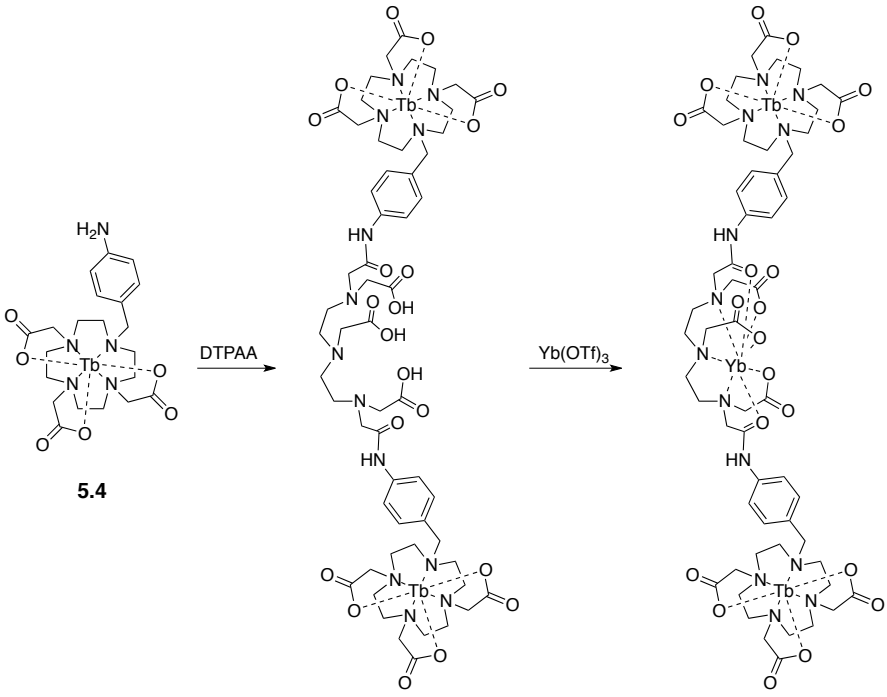


Figure 5-3. Strategy used by Faulkner et al. for the formation of heteromultimetallic complexes from lanthanide chelates used as building blocks.

Using a similar approach, the synthesis of a tetranuclear bimetallic complex was achieved through diazotisation, a synthetic approach that further illustrates the importance of the use of stable complexes as starting materials (see Figure 5-4).[7]

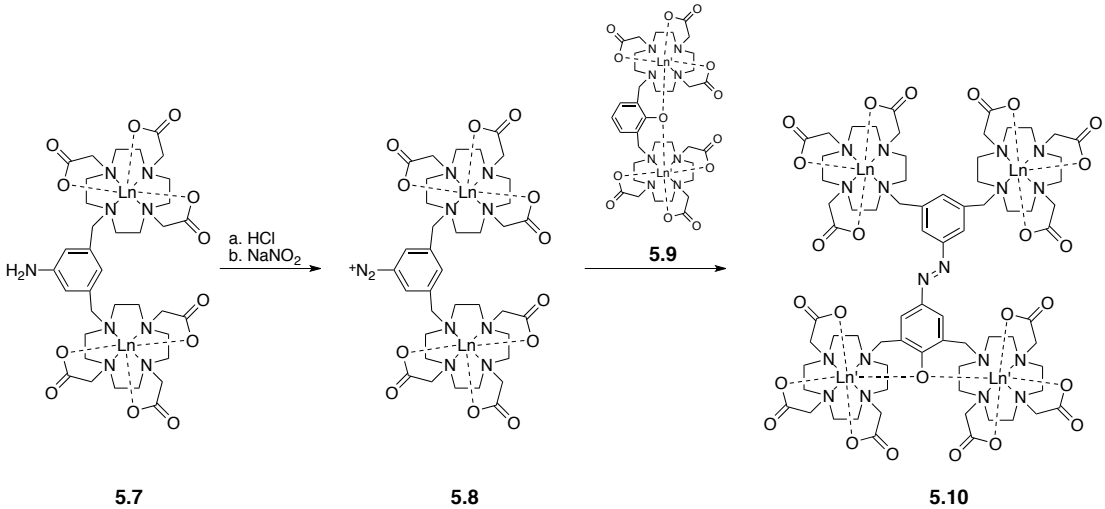


Figure 5-4. Formation of a heterotetrametallic lanthanide complex by diazotisation from two bimetallic building blocks.

A sequential metallation approach was instead used by Sames et al. in which the authors exploited the lability of lanthanide complexes of DTPA under acidic conditions. Here DOTA and DTPA binding pockets were first metallated with the same lanthanide ion; this was then followed by selective DTPA demetallation under acidic conditions while leaving the DOTA complex "untouched". Finally the DTPA pocket could be metallated again using a different lanthanide yielding a pure heterobimetallic f-f' complex as shown in Figure 5-5.[8]

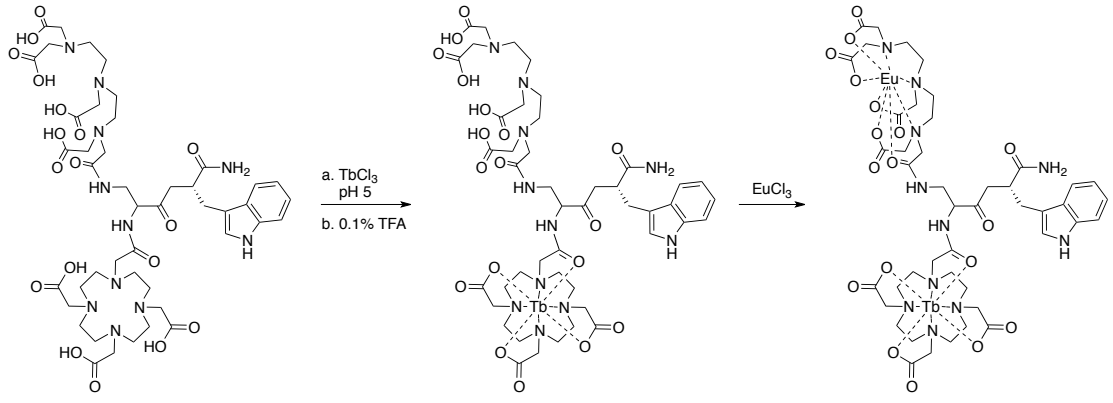


Figure 5-5. Synthetic strategies adopted by Sames et al. for the selective formation of heterobimetallic lanthanide complexes exploiting the kinetic lability of DTPA under acidic conditions.

Another strategy relies on the orthogonal protection approach employed by Faulkner et al.[9] In this case the authors showed that the order of deprotection is critical to avoid metal catalysed hydrolysis of the bound carboxamide in basic conditions. However this approach has limited use given the high number of synthetic steps and consequent low overall yield.

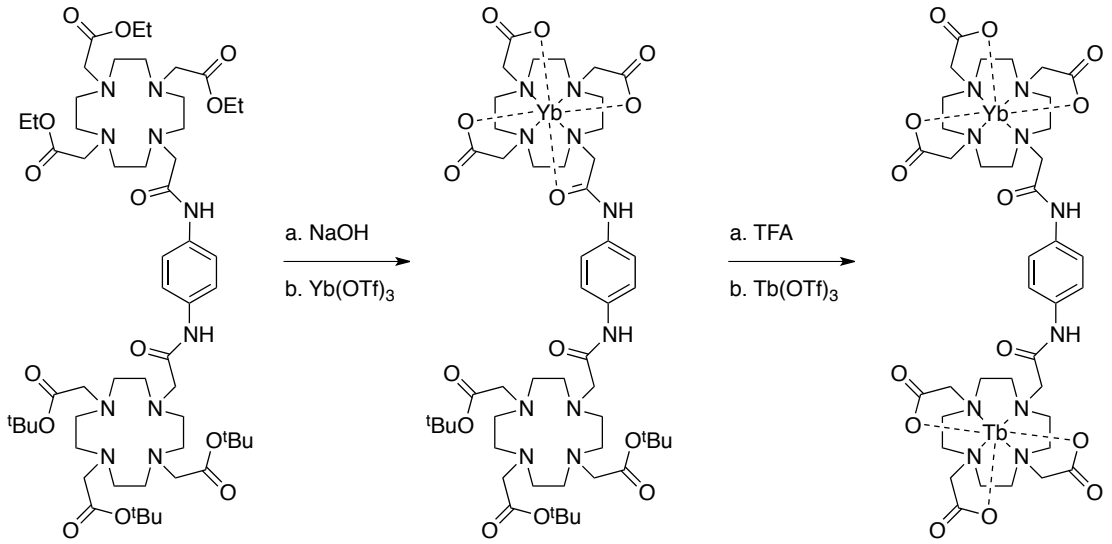


Figure 5-6. An alternative approach for the encapsulation of two lanthanides in identical binding pockets, exploiting orthogonal protection of the carboxylic groups on the ligands.

In this chapter a building block strategy will be employed for the formation of a class of purely heterobimetallic lanthanide complexes from readily available starting materials. By means of a "click" chemistry approach a series of heterobimetallic complexes are formed. In particular, the effect on the luminescence and NMR properties, given by two different metals in the same molecular structure, are elucidated.

5.2 Synthesis and characterisation of azido-appended complexes

5.2.1 Introduction

As mentioned above, the use of lanthanide complexes as building blocks would certainly be advantageous for the development of structurally diverse architectures containing different lanthanide ions. Also, a strategy for the straightforward formation of pure hetero-multimetallic complexes would be highly desirable, especially if the starting building blocks are easy to obtain and widely exploitable in a different range of applications. The need to use harsh reaction conditions with a consequent possible demetallation of one or more metal complexes is certainly to avoid while mild reaction conditions, short reaction time and high yield of product formation are highly desirable features. A "click" chemistry approach was chosen, given our familiarity with using this reaction with alkyne substrates. Given the availability of the already mentioned class of alkyne appended lanthanide complexes, it was reasoned that a class of complexes containing an orthogonal azide group could constitute a useful synthon. Few examples of azide-appended lanthanide complexes are present in the literature and none of them contains a chromophore.[10, 11]

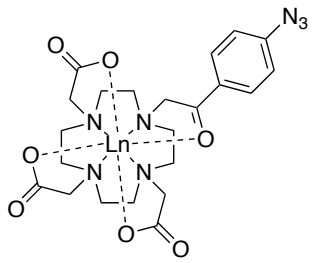


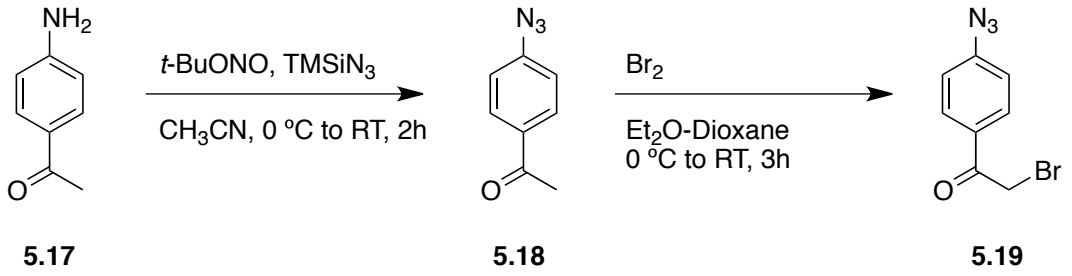
Figure 5-7. Target lanthanide complex containing an azide group appended to a chromophore.

The target molecule is depicted in Figure 5-7. This comprises a ketone moiety for direct coordination to the metal centre and an azido group linked to the aryl chromophore. It was envisaged that this structure could allow not only the further derivatisation of the molecule but also direct, through-bond communication between the two lanthanide centres in the heterobimetallic complex. Furthermore, while the

eight donor atoms on the ligand scaffold would provide increased stability, the presence of a chromophore would help to better understand the photophysical behaviour of the heterobimetallic complex in solution.

5.2.2 Synthesis

4-Azido acetophenone is a commercially available compound but it is only sold in milligram quantities and at high price: hence its synthesis was achieved starting from the inexpensive 4-aminoacetophenone using the general method reported by Moses et al.[12] The conversion of the amino group was achieved by treatment with *tert*-butyl nitrite to generate a diazonium salt *in situ*, followed by addition of azidotrimethylsilane. The product was isolated after washing with cold hexane in almost quantitative yield.



5.17 **5.18** **5.19**

Figure 5-8. Description of the synthesis of azidophenacyl bromide.

The bromination step to obtain azidophenacyl bomide was initially conducted in dichloromethane or chloroform in the presence of stoichiometric amount of molecular bromine as reported previously.[13] These conditions did not seem to produce any appreciable conversion to the target compound. Addition of catalytic amounts of aluminium trichloride to the reaction mixture mainly afforded the dibrominated product, and attempts to control the reaction by dropwise addition of Br_2 or by lowering the temperature all resulted in either incomplete conversion or dibrominated product. Surprisingly, the use of N-bromosuccinimide also failed to achieve any appreciable conversion. The product was eventually obtained upon addition of molecular bromine to 4-azidoacetophenone in a diethyl ether:dioxane 2:1 (*v:v*)

mixture, and was purified by flash column chromatography. The final compound was kept in the dark as exposure to light led to decomposition.

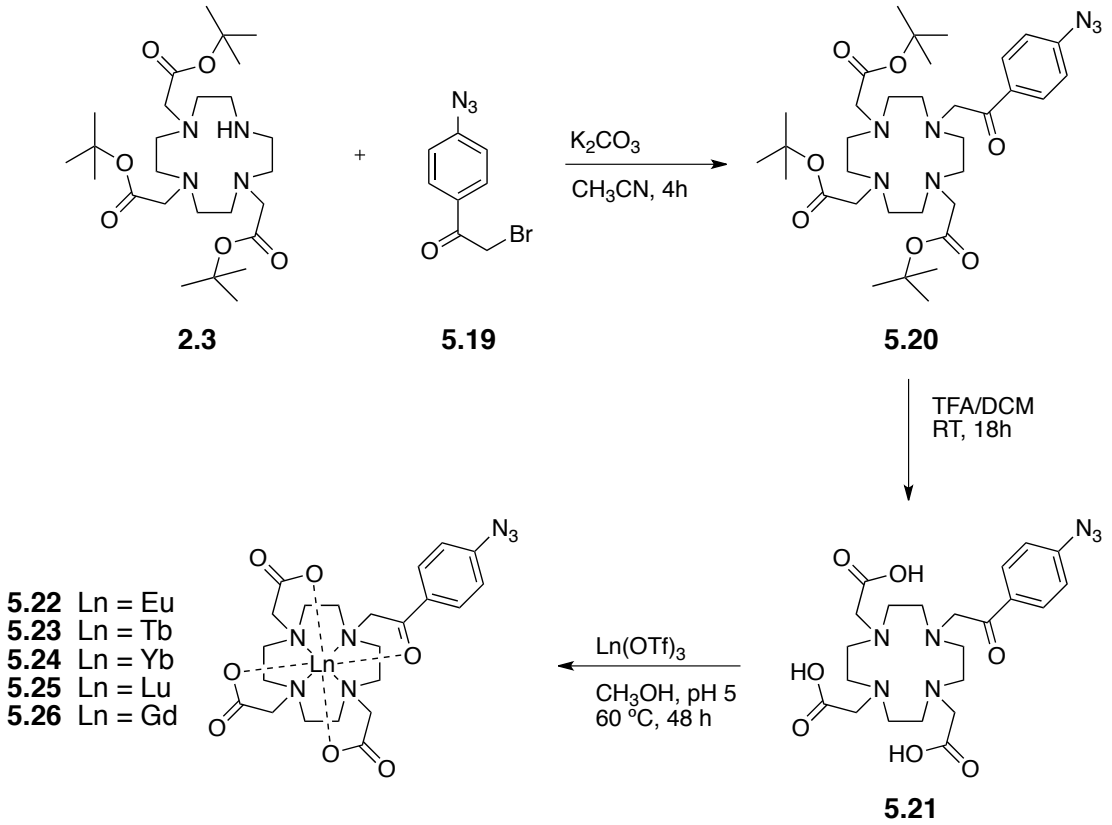


Figure 5-9. Synthetic scheme of the preparation of the azide appended lanthanide complexes.

Alkylation of the *tert*-butyl protected triester in basic conditions afforded the protected ligand **5.21**, which was isolated after purification by flash column chromatography on silica gel. Cleavage of the *tert*-butyl groups was achieved by treatment with TFA in dichloromethane. Complexation was carried out in methanol at 60 °C using the triflate salt of the appropriate lanthanide ion. Excess of lanthanide was precipitated as its insoluble hydroxide by raising the pH and filtering off the precipitate.

The metal complexes were successfully characterised by ^{1}H-NMR and accurate mass-spectrometry (see Figure 5-10). IR spectroscopy also showed the highly diagnostic peak (ca. 2100 cm^{-1}) corresponding to the presence of the azido group.

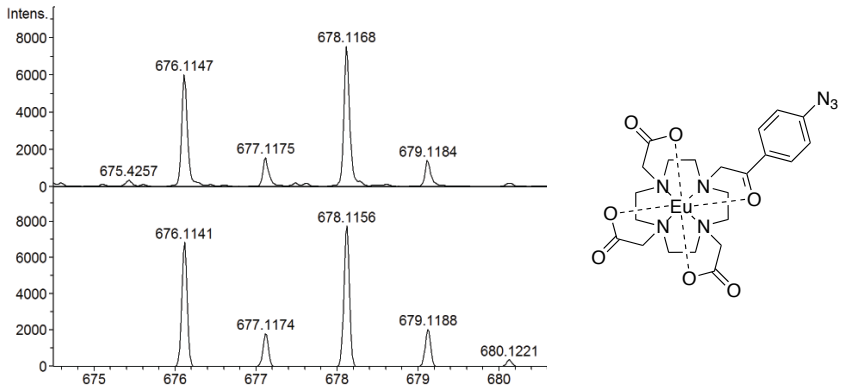


Figure 5-10. High-resolution ESMS showing the theoretical (bottom) and experimental (top) isotope distribution of **5.22**.

5.2.3 NMR spectroscopy characterisation

The ^{1}H-NMR spectrum of the europium complex **5.22** showed highly shifted resonances given the paramagnetic nature of this lanthanide ion. The four main resonances at low field represent the four different proton environment on the macrocycle backbone. The relative sharpness indicates that this is an eight-coordinate complex in which the ketone oxygen actively participates in the coordination. Indeed, variation of pH between 2 and 10 did not show any significant change in the spectrum, confirming that the complex remains in the SAP conformation and does not interchange with other structural isomers, at least on the NMR time scale (as opposed to the seven coordinate propargyl appended DO3A complexes shown in chapter 2).

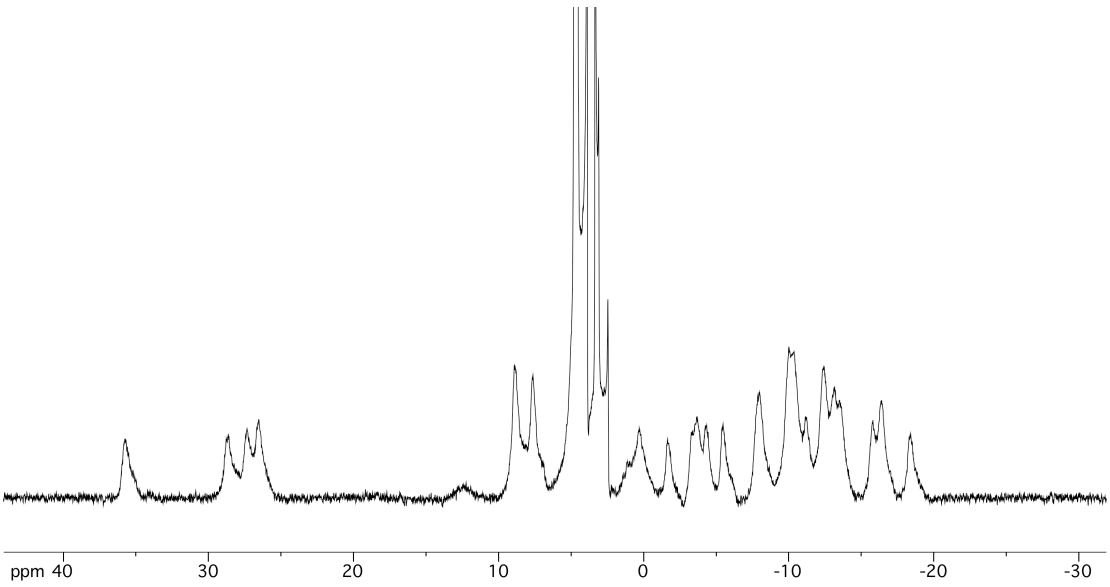


Figure 5-11. ^{1}H-NMR spectrum of **5.22** registered in D_2O at RT at pD 7.

Interestingly the ytterbium complex **5.24** gave rise to a slightly different spectrum with two sets of signals clearly arising from two distinct isomers in solution. Raising the pH to 10 resulted in the predominance of only one set of signals. This behaviour may suggest that binding of the carbonyl to the Lewis acidic lanthanide results in increased formation of the enolic form of the ligand (which might be expected to dominate at high pH). However, this must remain a hypothesis, as no similar

behaviour could be observed when the diamagnetic lutetium ion (which ought to have similar Lewis acidity) was used instead of ytterbium.

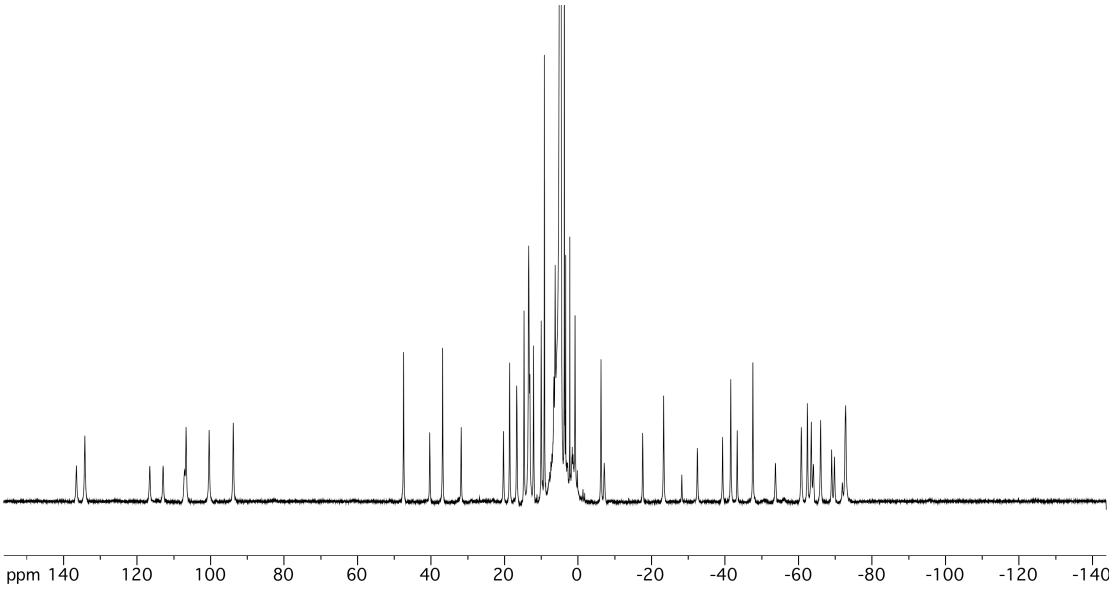


Figure 5-12. ^{1}H-NMR spectrum of **5.24** registered in D_2O at RT at pD 7.

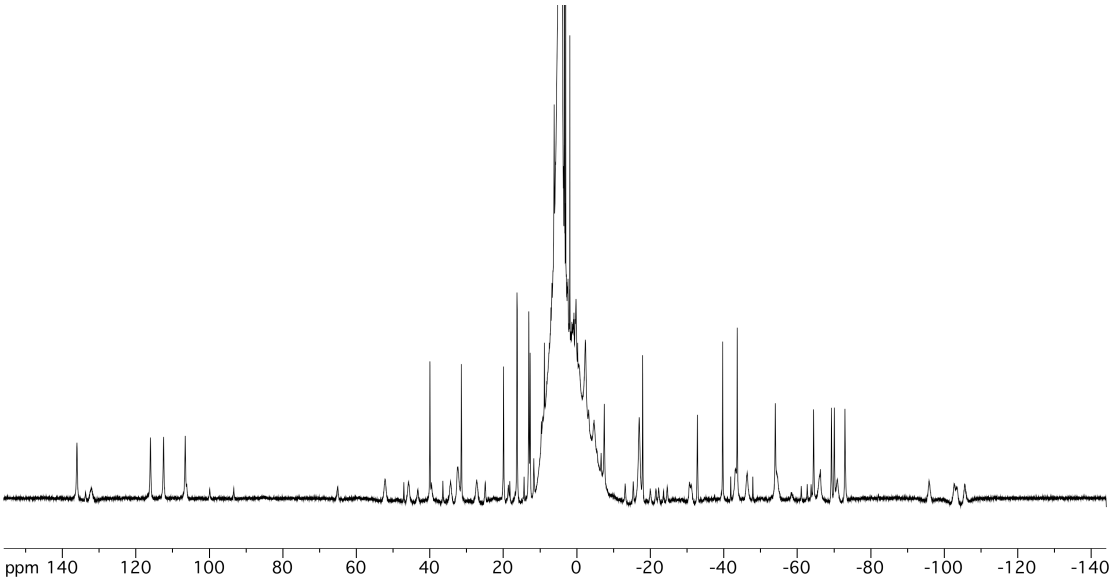


Figure 5-13. ^{1}H-NMR spectrum of **5.24** registered in D_2O at RT at pD 12.

5.2.4 Photophysical Studies

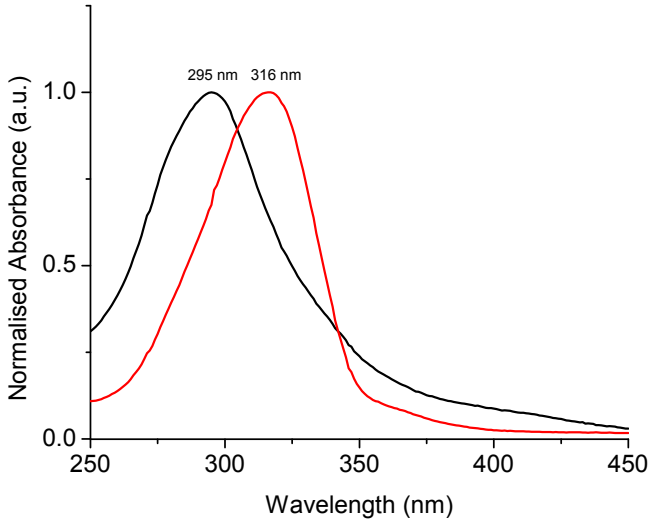


Figure 5-14. UV-Vis absorption spectrum of the ligand **5.21** and the complex **5.22** registered in H_2O.

Figure 5-14 shows the comparison of the UV-Vis absorption spectra of the ligand **5.21** and the Eu(III) complex **5.22**. The absorption spectrum of the ligand shows a strong band centred at 300 nm. This can be ascribed to an ILCT transition centred on the aromatic chromophore. Indeed, upon complexation a redshift in this absorption band is observed, further confirming the preliminary assumption. This is not surprising, given the electron donor and acceptor ability of the azide and ketone groups respectively. Addition of the trivalent lanthanide ion increases the polarisation of the ketone group in the excited state, stabilising the charge separated excited state and thus lowering its energy.

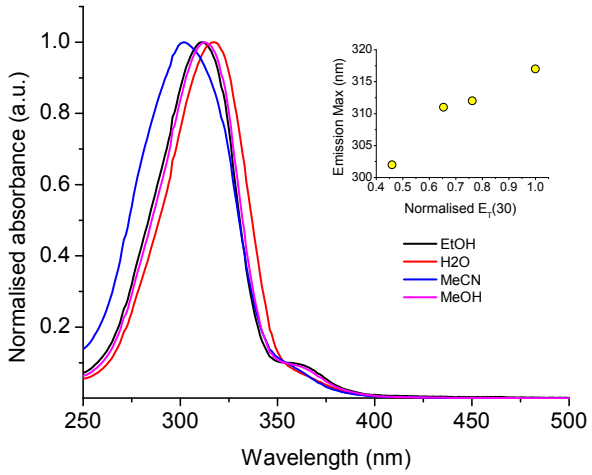


Figure 5-15. UV-Vis absorption spectra of complex **5.22** registered in solvent of increasing polarity. Inset: correlation between the maximum of the absorption band the normalized $E_t(30)$ parameter of polarity of the corresponding solvent.

To confirm the charge transfer nature of this transition a series of absorption spectra were measured in solvents of different polarities. As can be seen in Figure 5-15, the main absorption band is red shifted upon increasing the solvent polarity, as a consequence of an increased stabilisation of the charge separated excited state. Furthermore a positive correlation between the $E_T(30)$ parameter can be observed (inset Figure 5-15).[14]

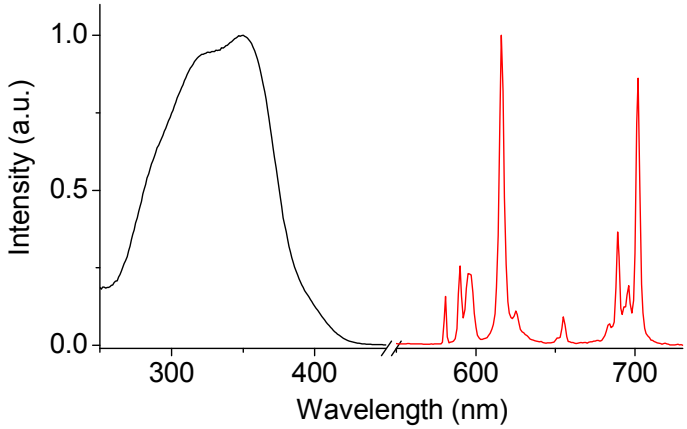


Figure 5-16. Excitation and emission spectrum of the Eu(III) complex **5.22** in H_2O.

The Eu(III) complex **5.22** shows strong luminescence upon excitation in the chromophore band. More interestingly it is possible to sensitise europium over a large

region of excitation wavelengths that include the visible spectrum. The lifetimes of the complexes prepared are tabulated in Table 5-1. From their values in D_2O and H_2O, the number of coordinated solvent molecules was determined according to the modified Horrocks' equation:

$$q = A_{Ln} \cdot (k_H - k_D - B_{Ln}) \qquad (5.1)$$

The value of q for **5.22** further confirms the octadentate nature of the ligand in solution, with only one water molecule to saturate the metal coordination sphere. The Yb(III) complex **5.24** also showed strong luminescence, with lifetime values in line with other reported molecules of the same family. In this case the calculated hydration number (q =1.4) also confirms that the ketone is indeed actively participating in the coordination.

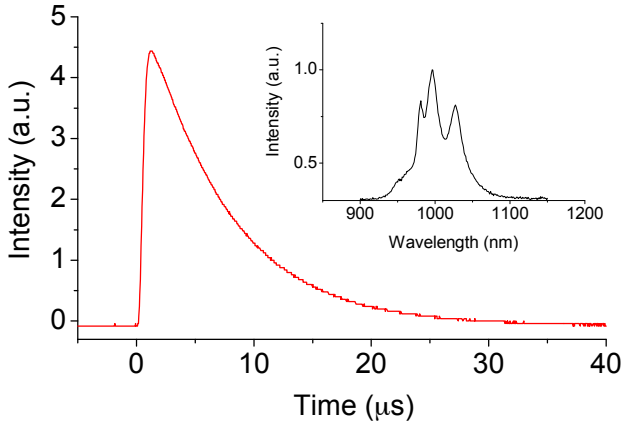


Figure 5-17. Emission decay of the excited state of Yb(III) in **5.24** upon excitation at 337 nm in D_2O. Inset: total emission spectrum of **5.24** upon excitation at 360 nm in D_2O.

In the case of complex **5.23**, the azidophenacyl chromophore was found to be a poor sensitiser of Tb(III) centred luminescence as indicated from the still intense fluorescence originating from the aryl chromophore when exciting into the chromophore manifold itself (Figure 5-18).

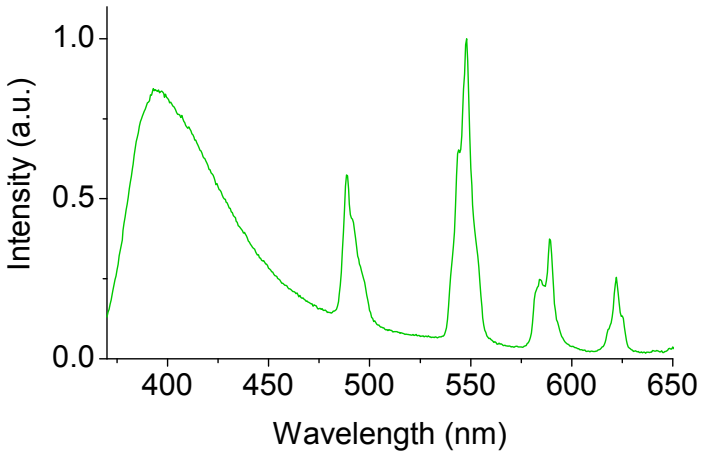


Figure 5-18. Emission spectrum of Tb(III) complex **5.23** obtained upon excitation at 350 nm in H_2O.

This behaviour is not surprising given the low energy of the organic chromophore triplet state relative to the $^5D_4$ excited state of Tb(III), as measured from the Gd(III) analogue (Figure 5-19). In this case, back energy transfer through thermal repopulation of the antenna chromophore is a feasible pathway of quenching of the lanthanide excited state and lifetime measurements further confirmed this hypothesis. Terbium complexes of DO3A derivatives typically show lifetime of the order of 2-3 ms in deuterated solvents even in seven-coordinate complexes; in this case the excited state lifetime of the complex was found to be 1.2 ms in deuterium oxide: suggesting that back energy transfer is indeed taking place.

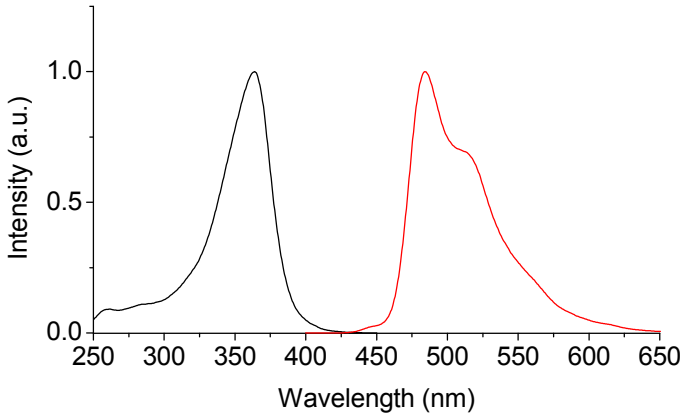


Figure 5-19. Excitation and emission spectrum of the Gd(III) complex **5.26** registered at 77 K.

Table 5-1. Luminescence lifetimes of the azide containing complexes and corresponding hydration number q.

Compound	λ_{ex}/nm	λ_{em}/nm	τ_{H2O}/μs	τ_{D2O}/μs	q
5.22	300	615	420	1020	1.4
5.23	300	545	320	870	-
5.24	337	980	0.61	6.41	1.4

In order to investigate the origin of this quenching, a sample of **5.23** in deuterium oxide was deoxygenated through several freeze-pump-thaw cycles. Figure 5-20 shows a comparison between the same sample in deoxygenated and aerated conditions. While the characteristic emission profile of terbium remains unchanged, the residual emission attributed to the aryl chromophore undergoes a noticeable increase. In addition, the values of lifetimes in the absence of oxygen did not show an appreciable change. This indicates that triplet oxygen is responsible only for the quenching of the aryl centred triplet state and as a consequence its removal increases the yield of radiative processes from the chromophore excited states only.

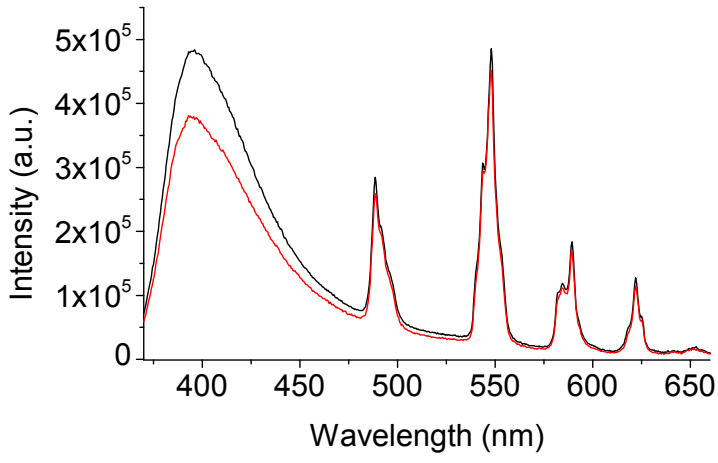


Figure 5-20. Comparison of fluorescence spectra of complex **5.23** before (red line) and after (black line) deoxygenation of the sample.

As far as the population of the lanthanide excited state is concerned, it is reasonable to assume that its main feeding state is not a triplet, as this would have been quenched

by triplet oxygen, but a singlet and that the main mechanism of quenching is through low lying excited states, likely to be of ILCT character, given the nature of the chromophore (see Figure 5-21 for a proposed Jablonski diagram for this particular system).

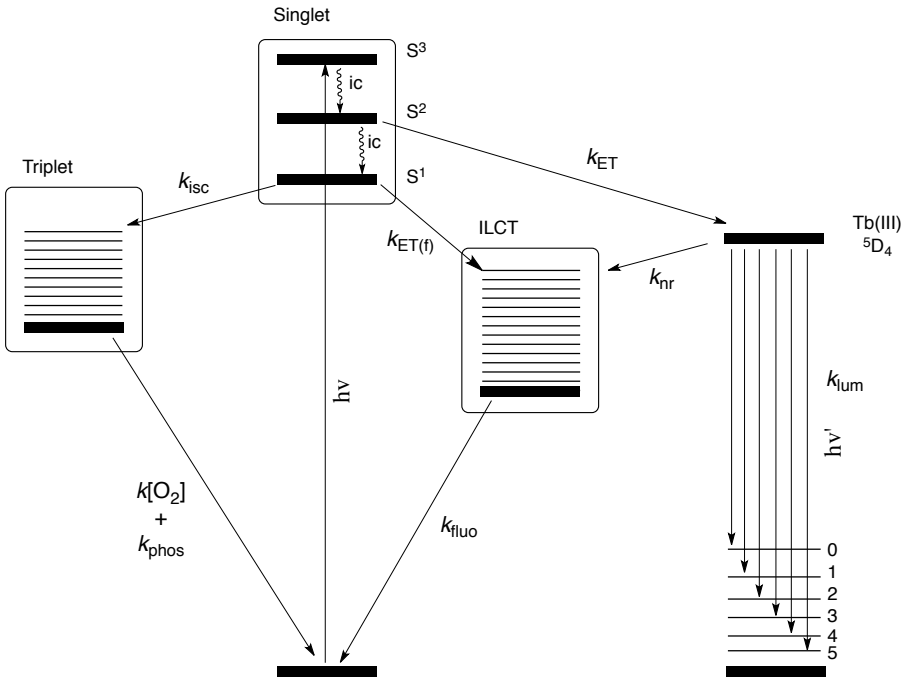


Figure 5-21. Sketch of the proposed energy transfer mechanisms taking place in the Tb(III) complex **5.23**.

Unfortunately other energy transfer mechanisms could not be investigated with the instrumentation available, hence a definitive answer on the real mechanism of energy transfer in **5.23** cannot be given and other mechanisms faster than the quenching of the chromophore triplet state by oxygen cannot be ruled out.

5.3 Preparation and study of f-f' heterobimetallic complexes

5.3.1 Introduction

While the structure of the DO3A-based ligand provides excellent kinetic and thermodynamic stability, the presence of an azido group allows for further functionalisation once the lanthanide complex is formed. In particular, the coupling with the class of propargyl-DO3A complexes would afford pure heterobimetallic

complexes with excellent selectivity and in straightforward fashion. The use of mild reaction conditions and the kinetic inertness of the starting lanthanide complexes would ensure the formation of kinetically and thermodynamically stable heterobimetallic complexes where no transmetallation should occur between the binding pockets. Furthermore, it was reasoned that the conjugation of the bridging chromophore system would be reflected in a change of photophysical properties and could allow the study of f-f' through bond communication.

5.3.2 Synthesis

The coupling between the two lanthanide complexes was achieved under classical Cu(I) "click" chemistry conditions. The reaction was conducted in methanol and the Cu(I) catalyst was produced *in situ* by reduction of Cu(II) using sodium ascorbate. It was found that an excess of alkyne was required to drive the reaction to completion, probably due to the apparently low reactivity of the azide group (see also the rotaxane reaction).

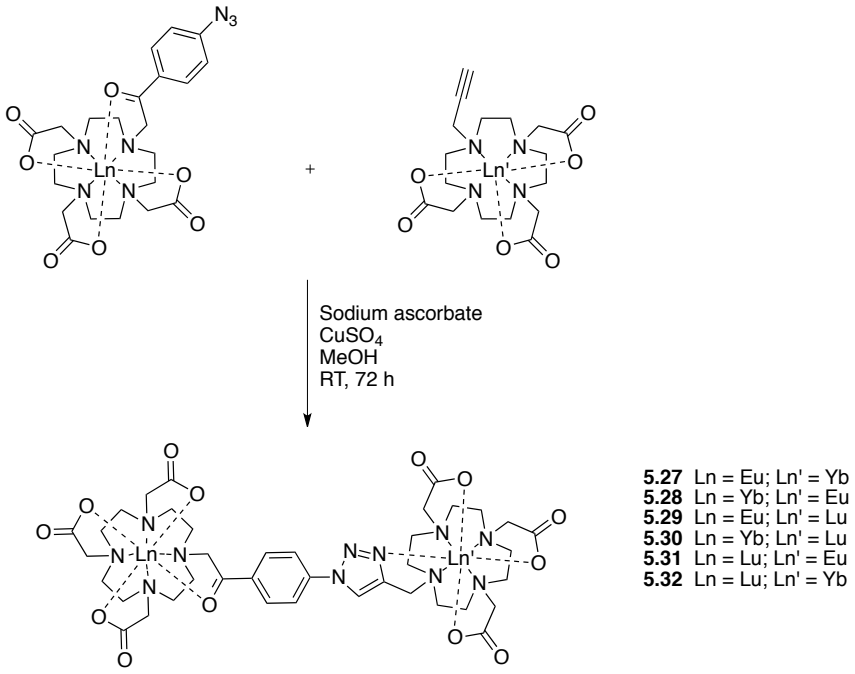


Figure 5-22. Description of the synthesis of the *f-f'* heterobimetallic complexes.

Alternative reaction conditions (such as the use of water or methanol/dichloromethane mixtures or alternative sources of Cu(I)) either did not improve the rate of conversion to the products or didn't show any conversion to the target molecule. The final product was purified by dialysis using a 1000 MWCO cellulose membrane in order to remove any unreacted starting material and selectively retain the target compound. The bimetallic complexes were characterised by paramagnetic ^{1}H-NMR, MALDI-MS, absorption and luminescence spectroscopy.

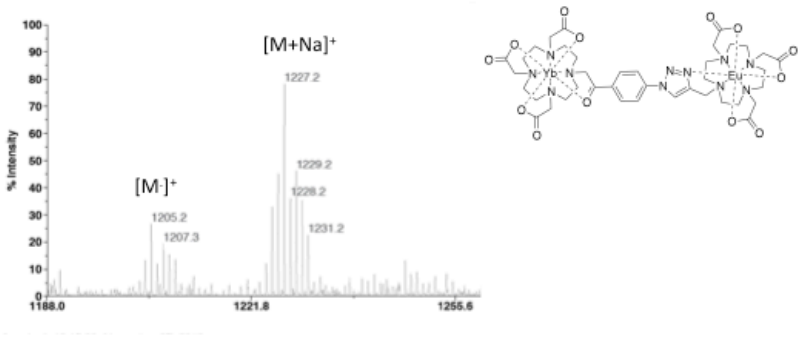


Figure 5-23. MALDI-MS of molecule **5.28** showing the isotopic pattern of the Yb-Eu couple.

5.3.3 NMR spectroscopy characterisation

From the NMR study of the bimetallic complexes it is clear that each lanthanide ion is in a rigid binding pocket, implying that the ligand is octadentate. Indeed all ^{1}H-NMR spectra show sharp resonances indicating that all isomers in solution are in slow exchange on the NMR time scale. Depending on the lanthanide couple, there are some resonances dominating the spectrum. For example in complex **5.28**, resonances corresponding to the axial ring proton of the europium binding pocket are subsumed by low shifted peaks ascribable to the ytterbium complex (see Figure 5-24).

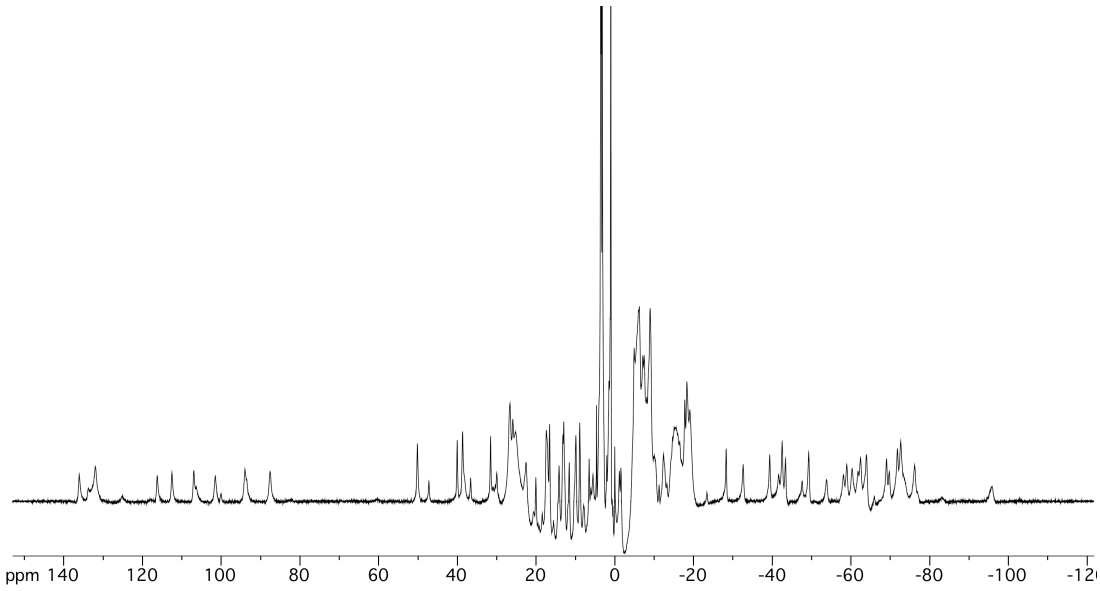


Figure 5-24. ^{1}H-NMR spectrum of **5.28** registered in D_2O at pD 7.

Judging from the wealth of NMR resonances, it can be deduced that more than one diastereoisomer is present in solution, with the original SAP and TSAP enantiomeric pairs of each lanthanide binding pocket now forming NMR distinguishable species. In the spectrum of **5.28** in Figure 5-24, there are eight resonances attributable to the four axial ring protons surrounding the Yb(III) ion. This is due to the effect of a second chiral centre given by the Eu(III) binding pocket. By contrast, in the case of complex **5.27**, the effect of a second chiral centre is not so evident, with only a splitting of the Yb(III) axial ring protons signals and the presence of a minor isomer indicated by an additional set of upshifted resonances at ca. 60 ppm (see Figure 5-25). Although in

both these complexes the NMR spectra are dominated by signals of protons close the Yb(III) centre, the presence of shifted resonances attributable to the Eu(III) binding site is nonetheless evident in the region between 40 and -40 ppm.

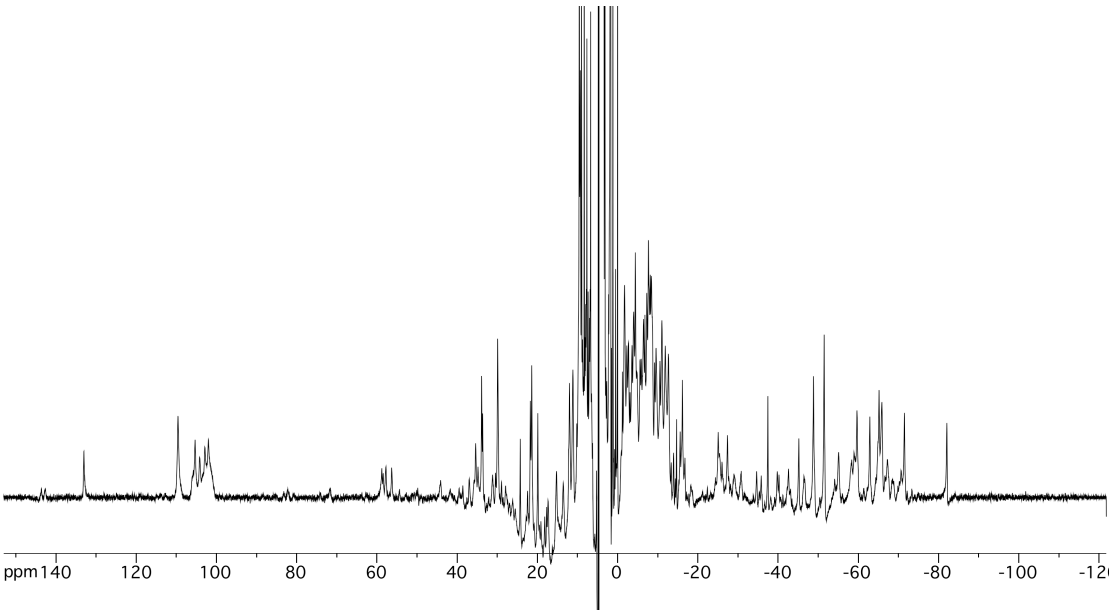


Figure 5-25. ^{1}H-NMR spectrum of **5.27** registered in D_2O at pD 7.

Overall, upon formation of the heterometallic complex, the NMR spectrum undergoes a drastic change, as can be noticed from the comparison of the NMR profile of the products with the starting lanthanide complexes containing azide and alkyne groups (see this chapter and chapter 2). This is partly due to the presence of a second eight coordinate species upon formation of the triazole group, but also to the presence of two chiral centres, given by two DO3A-based lanthanide complexes. This affords a theoretical total of eight NMR distinguishable enantiomeric pairs in solution with the consequent appearance of several resonances. In practice some species will be more favoured over the others, not only thermodynamically but also statistically, with a consequent lower number of dominating isomers in solution and hence of proton signals. Indeed, this is evident for the axial ring protons resonances of the lanthanide binding pocket containing the ketone group. By contrast, this is not the case for the axial ring protons resonances of the triazole-containing lanthanide binding pocket, where only a minor splitting was observed. This effect is clearly seen in

heterobimetallic complexes containing one Lu(III) ion, where the use of a diamagnetic metal simplifies the spectrum due to the presence of only one paramagnetically shifted set of resonances (see for example Figure 5-26).

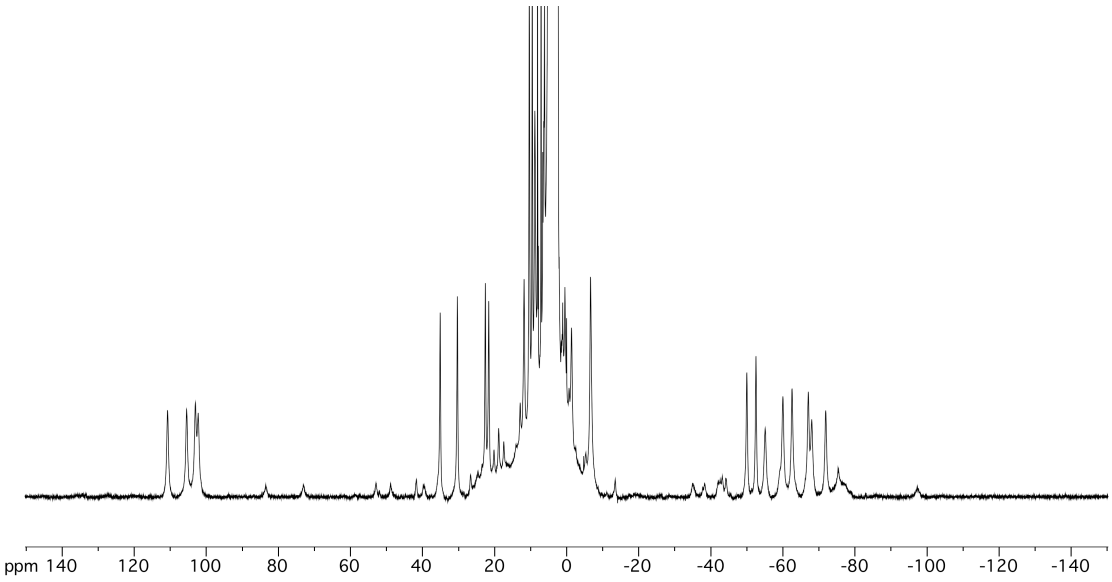


Figure 5-26. ^{1}H-NMR spectrum of **5.32** registered in D_2O at pD 7.

A general aspect of NMR behaviour in solution can then be noticed. When the paramagnetic lanthanide is situated in the triazole-containing pocket, only one major set of resonances for the axial ring protons of its lanthanide binding site is present in the NMR spectrum, indicating that there is one dominating species in solution with minor species visible and accounting for less than 5 %. On the contrary, when the paramagnetic lanthanide is in the ketone pocket the situation is different, with clearly more than one isomeric species present, indicating that in this case there is not a thermodynamically favoured conformation that dominates in solution but at least two NMR distinguishable species in a 1:1 ratio.

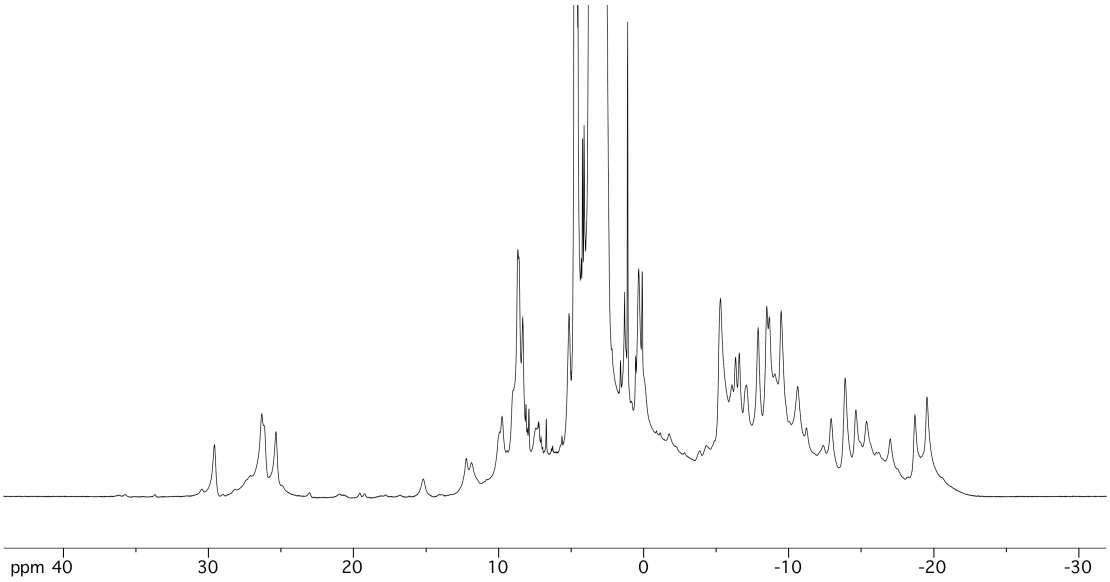


Figure 5-27. ^{1}H-NMR spectrum of **5.31** registered in D_2O at pD 7.

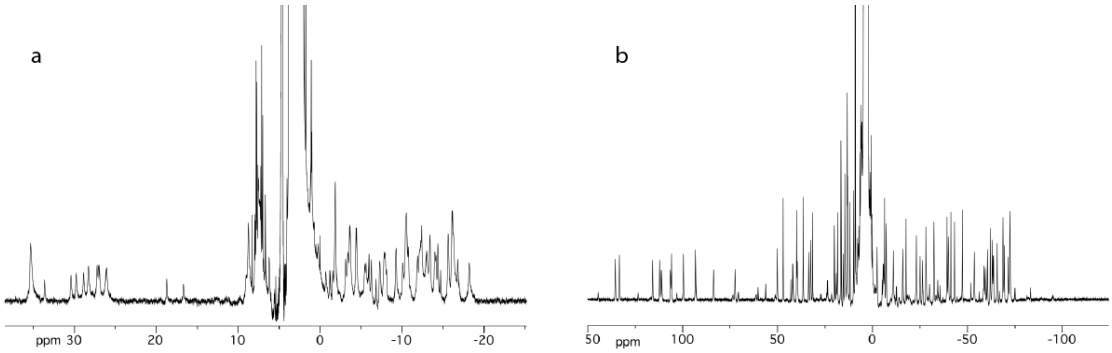


Figure 5-28. ^{1}H-NMR spectra of **5.29** (a) and **5.28** (b) registered in D_2O at pD 7

5.3.5 Photophysical characterisation

The excited state lifetimes, together with the calculated hydration numbers of each heterobimetallic complex synthesised, are summarised in Table 5-2. The photophysical behaviour of each bimetallic complex was characterised using steady state and time-resolved fluorescence together with UV-Vis absorption spectroscopy.

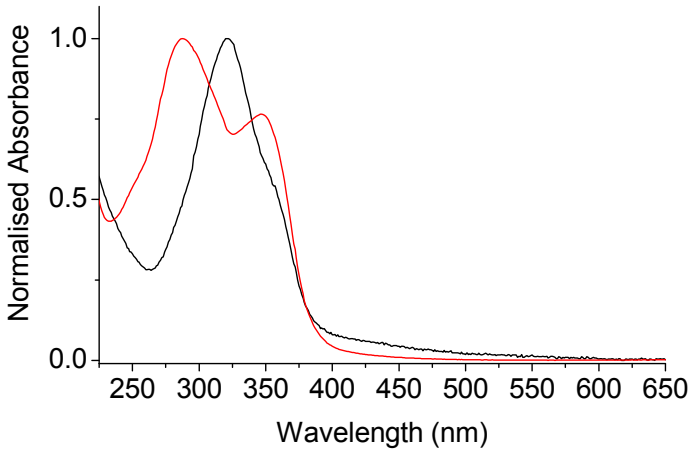


Figure 5-29. Comparison of the UV-Vis absorption spectra of **5.22** (black line) and **5.27** (red line) registered in H_2O.

The complexes show absorption profiles compatible with the presence of the newly formed triazole chromophore with the characteristic n-π* electronic transition at ca. 280 nm. Furthermore, the poor solvatochromic behaviour of the bridging chromophore suggests either the absence of any CT transition or a poor solvation of the bridging unit due to the steric requirements of the bulky DO3A complexes. Indeed the absorption spectrum did not show an appreciable change upon changing the solvent polarity, as it would be expected from the product, where the absence of a donor group such as the azide prevents the formation of a charge transfer state, confirming the successful outcome of the reaction.

In the case of the **5.27** and **5.28** complexes containing the Eu-Yb couple, excitation into the chromophore manifold gave rise to sensitised luminescence from both lanthanide ions in the visible and near IR region of the spectrum. A close inspection of the characteristic luminescence profile of europium in each of the complexes

reveals marked differences with the starting molecules, particularly in the ΔJ_1 and ΔJ_2 transitions. While in the azido complex **5.22** the ΔJ_2 transition dominates the spectrum, the formation of the triazole group upon reaction with the Yb(III) alkyne DO3A complex (**2.7**) results in a remarkable change of its relative intensity compared to the ΔJ_1 band. This is to be expected, given the hypersensitivity of the $^5D_0$ -$^7F_2$ transition to changes in the ligand environment. The splitting in the ΔJ_1 band is instead related to the local symmetry in the donor sets. In both **5.22** and **5.27** the splitting and number of peaks indicate a lower symmetry site, and although a rigorous analysis would require high-resolution studies, it is nonetheless evident that the profiles are remarkably different.

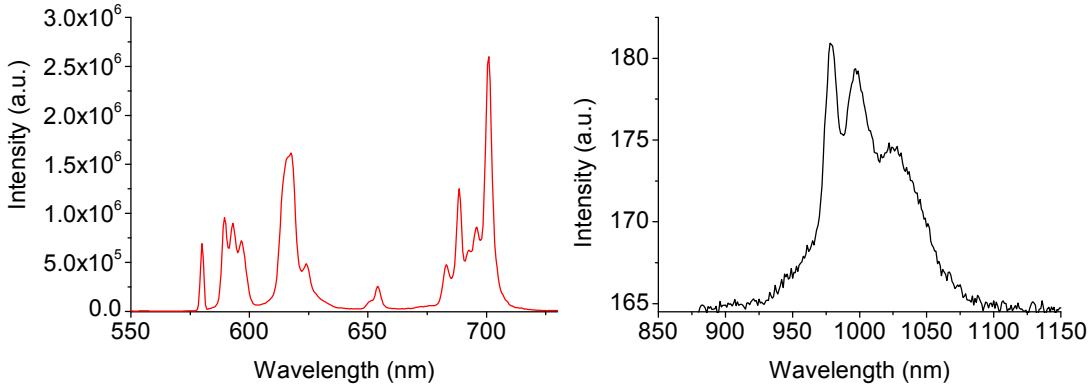


Figure 5-30. Fluorescence spectra of **5.27** originating from Eu(III) (left) and from the Yb(III) (right) centres, upon excitation at 320 nm, in D_2O.

The luminescence observed in the near IR region for complex **5.27** indicates a successful sensitisation of Yb(III) upon formation of the bridging ligand, unlike its precursor **2.7**, non-luminescent due to the lack of a sensitising chromophore. The number of inner sphere water molecules obtained by time resolved luminescence spectroscopy measurements are tabulated in Table 5-2. The decrease in the hydration number going from **5.22** to **5.27** indicates a more sterically hindered local environment around the Eu(III) and Yb(III) centres, with the latter showing a value lower than unity due to the lanthanide contraction. The same is true for **5.28**, where

both lanthanides display a q value of one, compatible with an eight-coordinate complex.

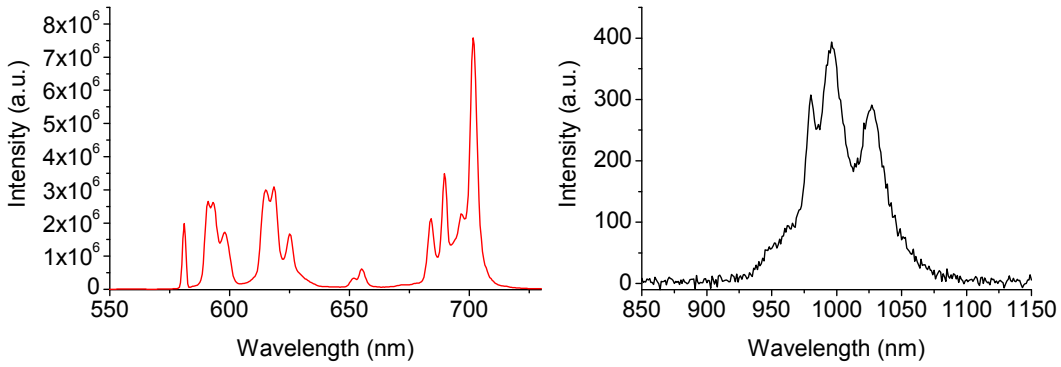


Figure 5-31. Fluorescence spectra of **5.28** originating from Eu(III) (left) and from the Yb(III) (right) centres, upon excitation at 320 nm, in D_2O.

Figure 5-31 shows the luminescence emission of complex **5.28**. Both spectra show the typical europium and ytterbium luminescent bands, indicating that the bridging chromophore is a good sensitiser for both lanthanides as expected from the results obtained for **5.27**. The emission profile displayed by Eu(III) is remarkably similar to other complexes derived from **2.6** upon CuAAC "click" chemistry reaction.[15, 16] The values of lifetimes are in line with the values obtained with other luminescent complexes based on the DO3A ligand, indicating the absence of any detrimental non-radiative process. Furthermore, excitation into the europium f-f manifold on either complexes at 580 nm or at 397 nm did not result in any detectable luminescence from the Yb(III) $^2F_{5/2}$ excited state, suggesting inefficient energy transfer between the two ions.

In a comparison between the two complexes containing the Yb(III)-Eu(III) couple (**5.27** and **5.28**), it is worth noting that, due to the different local environment around each lanthanide ion in each of these complexes, the two emission spectra look remarkably different, both in the splitting of the $^2F_{5/2}$ to $^2F_{3/2}$ ytterbium transition at 980 nm and in the ΔJ_1 and ΔJ_2 hypersensitive europium transitions at 590 and 615 nm respectively. By comparison with other Eu-DO3A complexes containing the triazole

group presented in other sections, the resemblance of the emission spectra is clear, indicating not only that the reaction has taken place, but also that during the reaction no transmetallation occurred. More importantly, the heterobimetallic array proved to be kinetically robust, with no observable change in the visible and near IR emission profile from the same solution after a period of at least three months, indicating the each lanthanide remains closely associated with its ligand and hence no transmetallation takes place, since this could be easily detected by a change in the fine structure of the emission spectrum.

Table 5-2. Tabulated values of luminescence lifetimes of the *f-f'* heterobimetallic complexes discussed in this chapter.

Compound	λ_{ex}/nm	λ_{em}/nm	τ_{H2O}/μs	τ_{D2O}/μs	**q**
5.27	300	615	640	1880	0.9
	337	980	1.29	5.67	0.5
5.28	300	615	590	1810	1.1
	337	980	0.73	6.51	1.1
5.29	280	615	0.63	1.76	0.9
5.30	337	980	0.76	7.32	1.1
5.31	300	616	600	1920	1.1
5.32	337	980	1.09	5.16	0.6

5.4 Conclusions

In this chapter a new class of luminescent lanthanide complexes has been synthesised and their photophysical properties have been studied. The chromophore employed allows for visible sensitisation of Eu(III) and strong emission in the near IR when Yb(III) is employed. From the solvatochromic behaviour and study of the photophysics of the terbium analogue it was suggested that sensitisation, where energetically allowed, occurs via a singlet ILCT state. Furthermore, the presence of an azido group on the chromophore itself could be exploited for the further functionalisation of the complex, demonstrating the versatility of this novel synthon for the formation of multiplexed covalently linked structures. Envisaging a conjugated bridging chromophore that could be exploited for triggering lanthanide to lanthanide communication, a series of heterobimetallic *f-f'* arrays was formed by click chemistry between the azido and the family of alkyne functionalised lanthanide complexes. NMR spectroscopy and photophysical studies techniques were employed in order to characterise the behaviour of these compounds in solution. Unfortunately, no evidence for communication between the two metal centres could be found. Although it was hoped that this would be the case, this is not necessarily a disadvantage, since a heterobimetallic array formed by discrete and independent luminescent centres could be exploited in the preparation of responsive dual emissive probes, where a reference luminescent channel for ratiometric detection is directly integrated in the chemical structure and whose properties are not amenable to change during the recognition event. More importantly it has been demonstrated that, by employing kinetically stable building blocks, a class of true *f-f'* heterobimetallic arrays can be formed, with no signs of transmetallation over a period of months.

5.5 References

1. T. Koullourou, L. S. Natrajan, H. Bhavsar, S. J. A. Pope, J. Feng, J. Narvainen, R. Shaw, E. Scales, R. Kauppinen, A. M. Kenwright and S. Faulkner, *J. Am. Chem. Soc.*, 2008, **130**, 2178-2179.
2. C. S. Bonnet and É. Tóth, *C. R. Chim.*, 2010, **13**, 700-714.
3. L. Frullano, C. Catana, T. Benner, A. D. Sherry and P. Caravan, *Angew. Chem., Int. Ed.*, 2010, **49**, 2382-2384.
4. C. P. Gros, A. Eggenspiller, A. Nonat, J.-M. Barbe and F. Denat, *MedChemComm*, 2011, **2**, 119-125.
5. N. André, R. Scopelliti, G. Hopfgartner, C. Piguet and J.-C. G. Bünzli, *Chem. Commun.*, 2002, 214-215.
6. S. Faulkner and S. J. A. Pope, *J. Am. Chem. Soc.*, 2003, **125**, 10526-10527.
7. M. P. Placidi, A. J. L. Villaraza, L. S. Natrajan, D. Sykes, A. M. Kenwright and S. Faulkner, *J. Am. Chem. Soc*, 2009, **131**, 9916-9917.
8. M. S. Tremblay and D. Sames, *Chem. Commun.*, 2006, 4116-4118.
9. L. S. Natrajan, A. J. L. Villaraza, A. M. Kenwright and S. Faulkner, *Chem. Commun.*, 2009, 6020-6022.
10. D. J. Mastarone, V. S. R. Harrison, A. L. Eckermann, G. Parigi, C. Luchinat and T. J. Meade, *J. Am. Chem. Soc.*, 2011, **133**, 5329-5337.
11. C. Szijjarto, E. Pershagen and K. E. Borbas, *Dalton Trans.*, 2012, **41**, 7660-7669.
12. K. Barral, A. D. Moorhouse and J. E. Moses, *Org. Lett.*, 2007, **9**, 1809-1811.
13. A. G. Habeeb, P. N. Praveen Rao and E. E. Knaus, *J. Med. Chem.*, 2001, **44**, 3039-3042.
14. C. Reichardt, *Chem. Rev.*, 1994, **94**, 2319-2358.
15. M. Jauregui, W. S. Perry, C. Allain, L. R. Vidler, M. C. Willis, A. M. Kenwright, J. S. Snaith, G. J. Stasiuk, M. P. Lowe and S. Faulkner, *Dalton Trans.*, 2009, 6283-6285.
16. G. J. Stasiuk and M. P. Lowe, *Dalton Trans.*, 2009, 9725-9727.

6 Synthesis and study of lanthanide bioconjugates

6.1 Introduction

The unique luminescence and magnetic properties of lanthanides renders their complexes ideal candidates for use as bioimaging probes. Gadolinium compounds have been widely used over the last twenty years as MRI contrast agents, and luminescent lanthanide probes are becoming more popular with the development of novel fluorescence lifetime microscopy techniques. The main advantage of lanthanide-containing probes is their chemical properties. Given the almost identical chemical behaviour, the same "line" of complexes can be exploited both as MRI and as luminescent probes, not to mention the possibility for multi emissive probes exploiting multimodal imaging through PET-MRI, luminescence and MRI and PARACEST contrast agents.[1-3] From the synthesis of a single type of complex, one automatically has several properties available just by changing the lanthanide ion employed, providing scope to explore a range of imaging modalities.

The formation of lanthanide conjugates is then highly desirable and, more importantly, the ability to form several biologically active lanthanide conjugates from the same starting material would be ideal. In the previous sections, lanthanide complexes based on the DO3A scaffold and containing an alkyne group have been established as versatile building blocks for the formation of kinetically stable derivatives bearing triazole pendant arms. The aim of this section is to demonstrate the use of this class of complexes to form lanthanide-containing bioconjugates, with a focus on preparing compounds that could act as substrates for the dopamine transporter protein (DAT). The expression of this protein decreases in line with the degeneration of dopaminergic neurons observed in Parkinson's and related diseases.[4-7] Hence, by specifically targeting this protein, one can monitor its level of expression

and indirectly the activity of dopaminergic neurons. Furthermore, by targeting a transporter protein, the concentration of the contrast agent would build up inside the cell, thus reaching a concentration of the order of at least tens of μM, suitable for MRI imaging, while requiring a low dosage thanks to its intrinsic specificity for the DAT.[8]

Current methods for the diagnosis and monitoring of the progression of this disease are mainly based on PET and SPECT radiotracers. The biological processes monitored by these compounds are several and can range from the assessment of the uptake of a certain bioactive molecule to the binding of the radiotracer to a specific receptor in the synaptic cleft. Indeed, ^{18}F labelled L-DOPA, known as [^{18}F]fluorodopa, is used to monitor the population of dopaminergic neurons indirectly by monitoring the activity of the aromatic acid decarboxylase enzyme (AADC) in the cytosol. In a different approach, [^{11}C]dihydrotetrabenazine (DTBZ) is used as a PET radiotracer able to target the VMAT2 transporter, responsible for the transport of the family of monoamines from the cytosol into synaptic vesicles.[9, 10] It was hence reasoned that by using MRI-active bioconjugates it would be possible to increase the spatial resolution of current methods, in the case of Gd(III) derivative, or even allow *in vitro* studies by luminescence spectroscopy in the case of analogues employing luminescent lanthanides.

In this chapter, alkyne-containing lanthanide complexes are used as a starting material for the preparation of aldehyde appended derivatives of triazolyl(DO3A). It will be shown that such systems have considerable scope for the preparation of bioactive conjugates with biologically active compounds containing amino groups, and that they have considerable potential as building blocks for generating contrast in biological imaging experiments.

6.2 Aldehyde appended lanthanide complexes

6.2.1 Synthesis

Complexes containing a pendent aldehyde group were prepared via a CuAAC "click" chemistry approach by reaction of the propargyl DO3A lanthanide complexes with 3-azidopropanal (**6.2**). The latter was itself obtained by nucleophilic addition of an azide group to the propenal (**6.1)** under acidic conditions (see Figure 6-1).

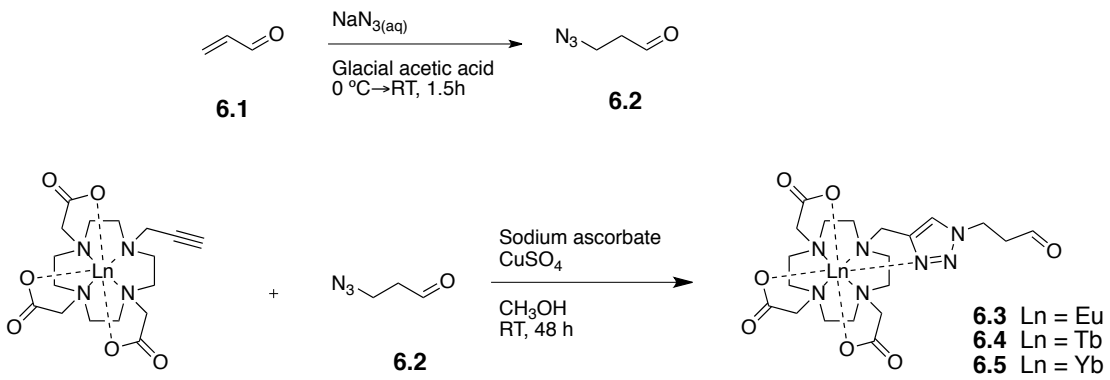


Figure 6-1. Synthesis scheme of the aldehyde appended lanthanide complexes discussed in this chapter.

The reaction between the alkyne complexes and compound **6.2** was carried out in methanol to provide a good solubility for both the reactants and catalytic amounts of Cu(I) were generated *in situ* by reduction of Cu(II) with sodium ascorbate using the procedure originally reported by Sharpless et al.[11] The products were be purified by dialysis and characterised by paramagnetic NMR, MS and fluorescence spectroscopy.

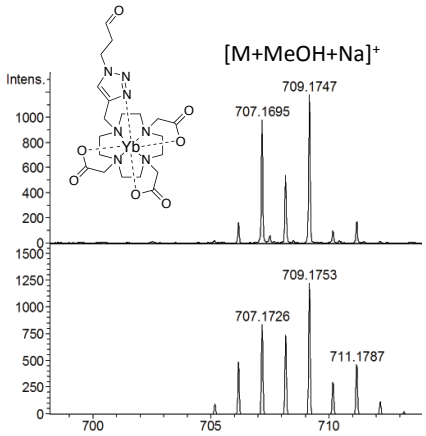


Figure 6-2. High resolution ESMS of compound **6.5** (top) with the theoretical isotope distribution (bottom).

6.2.2 NMR spectroscopy characterisation

The formation of the triazole group upon "click" reaction between alkyne and azide appended starting materials is clearly inferred from the ^{1}H-NMR spectrum of the paramagnetic Eu(III) and Yb(III) complexes, **6.3** and **6.4** respectively. There are four upshifted signals attributable to four different axial ring protons around the lanthanide ion. Both spectra show sharp resonances, indicating the presence of an eight coordinate species in solution, with a clear predominance for the SAP structure in both complexes. Close inspection of the NMR spectrum reveals a set of less shifted, broader resonances that account for the presence of the TSAP isomer: integration of these peaks suggests that the SAP/TSAP ratio is around 10:1 (see Figure 6-3).

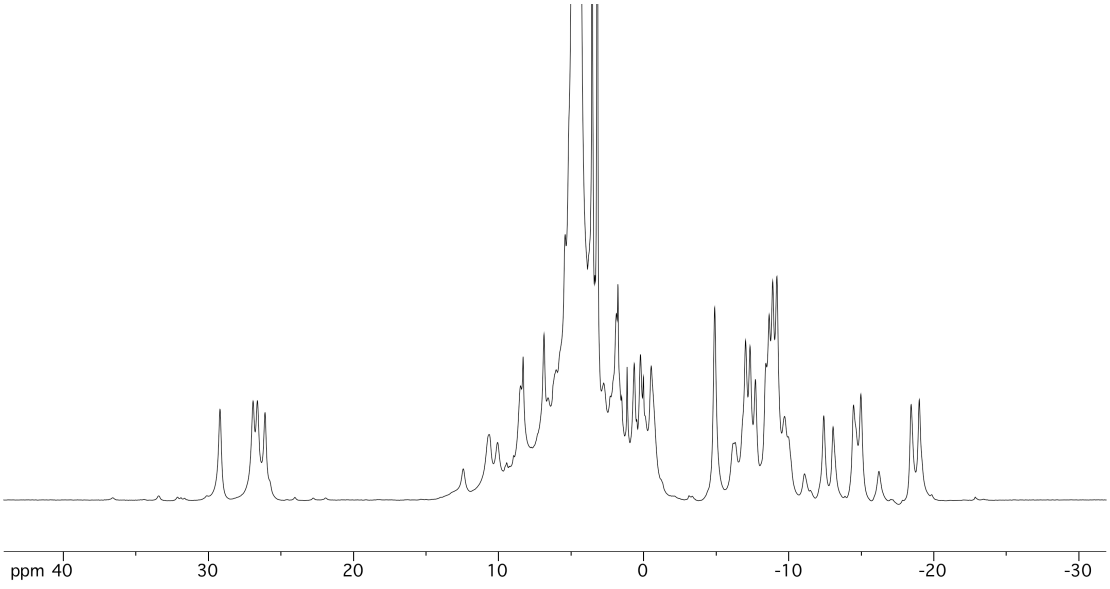


Figure 6-3. ^{1}H-NMR spectrum of **6.3** registered in D_2O at RT at pD 7.

This is in broad agreement with the paramagnetic NMR of chemical structures derived from the alkyne-DO3A complexes upon "click" reaction and presented in other sections of this work. It also demonstrates that there are only small changes to the balance between isomers in solution, with slow exchange between the isomers implying a strong interaction between the triazole and the metal ion in the binding pocket.

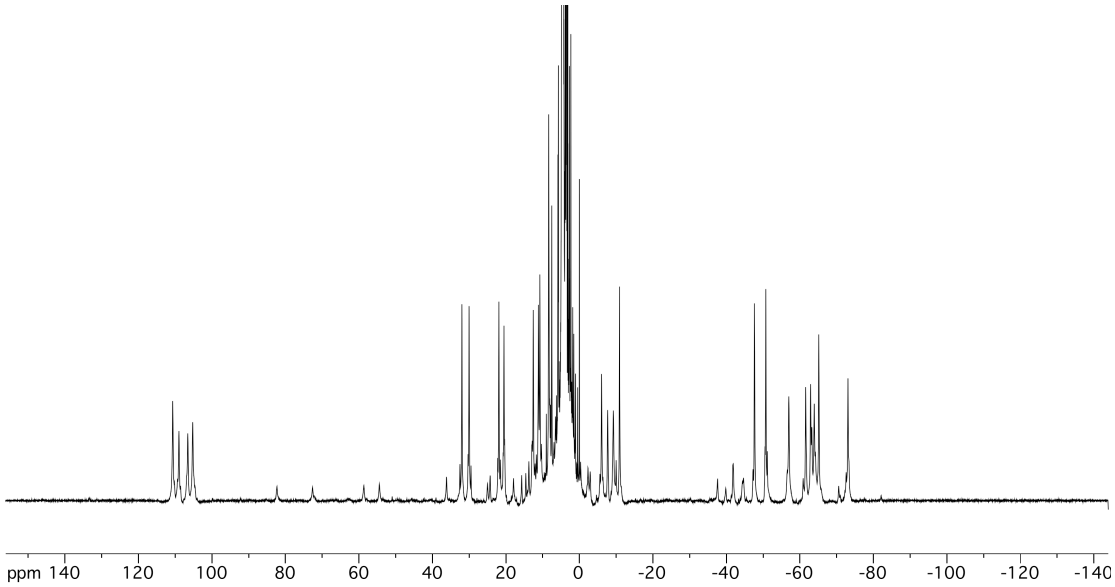


Figure 6-4. ^{1}H-NMR spectrum of the Yb(III) complex **6.5** registered in D_2O at RT at pD 7.

The NMR spectra imply that the same structure is adopted in solution for all the complexes studied, with the Tb(III) complex **6.4** in particular showing the group of four resonances for the most shifted axial ring protons into the lowest frequency of the spectrum, due to the difference in sign of the *D* factor in the Bleaney equation, and displaying a second set of broader resonances that can be attributed to the open TSAP conformation.

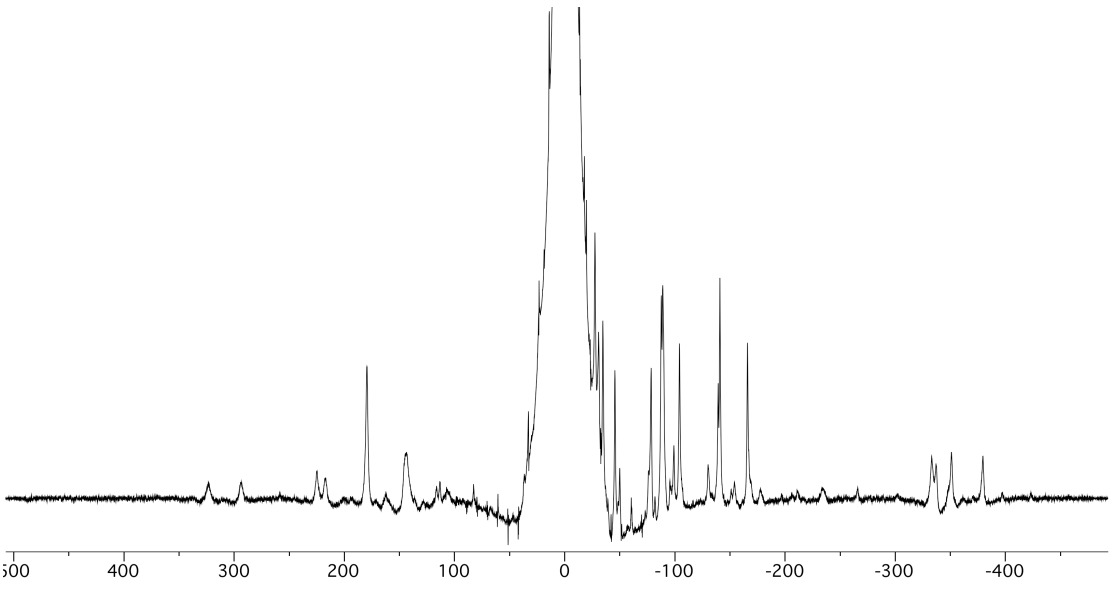


Figure 6-5. ^{1}H-NMR spectrum of the Tb(III) complex **6.4** registered in D_2O at RT at pD 7.

6.2.3 Photophysical characterisation

The photophysical properties of the luminescent lanthanide complexes containing the aldehyde motif were studied in order confirm the speciation of the complexes in solution. The emission spectra of complexes **6.3** and **6.4** are shown in Figure 6-6. Both complexes could be excited into the triazole excited state manifold, showing the typical red and green fluorescence respectively. Time resolved luminescence shed further light on the characterisation of the metal complexes in solution, with a hydration number close to one for all complexes synthesised. Indeed this confirms the octadentate nature of the ligand upon formation of the triazole. Moreover, the lifetime values of **6.4** are compatible with the values obtained for complexes based on a DOTA like structure, indicating that the chromophore triplet state is high enough in energy to populate the Tb(III) $^5D_4$ emissive state with no back energy transfer occurring.

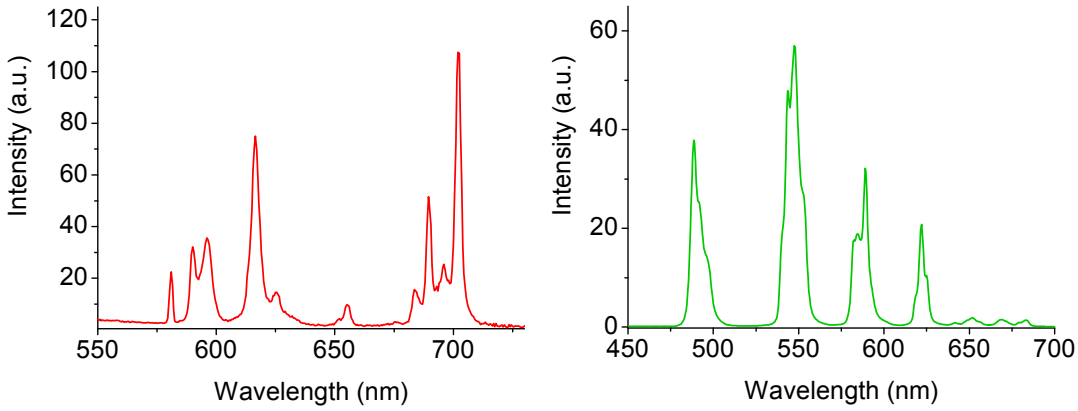


Figure 6-6. Emission spectra of Eu(III) complex **6.3** (left) and Tb (III) complex **6.4** (right) obtained upon 317 nm and 280 nm excitation respectively.

Interestingly, the Yb(III) analogue **6.5** proved to be weakly luminescent even in D_2O-with the values of lifetime hence drastically affected by instrumental error. The value of q in this case should then be taken with extreme care, with a real number of coordinated water molecules more likely close to unity, following the lanthanide contraction.

Table 6-1. Tabulated values of luminescence lifetime for the aldehyde appended lanthanide complexes discussed in this chapter.

Compound	λ_{ex}/nm	λ_{em}/nm	τ_{H2O}/μs	τ_{D2O}/μs	q
6.3	317	616	520	1560	1.2
6.4	280	545	1740	2730	0.7
6.5	337	980	2.58	3.02	0

6.3 Lanthanide bioconjugates containing a dopamine group

Having established the possibility of preparing octadentate lanthanide complexes containing an aldehyde moiety by a straightforward method and having assessed their properties in solution, both via paramagnetic ^{1}H-NMR and luminescence studies, their use as synthetic precursors for reductive amination reactions with biologically important substrates was evaluated. As mentioned earlier, the homeostasis of dopamine and its derivatives is crucial and its perturbation is thought to be the main cause for neurodegenerative diseases such as PD. This molecule was chosen as a first amine-containing biologically active compound that could serve to target the DAT protein.

6.3.1 Synthesis

The preparation of the dopamine conjugate is depicted in Figure 6-7. The conjugation of the lanthanide complex and dopamine was achieved through a reductive amination reaction between the aldehyde moiety present in the structure of **6.3** and the amino group of dopamine, using $NaBH_3CN$ as the reducing agent. The reaction was carried out in the dark and the product stored in the dark, given the photosensitivity and tendency to polymerise of the catechol fragment, especially at basic pH.

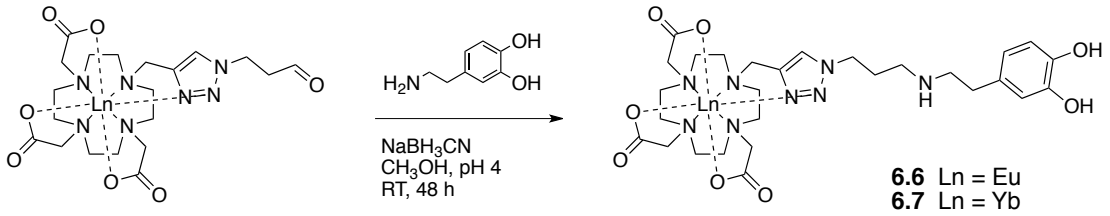


Figure 6-7. Description of the synthesis of the lanthanide containing bioconjugates.

NMR spectroscopy, mass spectrometry and photophysical measurements all provided clear evidence of the formation of the dopamine-appended bioconjugates. Figure 6-4 shows the accurate mass spectrum of the Eu(III) bioconjugate **6.6**.

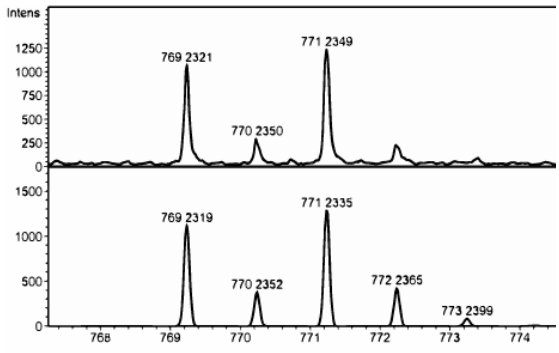


Figure 6-8. High resolution ESMS profile of the Eu(III) complex **6.6** showing the experimental (top) and theoretical (bottom) isotope pattern.

6.3.2 NMR spectroscopy characterisation

Upon reaction with dopamine, the local environment of the metal ion is not changed. It is then not surprising that the paramagnetic ^{1}H-NMR shows almost identical resonances as these represents only protons in close proximity to the lanthanide while a chemical change at the periphery will not affect the number of shifted signals in the spectrum. It is worth noting that although the overall spectra are very similar, the presence of broader signals in complex **6.6** compared to its parent derivative **6.3**, might be due to an increase in structure size and hence a lesser degree of fluxionality, at least on the time scale of the NMR experiment.

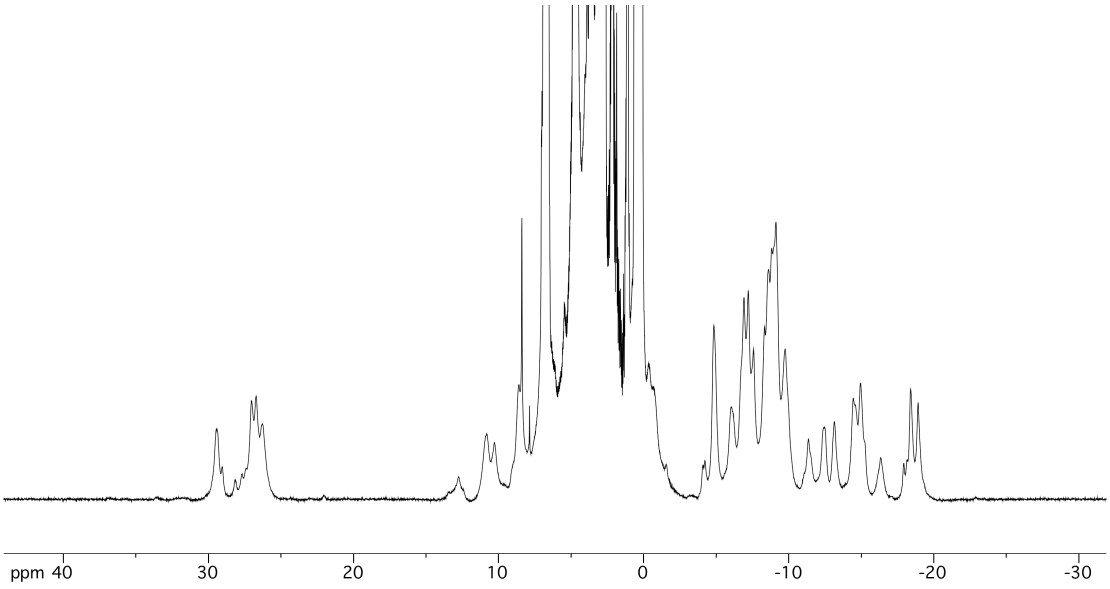


Figure 6-9. ^{1}H-NMR spectrum of **6.6** registered in D_2O at RT at pD 7.

This behaviour is accentuated in the Yb(III) complex **6.7** whose ^{1}H-NMR spectrum shows some splitting in the resonances corresponding to the axial ring proton. This seems to indicate that the complex is indeed in slow exchange between different conformations in solution but that their structures do not differ significantly. Also, a number of other sets of resonances are present in the NMR spectrum of **6.7**. It is likely that these are due to the presence of by-products of degradation of the complex upon long exposure to light.

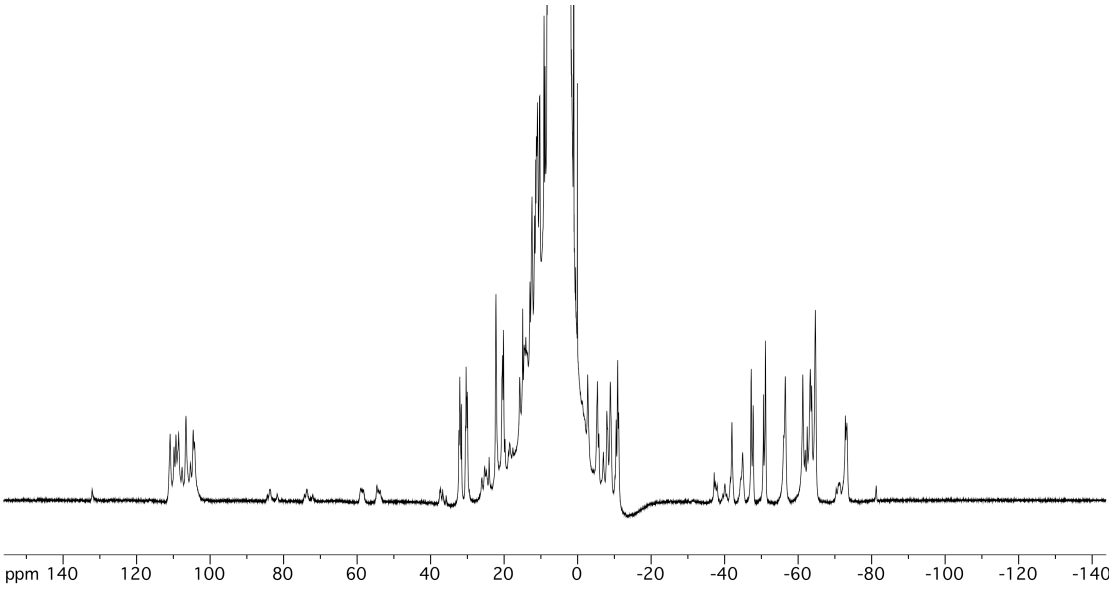


Figure 6-10. ^{1}H-NMR spectrum of **6.7** registered in D_2O at RT at pD 7.

6.3.3 Photophysical characterisation

Figure 6-11 shows the comparison between the UV-Vis absorption spectra of **6.3** and that of **6.6**. The presence of the strong absorption band at 280 nm is characteristic of the π-π* electronic transition of the catechol moiety and this subsumes the less intense transition attributable to the triazole group.

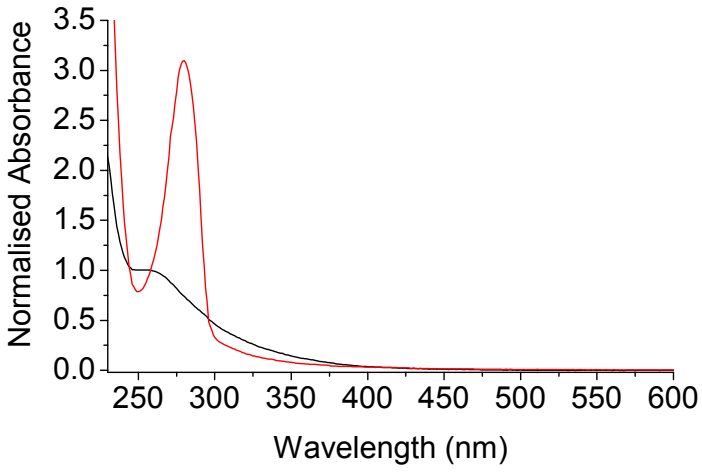


Figure 6-11. Comparison of the UV-Vis absorption spectra of complexes **6.3** (black line) and **6.6** (red line).

Excitation at 337 nm using a nitrogen laser resulted in near IR emission at 980 nm in the case of the Yb(III) complex **6.7**. The values of lifetime were significantly different from the starting aldehyde containing molecule **6.5**, thus indicating that the new aromatic chromophore is actively participating in the sensitisation of the Yb(III) $^2F_{5/2}$ excited state. Also, the intensity of luminescence of this complex was much higher than its parent compound **6.5** suggesting that the catechol group is directly influencing the sensitisation mechanism. The measurement of the lifetimes of luminescence in water and deuterium oxide once again allowed the determination of the hydration number using the modified Horrocks' equation. These values are tabulated in Table 6-2 and confirm what was clear from the NMR spectra, that is, the eight coordinate nature of the complexes and the minimal perturbation in the local environment of the metal ion.

Table 6-2. Tabulated values of luminescence lifetime for the dopamine appended lanthanide complexes.

Compound	λ_{ex}/nm	λ_{em}/nm	τ_{H2O}/μs	τ_{D2O}/μs	**q**
6.6	320	616	510	971	0.8
6.7	337	980	1.00	5.32	0.7

From the excitation spectrum of the Eu(III) derivative **6.6** it is quite clear that the catechol chromophore does not participate in europium sensitisation and the overall efficiency of sensitisation from the triazole chromophore seems to be quite poor given the still visible direct excitation peak of Eu(III) at ca. 395 nm. Nonetheless, excitation of the triazole moiety at 320 nm was able to sensitise luminescence from Eu(III) characterised by its typical fluorescence spectrum shown in Figure 6-12.

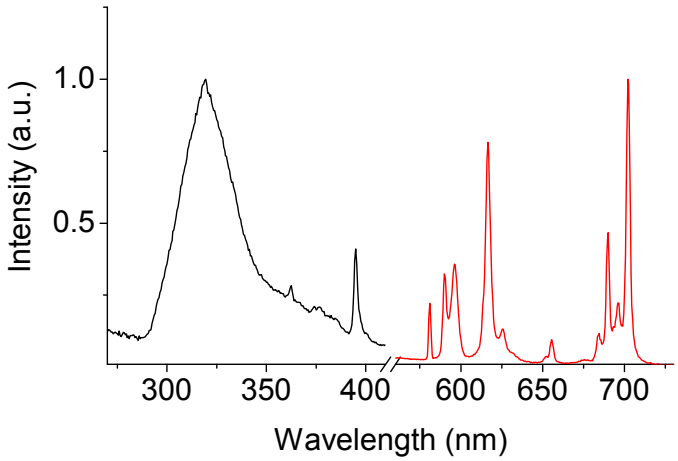


Figure 6-12. Emission and excitation spectra of the Eu(III) complex **6.6** in H_2O.

6.3.4 Uptake experiments

In collaboration with Dr Keith Brain at the University of Birmingham, preliminary experiments were undertaken to assess the ability of the Eu(III) bioconjugate **6.6** to target the dopamine transporter protein (DAT). All experiments were performed on the PC12 cell line. The choice of these cells was due to their ability to express the dopamine transporter DAT and to their differentiation into nerve-like cells when treated with nerve growth factor (NGF), making them ideal candidates for uptake experiments of **6.6** via the DAT protein.

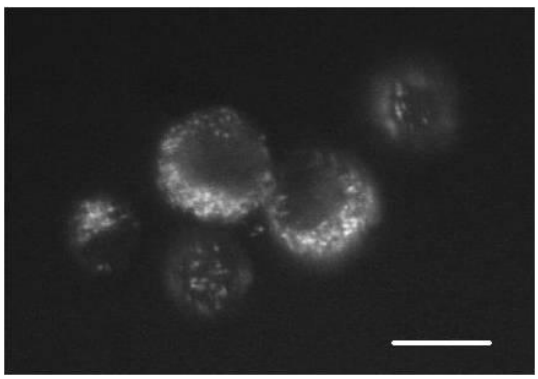


Figure 6-13. Epifluorescence image of PC-12 cells loaded with **6.6** (30μM). Scale bar 10μm.

Figure 6-13 shows an epifluorescence image of these cells upon incubation with **6.6**. It is evident that indeed the probe undergoes uptake and that it is internalised into the

cell. Furthermore, control experiments confirmed the uptake via the DAT transporter, as shown in Figure 6-14. In this experiments, the uptake assays were performed with and without the presence of a dopamine uptake inhibitor for DAT (GBR 12909). It can be noticed that, in the presence of the inhibitor, the uptake of the Eu(III) compound is effectively decreased, as a consequence of the saturation of the binding site by the inhibiting molecule GBR 12909.

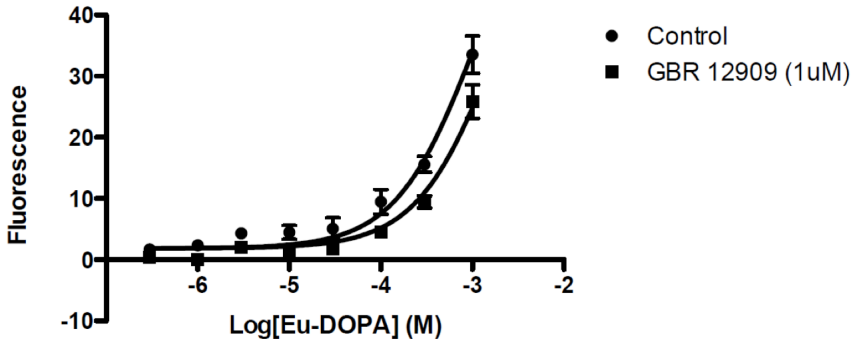


Figure 6-14. Uptake experiments of **6.6** with and without the presence of DAT inhibitor, showing a lower uptake of **6.6** in the presence of inhibition.

Preliminary experiments on the selectivity of uptake of the Eu(III) compound **6.6** by other cell lines were also undertaken, with the aim to understand, at least at an initial stage, whether the uptake of these complexes was mediated by the dopamine transporter (DAT). In particular, mesenteric artery labelling was attempted by comparing the uptake of the compound under study with a commercially available standard fluorescent substrate (NTUA) that targets the noradrenaline transporter pathway. Since the mesenteric artery does not express DAT, but only exhibits transport through the noradrenaline pathway, such a cell line is ideal to study specificity. While the NTUA is internalised by the artery, as signalled by the remaining fluorescence signal after washing, the same is not true for compound **6.6** indicating that the europium complex is targeted specifically to the DAT pathway. Furthermore, preliminary toxicological studies indicated that there is no increase in cell mortality in cell lines to which compound **6.6** is administered.

Clearly, there is considerable scope for further study on this system, and Dr Brain's group are currently pursuing investigations of uptake kinetics in other cell lines and in viscera.

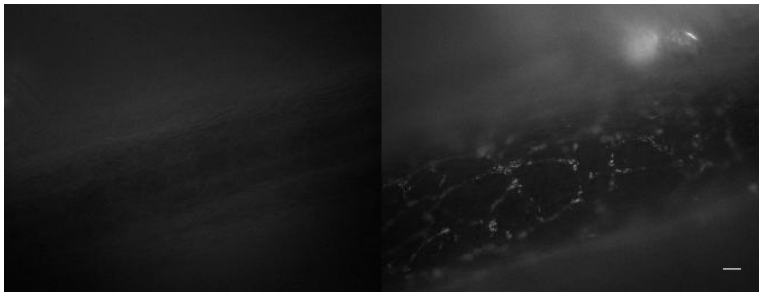


Figure 6-15 Comparison of residual fluorescence on a sample of mesenteric artery upon incubation with compound **6.6** (left) or with NTUA, a commercially available fluorescent substrate for the noradrenaline transporter (right).

6.4 Lanthanide bioconjugates containing an L-DOPA group

6.4.1 Introduction

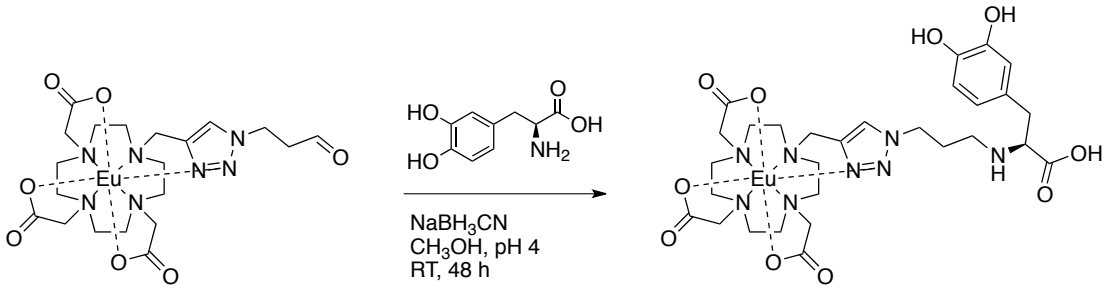
Given the successful reaction of the aldehyde-appended lanthanide complexes with dopamine, and the promising preliminary results about the biological activity the Eu(III) analog showed, it was reasoned that the same synthetic strategy could be adopted for the formation of a larger class of bioconjugates starting from biologically active compounds containing an amine group.

While dopamine itself constitutes a model substrate for the DAT, its chemical nature does not give this molecule the ability to cross the blood brain barrier and thus it cannot access dopaminergic neurons under physiological conditions. Thus, aside from being a potential reference compounds for *in vitro* experiments, lanthanide bioconjugates of dopamine may not be suitable candidates for whole animal applications.

Unlike dopamine, L-DOPA can cross the blood brain barrier and indeed, once internalised into the central nervous system, it is enzymatically converted into dopamine. It was thus reasoned that the ability of L-DOPA could be exploited to

enhance the pharmacokinetic properties of lanthanide bioconjugates towards their internalisation into the central nervous system where it could target the DAT protein. The synthetic strategy had already been optimised while the versatility of the aldehyde appended building blocks could be once again exploited.

6.4.2 Synthesis



6.3 **6.8**

Figure 6-16. Schematic description of the synthesis of L-DOPA lanthanide bioconjugates.

Starting from the aldehyde appended Eu(III) complex **6.3**, the chemical modification proceeded in the same fashion outlined previously. L-DOPA and **6.3** were coupled via reductive amination, and the complex obtained was purified by dialysis. NMR spectroscopy, mass spectrometry and photophysical studies helped to characterise the product obtained.

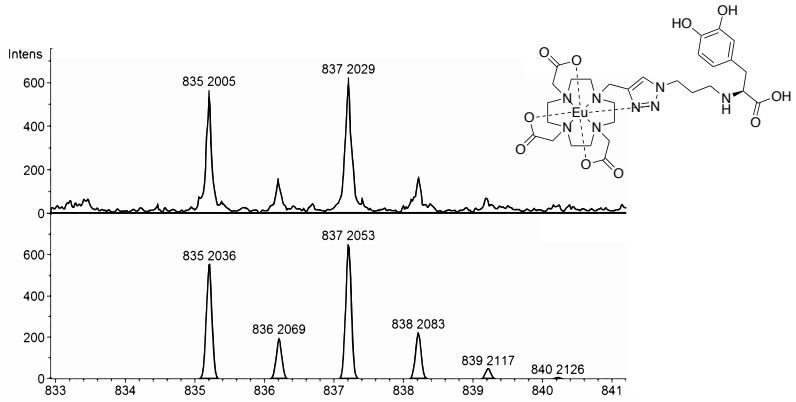


Figure 6-17. High resolution ESMS of **6.8** showing the experimental (top) and theoretical (bottom) isotope pattern.

6.4.3 NMR spectroscopy characterisation

From the paramagnetic NMR spectrum shown in Figure 6-18, it can be deduced that proton environment around the paramagnetic metal ion has undergone a negligible change and that the speciation in solution has mainly remained unchanged, with only one major isomer dominating the spectrum. It is worth noting that the presence of a chiral centre does not affect the overall spectrum, given the this does not alter the thermodynamic equilibrium between the diastereoisomers in solution, with the SAP clearly still being the most stable conformation over the TSAP isomer. As in the case of the dopamine bioconjugates, the presence of overall broader signals for **6.8** when compared to the parent aldehyde appended complex **6.3**, may be an indication of a, less fluxional structure in solution.

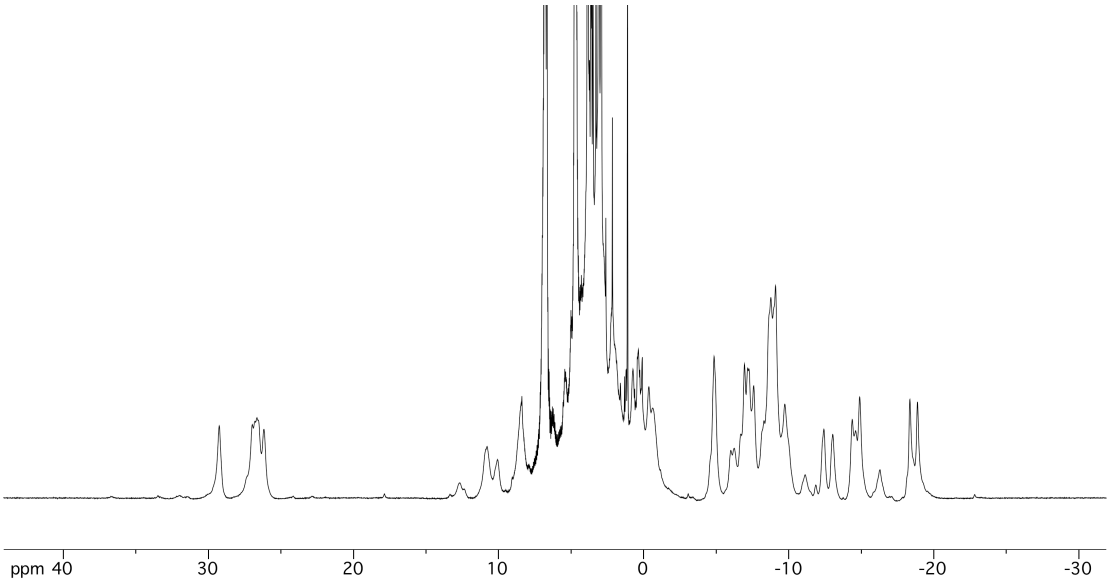


Figure 6-18. 1H-NMR spectrum of **6.8** registered in D_2O at RT at pD 7.

6.4.4 Photophysical characterisation

Figure 6-19 shows the emission spectrum of **6.8** together with its excitation and UV-Vis absorption profiles. The complex proved to be luminescent upon excitation into the visible, even though the presence of the Eu(III) $^7F_0$ to $^5L_6$ direct excitation peak indicates that the energy transfer process is not particularly efficient.

Indeed, due to the electron rich nature of the catechol group, an alternative quenching pathway might be envisaged in which an LMCT state forms upon electron transfer between the aromatic group and the lanthanide ion. This would inevitably lead to non-radiative depopulation of the emissive $^5D_0$ state of Eu(III) since this newly formed LMCT state is lower in energy. This behaviour has indeed been observed in the literature, with a dynamic quenching taking place between catechol derivatives and a series of europium complexes and is explained in more detail in chapter 2.[12]

Nonetheless, subtly different behaviour from its precursor was observed in the case of complex **6.8**, with values of lifetimes comparable with the corresponding aldehyde complex **6.3**, indicating that the main Eu(III) emissive state ($^5D_0$) does not undergo depopulation via the formation of a LMCT state. Sensitisation via the triazole is the main energy transfer pathway in this case, though the characteristic peak at 397 nm suggests that indirect excitation has a limited efficiency. The reduced effectiveness of the electron-transfer mediated non-radiative quenching process is not surprising, given the distance separating the electron rich catechol and the metal centre and the absence of a conjugated bridge between them.

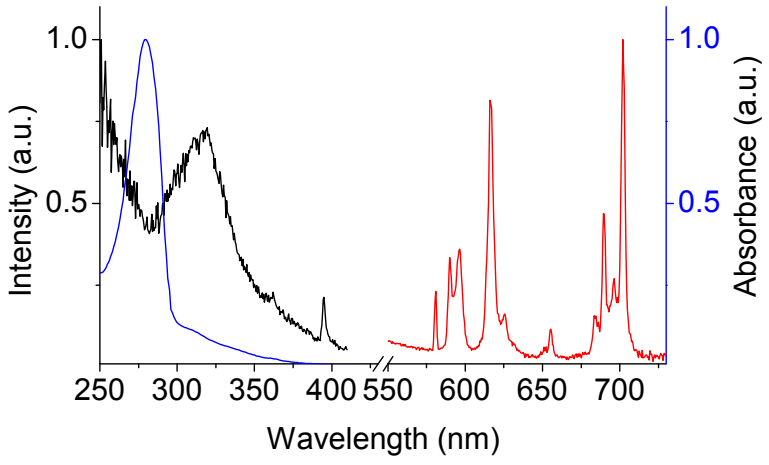


Figure 6-19. Emission spectrum of the Eu(III) compound **6.8** also showing the corresponding excitation spectrum (black line) and UV-Vis spectrum.

Indeed, excitation and UV-Vis absorption spectra of the compound do not overlap, confirming the absence of effective communication between lanthanide and catechol and the presence of only the triazole group as the sensitising unit.

Table 6-3. Luminescence lifetime values for the Eu(III) complex appended with L-DOPA.

Compound	λ_{ex}/nm	λ_{em}/nm	τ_{H2O}/μs	τ_{D2O}/μs	**q**
6.8	320	616	530	1410	1.1

6.5 Conclusions

In this chapter a class of lanthanide complexes containing an aldehyde moiety have been prepared in one simple step from readily available and widely versatile starting materials. Aiming to the development of a contrast agent with the potential to target dopaminergic neurons, it has been shown that this newly formed building block can be coupled to dopamine and L-DOPA via reduction amination upon mild reaction conditions. The corresponding bioconjugates containing Eu(III) have been studied in solution by means of paramagnetic ^{1}H-NMR and luminescence and their speciation in solution has been confirmed. Some very promising results have been obtained in *in vitro*/*in vivo* experiments that suggested the selective uptake of the Eu(III) probe into dopaminergic neurons through the DAT transporter. These results are indeed only a first step towards an exhaustive study of the biological activity of lanthanide containing bioconjugates aiming to target and image dopaminergic neurons.

6.6 References

1. M. Woods, D. Woessner and A. Sherry, *Chem. Soc. Rev.*, 2006, **35**, 500-511.
2. L. Frullano, C. Catana, T. Benner, A. D. Sherry and P. Caravan, *Angew. Chem., Int. Ed.*, 2010, **49**, 2382-2384.
3. T. Koullourou, L. S. Natrajan, H. Bhavsar, S. J. A. Pope, J. Feng, J. Narvainen, R. Shaw, E. Scales, R. Kauppinen, A. M. Kenwright and S. Faulkner, *J. Am. Chem. Soc.*, 2008, **130**, 2178-2179.
4. P. Seeman and H. B. Niznik, *Faseb J.*, 1990, **4**, 2737-2744.
5. R. R. Gainetdinov, S. R. Jones, F. Fumagalli, R. M. Wightman and M. G. Caron, *Brain Res. Rev.*, 1998, **26**, 148-153.
6. J. G. Nutt, J. H. Carter and G. J. Sexton, *Ann Neurol*, 2004, **55**, 766-773.
7. S. J. Chinta and J. K. Andersen, *Int. J. Biochem. Cell Biol.*, 2005, **37**, 942-946.
8. P. Caravan, *Chem. Soc. Rev.*, 2006, **35**, 512-523.
9. B. Ravina, D. Eidelberg, J. E. Ahlskog, R. L. Albin, D. J. Brooks, M. Carbon, V. Dhawan, A. Feigin, S. Fahn, M. Guttman, K. Gwinn-Hardy, H. McFarland, R. Innis, R. G. Katz, K. Kieburtz, S. J. Kish, N. Lange, J. W. Langston, K. Marek, L. Morin, C. Moy, D. Murphy, W. H. Oertel, G. Oliver, Y. Palesch, W. Powers, J. Seibyl, K. D. Sethi, C. W. Shults, P. Sheehy, A. J. Stoessl and R. Holloway, *Neurology*, 2005, **64**, 208-215.
10. A. W. Michell, S. J. G. Lewis, T. Foltynie and R. A. Barker, *Brain*, 2004, **127**, 1693-1705.
11. V. V. Rostovtsev, L. G. Green, V. V. Fokin and K. B. Sharpless, *Angew. Chem. Int. Ed. Engl.*, 2002, **41**, 2596-2599.
12. F. Kielar, C. P. Montgomery, E. J. New, D. Parker, R. A. Poole, S. L. Richardson and P. A. Stenson, *Org. Biomol. Chem.*, 2007, **5**, 2975-2982.

7 Conclusion and Future Perspective

This work has demonstrated the scope and versatility of Click chemistry applied to lanthanide containing complexes. Furthermore, the products obtained from such reactions have been used to demonstrate a number of concepts, including:

7.1 Redox Mediated Switching of Lanthanide luminescence

This work covered the basics of the modulation of lanthanide luminescence by changing the redox potential of the environment and hence gives ample scope for further development. Our results represent the first application of such an approach, and have demonstrated that a simple spectroelectrochemical set-up can yield remarkable data. The efficiency of modulation itself must be improved. In particular, the use of lanthanide probes with high luminescence quantum yield in their "ON" redox state would be advantageous, while total quenching in the "OFF" state is also highly desirable.

Future work could focus on the development of chromophores that are able to sensitise lanthanide luminescence and whose photophysical properties can be changed by a redox event. Ideally, such a chromophore would have strong absorption in the visible region and a high efficiency of lanthanide sensitisation.

7.2 Anion modulated luminescence in lanthanide appended rotaxanes

Aside from demonstrating the first route to lanthanide appended rotaxanes, this work has clearly shown that the use of an octadentate lanthanide complex, even if neutral, will compete effectively with the rotaxane cavity in binding experiments with anions in any solvent system, and that is a much more effective anion binding site in

competitive media. While binding to the metal appears to be strong even in competitive solvent mixtures, the selectivity between monodentate anions is poor due to the lack of directionality for pure electrostatic interactions. These difficulties could be circumvented by a supramolecular structure in which the lanthanide centre is a structural component of the anion binding cavity. This would lead to a synergistic effect, allowing hydrogen bonding (or other supramolecular interactions) to supplement the anion binding by the macrocycle, while the nature of the cavity itself can be used to engender selectivity.

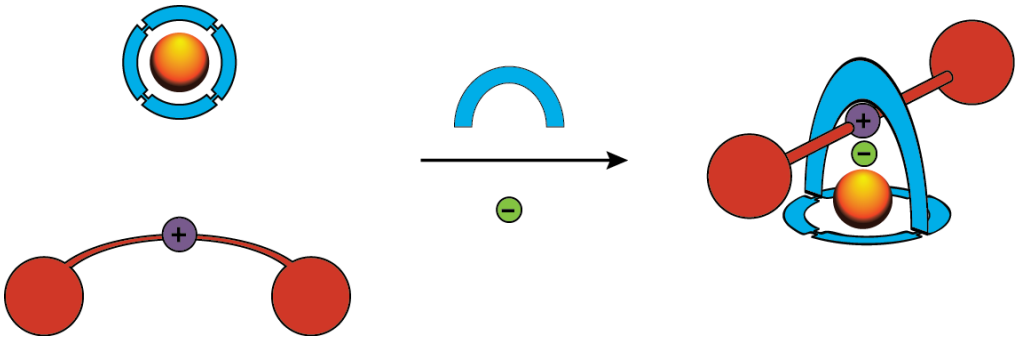


Figure 7-1. Sketch of a possible design of a supramolecular architecture where a lanthanide complex and a binding cavity are exploited to interact with anions in the same binding domain.

7.3 Multi-macrocyclic structures containing lanthanide complexes

The alkyne containing complexes prepared in this thesis are amenable to a vast range of functionalisation via Cu(I) "click" chemistry, and it has been possible to extend the concept just described to systems in which two arms on a cyclen complex are joined together through a second macrocyclic bridge. While the reaction to form such a bismacrocyclic structure was not entirely successful, the routes investigated show promise and could potentially be optimised. The use of a templating anion should improve the efficiency of the reaction by leading to preorganisation of the bis-azide molecule. The macrocycle can then be tested for sensing purposes or used for assembling supramolecular structures.

7.4 Behaviour of heterobimetallic *f-f'* lanthanide arrays

The class of azide-containing lanthanide complexes are amenable to several derivatisations by means of Cu(I) "click" chemistry. In my thesis, this new molecule has been shown to have considerable scope as a Click substrate in its own right. Further studies can be envisaged: in particular, the preparation of multimetallic systems containing several Gd(III) centres can potentially lead to MRI contrast agents with high relaxivity. The advantage of using azide functionalised Gd(III) complexes is that these can be arranged around a central "hub" containing multiple alkyne sites while keeping the system rigid through conjugation. By contrast with the class of alkyne containing complexes, this approach to multinuclear arrays avoids the use of molecules that contain many azide groups and constitute a possible safety hazard.

The mechanism of sensitisation of lanthanide luminescence in the class of heterobimetallic compounds merits further study in depth, in particular with regard to the possibility of communication between lanthanide centres and the effect of different bridging units between them.

7.5 Synthesis and study of lanthanide bioconjugates

We have shown that it is possible to target the dopamine transporter pathway using simple bioconjugates derived from propargyl DO3A complexes. This work is still ongoing, but the demonstration of the effect gives great scope for further development, particularly through optimising both the photophysical properties and the bioactivity of the compounds, and through demonstrating the nature of the uptake pathway beyond doubt. For optical studies, the incorporation of chromophores that absorb at longer wavelengths is almost imperative, while variation of the emissive lanthanide is also desirable. If continuing uptake can be demonstrated *in vivo* to the point where micromolar concentrations of the probe can build up inside cells, it is possible to conceive the use of MRI to study the central nervous system. Much clearly

remains to be done, but this thesis clearly illustrates both the scope and potential of Click chemistry with lanthanide complexes.

8 Experimental

8.1 General procedures

Commercially available solvents and chemicals were used without further purification unless otherwise stated. Where dry solvents were used, they were degassed with nitrogen, dried by passing through an MBraun MPSP-800 column and then used immediately. Water was deionised and microfiltered using a Milli-Q Millipore machine. Tetrabutylammonium (TBA) salts were stored under vacuum in a desiccator. Propargyl bromide was used as a solution of 80% wt. in toluene. All other reagents were purchased and used as received. Silica gel for flash column chromatography was purchased from Merck (Geduran 60, 230-400 mesh) and neutral alumina was purchased from Sigma-Aldrich (Merck 90, 70-230 mesh) and soaked in ethyl acetate before use. Size exclusion chromatography used Bio-Beads SX-3 as stationary phase and toluene as mobile phase. Silica TLC plates were TLC Silica gel 60 purchased from Merck. Dialysis was performed using a dialysis chamber purchased from Sigma-Aldrich and using the appropriate cellulose membrane (MWCO = 500 or 1000 as indicated). The sample was dissolved in water and the chamber was placed in 2 L conical flask filled with water. The water was changed at least twice a day.

NMR spectra were registered at 295 K unless otherwise state. 300 MHz ^{1}H or 76 MHz ^{13}C NMR spectra were recorded on a Varian Mercury 300 spectrometer. 500 MHz ^{1}H or 126 MHz ^{13}C NMR spectra were recorded on a Bruker AVIII 500 spectrometer or a Bruker AVII 500 with ^{13}C cryoprobe. 700 MHz ^{1}H spectra were recorded on a Varian VNMRS-700. All chemical shift (δ) values are given in parts per million and were referenced to the residual solvent peak.

Low-resolution mass spectra were recorded on a Micromass LCT Premier XE spectrometer. Accurate masses were determined to four decimal places using Bruker μTOF and Micromass GCT spectrometers. MALDI-TOF mass spectra were recorded on a Waters MALDI Micro MX or recorded by the staff at the National Mass Spectrometry Service Centre facility in Swansea using a Voyager DE-STR MALDI-TOF system. IR spectra were recorded using a Bruker Tensor 27 FT-IR equipped with an ATR unit.

UV-Vis spectra were recorded on a PG T60 U UV-Vis spectrometer. Luminescence spectra were measured either on a Perkin Elmer LS55 on a Horiba Jobin Yvon FluoroLog-3 equipped with a Hamamatsu R928 PMT detector and a double-grating emission monochromator. The spectra were corrected to take into account the energy profile of the lamp and the detector sensitivity at each wavelength using the manufacturer correction file. For emissions in the 800-1150 nm region a liquid-nitrogen cooled NIR-PMT detector was used. Lifetimes were recorded using the flash lamp present in the instruments and the decay curves were fitted to a single exponential decay using an Excel spreadsheet or the Origin software. In the case of lifetime luminescence measurements of ytterbium complexes, the sample was excited using a pulsed nitrogen laser (PTI- 3301-337nm) or using a dye laser (PTI-3302). Light emitted at right angles to the excitation beam was focused onto the slits of the monochromator (PTI120), which was used to select the appropriate wavelength. The growth and decay of the luminescence at selected wavelengths was detected using a germanium photodiode (Edinburgh Instruments, EI-P) and recorded using a digital oscilloscope (Tektronix TDS220) before being transferred to the computer for analysis. Luminescence lifetimes were obtained by iterative reconvolution of the detector response (obtained by using a scatter) with exponential components for growth and decay of the metal centred luminescence using a spreadsheet running in Microsoft Excel. The time-resolved emission (TRES) spectra for the complexes were obtained by measuring the growth and decay of the luminescence at each series of wavelengths.

Electrochemical experiments were performed directly inside a Perkin Elmer LS55 Spectrometer using a Starna® sub-micro type 26 fluorimeter cell (geometric volume 100 μL). The three electrode setup consisted of a fine Pt mesh as a working electrode, a Pt wire as a counter electrode and a no leak Ag/AgCl reference electrode (Cypress system). The electrodes were positioned so as not to disturb the luminescence measurements. The total volume of the sample was ca. 140 μL of supporting electrolyte solution (0.1M $NaClO_4$) containing 2 mM of complex in de-ionised and microfiltered H_2O. Cyclic voltammograms were performed on a microAutolab type II/GPES (General Purpose Electrochemical System – Version 4.9), Eco Chemie. Chronoamperometry was employed to cycle between oxidative (0.6 V) and reductive (0 V) potentials for 30 and 40 minutes respectively. Synchronized luminescence measurements were taken *in situ.*

For the X-ray analysis of **2.9**, the crystal was mounted using the oil drop technique, in perfluoropolyether oil at 150(2) K using a Cryostream N_2 open-flow cooling device.[1] Diffraction data were collected using graphite monochromatic Mo-K_α radiation (λ = 0.71073 Å) on a Nonius Kappa CCD diffractometer. A series of ω-scans was performed in such a way as to collect a complete data set to a maximum resolution of 0.77 Å. Data reduction including unit cell refinement and inter-frame scaling was carried out using DENZO-SMN/SCALEPACK.[2] Intensity data were processed and corrected for absorption effects by the multi-scan method, based on repeat measurements of identical and Laue equivalent reflections. Structure solution was carried out with direct methods using the program SIR92[3] within the CRYSTALS software suite.[4] In general, coordinates and anisotropic displacement parameters of all non-hydrogen atoms were refined freely except where disorder necessitated the use of "same distance restraints" together with thermal similarity and vibrational restraints to maintain sensible geometry/displacement parameters. Hydrogen atoms were generally visible in the difference map and refined with soft restraints prior to inclusion in the final refinement using a riding model.[5]

Fluorescence titrations were carried out using a Horiba Fluorolog-3 spectrometer at room temperature. Typically, a 1.8 ml solution of host (ca. 1 x 10^{-5} M) in dichloromethane or dichloromethane/methanol (1:1 *v/v*) was titrated with a solution of the anion of interest in the same solvent (ca. 3 x 10^{-3-} M). Depending on the strength of the binding, up to 40 equivalents of the anionic guest were added. The final volume of the host-guest mixture did not exceed 1.89 ml.

Fitting using Dynafit

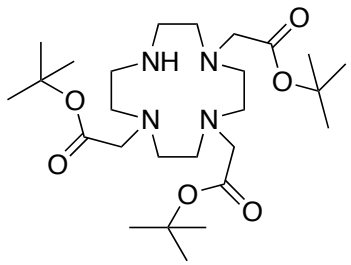
Dynafit was used to fit the responses observed in the luminescence spectrum of the Eu complexes upon addition of anion to the solution. As the dilution method was used for the titrations, the concentration independent intensity ratio was used to determine the association constant. If intensities had to be incorporated into the model, only data obtained with a dilution of less than 5% were employed.

Example of Dynafit script

```
[task]
data = equilibra task = fit
[mechanism] Eurotaxane + Cl <==> Eurotaxane.Cl
[constants] K1 = 100000 ??
[concentrations] Eurotaxane = 3.916e-005
[equilibria] variable Cl
: K1 assoc
file
C:\Users\Manuel\Desktop\Eu_rotaxane\MT354_DCM\Dynafit_input\MT354_DCM_Cl_DJ=2_DJ1.txt
| response Eurotaxane=15490 ?, Eurotaxane.Cl=30000 ? file
C:\Users\Manuel\Desktop\Eu_rotaxane\MT354_DCM\Dynafit_input\MT354_DCM_Cl_DJ=2_DJ4.txt
|response Eurotaxane=16480 ?, Eurotaxane.Cl=30000 ?
;file
C:\Users\Manuel\Desktop\Eu_rotaxane\MT354_DCM\Dynafit_input\MT354_DCM_Cl_DJ=2_DJ0.txt
|response Eurotaxane=16480 ?, Eurotaxane.Cl=30000
[output] directory
C:\Users\Manuel\Desktop\Eu_rotaxane\MT354_DCM\Dynafit_output\MT354_DCM_Cl_DJ_ratios_al
l\
[end]
```

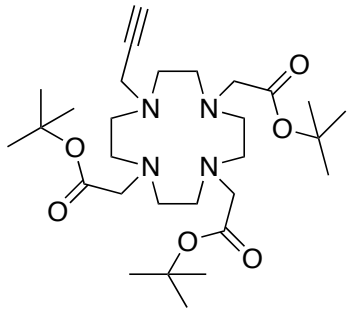
8.2 Synthesis

1,4,7-Tris(*tert*-butoxycarbonylmethyl)-1,4,7,10-tetraazacyclododecane, hydrobromide salt[6] (2.3)



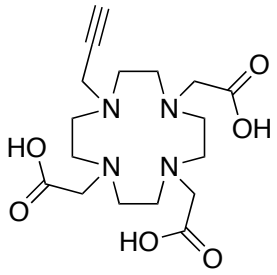
Cyclen (5.00 g, 29 mmol) was dissolved in dry acetonitrile (120 ml). Sodium hydrogen carbonate (8.04 g, 96 mmol) was added to this solution. The resulting suspension was placed in an ice bath and stirred vigorously for 30 minutes. Tert-butyl bromoacetate (18.72 g, 96 mmol) was then added dropwise over 30 min. Once the addition was completed the reaction was left stirring at RT under nitrogen for 48 h. The inorganic solid was removed by filtration and the solvent was evaporated under reduced pressure leaving a beige solid. The final product was obtained by multiple recrystallisations from hot toluene and was isolated as a white solid. (9.13 g, 53 %). ^{1}H NMR (300 MHz; $CDCl_3$): δ 10.04 (s, br, 1H), 3.38 (s, 4H), 3.29 (s, 2H), 3.10 (s, br, 4H), 2.90 (s, br, 12H), 1.46 (s, 27H). ^{13}C NMR (76 MHz; CDCl3): δ 170.5, 81.7, 58.2, 51.3, 49.2, 47.5, 28.1. LR-ESMS: *m/z* calc. for $[M+H]^+$ 515.38, found 515.35.

1,4,7-Tris(*tert*-butoxycarbonylmethyl)-10-(prop-2-ynyl)-1,4,7,10-tetraazacyclododecane[7, 8] (2.4)



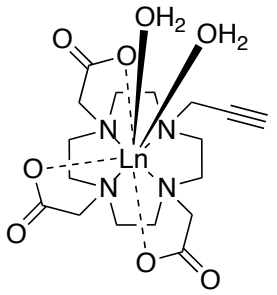
To a solution of **2.3** (2.50 g, 4.2 mmol) in 30 ml of dry acetonitrile was added potassium carbonate (1.45 g, 10.5 mmol) and this suspension was left stirring for 20 min. Propargyl bromide (0.62 g, 4.2 mmol) was added dropwise while keeping the reaction flask in an ice bath. The reaction was left stirring under nitrogen for 8 h at RT and monitored by ES-MS. The inorganic solids were removed by filtration and the solvent evaporated under reduced pressure. The product was obtained as a beige oil after successive filtrations from toluene to remove residual inorganic solid. (2.14 g, 92 %). ^{1}H NMR (300 MHz; $CDCl_3$): δ 3.43 (d, J = 2.0, 2H), 3.28 (s, 6H), 2.82-2.79 (m, 12H), 2.69 (m, 4H), 2.14 (t, J = 2.0, 1H), 1.45 (s, 27H). ^{13}C NMR (76 MHz; $CDCl_3$): δ 171.2, 129.1, 128.3, 125.4, 80.8, 79.4, 72.6, 56.9, 52.2, 51.90, 51.71, 43.2, 28.3. LR-ESMS: *m/z* calc. for $[M+H]^+$ 553.40, found 553.37.

1,4,7-Tris(carboxymethyl)-10-(prop-2-ynyl)-1,4,7,10-tetraazacyclododecane[7, 8] (2.5)



Compound **2.4** (0.7 g, 1.26 mmol) was dissolved in DCM (8 mL) and TFA (8 mL) was added dropwise. The solution was stirred overnight at RT. The solvent was removed under reduced pressure and the residue dissolved in the minimum amount of methanol and precipitated with diethyl ether. Trituration with diethyl ether yielded the TFA salt of the title compound as a white solid in quantitative yield. ^{1}H NMR (300 MHz; D_2O): δ 3.84-3.66 (br, 8H), 3.31-3.22 (m, br, 16H), 2.82 (s, br, 1H). ^{13}C NMR (75MHz, D_2O) δ = 31.38, 36.89, 43.61, 45.49, 48.86, 49.74, 51.78, 52.86, 53.10, 53.28, 54.44, 56.84, 72.62, 77.65, 171.98, 174.36. LR-ESMS: *m/z* calc. for $[M+H]^+$ 384.20, found 385.22.

General method for the synthesis of the lanthanide complexes from 2.5



To a solution of the ligand in methanol the appropriate lanthanide triflate salt was added (1.05 eq.) and the reaction mixture was stirred at 40º C for 30 min. The pH was adjusted to 4 by dropwise addition of an aqueous NaOH solution. The reaction was

left stirring at 40 ºC for 48 h. The methanol was removed under reduced pressure leaving an oil that was dissolved in water. The pH of this solution was adjusted to 10 by addition of aqueous NaOH to remove excess of lanthanide as its insoluble hydroxide. The resulting precipitate was centrifuged and the supernatant filtered. The solvent was removed under reduced pressure to obtain the product as a white solid.

2.6 (Ln: Eu)**.** Yield: 92%. ^{1}H NMR (300 MHz; D_2O): δ 23.3 (s), 14.0 (s), 11.5 (s), 10.2 (s), -3.9 (s), -6.1 (s), -6.6 (s), -9.5 (s), -11.2 (s), -11.7 (s), -12.5 (s), -12.7 (s), -13.1 (s), -14.8 (s), -17.7 (s). Only resolved peaks outside 0 to 10 ppm region are reported. MALDI-MS (α- MeOH): *m/z* calc. for $[M+Na]^+$ 556.36, found 555.43. Luminescence: H_2O: 0.40 ms, D_2O: 1.85. q=2.1.

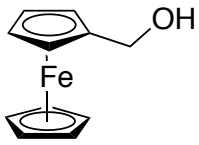
2.7 (Ln: Yb)**.** Yield: 87%. ^{1}H NMR (300 MHz; D_2O): δ 85.7, 62.6, 53.3, 39.7, 29.9, 23.9, 23.5, 12.4, -4.9, -8.4, -11.1, -12.1, -17.9, -18.3, -20.1, -30.1, -52.5, -56.9. Only resolved peaks outside 0 to 10 ppm region are reported. LR-ESMS: *m/z* calc. for $[M+Na]^+$ 578.11, found 578.13.

2.8 (Ln: Gd)**.** Yield: 91%. LR-ESMS: *m/z* calc. for $[M+Na]^+$ 562.09, found 562.14. IR-ATR(cm^{-1}): 1598, 1256, 1170, 1035, 630.

2.9 (Ln: Lu) Yield: 92%. ^{1}H NMR (300 MHz; D_2O): δ 3.93 (s, br, 1H), 3.33 (s, br, 8H), 3.03-2.63 (m, br, 17H). LR-ESMS: *m/z* calc. for $[M+Na]^+$ 579.11, found 579.15.

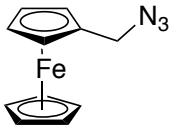
2.29 (Ln: Tb). Yield: 89%. ^{1}H NMR (500 MHz; D_2O, pD7): δ 333.9, 317.1, 275.1, 141.3, 87.3, 72.3, -49.9, -63.8, -80.2, -84.6, -93.8, -101.3, -154.2, -162.9, -176.4, -196.9, -208.4, -227.6, -313.0. Only resolved peaks related to the major isomer outside the +40 to -40 ppm region reported. MALDI-MS (α- MeOH): calc. for $[M+Na]^+$ 563.32, found 565.01. Lifetimes: H_2O: 1.13 ms, D_2O: 2.69 ms; q=2.3.

Synthesis of hydroxymethyl ferrocene[9] (2.11)



Ferrocene carboxyaldehyde (0.5 g, 2.3 mmol) was dissolved in methanol (25 ml) and cooled at 0 °C in an ice bath. $NaBH_4$ (0.44 g, 11.5 mmol) was dissolved in an aqueous solution of sodium hydroxide (2 M) and then added via a cannula. The resulting mixture was stirred for 16 h at RT. The solvent was evaporated under reduced pressure to leave an aqueous solution that was extracted with diethyl ether (3 × 30 mL). The organic layer was washed with water (2 × 30 mL), dried over anhydrous $MgSO_4$ and filtered through Celite. The solvent was evaporated under reduced pressure to leave the product as a crystalline light orange solid in quantitative yield. ^{1}H NMR (300 MHz; $CDCl_3$): δ 4.32 (s, 2H), 4.25 (s, 2H), 4.19 (s, 7H). ^{13}C NMR (76 MHz; $CDCl_3$): δ 89.10, 69.10, 68.40, 61.10.

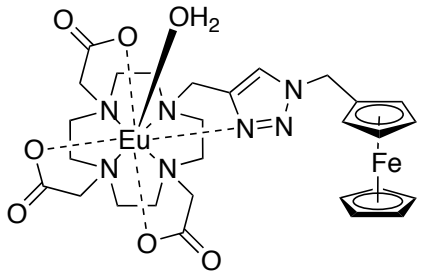
Synthesis of azidomethyl ferrocene[10] (2.12)



Hydroxymethyl ferrocene **2.11** (0.10 g, 0.41 mmol) was dissolved in glacial acetic acid (3 ml) and sodium azide (0.27 g, 4.1 mmol) was added. This solution was stirred for 3 h in an oil bath at 60 ºC. The reaction mixture was diluted with 50 ml of DCM and extracted with a saturated solution of $NaHCO_3$ (3 x 50 ml), dried over anhydrous $MgSO_4$ and filtered. After evaporation of the solvent under reduced pressure the product was purified by silica gel chromatography (EtOAc/hexane 1:25) to obtain a

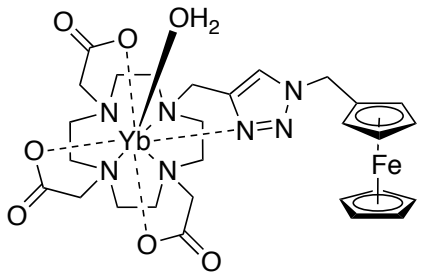
yellow oil that was stored in the dark. (94 mg, 85 %). ^{1}H NMR (300 MHz; $CDCl_3$): δ 4.24 (s, 2H), 4.20 (s, 2H), 4.17 (s, 5H), 4.12 (s, 2H). ^{13}C NMR (76 MHz; $CDCl_3$): δ 82.1, 68.72, 68.60, 50.8. LR-ESMS: : *m/z* calc. for $[M+H]^+$ 242.04, found 242.30.

Eu(III)-1,4,7-Tris(carboxymethyl)-10-[(1*H*-1,2,3-triazol-1-yl)methyl ferrocene]-1,4,7,10-tetraazacyclododecane (2.13)



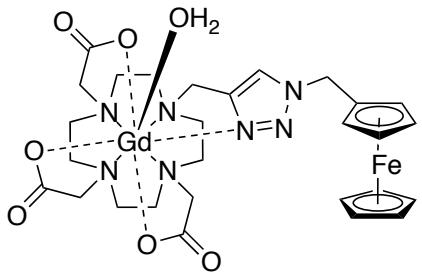
Compounds **2.12** (32.5 mg, 0.135 mmol) and **2.6** (60 mg, 0.112 mmol) were dissolved in 10 mL of methanol. Sodium ascorbate (4.7 mg, 0.023 mmol) and copper(II) sulfate pentahydrate (1.7 mg, 0.007 mmol) were added and the mixture was left stirring for 24 h at RT. The solvent was removed under reduced pressure and the oil obtained was redissolved in methanol. Unreacted ferrocene azide was removed by extractions with hexane (4 x 30 mL). The product was obtained by trituration with diethyl ether as a light yellow powder (71 mg, 82%). Copper and sodium ascorbate traces were eliminated by dialysis and the product was further treated with a copper scavenger (Quadrasil TA). ^{1}H-NMR (300 MHz; D_2O): δ 29.8, 29.4, 28.7, 27.6, 27.1, 26.8, -4.2, -4.7, -5.1, -7.2, -8.6, -8.9, -9.3, -9.6, -9.9, -11.2, -12.3, -13.5, -14.9, -15.4, -16.5, -18.9, -19.5. Only resolved peaks outside 0 to10 ppm region are reported. HR-ESMS: *m/z* calc. for $[M+Na]^+$ 798.119, found 798.118. IR-ATR(cm^{-1}): 1599 (C=O). UV-Vis (H_2O) λ_{max}: 259 nm (ε= 2640 $M^{-1}cm^{-1}$), 423 nm (ε= 142 $M^{-1}cm^{-1}$).

Yb(III)-1,4,7-Tris(carboxymethyl)-10-[(1*H*-1,2,3-triazol-1-yl)methyl ferrocene]-1,4,7,10-tetraazacyclododecane (2.14)



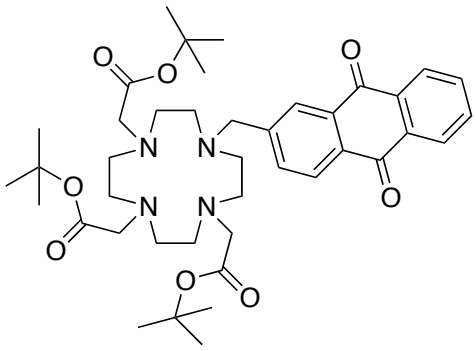
Compounds **2.12** (60 mg, 0.252 mmol) and **2.7** (133 mg, 0.240 mmol) were dissolved in 20 mL of methanol. Sodium ascorbate (4.8 mg, 0.024 mmol) and copper(II) sulfate pentahydrate (3.0 mg, 0.012 mmol) were added and the mixture was left stirring for 24 h at RT. The solvent was removed under reduced pressure and the oil obtained was redissolved in methanol. Unreacted ferrocene azide was removed by extractions with hexane (6 x 30 mL). The product was obtained by trituration with diethyl ether as a light yellow powder (162 mg, 85%). Copper and sodium ascorbate traces were eliminated by dialysis and the product was further treated with a copper scavenger (Quadrasil TA). ^{1}H-NMR (300 MHz; D_2O): δ 122.9, 120.5, 116.9, 114.5, 37.6, 32.6, 25.3, 24.6, -11.1, -53.1, -56.6, -68.8, -72.1, -72.6, -74.6, -83.0. Only resolved peaks outside -10 to 20 ppm region are reported. HR-ESMS: *m/z* calc. for $[M+Na]^+$ 819.136, found 819.136. IR-ATR(cm^{-1}): 1585 (C=O). UV-Vis (H_2O) λ_{max}: 262 nm (ε= 2580 $M^{-1}cm^{-1}$), 423 nm (ε= 78 $M^{-1}cm^{-1}$).

Gd(III)-1,4,7-Tris(carboxymethyl)-10-[(1*H*-1,2,3-triazol-1-yl)methyl ferrocene]-1,4,7,10-tetraazacyclododecane (2.15)



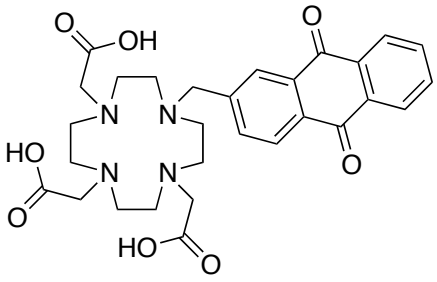
Compounds **2.12** (49 mg, 0.203 mmol) and **2.8** (91 mg, 0.169 mmol) were dissolved in 15 mL of methanol. Sodium ascorbate (4.0 mg, 0.016 mmol) and copper(II) sulfate pentahydrate (7.0 mg, 0.035 mmol) were added and the mixture was left stirring for 24 h at RT. The solvent was removed under reduced pressure and the oil obtained was redissolved in methanol. Unreacted ferrocene azide was removed by extractions with hexane (4 x 30 mL). The product was obtained by trituration with diethyl ether as a light yellow powder (113 mg, 85 %). Copper and sodium ascorbate traces were eliminated by dialysis and the product was further treated with a copper scavenger (Quadrasil TA). HR-ESMS: *m/z* calc. for $[M+Na]^+$ 803.122, found 803.121. IR-ATR(cm^{-1}): 1604 (C=O). UV-Vis (H_2O) λ_{max}: 255 nm (ε= 1574 $M^{-1}cm^{-1}$), 425 nm (ε= 47 $M^{-1}cm^{-1}$).

1,4,7-Tris(*tert*-butoxycarbonylmethyl)-10-(2-methylanthraquinone)-1,4,7,10-tetraazacyclododecane (2.17)



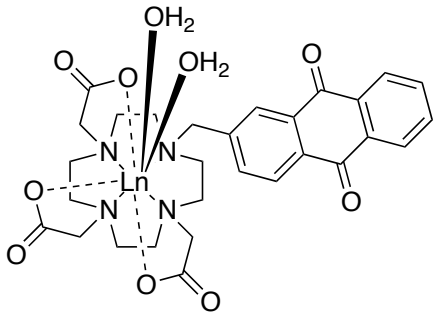
To a solution of **2.3** (1.5 g, 2.5 mmol) in 20 ml of dry acetonitrile was added potassium carbonate (0.69 g, 5.0 mmol) and this suspension was left stirring for 20 min. 2-Bromomethyl-anthraquinone (0.75 g, 2.5 mmol) was added while keeping the reaction flask in an ice bath. The reaction was left stirring under nitrogen for 8 h at RT and monitored by ES-MS. The inorganic solid was removed by filtration and the solvent evaporated under reduced pressure. The crude product was obtained as an amber oil and was purified by column chromatography on neutral alumina (DCM/MeOH 95:5 to 80:20) to obtain a yellow solid (0.55g, 30%). X-ray quality crystals were obtained by slow diffusion of hexane in dichloromethane. ^{1}H-NMR (300 MHz; d^{6}-dmso, 373 K): δ 8.25-8.17 (m, 4H), 7.97-7.91 (m, 3H), 3.80 (s, 2H), 3.26 (s, 2H), 3.16 (s, 4H), 2.73 (m, br, 16H), 1.46 (s, 10H), 1.39 (s, 17H). ^{13}C NMR (76 MHz; d^{6}-dmso): δ 180.5, 169.23, 168.21, 159.92, 159.22, 141.15, 137.90, 136.55, 135.56, 135.15, 134.01, 125.12, 115.55, 113.10, 81.8, 62.2, 49.3, 43.2, 42.5, 28.1. HR-ESMS: *m/z* calc. for $[M+Na]^{+}$ 757.415, found 757.414.

1,4,7-Tris(carboxymethyl)-10-(2-methylanthraquinone)-1,4,7,10-tetraazacyclododecane (2.18)



Compound **2.17** (0.7 g, 1.26 mmol) was dissolved in DCM (8 mL) and TFA (8 mL) was added dropwise. The solution was stirred at RT for 24 h. The solvent was removed under reduced pressure and the residue dissolved in the minimum amount of methanol and precipitated with diethyl ether. Trituration with diethyl ether yielded the TFA salt of the title compound as a white solid in quantitative yield. ^{1}H NMR (300 MHz; d^{6}-dmso, 353 K): δ 8.26 (dd, J = 5.5, 3.5, 4H), 7.99 (m, 3H), 4.25 (s, 2H), 3.66 (s, 2H), 3.58 (s, 4H), 3.12 (s, br, 4H), 3.03 (s, 12H). ^{13}C NMR (76 MHz; d^{6}-dmso): δ 48.74, 50.13, 53.78, 56.29, 115.48, 119.43, 127.32, 133.39, 133.45, 135.14, 135.26, 136.19, 136.88, 143.05, 158.52, 158.94, 170.41, 171.33, 182.86. HR-ESMS: *m/z* calc. for $[M+H]^{+}$ 567.246, found 567.245.

General method for the synthesis of the lanthanide complexes from 2.18



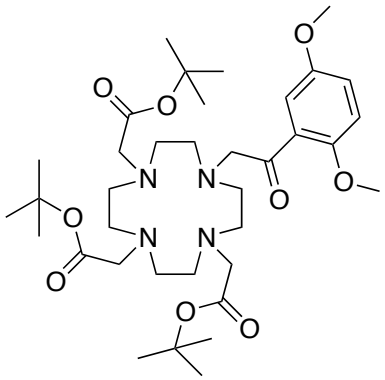
To a solution of the ligand in methanol the appropriate lanthanide triflate salt was added (1.05 eq.) and the reaction mixture was stirred at 40º C for 30 min. The pH was adjusted to 4 by dropwise addition of an aqueous NaOH solution. The reaction was left stirring at 40º C for 48 h. The methanol was removed under reduced pressure leaving an oil that was dissolved in water. The pH of this solution was adjusted to 10 by addition of aqueous NaOH to remove excess of lanthanide as its insoluble hydroxide. The resulting precipitate was centrifuged and the supernatant filtered to remove solid impurities. The solvent was removed under reduced pressure to obtain the product as an amber solid.

2.19 (Ln: Eu)**.** Yield: 88%. ^{1}H NMR (300 MHz; d^{6}-dmso): δ 37.80, 31.74, 28.78, 12.48, -4.11, -4.62, -6.47, -7.44, -9.53, -10.97, -15.02, -16.61, -17.52, -21.34, -22.93. Only resolved peaks outside 0 to 10 ppm region are reported. HR-ESMS: *m/z* calc. for $[M+H]^{+}$ 717.143, found 717.142. UV-Vis (H_2O) λ_{max}: 256, 334 nm. Lifetimes: 0.39 ms (H_2O); 1.28 ms (D_2O); q=1.8.

2.20 (Ln: Yb). Yield 85%. ^{1}H NMR (300 MHz; d^{6}-dmso): δ 143.56, 128.55, 67.95, 60.78, 48.88, 43.96, 40.44, 31.11, 25.21, 21.64, 20.21, 14.38, 12.61, -17.30, -22.24, -26.39, -43.11, -53.68, -55.63, -62.74, -64.90, -79.52, -81.30, -84.42, -96.44, -100.05, -108.79. Only resolved peaks outside 0 to 10 ppm region are reported. HR-ESMS: *m/z* calc. for $[M+Na]^{+}$ 760.143, found 760.140. UV-Vis (H_2O) λ_{max}: 257, 334 nm.

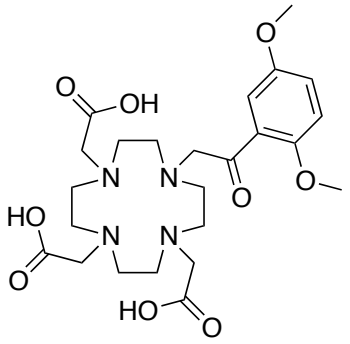
2.21 (Ln: Gd). Yield 88%. UV-Vis (H_2O) λ_{max}: 254, 332 nm. E_T = 25000 cm^{-1}. LR-ESMS: *m/z* calc. for $[M+Na]^+$ 720.14, found 720. 21.

1,4,7-Tris(*tert*-butoxycarbonylmethyl)-10-(2',5'-dimethoxy-2-acetophenone)-1,4,7,10-tetraazacyclododecane (2.23)



To a solution of **2.3** (2.0 g, 3.4 mmol) in 25 ml of dry acetonitrile was added potassium carbonate (0.97 g, 7.0 mmol) and this suspension was left stirring for 20 min. 2-Bromo-2′,5′-dimethoxyacetophenone (**2.22**) (0.88 g, 3.4 mmol) was added while keeping the reaction flask in an ice bath. The reaction was left stirring under nitrogen for 16 h at RT and monitored by ES-MS. The inorganic solids were removed by filtration and the solvent evaporated under reduced pressure. The crude product was obtained was purified by column chromatography on neutral alumina (DCM/MeOH 95:5 to 80:20) to obtain a yellow solid (1.28g, 54%). ^{1}H NMR (300 MHz; d^6-dmso 353 K): δ 7.20-7.18 (m, 1H), 7.15-7.10 (m, 2H), 3.89 (s, 2H), 3.84 (s, 3H), 3.73 (s, 3H), 3.03 (s, 6H), 2.70 (s, br, 8H), 2.36 (s, br 8H), 1.46 (s, 9H), 1.39 (s, 18H). ^{13}C NMR (76 MHz; d^6-DMSO): δ 28.10, 48.60, 48.98, 50.26, 50.64, 51.08, 54.06, 56.80, 58.68, 115.51, 116.10, 118.11, 119.16, 119.90, 120.89, 155.43, 157.76, 164.23, 165.01, 175.14. LR-ESMS: *m/z* calc. for $[M+Na]^+$ 715.87, found 714.47.

1,4,7-Tris(carboxymethyl)-10-(2',5'-dimethoxy-2-acetophenone)-1,4,7,10-tetraazacyclododecane (2.26)



Compound **2.26** (1.0 g, 1.90 mmol) was dissolved in DCM (8 mL) and TFA (8 mL) was added dropwise. The solution was stirred at RT for 24 h. The solvent was removed under reduced pressure and the residue dissolved in the minimum amount of methanol and precipitated with diethyl ether. Trituration with diethyl ether yielded the TFA salt of the title compound as a white solid in quantitative yield. ^{1}H NMR (500 MHz; D_2O): δ 7.14 (dd, 1H), 7.11-7.10 (m, 2H), 4.52 (s, 2H), 4.08 (s, 2H), 3.85 (s, 3H), 3.82 (s, 3H), 3.61-3.03 (m, br, 24H). ^{13}C NMR (126 MHz; D_2O): δ 46.80, 47.86, 50.09, 51.44, 52.33, 53.88, 55.90, 56.56, 113.31, 115.14, 117.31, 117.46, 118.60, 119.78, 152.17, 153.06, 162.82, 163.10, 173.40. HR-ESMS: *m/z* calc. for $[M+H]^+$ 525.256, found 525.254.

General method for the synthesis of the lanthanide complexes from 2.26

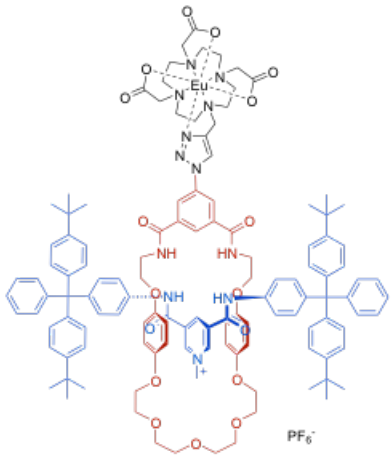
To a solution of the ligand in methanol the appropriate lanthanide triflate salt was added (1.05 eq.) and the reaction mixture was stirred at 40º C for 30 min. The pH was adjusted to 4 by dropwise addition of an aqueous NaOH solution. The reaction was left stirring at 40º C for 48 h. The methanol was removed under reduced pressure leaving an oil that was dissolved in water. The pH of this solution was adjusted to 10 by addition of aqueous NaOH to remove excess of lanthanide as its insoluble

hydroxide. The resulting precipitate was centrifuged and the supernatant filtered. The solvent was removed under reduced pressure to yield the product as a yellow solid.

2.27 (Ln: Eu). Yield: 94 %. ^{1}H NMR (300 MHz; D_2O): δ 35.85, 28.34, 27.52, 26.33, 10.52, -2.10, -3.33, -4.24, -4.84, -7.21, -8.01, -9.99, -15.91, -17.55. Only resolved peaks outside 0 to 10 ppm region are reported. HR-ESMS: *m/z* calc. for $[M+Na]^+$ 697.135, found 697.137. UV-Vis (H_2O) λ_{max}: 268, 373 nm. Lifetimes: 0.27 ms (H_2O); 0.49 ms (D_2O); q=1.7.

2.28 (Ln: Yb). Yield 89%. ^{1}H NMR (300 MHz; D_2O): δ 136.71, 107.01, 102.78, 94.10, 47.84, 36.68, 21.60, 20.50, 12.77, 12.00, -1.28, -7.37, -26.99, -41.03, -46.31, -57.22, -62.51, -64.05, -66.68, -73.72. Only resolved peaks outside 0 to 10 ppm region are reported. HR-ESMS: *m/z* calc. for $[M+Na]^+$ 718.153, found 718.152. UV-Vis (H_2O) λ_{max}: 267, 370 nm. Lifetimes: 0.72 μs (H_2O); 8.09 μs (D_2O); q=1.2.

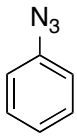
Synthesis of the lanthanide appended rotaxane (3.5)



To a solution of azide rotaxane **3.4** (40 mg, 0.02 mmol) in CH_2Cl_2/MeOH (4:1, 5 mL) was added the **2.6** (35 mg, 0.07 mmol). The solution was stirred for 5 minutes before $Cu(I)(MeCN)_4PF_6$ (0.1 molar eq.) and tris[(1-benzyl-1*H*-1,2,3-triazol-4-

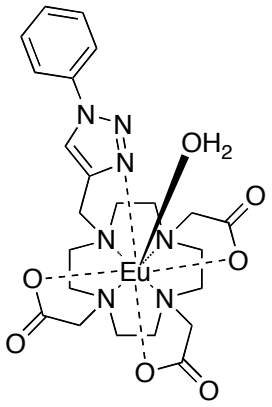
yl)methyl]amine (TBTA) (0.1 molar eq.) were added. The solution was stirred for 48 h at RT under nitrogen. The solvent was removed under reduced pressure and the crude solid was dissolved in DCM (10 mL) and washed with H_2O (2 × 10 mL), with NH_4PF_6(aq) (0.1 M; 10 × 10 mL) and H_2O (2 × 10 mL) to ensure the presence of only PF_6^- as the counter ion. After removal of the organic solvent under reduced pressure, the crude solid was redissolved in toluene and filtered. Purification by size-exclusion chromatography (Bio-Beads SX-3/ toluene) gave the compound as a yellow solid (38 mg, 81%). ^{1}H NMR (500 MHz; CD_3OD/CD_2Cl_2 1:1): δ 34.25, 30.13, 29.97, 27.92, -3.99, -4.73, -5.54, -6.14, -7.46, -8.06, -8.65, -11.77, -12.33, -16.16, -16.44, -17.18, -17.74, -19.70, -21.14. Only resolved peaks outside 0 to 10 ppm region are reported. HR-ESMS: *m/z* calc. for $[M\text{-}PF_6+Na]^+$ 1116.977, found 1116.980. Lifetime: DCM: 0.85 ms.

Azidobenzene[11] (3.7)



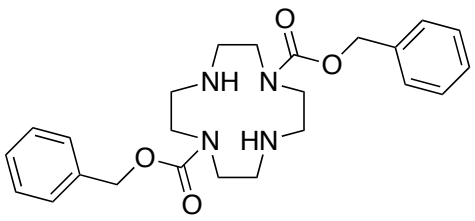
Aniline (**3.6**) (204 mg, 2.2 mmol) was dissolved in anhydrous acetonitrile (6 mL) and this solution was left to cool in an ice-water bath for ten minutes. To this *t*-BuONO was added (340 mg, 3.3 mmol) followed by dropwise addition of $TMSN_3$ (305 mg, 2.6 mmol). After stirring under nitrogen atmosphere at room temperature for 1 h 30 minutes, the solvents were removed under reduced pressure and the product was purified by silica gel chromatography (hexane) to obtain a pale yellow oil (224 mg, 86%). ^{1}H-NMR (300 MHz; $CDCl_3$): 7.38-7.33 (m, 2H), 7.14 (td, J = 7.4, 1.3 Hz, 1H), 7.05-7.02 (m, 2H) identical to the spectrum reported in the literature.

Eu(III)-1,4,7-Tris(carboxymethyl)-10-[(1*H*-1,2,3-triazol-1-yl)benzene]-1,4,7,10-tetraazacyclododecane (3.8)



Complex **2.6** (44 mg, 0.08 mmol) was dissolved in water (2.5 mL) and to this azidobenzene (**3.7**) (20 mg, 0.17 mmol), dissolved in *tert*-butanol (2.5 mL), was added, followed by sodium ascorbate (2 mg, 0.008 mmol) and $CuSO_4$ (41 μL of a 0.1 M solution in water). This solution was left stirring at RT under nitrogen for 48 h. The solvents were then removed under reduced pressure and the solid obtained was washed with diethyl ether to remove excess of azidobenzene. The residual solid was redissolved in water and subjected to purification by dialysis for 3 days ^{1}H-NMR (300 MHz; D_2O, pD 8): δ -19.39, -18.42, -11.16, -8.49, -4.96, 11.68, 25.86, 26.70, 27.13, 29.62. HR-ESMS: *m/z* calc. for $[M+Na]^+$ 676.136, found 676.138. Lifetimes: H_2O: 0.54 ms; D_2O: 1.69 ms, q: 1.2.

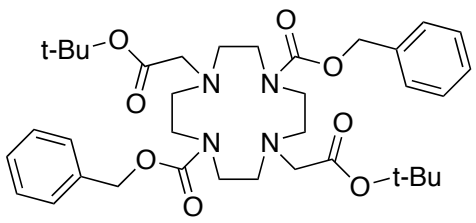
1,7-Bis(benzylcarbamate) -1,4,7,10-tetraazacyclododecane[12] (4.3)



A solution of cyclen (2.0 g, 11.6 mmol) in chloroform (80 mL) was cooled in an ice bath. Benzyl chloroformate (3.96 g, 23.2 mmol) was added dropwise. The reaction

gave rise to abundant white solid formation and was stirred for 16 h at RT under nitrogen. The solvent was removed under reduced pressure and diethyl ether was added to the remaining cake. This was washed with diethyl ether several times to give the product as the dihydrochloride salt as a white solid (5.8 g, 97%). The free base was obtained by adding NaOH (100 mL, 3 M) to the solid and extracting the aqueous phase with chloroform (3 x 50 mL). The extracts were combined and dried over K_2CO_3. The solvent was removed under reduced pressure giving the product as a clear oil (4.8 g, 94%). ^{1}H NMR (300 MHz; $CDCl_3$): δ 7.30 (m, 10H), 5.15 (s, 4H), 3.42 (d, J = 5.0, 8H), 2.85 (t, J = 5.0, 8H). LR-ESMS: *m/z* calc. for $[M+H]^+$ 441.25, found 441.22

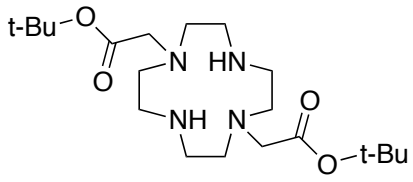
1,7-Bis(benzylcarbamate)-4,10-bis(*tert*-butoxycarbonylmethyl)-1,4,7,10-tetraazacyclododecane (4.4)



Compound 4.3 (2.0 g, 4.54 mmol) was dissolved in dry acetonitrile (60 ml) and K_2CO_3 (1.57 g, 11.35 mmol) was added. This mixture was stirred for 20 min and cooled to 0 ºC in an ice bath. Tert-butyl bromoacetate (1.77 g, 9.10 mmol) was added dropwise over 30 min and the reaction was left stirring under nitrogen for 16 h at RT. The inorganic solid was filtered off and the solvent was evaporated under reduced pressure. The product was purified by silica gel chromatography (DCM/MeOH 95:5 to 80:20 *v:v*) (2.3 g, 76%). Alternatively the product could be recrystallised from chloroform/hexane at -18 ºC. ^{1}H NMR (300 MHz; $CDCl_3$): δ 7.36-7.27 (m, 10H), 5.13 (s, 4H), 3.43-3.33 (br, 12H), 2.88 (s, 8H), 1.44 (s, 18H). ^{13}C NMR (76 MHz; $CDCl_3$): δ 170.5, 156.4, 136.8, 128.4, 127.89, 127.84, 80.9, 66.9, 55.9, 54.33, 54.26,

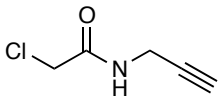
54.19, 54.14, 54.08, 54.05, 53.99, 53.95, 47.02, 47.00, 46.94, 46.6, 28.1. LR-ESMS: *m/z* calc. for $[M+K]^+$ 707.34, found 707.41.

1,7- Bis(*tert*-butoxycarbonylmethyl)-1,4,7,10-tetraazacyclododecane (4.5)



Compound **4.4 (**2.5 g, 3.7 mmol) was placed in a round bottom flask charged with Pd/C (0.5 g) and ethanol (50 ml). This suspension was bubbled with H_2 for 5 min and then left stirring under a balloon charged with H_2 for 48 h at RT. The mixture was filter over celite and the solvent was removed under reduced pressure. The oil obtained was dissolved in methanol and precipitated with diethyl ether. The supernatant was decanted off and the solid was dried under reduced pressure to give the product as a white powder (1.4 g, 95%). ^{1}H NMR (300 MHz; $CDCl_3$): δ 3.40 (s, 4H), 2.96 (t, J = 5.0, 8H), 2.78 (t, J = 5.0, 8H), 1.44 (s, 18H). LR-ESMS: *m/z* calc. for $[M+H]^+$ 401.56, found 401.77

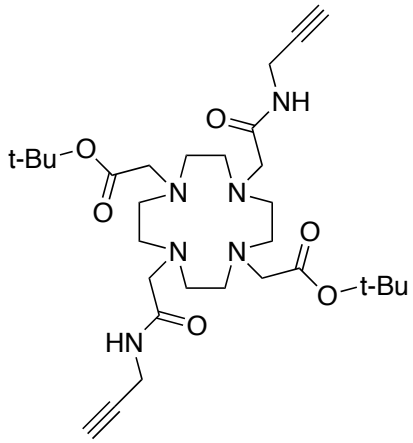
N-(propargyl)-chloroacetamide (4.6)



Propargylamine (1.7 g, 31.2 mmol) was dissolved in dry DCM (50 ml) and cooled to 0 ºC in an ice bath. Chloroacetyl chloride (1.76 g, 15.6 mmol) was added dropwise and the reaction mixture was left to stir for 30 min at RT under nitrogen. The reaction was washed with water (4 x 30 ml) and brine (2 x 30 ml). The organic solvent was

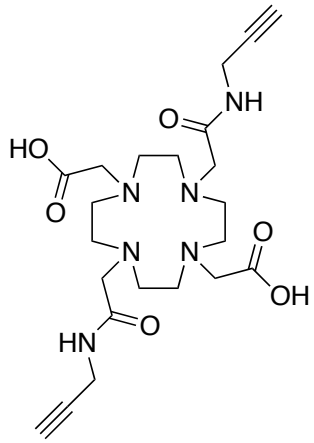
dried over anhydrous $NaSO_4$, filtered and evaporated under reduced. The product was isolated as a brown solid and used immediately. ^{1}H NMR (300 MHz; $CDCl_3$): δ 6.78 (s, 1H), 4.10 (dd, J = 5.5, 2.5, 2H), 4.06 (s, 2H), 2.27 (t, J = 2.5, 1H). ^{13}C NMR (76 MHz; $CDCl_3$): δ 166.2, 79.0, 72.4, 42.7, 29.8.

1,7-Bis(*tert*-butoxycarbonylmethyl)-4,10-bis[(N-propargyl)-acetamide)]-1,4,7,10-tetraazacyclododecane (4.7)



To a solution of compound **4.5** (2.1 g, 5.2 mmol) dissolved in acetonitrile (40 ml) was added K_2CO_3 (1.81 g, 13.1 mmol). To this suspension was added a catalytic amount of KI and compound **4.6** (1.5 g, 11.4 mmol). The reaction was left stirring under nitrogen for 16 h in an oil bath at 60 ºC. The inorganic solid was removed by filtration and the solvent was evaporated under reduced pressure. The product was obtained as a white solid by recrystallisation from chloroform/hexane at -18 ºC (1.52 g, 49%). ^{1}H NMR (300 MHz; $CDCl_3$): δ 8.68 (t, J = 5.2, 2H), 4.07 (dd, J = 5.0, 2.5, 4H), 3.28 (s, 4H), 3.10 (s, 4H), 2.86 (t, J = 2.0, 8H), 2.60 (dt, J = 5.0, 2.0, 8H), 2.19 (t, J = 2.5, 2H), 1.44 (s, 18H). ^{13}C NMR (76 MHz; $CDCl_3$): δ 28.01, 28.78, 52.12, 55.59, 56.05, 58.20, 70.95, 79.95, 81.14, 169.95, 171.32. HR-ESMS: *m/z* calc. for $[M+H]^+$ 591.387, found 591.387.

1,7-Bis(carboxymethyl)-4,10-bis[(N-propargyl)-acetamide)]-1,4,7,10-tetraazacyclododecane (4.8)



Compound **4.7** (0.7g, 1.2 mmol) was dissolved in DCM (8 ml) and TFA is added dropwise. The solution was left stirring for 24 h at RT. The solvent was removed under reduced pressure to leave a sticky solid that was washed several times with DCM before being dissolved in methanol and precipitated with diethyl ether. The solvents were decanted off and the solid was dried under reduced pressure to leave the product as an off white powder. (0.56 g, 98%). ^{1}H NMR (300 MHz; D_2O): δ 3.85 (d, J = 2.5, 4H), 3.71-3.10 (br, 24H), 2.45 (t, J = 2.5, 2H). ^{13}C NMR (76 MHz; D_2O): δ 188.3, 162.9, 162.4, 118.1, 114.2, 110.3, 106.9, 79.1, 72.0, 55.1, 53.1, 50.5-48.9 (br), 49.4, 48.9, 28.7. HR-ESMS: *m/z* calc. for $[M+Na]^+$ 501.243, found 501.243.

General method for the synthesis of the lanthanide complexes from 4.8

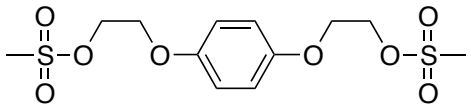
To a solution of the ligand in methanol the appropriate lanthanide triflate salt was added (1.05 eq.) and the reaction mixture was stirred at 40º C for 30 min. The pH was adjusted to 4 by dropwise addition of an aqueous NaOH solution. The reaction was left stirring at 40º C for 48 h. The methanol was removed under reduced pressure leaving an oil that was dissolved in water. The pH of this solution was adjusted to 10 by addition of aqueous NaOH to remove excess of lanthanide as its insoluble

hydroxide. The resulting precipitate was centrifuged and the supernatant filtered. The solvent was removed under reduced pressure to obtain the product as a white powder.

4.9 (Ln: Eu). Yield: 90 %. ^{1}H NMR (300 MHz; D_2O): δ 29.88 (s), 27.80 (s), 6.28 (s), 5.34 (s), 1.18 (s), -4.94 (s), -6.69 (s), -8.68 (s), -9.20 (s), -12.28 (s), -12.99 (s), -14.87 (s), -17.97 (s). Only resolved resonance outside 0-5 ppm region are reported. HR-ESMS: *m/z* calc. for $[M]^+$ 629.159, found 629.161. Lifetime: 0.53 ms (H_2O), 2.13 ms (D_2O), q=1.2.

4.10 (Ln: Tb). Yield: 89%. ^{1}H NMR (500 MHz; D_2O): δ 278.79 (s), 254.48 (s), 215.41 (s), 141.52 (s), 11.65 (s), -39.32 (s), -53.84 (s), -125.78 (s), -142.83 (s), -339.72 (s), -376.47 (s). Only resolved resonances outside 0-10 ppm region are reported. HR-ESMS: *m/z* calc. for $[M]^+$ 635.163, found 635.162. Lifetime: 1.57 ms (H_2O), 2.80 ms (D_2O), q=1.1.

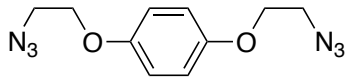
2,2'-(1,4-Phenylenedioxy)-ethyl methanesulfonate[13] (4.12)



Compound **4.11** (6.0 g, 30.3 mmol) was dissolved in dry dichloromethane (100 ml) and triethylamine was added (13 ml, 93 mmol). This solution was cooled to ºC in an ice bath and methanesulfonyl chloride (7 ml, 91 mmol) was added dropwise over 10 min. This mixture was stirred for 30 min and then washed with cold 1M HCl (3 x 40 ml), sat. $NaHCO_3$ (3 x 40 ml) and brine (2 x 40 ml). The organic solvent was dried over anhydrous $MgSO_4$ and then, filtered and evaporated under reduced pressure to give the product as an off-white solid (10.3 g, >95%). ^{1}-H NMR (300 MHz; $CDCl_3$): δ 6.83 (s, 4H), 4.54-4.51 (m, 4H), 4.19-4.16 (m, 4H), 3.06 (s, 6H). ^{13}C NMR (76 MHz;

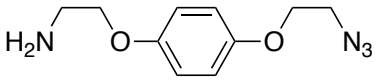
$CDCl_3$): δ 153.1, 116.2, 68.5, 66.9, 38.1. LR-ESMS: *m/z* calc. for $[M+Na]^+$ 377.03, found 377.04.

2,2'-(1,4-Phenylenedioxy)-bis(ethyl azide)[13] (4.13)



Compound **4.12** (3.0 g, 8.5 mmol) was dissolved in DMF and sodium azide was added. This mixture was heated in an oil bath at 90 ºC for 16 h under nitrogen. The formed solid was filtered off and the solvent removed under reduced pressure. The resulting solid was dissolved in diethyl ether and this solution was washed with water (3 x 50 ml) and brine (2 x 50 ml), dried over $MgSO_4$ and filtered. Upon evaporation of the solvent under reduced pressure the product was isolated as a low melting point solid (1.8 g, 85%). ^{1}H NMR (300 MHz; $CDCl_3$): δ 6.87 (s, 4H), 4.11 (t, J = 5.0, 4H), 3.57 (t, J = 5.0, 4H). ^{13}C NMR (76 MHz; $CDCl_3$): δ 152.9, 115.8, 67.7, 50.3. LR-ESMS: *m/z* calc. for $[M+Na]^+$ 271.01, found 271.25.

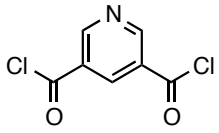
2-(4-(2-Azidoethoxy)phenoxy)ethanamine[13] (4.14)



Compound **4.13** (1.2 g, 4.8 mmol) was dissolved in diethyl ether/ethyl acetate 1:1 (*v:v*) (15 ml) with 5 % in volume of HCl. Triphenylphosphine (1.27 g, 4.8 mmol), dissolved in diethyl ether with 5 % in volume of HCl, was added dropwise over 30 min while keeping the reaction flask in an ice bath. The mixture was left stirring for 24 h at RT under nitrogen. The two phases were separated and the aqueous layer was

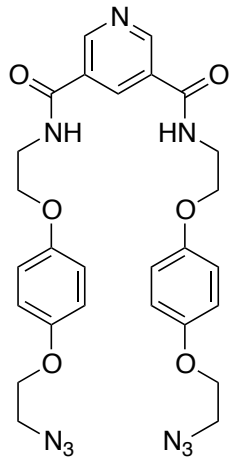
washed with dichloromethane (2 x 20 ml) and basified using NaOH to pH 10-12. The resulting suspension was extracted with dichloromethane (3 x 30 ml). The combined organic solvent was dried over anhydrous $MgSO_4$, filtered and evaporated under reduced pressure to obtain the product as a pale yellow oil (0.4 g, 37%). ^{1}H NMR (300 MHz; $CDCl_3$): δ 6.83 (s, 4H), 4.06 (t, J = 5.0, 2H), 3.90 (t, J = 5.0, 2H), 3.53 (t, J = 5.0, 2H), 3.02 (t, J = 5.0, 2H). ^{13}C NMR (76 MHz; $CDCl_3$): δ 152.4, 115.6, 70.7, 67.6, 50.2, 41.6. LR-ESMS: *m/z* calc. for $[M+Na]^+$ 245.24, found 245.32.

3,5-Pyridinedicarboxylic acid chloride (4.15)



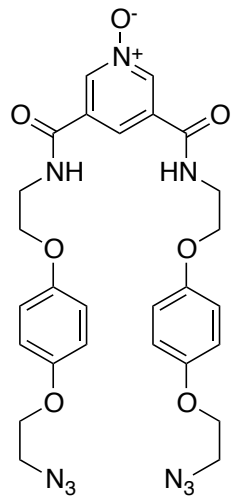
To a suspension of 3,5-pyridinedicarboxylic acid in dry dichloromethane was added an excess of thionyl chloride followed by 2 drops of DMF. The reaction mixture was left stirring at RT for 3 h or longer, depending on the scale of the reaction. Completion of the reaction was checked by TLC, few drops of the reaction mixture were quenched by few drops of methanol forming the methyl ester. Presence of only methyl ester on the TLC plate indicated the completion of the reaction. The solvent was removed under reduced pressure and the resulting solid was used immediately without further purification.

Pyridine bis-azide (4.16)



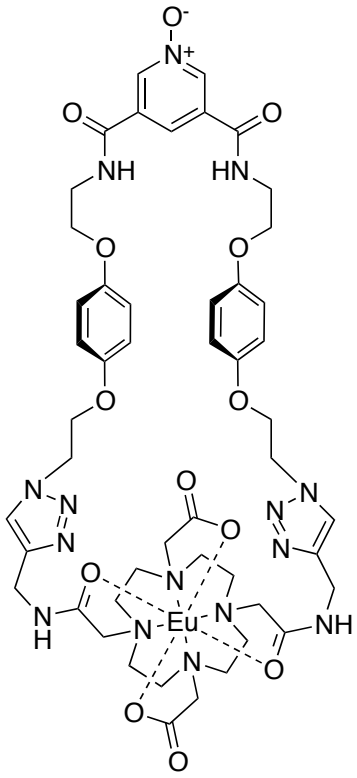
Compound **4.14** (1.89 g, 8.5 mmol) was dissolved in dry DCM (50 ml) and to this solution was added triethylamine (2.5 ml, 17.9 mmol). A solution of compound **4.15** (1.73 g, 8.5 mmol) in dry DCM (30 ml) was added dropwise over 30 min while keeping the reaction under nitrogen and in an ice bath. The reaction was left stirring for 16 h at RT under nitrogen. The organic solvent was washed with 0.1 M $HCl_{(aq)}$ (3 x 30 ml) and sat. $NaHCO_{3(aq)}$. The solvent was dried over anhydrous $MgSO_4$, filtered and evaporated under reduced pressure to leave a yellow solid that was purified by silica gel chromatography (DCM/MeOH 9:1 *v:v*). The product was obtained as an off white solid (1.1 g, 22%). ^{1}H NMR (500 MHz; $CDCl_3$): δ 9.13 (d, J = 2.0, 2H), 8.49 (t, J = 2.0, 1H), 6.86 (s, 8H), 6.79 (t, J = 5.5, 2H), 4.12 (m, 8H), 3.89 (t, J = 5.5, 4H), 3.58 (t, J = 5.5, 4H). ^{13}C NMR (126 MHz; CDCl3): δ 164.8, 152.9, 150.6, 133.6, 129.7, 115.8, 115.5, 67.6, 67.1, 50.2, 39.8. HR-ESMS: *m/z* calc. for $[M+Na]^+$ 598.213, found 598.213.

Pyridine N-oxide bis-azide (4.17)



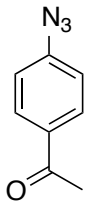
Compound **4.16** (0.195 g, 0.33 mmol) was dissolved in a 1:1 mixture of 2-butanone/water (50 ml) and $NaHCO_3$ (0.86 g, 10.2 mmol) was added. This mixture was left stirring vigorously while a saturated solution of Oxone (0.63 g, 1.02 mmol) in water (4 ml) was added dropwise over 20 min. The reaction mixture was stirred vigorously for 2 h at RT. NaCl (2.4 g, 41 mmol) was added to the reaction and the aqueous layer was extracted with chloroform (3 x 50 ml). The organic layer was collected, dried over anhydrous $MgSO_4$ and filtered. The solvent was evaporated under reduced pressure to leave the product as a white powder (0.18 g, 92%). ^{1}H NMR (500 MHz; $CDCl_3$): δ 8.60 (s, 4H), 8.16 (s, 1H), 6.71 (s, 8H), 3.97 (s, 8H), 3.66 (s, 4H), 3.43 (s, 4H). ^{13}C NMR (126 MHz; $CDCl_3$): δ 162.9, 153.0, 152.6, 140.00, 139.88, 133.8, 125.7, 115.6, 115.4, 50.1, 40.1. HR-ESMS: *m/z* calc. for $[M+Na]^+$ 614.208, found 614.206.

Attempted synthesis of compound 4.18



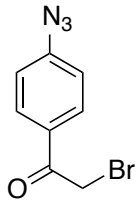
Compounds **4.9** (37 mg, 0.06 mmol) and **4.17** (35 mg, 0.06 mmol) were suspended in a 1:1 mixture of t-butanol/water (25 ml). TBTA (2.2 mg, 0.006 mmol) and $Cu(I)(MeCN)_4PF_6$ (3.2 mg, 0.006 mmol) were added and the reaction mixture was stirred while heating in an oil bath at 70 ºC under nitrogen. TLC and ESMS showed the development of a new band with Rf ~ 0 the ion adduct in the mass spectrum. In particular the ESMS spectrum showed sign of the product as the $[M]^+$ adduct (theoretical 1120.38 m/z, found 1120.45 m/z), $[M+H_2O]^+$ (theoretical 1238.39 m/z, found 1239.72 m/z) and also of the interpenetrated species in which one bis-azide molecule is interpenetrated into the "clicked" macrocycle to form a pseudo-catenate detected as the adduct $[M+bis\text{-}azide+H^+]^{2+}$ (theoretical 906.30 m/z, found 906.35 m/z). After 72 h the solvent was evaporated under reduced pressure. Any attempts to purify the product by recrystallisation or column chromatography failed, most likely due to the amphiphilic nature of the molecule and hence its high affinity to silica but insolubility in polar solvents.

4-Azido acetophenone[11] (5.18)



4-Aminoacetophenone (**5.17**) (1.5 g, 11.1 mmol) was dissolved in anhydrous acetonitrile (30 ml) and this solution was left to cool in an ice-water bath for ten minutes. To this *t*-BuONO was added (1.72 g, 16.6 mmol) followed by dropwise addition of $TMSN_3$ (1.53 g, 13.3 mmol). After stirring under nitrogen atmosphere at RT for 2 h, the solvent was removed under reduced pressure. The resulting brown solid was washed with cold hexane and the solid was dried under reduced pressure to give the product as an orange crystalline solid (1.71 g, 96 %). ^{1}H NMR (300 MHz; $CDCl_3$): δ 7.96 (d, J = 8.5, 2H), 7.09 (d, J = 8.5, 2H), 2.58 (s, 3H). ^{13}C NMR (76 MHz; $CDCl_3$): δ 196.5, 144.8, 133.7, 130.2, 118.9, 26.4. IR-ATR(cm^{-1}): 2095 (N_3), 1683 (C=O).

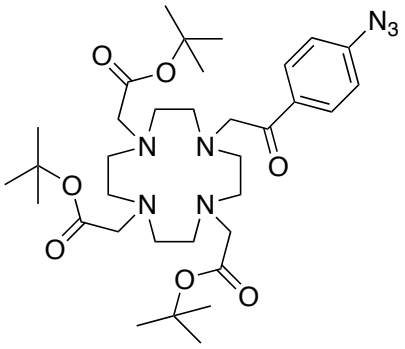
4-Azidophenacyl bromide (5.19)



1-Azidoacetophenone (4.8 g, 29.8 mmol) was dissolved in diethyl ether (15 mL) and dioxane (8 mL) and kept in an ice bath while Br_2 was added dropwise (1.5 mL, 29.8 mmol). The reaction was left stirring at RT monitoring its progression by TLC. After typically 3 hours all starting material was consumed. Water was then added to the organic mixture (30 mL) and the aqueous layer was extracted with diethyl ether (3 x

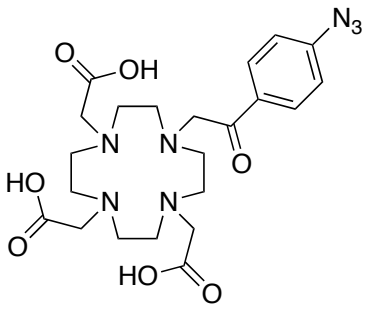
30 mL). The organic solvents were dried with brine, then with $MgSO_4$ before being evaporated. The crude product was purified by silica gel chromatography (1:1 (*v:v*) DCM:petroleum ether) to obtain the a pale yellow solid (2.5 g, 35%) which was found to be identical with that of a commercial sample (obtained from Sigma-Aldrich). ^{1}H-NMR (300 MHz; $CDCl_3$,): δ 7.99 (2 H, d, *J* =8.5 Hz), 7.11 (2 H, d, *J* =8.5), 4.40 (2 H, s). ^{13}C NMR (76 MHz; $CDCl_3$): δ 190.4, 146.4, 131.5, 131.0, 119.8, 31.1. IR-ATR(cm^{-1}): 2096 (N_3), 1678 (C=O).

1,4,7-Tris(*tert*-butoxycarbonylmethyl)-10-(4'-azido-2'-acetophenone)-1,4,7,10-tetraazacyclododecane (5.20)



To a solution of **2.3** (0.93 g, 1.56 mmol) in dry acetonitrile (50 ml), potassium carbonate was added (0.43 g, 3.12 mmol) followed by **5.19** (0.38 mg, 1.56 mmol). This suspension was left stirring at RT under nitrogen for 3 h. The reaction was filtered and the solvent was removed under reduced pressure. The crude product was purified by silica gel column chromatography (DCM/MeOH 90:10) to obtain an orange solid. (860 mg, 82%). ^{1}H NMR (300 MHz; DMSO-d_6): δ 8.09 (d, J = 8.5, 2H), 7.21 (d, J = 8.5, 2H), 3.91 (s, 2H), 3.20 (m, br, 8H), 3.04 (s, br, 8H), 2.68 (m, br, 4H), 1.45 (s, 27H). ^{13}C NMR (76 MHz; $CDCl_3$): δ: 206.3, 172.0, 129.86, 129.83, 119.1, 110.8, 81.9, 60.9, 57.1, 56.5, 48.9, 45.4, 27.93, 27.88. HR-ESMS: *m/z* calc. for $[M+Na]^+$ 696.405, found 696.405.

1,4,7-Tris(carboxylmethyl)-10-(4'-azido-2-acetophenone)-1,4,7,10-tetraazacyclododecane (5.21)



To a solution of **5.20** (0.4 g, 0.59 mmol) in DCM (5 ml), TFA (5ml) was added dropwise. The reaction was stirred at RT for 48 h, the solvents were removed under reduced pressure and the product was obtained quantitatively from methanol by precipitation using diethyl ether. ^{1}H-NMR (300 MHz; DMSO-d_6, 353 K): δ 8.00 (d, *J* = 8.8 Hz, 2H), 7.26 (d, *J* = 8.7 Hz, 2H), 4.63 (s, 2H), 3.68 (m, 6H), 3.20-3.16 (m, 4H), 3.06 (s, br, 12H). ^{13}C NMR (126 MHz; DMSO-d_6): δ 173.0, 158.6, 158.4, 158.1, 157.9, 131.7, 131.5, 130.3, 126.2, 119.53, 119.40, 119.24, 118.6, 116.2, 113.8, 53.60, 53.56, 53.53, 52.07, 52.04, 48.99, 48.81. HR-ESMS: *m/z* calc. for $[M+H]^+$ 506.236, found 506.234.

General method for the synthesis of the lanthanide complexes from 5.21

To a solution of the ligand in methanol the appropriate lanthanide triflate salt was added (1.05 eq.) and the reaction mixture was stirred at 40º C for 30 min. The pH was adjusted to 4 by dropwise addition of an aqueous NaOH solution. The reaction was left stirring at 40º C for 48 h. The methanol was removed under reduced pressure leaving an oil that was dissolved in water. The pH of this solution was adjusted to 10 by addition of aqueous NaOH to remove excess of lanthanide as its insoluble hydroxide. The resulting precipitate was centrifuged and the supernatant filtered. The solvent was removed under reduced pressure to yield the product as an orange solid.

5.22 (Ln: Eu). Yield: 89%. ^{1}H-NMR (300 MHz; D_2O, pD7): δ 35.8, 28.6, 27.3, 26.5, 8.9, 7.6, -1.7, -3.7, -4.4, -5.5, -7.9, -10.4, -12.4, -13.1, -16.4, -18.5. Only resolved peaks outside 0 to 5 ppm are reported. HR-ESMS: *m/z* calc. for $[M+Na]^+$ 678.116, found 678.117. IR-ATR (cm^{-1}): 2106 (N_3), 1594 (C=O). UV-Vis: λ_{max}: 318 nm Luminescence lifetimes: H_2O: 0.42 ms, D_2O: 1.02 ms, q=1.4.

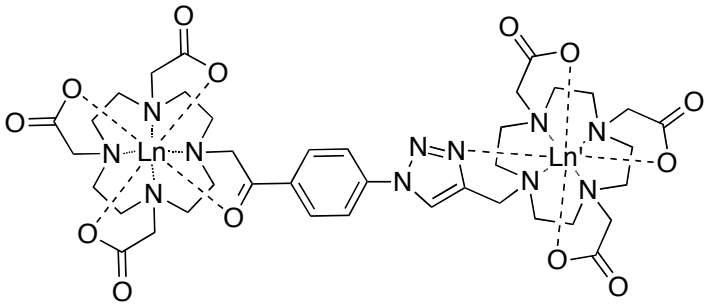
5.23 (Ln: Tb). Yield: 87%. ^{1}H NMR (500 MHz; D_2O, pD7): δ 299.8, 274.8, 257.9, 254.7, 220.8, 203.9, 186.6, 132.4, 124.6, 107.9, 105.4, -77.1, -82.3, -94.2, -96.3, -98.9, -103.6, -138.8, -152.1, -156.6, -179.8, -247.8, -337.2, -357.9, -426.1, -433.6. Only resolved peaks outside -20 to 20 ppm are reported. LR-ESMS: *m/z* calc. for $[M+H]^+$ 662.14, found 664.17. IR-ATR (cm^{-1}): 2103 (N_3), 1587 (C=O). UV-Vis: λ_{max}: 329 nm. Luminescence lifetimes: H_2O: 0.32 ms, D_2O: 0.87 ms.

5.24 (Ln: Yb). Yield: 86%. ^{1}H-NMR (300 MHz; D_2O, pD7): major isomer: δ 136.0, 108.1, 101.6, 94.9, 48.1, 37.3, 18.9, 13.4, -6.4, -23.8, -42.2, -48.4, -63.5, -64.3, -67.0, -70.2, -73.9; minor isomer: δ 138.3, 118.1, 114.3, 108.4, 40.8, 32.1, 20.5, 16.8, -7.4, -17.9, -22.0, -28.8, -33.2, -39.9, -44.0, -54.6, -61.7, -70.2, -70.8, -73.1. Only resolved peaks outside -20 to 20 ppm are reported. HR-ESMS: *m/z* calc. for $[M+Na]^+$ 699.133, found 699.133. IR-ATR (cm^{-1}): 2107 (N_3), 1591 (C=O). UV-Vis: λ_{max}: 322 nm. Luminescence lifetimes: H_2O: 0.61 μs, D_2O: 6.4 μs, q=1.4.

5.25 (Ln: Lu). Yield: 88%. ^{1}H NMR (300 MHz; D_2O): δ 8.17 (d, J = 8.8, 2H), 7.26 (d, J = 8.7, 2H), 3.53 (br, 16H), 2.84 (br, 8H), 2.56 (br, 4H). HR-ESMS: *m/z* calc. for $[M+Na]^+$ 700.135, found 700.135. IR-ATR (cm^{-1}): 2105 (N_3), 1596 (C=O).

5.26 (Ln: Gd) Yield: 85%. HR-ESMS: *m/z* calc. for $[M+Na]^+$ 683.119, found 683.119. $E_T \sim 22000\ cm^{-1}$. UV-Vis: λ_{max}: 317 nm. IR-ATR (cm^{-1}): 2106 (N_3), 1595 (C=O).

General procedure for the synthesis of Ln.2.Ln' heterobimetallic complexes



To 1 equivalent of Ln azide dissolved in water, 3 equivalents of Ln alkyne were added, followed by sodium ascorbate (0.10 req) and copper (II) sulfate (0.05 eq.). This solution was stirred at RT for 3 days, microfiltered and dialysed for 3 days using a 1000 MWCO membrane. The solvent was removed under reduced pressure to obtain a glassy solid which was redissolved in methanol and precipitated with diethyl ether. Removal of solvent afforded the product as a light green solid in 80-90% yield based on starting azide.

5.27. Yield 85 %. ^{1}H-NMR (700 MHz; D_2O, 293 K, pD7): δ 133.0, 109.6, 105.3, 104.2, 102.9, 101.9, 35.4, 33.9, 29.9, 24.3, 21.4, 19.9, -25.1, -27.4, -37.5, -45.2, -48.9, -51.5, -59.7, -62.9, -65.2, -65.9, -71.5, -82.1. Only resolved peaks outside -20 to 10 ppm are reported MALDI-MS: *m/z* calc. for $[M+H]^+$ 1209.9, found 1209.2. UV-Vis: λ_{max}: 288, 347 nm. Luminescence lifetimes: Eu: H_2O: 0.64 ms, D_2O: 1.88 ms,, q=0.9. Yb: H_2O: 1.29 μs, D_2O: 5.67 μs, q=0.5.

5.28. Yield 81 %. ^{1}H NMR (700 MHz; D_2O, 293 K, pD7): δ 133.0, 109.6, 105.3, 104.2, 102.9, 101.9, 35.4, 33.9, 29.9, 24.3, 21.4, 19.9, -25.1, -27.4, -37.5, -45.2, -48.9, -51.5, -59.7, -62.9, -65.2, -65.9, -71.5, -82.1. Only resolved peaks outside -20 to 10 ppm are reported. MALDI-MS: *m/z* calc. for $[M+H_2O+H]^+$ 1227.9, found 1227.1. UV-Vis: λ_{max}: 287, 347 nm. Luminescence lifetimes: Eu: H_2O: 0.59 ms, D_2O: 1.81 ms,, q=1.1. Yb: H_2O: 0.73 μs, D_2O: 6.51 μs, q=1.1.

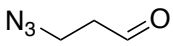
5.29. Yield 81 %. ^{1}H NMR (700 MHz; D_2O, pD 7): δ 35.4, 33.6, 30.4, 29.8, 28.9, 28.3, 27.2, 27.0, 26.1, 18.6, 16.7, -1.9, -3.1, -3.4, -3.6, -4.4, -5.4, -5.9, -6.3, -6.8, -7.3, -7.8, -9.3, -10.1, -10.6, -11.8, -12.4, -13.0, -13.4, -14.0, -14.4, -15.6, -16.1, -16.8, -18.2. Only resolved peaks outside 0 to 10 ppm are reported UV-Vis: λ_{max}: 317, 355 nm. Luminescence lifetimes: Eu: H_2O: 0.63 ms, D_2O: 1.76 ms, q=0.9.

5.30. Yield 83%. ^{1}H NMR (500 MHz; D_2O, pD 7): δ 135.5, 133.2, 115.8, 112.1, 111.2, 106.5, 105.9, 99.7, 93.2, 83.7, 72.3, 50.1, 47.1, 39.9, 36.5, 33.7, 32.6, 31.5, 20.0, 18.4, 16.6, 14.6, 13.2, -2.3, -6.3, -7.4, -11.0, -16.1, -17.6, -23.2, -25.0, -26.4, -28.0, -32.3, -39.2, -39.9, -41.4, -43.2, -47.3, -53.6, -58.8, -59.5, -60.5, -62.1, -63.1, -63.6, -65.7, -68.7, -69.4, -71.4, -72.3. Only resolved peaks outside 0 to 10 ppm are reported. MALDI-MS: *m/z* calc. for $[M+H_2O+H]^+$ 1250.9, found 1251.9. UV-Vis: λ_{max}: 312, 341 nm. Luminescence lifetimes: Yb: H_2O: 0.76 μs, D_2O: 7.32 μs, q=1.1.

5.31. Yield: 87%. ^{1}H NMR (500 MHz; D_2O, pD 7): δ 29.6, 26.3, 26.2, 25.4, 15.2, 12.2, 11.9, -5.3, -6.3, -6.6, -7.1, -7.9, -8.5, -8.7, -9.5, -10.6, -12.9, -13.9, -14.6, -15.4, -17.0, -18.7, -19.5. Only resolved peaks outside 0 to 10 ppm are reported MALDI-MS: *m/z* calc. for $[M+2H_2O+CH_3OH+Na]^+$ 1301.9, found 1300.1. λ_{max}: 285, 353 nm Luminescence lifetimes: Eu: H_2O: 0.60 ms, D_2O: 1.92 ms, q=1.1.

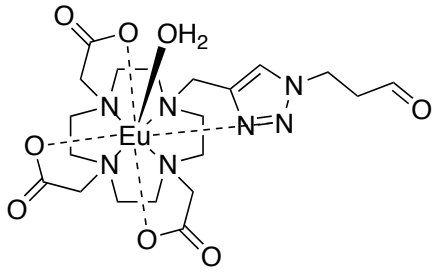
5.32. Yield: 82%. ^{1}H NMR (700 MHz; D_2O, pD 7): δ 109.2, 103.9, 101.4, 100.8, 34.6, 29.7, 22.3, 21.2, -49.3, -51.8, -54.4, -59.1, -61.7, -66.1, -66.9, -70.9. Only resolved peaks outside 0 to 10 ppm region reported. MALDI-MS: *m/z* calc. for $[M+H_2O+H]^+$ 1250.9, found 1252.0. UV-Vis: λ_{max}: 291, 359 nm. Luminescence lifetimes: Yb: H_2O: 1.09 μs, D_2O: 5.16 μs, q=0.6.

2-Azidopropanal[14] (6.2)



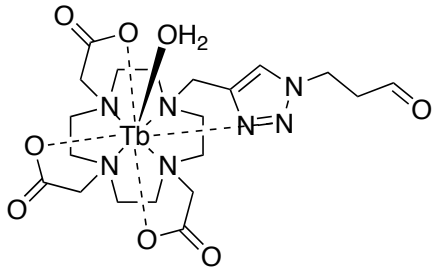
Acrolein (**6.1**) (1.1 g, 19.6 mmol) was dissolved in glacial acetic acid (3 ml) and the resulting solution was cooled in an ice salt bath for 20 min. A solution of sodium azide (1.95 g, 30.0 mmol) in water (7 ml) was added dropwise over 1 h while keeping the reaction flask in an ice salt bath. The reaction mixture was left stirring for 30 min at RT under nitrogen. The reaction mixture was extracted with diethyl ether (2 x 10 ml) and the organic phase was washed with a saturated solution of $NaHCO_{3(aq)}$ (4 x 20 ml), water (2 x 20 ml) and dried over anhydrous $MgSO_4$. The solvent was removed under reduced pressure leaving the product as a volatile oil that was used immediately (1.01 g, 52%). Given the very poor stability of the product, it was freshly prepared each time and used immediately. The product showed to decompose at RT within hours hence only a ^{1}H-NMR spectrum was registered. ^{1}H NMR (300 MHz; $CDCl_3$): δ 9.81 (s, 1H), 3.62 (t, J = 6.3, 2H), 2.74 (td, J = 6.3, 0.9, 2H). When the product was stored at 4-8 ºC decomposition occurred within days, leading to the formation of a insoluble sticky solid. Even when stored at -18 ºC the product decomposed within a few weeks.

Eu(III)-1,4,7-Tris(carboxymethyl)-10-[(1*H*-1,2,3-triazol-1-yl)propionaledhyde]-1,4,7,10-tetraazacyclododecane (6.3)



The EuDO3A propargyl complex (**2.6**) (106 mg, 0.19 mmol) and 2-azidopropanal (**6.2**) (83 mg, 0.84 mmol) were dissolved in methanol. $CuSO_4$ $5H_2O$ (4.8 mg, 0.02 mmol) and sodium ascorbate (8 mg, 0.04 mmol) were added and the reaction mixture was stirred for 16 hours at RT under nitrogen. After removal of solvent under reduced pressure the so formed sticky solid was re-dissolved in 10 mL of water and extracted with DCM (3x10mL) and the organic phase was discarded. Removal of water yielded a pale yellow solid that was dialysed against water using a 500MWCO membrane for 2 days. Removal of residual solvent under reduced pressure yielded a white off solid (115 mg, 91%). ^{1}H NMR (300 MHz, D_2O, pD 7): δ 29.4, 27.1, 26.8, 26.3, 8.50, 6.99, 6.26, 3.68, 3.34, -4.81, -6.95, -7.22, -7.56, -8.56, -8.78, -9.08, -9.83, -12.3, -13.0, -14.4, -14.9, -16.1, -18,4, -18.9. Only resolved peaks outside 0 to 10 ppm are reported HR-ESMS: *m/z* calc. for $[M+CH_3OH+Na]^+$ 688.1575, found 688.1573. UV-Vis: λ_{max}: 256 nm. Luminescence lifetimes: Eu: H_2O: 0.52 ms, D_2O: 1.56 ms, q=1.2.

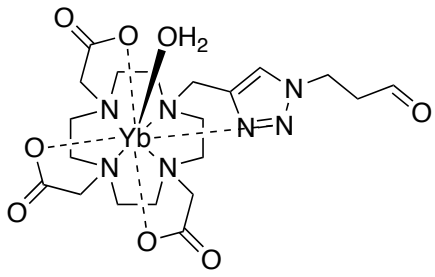
Tb(III)-1,4,7-Tris(carboxymethyl)-10-[(1*H*-1,2,3-triazol-1-yl)propionaledhyde]-1,4,7,10-tetraazacyclododecane (6.4)



The TbDO3A propargyl complex (**2.29**) (55 mg, 0.09 mmol) and 2-azidopropanal (**6.2**) (36 mg, 0.36 mmol) were dissolved in methanol. $CuSO_4$ $5H_2O$ (2.2 mg, 0.01 mmol) and sodium ascorbate (4 mg, 0.02 mmol) were added and the reaction mixture was stirred for 16 hours at RT under nitrogen. After removal of solvent under reduced pressure the so formed sticky solid was redissolved in 10 mL of water and extracted with DCM (3x10mL) and the organic phase was discarded. Removal of water yielded

a pale yellow solid that was dialysed in a large excess of water using a 500MWCO membrane for 2 days. Removal of residual solvent under reduced pressure yielded a white off solid (53 mg, 92%). ^{1}H NMR (500 MHz; D_2O, pD 7): δ 323.52, 293.59, 225.85, 217.19, 179.64, 143.73, -27.45, -30.76, -34.64, -45.54, -49.92, -78.45, -87.66, -88.99, -99.12, -104.16, -130.10, -139.26, -140.84, -165.90. Only resolved peaks outside -20 to 20 ppm are reported. LR-ESMS: *m/z* calc. for $[M+Na]^+$ 662.1, found 662.1. UV-Vis: λ_{max}: 268 nm. Luminescence lifetimes: Tb: H_2O: 1.74 ms, D_2O: 2.73 ms, q=0.7.

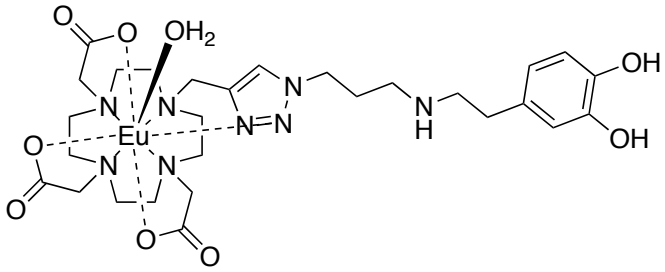
Yb(III)-1,4,7-Tris(carboxymethyl)-10-[(1*H*-1,2,3-triazol-1-yl)propionaledhyde]-1,4,7,10-tetraazacyclododecane (6.5)



The YbDO3A propargyl complex (**2.7**)(73 mg, 0.13 mmol) and 2-azidopropanal (**6.2**) (52 mg, 0.53 mmol) were dissolved in methanol. $CuSO_4$ $5H_2O$ (1.8 mg, 0.007 mmol) and sodium ascorbate (3 mg, 0.015 mmol) were added and the reaction mixture was stirred for 16 hours at RT under nitrogen. After removal of solvent under reduced pressure the so formed sticky solid was redissolved in 10 mL of water and extracted with DCM (3x10mL) and the organic phase was discarded. Removal of water yielded a pale yellow solid that was dialysed against a large excess of water using a 500 MWCO membrane for 2 days. Removal of residual solvent under reduced pressure yielded an off-white solid (65 mg, 77%). ^{1}H NMR (500 MHz; D_2O, pD 7): δ 110.7, 109.0, 106.6, 105.2, 32.0, 30.0, 21.9, 20.5, 12.6, 11.1, 10.8, -6.0, -7.7, -9.2, -10.9, -47.6, -50.7, -57.0, -61.6, -62.9, -63.9, -65.2, -73.1. Only resolved peaks outside 0 to

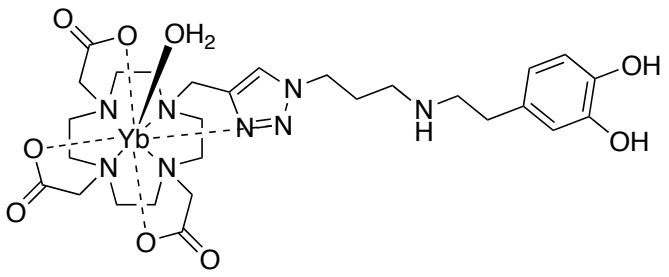
10 ppm are reported. HR-ESMS: *m/z* calc. for $[M+CH_3OH+Na]^+$ 709.175, found 709.175. UV-Vis: λ_{max}: 285 nm. Luminescence lifetimes: Yb: H_2O: 2.58 μs, D_2O: 3.02 μs; q=0.

Eu(III) dopamine conjugate (6.6)



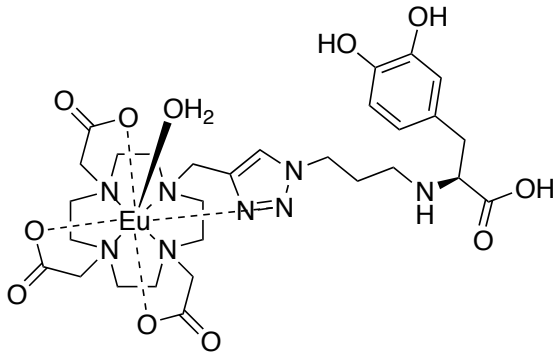
Compound **6.3** (49 mg, 0.08 mmol) was dissolved in methanol and dopamine hydrochloride (23 mg, 0.12 mmol) was added. To this mixture $NaBH_3CN$ (5 mg, 0.08 mmol) was added and the pH of the solution was brought to 4-5 using TFA. The reaction mixture was left stirring at RT for 48 h while keeping the reaction flash in the dark and under nitrogen. The solvent was removed under reduced pressure and the crude product was re-dissolved in water and subjected to dialysis against water for two days using a 500 MWCO membrane while keeping the system in the dark. Upon removal of the solvent under reduced pressure the product was obtained as an off-white solid (48 mg, 75 %). ^{1}H NMR (500 MHz; D_2O, pD7): δ 29.4, 27.0, 26.7, 26.3, 12.8, 10.8, 10.3, -4.8, -6.0, -6.9, -7.2, -8.3, -8.6, -8.8, -9.1, -9.8, -11.4, -12.5, -13.2, -14.5, -15.0, -16.3, -18.4, -18.9. Only resolved peaks outside 0 to 10 ppm are reported HR-ESMS: *m/z* calc. for $[M+H]^+$ 771.234, found 771.235. UV-Vis: λ_{max}: 279 nm. Luminescence lifetimes: Eu: H_2O: 0.51 ms, D_2O: 0.97 ms; q=0.8.

Yb(III) dopamine conjugate (6.7)



Compound **6.5** (23 mg, 0.04 mmol) was dissolved in methanol and dopamine hydrochloride (11 mg, 0.06 mmol) was added. To this mixture $NaBH_3CN$ (2.5 mg, 0.04 mmol) was added and the pH of the solution was brought to 4-5 using TFA. The reaction mixture was left stirring at RT for 48 h while keeping the reaction flash in the dark and under nitrogen. The solvent was removed under reduced pressure and the crude product was re-dissolved in water and subjected to dialysis against water for two days using a 500 MWCO membrane while keeping the system in the dark. Upon removal of the solvent under reduced pressure the product was obtained as an off-white solid (22 mg, 70 %). ^{1}H NMR (500 MHz; D_2O): δ 110.9, 109.8, 109.3, 108.6, 107.7, 106.6, 105.4, 104.6, 32.1, 30.4, 22.2, 20.2, -2.7, -5.4, -7.9, -8.9, -10.9, -42.0, -44.9, -47.2, -47.8, -50.6, -51.1, -56.5, -61.3, -63.3, -63.7, -64.7, -72.9. Only resolved peaks outside 0 to 20 ppm are reported. HR-ESMS: *m/z* calc. for $[M+H]^+$ 792.251, found 792.251. UV-Vis: λ_{max}: 281 nm. Luminescence lifetimes: Yb: H_2O: 1.00 μs, D_2O: 5.32 μs; q=0.7.

Eu(III) L-DOPA conjugate (6.8)



Compound **6.3** (34 mg, 0.05 mmol) was dissolved in methanol and 3,4-Dihydroxy-L-phenylalanine (15 mg, 0.08 mmol) was added. To this mixture $NaBH_3CN$ (3.3 mg, 0.05 mmol) was added and the pH of the solution was brought to 4-5 using TFA. The reaction mixture was left stirring at RT for 48 h while keeping the reaction flash in the dark and under nitrogen. The solvent was removed under reduced pressure and the crude product was redissolved in water and subjected to dialysis against water for two days using a 500 MWCO membrane while keeping the system in the dark. Upon removal of the solvent under reduced pressure the product was obtained as an off-white solid (28 mg, 69 %). ^{1}H NMR (500 MHz; D_2O, pD 7): δ 29.3, 27.0, 26.7, 26.2, 12.7, 10.8, 10.1, -4.9, -6.2, -7.0, -7.2, -7.3, -7.4, -8.8, -9.1, -9.7, -11.1, -12.4, -13.0, -14.4, -14.9, -16.3, -18.4, -18.9. HR-ESMS: *m/z* calc. for $[M+Na]^+$ 837.205, found 837.203. Uv-vis: λ_{max}: 279 nm. Luminescence lifetimes: Eu: H_2O: 0.53 ms, D_2O: 1.41 ms, q=1.1.

8.4 X-ray crystallographic data

Table 8-1. Summary of the X-ray crystallographic data.

	2.9	**2.17**	**4.7**
Chemical Formula	$C_{70}H_{102}Lu_4N_{16}O_{31}$ 12(H_2O) 4Na	$C_{43}H_{58}Br4_8O_8 \cdot 2(CH_2Cl_2)$ 1K 4Na	$C_{30}H_{50}N_6O_6$
FW	2671.79	1028.30	590.76
Crystal system	Monoclinic	Triclinic	Trigonal
Space group	P2/c	P-1	R-3
Crystal colour	Colourless	Yellow	Colourless
Crystal size (mm)	0.06 × 0.10 × 0.12	0.02 × 0.04 × 0.20	0.34 × 0.46 × 0.26
a (Å)	18.0616(2)	10.7801(2)	27.7817(3)
b (Å)	14.9690(2)	11.8149(2)	27.7817(3)
c (Å)	18.2262(3)	20.3072(4)	11.2438 (1)
α (°)	90	97.1183(8)	90
β (°)	108.6904(8)	92.9652(8)	90
γ (°)	90	95.3881(9)	120
V (Å^3)	4667.84(11)	2549.91(8)	7515.56(13)
Z	2	2	9
D_{calcd} (g/cm^3)	1.901	1.296	1.175
μ (mm^{-1})	4.313	1.148	0.082
F (000)	2660	1073	2880
Reflections collected	84881	18392	35076
Unique reflections (R_{int})	10639 (0.04)	10335 (0.035)	3801 (0.014)
R_1 ($I>2\sigma(I)$)	0.0641	0.0580	0.0369
wR'_2 (all data)	0.1680	0.0854	0.0680

8.5 References

1. J. Cosier and A. M. Glazer, *J. Appl. Crystallogr.*, 1986, **19**, 105-107.
2. Z. Otwinowski and W. Minor, in *Methods Enzymol.*, ed. Charles W. Carter, Jr., Academic Press, 1997, vol. Volume 276, pp. 307-326.
3. A. Altomare, G. Cascarano, C. Giacovazzo, A. Guagliardi, M. C. Burla, G. Polidori and M. Camalli, *J. Appl. Crystallogr.*, 1994, **27**, 435-435.
4. D. Watkin, R. Cooper and C. K. Prout, *Z. Kristallogr.*, 2002, **217**, 429-430.
5. R. I. Cooper, A. L. Thompson and D. J. Watkin, *J. Appl. Crystallogr.*, 2010, **43**, 1100-1107.
6. A. Dadabhoy, S. Faulkner and P. G. Sammes, *J. Chem. Soc. Perkin Trans. 2*, 2002, 348-357.
7. M. Jauregui, W. S. Perry, C. Allain, L. R. Vidler, M. C. Willis, A. M. Kenwright, J. S. Snaith, G. J. Stasiuk, M. P. Lowe and S. Faulkner, *Dalton Trans.*, 2009, 6283-6285.
8. G. Stasiuk and M. Lowe, *Dalton Trans.*, 2009, 9725.
9. R. Germaneau, R. Chavignon, J.-P. Tranchier, F. o. Rose-Munch, E. Rose, M. Collot and C. Duhayon, *Organometallics*, 2007, **26**, 6139-6149.
10. J. M. Casas-Solvas, E. Ortiz-Salmerón, J. J. Giménez-Martínez, L. García-Fuentes, L. F. Capitán-Vallvey, F. Santoyo-González and A. Vargas-Berenguel, *Chem. Eur. J.*, 2009, **15**, 710-725.
11. K. Barral, A. D. Moorhouse and J. E. Moses, *Org. Lett.*, 2007, **9**, 1809-1811.
12. L. M. De León-Rodríguez, Z. Kovacs, A. C. Esqueda-Oliva and A. D. Miranda-Olvera, *Tetrahedron Lett.*, 2006, **47**, 6937-6940.
13. D. E. Phipps and P. D. Beer, *Tetrahedron Lett.*, 2009, **50**, 3454-3457.
14. A. Davies, A. Donald and R. Marks, *J. Chem. Soc. C*, 1967, **1967**, 2109-2112.

ChemComm

RSC Publishing

COMMUNICATION

View Article Online
View Journal | View Issue

Preparation and study of an f,f,f′,f″ covalently linked tetranuclear hetero-trimetallic complex – a europium, terbium, dysprosium triad†

Cite this: *Chem. Commun.*, 2013, **49**, 783

Received 16th August 2012,
Accepted 6th December 2012

DOI: 10.1039/c2cc35931f

www.rsc.org/chemcomm

Published on 07 December 2012 on http://pubs.rsc.org | doi:10.1039/C2CC35931F
Downloaded by University of Oxford on 25 February 2013

Thomas Just Sørensen,*[ab] Manuel Tropiano,[a] Octavia A. Blackburn,[a] James A. Tilney,[a] Alan M. Kenwright[c] and Stephen Faulkner*[a]

A heterotrimetallic tetranuclear lanthanide complex containing two dysprosium ions, a terbium ion and a europium ion has been prepared by coupling three kinetically stable complexes together using the Ugi reaction. The covalently linked trimetallic system exhibits luminescence from all the different lanthanide centres.

Lanthanide complexes that can be applied as contrast media in imaging and assay have been widely investigated over the last quarter of a century:[1,2] a number of gadolinium complexes are in clinical use as MRI imaging agents,[3] while luminescent complexes have been developed for use in time resolved assay and microscopy.[4,5] Lanthanide luminescence has also been exploited in optical materials and displays.[5] From an early stage, luminescent complexes have been prepared that exploit the large absorption cross-section of aryl chromophores to overcome the inherently inefficient absorption properties of lanthanides themselves.[6] Such studies have been extended to the use of transition metal chromophores with very large extinction coefficients for metal-to-ligand charge transfer transitions.[7]

Heterometallic complexes assembled under thermodynamic control are well known in the world of d-block coordination chemistry, and well-defined heterometallic wheels and clusters have been widely described and applied.[8] Assembly of d-block systems under kinetic control is rarer, though good examples exist of exploiting the kinetic inertness of d^6 transition metal complexes in the preparation of heterometallic assemblies.[9]

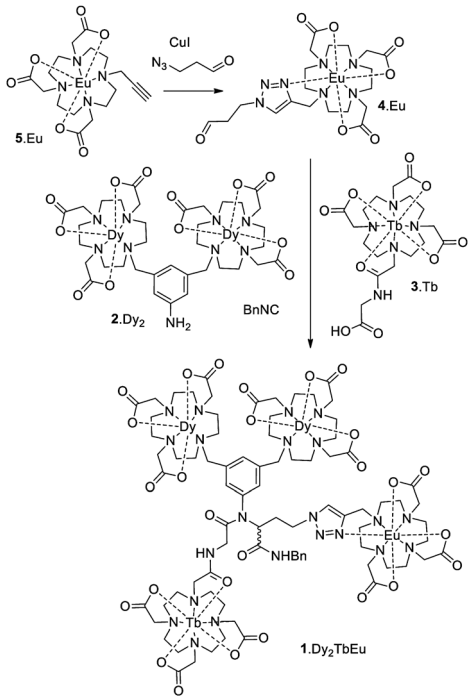
In the world of f-block chemistry, thermodynamic control will always give rise to mixtures and complex speciation. Exploitation of kinetic control can, however, provide access to heterometallic systems in which the position and coordination environment of each metal ion is clearly defined. The lanthanides tend to form labile complexes with simple ligands. As a consequence, while it is straightforward to differentiate between lanthanide and d-block transition metal sites in a compartmental ligand system, selection of one lanthanide over another cannot readily be achieved in systems under thermodynamic control. However, the clinical application of lanthanide complexes has entailed the development of kinetically stable systems that are sufficiently robust to be excreted intact, thus obviating the toxicity of lanthanide ions *in vivo*.[10] Heptadentate and octadentate derivatives of cyclen bearing carboxylate and carboxamide pendent arms form highly stable complexes.[10] In 2003, we exploited these properties in systems bearing reactive groups to prepare the first bimetallic lanthanide complexes.[11] Since then, we and others have extended the available methodologies to the point where it is possible to use a number of different approaches to access a wide variety of bimetallic systems.[12] We have been exploring the use of Ugi and Click chemistry to prepare lanthanide containing arrays.[13,14] In this paper, we report the use of an Ugi methodology to prepare what we believe to be the first complex containing three different kinds of lanthanide ions, and in which four kinetically stable binding pockets are linked together covalently. Such trimetallic systems can potentially be used to provide tri-colour emission, and are potentially of use in white light emissive devices and in multi-analyte sensing.

Our synthetic strategy involved preparing **1**·EuTbDy$_2$ by reacting three stable lanthanide complexes – **2**·Dy$_2$, – **3**·Tb and **4**·Eu together with benzylisocyanide as shown in Scheme 1. **2**·Dy$_2$ and **3**·Tb were prepared using procedures described in the literature for the preparation of their analogues.[15,16] **4**·Eu was prepared by click reaction of the known compound **5**·Eu[17] with 4-azidopropanal. The three building blocks were then reacted together under Ugi reaction conditions initiated by benzyl isocyanide in methanol, yielding **1**·EuTbDy$_2$, which was purified by filtration followed by dialysis with a 1000 Da molecular weight cut-off cellulose membrane. It should be noted that Ugi reactions on these systems only proceed to completion when the carboxylate pendent on **3**·Tb is protonated under the reaction conditions.

[a] *Chemical Research Laboratory, Oxford University, 12 Mansfield Road, Oxford OX1 3TA, England. E-mail: Stephen.Faulkner@chem.ox.ac.uk; Tel: +44 (0)1865 285148*
[b] *Nano-Science Center and Department of Chemistry, University of Copenhagen, Universitetsparken 5, DK-2100 København Ø, Denmark. E-mail: TJS@chem.ku.dk; Fax: +45 35320214; Tel: +45 35320213*
[c] *Department of Chemistry, University of Durham, South Road, Durham DH1 3LE, UK*

† Electronic supplementary information (ESI) available: Experimental detail on synthesis and characterization of the complexes: additional spectra and temporal profiles for the luminescence. See DOI: 10.1039/c2cc35931f

Published on 07 December 2012 on http://pubs.rsc.org | doi:10.1039/C2CC35931F
Downloaded by University of Oxford on 25 February 2013



Scheme 1 Synthesis of **1**·Dy_2TbEu.

NMR was used to probe the structure of the starting complexes and the Ugi product. **2**·Dy_2 exhibits strongly pH-dependent NMR spectra, which resolve into defined peaks only at high pH. Fig. 1 (top) shows the NMR spectrum at pD = 12. Below this pH, all signals are so broadened that no spectrum can be obtained. This is likely to be a consequence of exchange between isomeric forms of **2**·Dy_2 on a timescale close to that of the NMR experiment. By contrast, **3**·Tb and **4**·Eu exhibit clearly defined paramagnetically shifted NMR spectra that are independent of pH across a broad pH range (see Fig. SI1 and SI2, ESI†), reflecting slow exchange between the diastereomeric forms of the complexes with octadentate ligands. Following the Ugi reaction, the NMR spectrum clearly shows

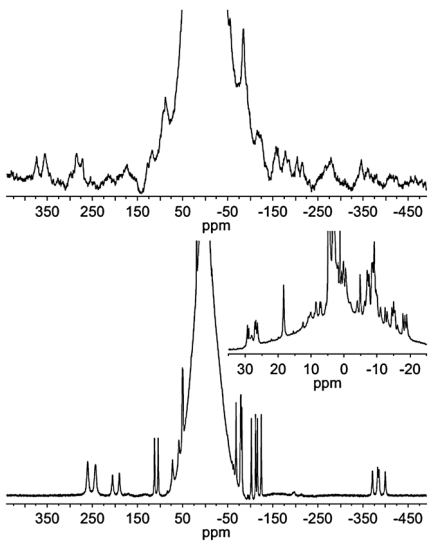


Fig. 1 ^{1}H NMR spectra (500 MHz, 298 K) of **2**·Dy_2 at pD = 12, (top) and of **1**·Dy_2TbEu (bottom).

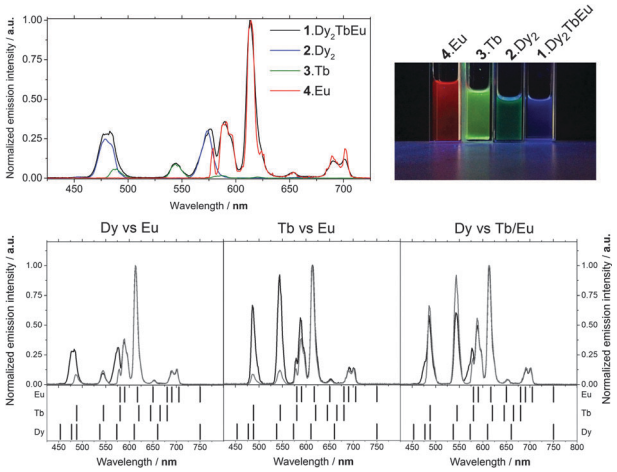


Fig. 2 Luminescence spectra of the complexes: Top: normalized luminescence spectra of the component complexes **1**·EuTbDy_2, **2**·Dy2, **3**·Tb, and **4**·Eu in D_2O. The photograph shows the complexes under UV illumination; Bottom: luminescence spectra of **1**·EuTbDy_2 in D_2O: Left: 300 nm excitation with 0.5 (black) and 3 ms (grey) delay time. Centre: 3 ms delay time with 260 (black) and 300 nm (grey) excitation. Right: 250 nm excitation with 0.5 (black) and 3 ms (grey) delay time. The emission lines of the individual lanthanide ions are indicated below the spectra.

evidence for macrocycle ring protons: Fig. 1 (bottom) shows the spectrum of **1**·Dy_2TbEu, clearly showing the reduced chemical shift range associated with europium, and the broader spread of peaks for the protons close to terbium. It is also instructive that the chemical shifts of the peaks associated with the terbium and europium binding pockets show only small variations compared with the shifts for analogous protons in the component complexes. This implies that the environments at the individual metal complexes are almost unchanged by the formation of the tetranuclear assembly.

1·Dy_2TbEu and the component complexes used to prepare it were luminescent, as can be seen from Fig. 2, while Table 1 summarizes their photophysical properties. It is clear from both the image and the spectra that the bands associated with emission span the visible part of the spectrum, and that relatively intense luminescence is observed.

Fig. 2 shows the luminescence spectrum of **1**·Dy_2TbEu and the precursor complexes, illustrating how it is composed of transitions from all the lanthanide ions. It is notable that none of the signals are

Table 1 Photophysical properties of **1**·Dy_2TbEu and the lanthanide containing building blocks used in its preparation

	Ln	τ dmso-d_6	τ H_2O	τ D_2O	q^a
1·Dy_2TbEu	Tb	2.76 ms	2.1 ms	3.5 ms	0.7
	Eu	1.61 ms	0.7 ms	2.9 ms	1.0
	Dy	~70 μs^b	<50 μs	<50 μs	—
2·Dy_2	Dy	250 μs	—^{b}	—^{b}	—
3·Tb	Tb	2.74 ms	1.92 ms	3.37 ms	0.8
4·Eu	Eu	1.30 ms	0.55 ms	1.69 ms	1.2

^{a} q, the number of inner sphere solvent molecules coordinated to the lanthanide centre, was calculated using the equation:[20] $q = A(\tau_{H_2O}^{-1} - \tau_{D_2O}^{-1} - B)$; for terbium A = 5.0 ms and B = 0.06 ms^{-1}, while for europium A = 1.2 ms and B = 0.25 ms^{-1}. ^{b} The instrumentation used in this study cannot determine lifetimes less than 100 μs to any degree of accuracy.

This journal is © The Royal Society of Chemistry 2013

Published on 07 December 2012 on http://pubs.rsc.org | doi:10.1039/C2CC35931F
Downloaded by University of Oxford on 25 February 2013

quenched entirely, but that the lifetime of the dysprosium luminescence in deuteriated DMSO is reduced significantly, consistent with energy transfer from the emissive state of dysprosium to the excited state manifolds of terbium and europium. The significant difference in lifetime between the dysprosium centred emission and that arising from terbium and europium enabled us to effectively gate out the dysprosium luminescence. Furthermore, the differences in lifetime between the terbium and europium centres are relatively small, meaning that (while they contribute differently to the spectrum at different time points after excitation), the signals cannot be separated completely. Direct excitation of all three lanthanides is possible and both the dysprosium centres and the europium centre can be excited *via* absorption by the triazolyl and amido-xylyl units. The terbium centre is sensitized by neither as is apparent in Fig. 2 and is confirmed by the excitation spectrum, see ESI† for details.

We recently reported the self-assembly of **2**·Eu_2 with the isophthalate anion and its derivatives.[18] **2**·Dy_2 displays very similar properties with isophthalate; the association constant for binding of isophthalate in methanol was found to be 1.6×10^6 M^{-1} [5×10^5–4×10^6] upon fitting data obtained from a luminescence titration using Dynafit.[19] This is significantly lower than the affinity of **2**·Eu_2 for isophthalate in 3 : 1 MeOH–H_2O mixtures (>20×10^6 M^{-1}).[19] The difference possibly results from the smaller size of the dysprosium ion reducing the size of the isophthalate binding pocket and increasing ligand repulsions in the ternary complex. Despite the affinity of **2**·Dy_2 for isophthalate, it is notable that **1**·Dy_2TbEu displayed no detectable affinity for isophthalate under the same conditions. It is clear that the tetranuclear complex is a much bulkier system, and it seems reasonable to suppose that crowding restricts the approach of isophthalate towards the binding pocket. When these observations on triazolyl or amidoxylyl chromophores are combined, and with the observed lifetime data, it is possible to draw some tentative conclusions about the solution structure of the molecule as a whole. It seems clear that the dysprosium and europium binding domains are close in space to one another, and that they restrict approach of the terbium containing domain towards the chromophore moieties. Furthermore, the steric bulk dictates that there is insufficient room for an isophthalate ion to bind in the dysprosium containing binding pocket: indicating either that a suitable binding conformation cannot be achieved, or alternatively that there is insufficient flexibility in the structure to accommodate the bound isophthalate.

The combined Click/Ugi strategy reported in this manuscript clearly gives scope for using a wide variety of building blocks in the preparation of trimetallic complexes. Variation to the structure is facile, since different aldehyde, amine and carboxylate functionalized lanthanide building blocks can be linked together by the same methodology. Furthermore, the isonitrile fragment lends itself to being a means to link a sensitizing chromophore to the architecture. In such second generation systems, it should be possible to vary the colour of the emission by varying the separation between this chromophore and the individual lanthanide centres, as this (in turn) will allow control of the efficiency of the energy transfer processes. This should allow the overall emission spectrum to be tuned to engineer white light emission. With these systems, it is also possible to envisage designing and developing imaging systems in which a single molecule can be used to generate multiple responses. We are currently exploring both these avenues.

We thank the Universities of Oxford and Durham for support, and the Danish Council for Independent Research, Technology and Production Sciences (grant 10-093546) for financial support for TJS, and the European Research Council ((FP7/2007-2013)/ERC-Grant Agreement Number 267426) for support for OAB, and EPSRC for a studentship for MT.

Notes and references

1 P. Caravan, J. J. Ellison, T. J. McMurry and R. B. Lauffer, *Chem. Rev.*, 1999, **99**, 2293–2352; C. Allain and S. Faulkner, *Future Med. Chem.*, 2010, **2**, 339; A. Thibon and V. C. Pierre, *Anal. Bioanal. Chem.*, 2009, **394**, 107–120; C. P. Montgomery, B. S. Murray, E. J. New, R. Pal and D. Parker, *Acc. Chem. Res.*, 2009, **42**, 925–937.
2 I. A. Hemmilä, *Applications of fluorescence in immunoassays*, Wiley, New York, Chichester, 1991; S. Faulkner and J. L. Matthews, *Fluorescent and Luminescent complexes for Biomedical Applications*, in *Comprehensive Coordination Chemistry*, Applications of Coordination Chemistry, ed. M. D. Ward, Elsevier, 2nd edn, 2004, vol. 9.
3 P. Caravan, *Chem. Soc. Rev.*, 2006, **35**, 512; R. Uppal, K. L. Ciesienski, D. B. Chonde, G. S. Loving and P. Caravan, *J. Am. Chem. Soc.*, 2012, **134**, 10799–10802.
4 A. Beeby, S. W. Botchway, I. M. Clarkson, S. Faulkner, D. Parker, A. W. Parker and J. A. G. Williams, *J. Photochem. Photobiol., B*, 2000, **57**, 83; L. Charbonniere, R. Ziessel, M. Guardigli, A. Roda, N. Sabbatini and M. Cesario, *J. Am. Chem. Soc.*, 2001, **123**, 2436.
5 J.-C. G. Bunzli, S. Comby, A. S. Chauvin and C. D. B. Vandevyver, *J. Rare Earths*, 2007, **25**, 257–274.
6 S. Faulkner, L. S. Natrajan, W. S. Perry and D. Sykes, *Dalton Trans.*, 2009, 3890.
7 M. D. Ward, *Coord. Chem. Rev.*, 2007, **251**, 1663; S. Faulkner and D. Sykes, *Lanthanide Assemblies*, in *Lanthanide Luminescence*, ed. P. Hanninen and H. Härmä, Springer Series on Fluorescence, Springer, Heidelberg, 2011, vol. 7.
8 for reviews see G. A. Timco, T. B. Faust, F. Tuna and R. E. P. Winpenny, *Chem. Soc. Rev.*, 2011, **40**, 3067–3075; G. Aromi, P. Gamez and J. Reedijk, *Coord. Chem. Rev.*, 2008, **252**, 964–989.
9 for a review see, L. Flamigni, J. P. Collin and J. P. Sauvage, *Acc. Chem. Res.*, 2009, **41**, 857–871.
10 M. Port, J. M. Idee, C. Medina, C. Robic, M. Sabatou and C. Corot, *Biometals*, 2008, **21**, 469–490.
11 S. J. A. Pope and S. Faulkner, *J. Am. Chem. Soc.*, 2003, **125**, 10526–10527.
12 L. S. Natrajan, A. J. L. Villaraza, A. M. Kenwright and S. Faulkner, *Chem. Commun.*, 2009, 6020–6022; M. P. Placidi, A. J. L. Villaraza, L. S. Natrajan, D. Sykes, A. M. Kenwright and S. Faulkner, *J. Am. Chem. Soc.*, 2009, **131**, 9916–9917; M. S. Tremblay and D. Sames, *Chem. Commun.*, 2006, 4116–4117.
13 M. Main, M. M. Meloni, M. Jauregui, D. Sykes, S. Faulkner, A. M. Kenwright and J. S. Snaith, *Chem. Commun.*, 2008, 5212; L. Tei, G. Gugliotta, S. Avedano, G. B. Giovenzana and M. Botta, *Org. Biomol. Chem.*, 2009, **7**, 4406–4414.
14 M. Jauregui, W. S. Perry, C. Allain, L. R. Vidler, M. C. Willis, A. M. Kenwright, J. S. Snaith, G. Stasiuk, M. P. Lowe and S. Faulkner, *Dalton Trans.*, 2009, 6283; M. Tropiano, N. L. Kilah, M. Morten, H. Rahman, J. J. Davis, P. D. Beer and S. Faulkner, *J. Am. Chem. Soc.*, 2011, **133**, 11847–11849; M. Tropiano, C. J. Record, E. Morris, H. S. Rai, C. Allain and S. Faulkner, *Organometallics*, 2012, **31**, 5673–5676.
15 M. P. Placidi, L. S. Natrajan, D. Sykes, A. M. Kenwright and S. Faulkner, *Helv. Chim. Acta*, 2009, **92**, 2427–2438.
16 H. Schmitt-Willich, J. Platzek and K. D. GraskeB. Raduechel, *Method for producing metal complex carboxylic acid amides*, Patent DE19961052386 19961204, 1996.
17 G. J. Stasiuk and M. P. Lowe, *Dalton Trans.*, 2009, 9725–9727.
18 J. A. Tilney, T. J. Sørensen, B. P. Burton-Pye and S. Faulkner, *Dalton Trans.*, 2011, 12063–12066.
19 P. Kuzmic, *Anal. Biochem.*, 1996, **237**, 260–273.
20 A. Beeby, I. M. Clarkson, R. S. Dickins, S. Faulkner, D. Parker, L. Royle, A. S. de Sousa, J. A. G. Williams and M. Woods, *J. Chem. Soc., Perkin Trans. 2*, 1999, 493–503.

Langmuir

Article

pubs.acs.org/Langmuir

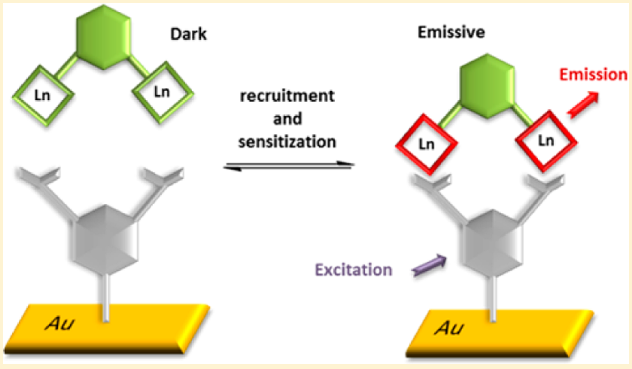
Reversible Recruitment and Emission of DO3A-Derived Lanthanide Complexes at Ligating Molecular Films on Gold

Joshua Lehr, Jamie Bennett, Manuel Tropiano, Thomas J. Sørensen, Stephen Faulkner, Paul D. Beer, and Jason J. Davis*

Department of Chemistry, University of Oxford, South Parks Road, Oxford OX1 3TA, United Kingdom

Supporting Information

ABSTRACT: The recruitment of DO3A-derived lanthanide complexes by ligation to isophthalic acid and catechol-modified gold surfaces, and their resulting sensitization, is reported herein. Predictably pH-dependent surface recruitment is associated with the expected fingerprint europium and terbium emission characteristics. The intensity of the lanthanide luminescence scales exponentially with spacer length, indicating a strong quenching interaction between the lanthanide and the gold surface. The switchable catechol oxidation state provides a means of electrochemically triggering the release of prior ligated complexes.



INTRODUCTION

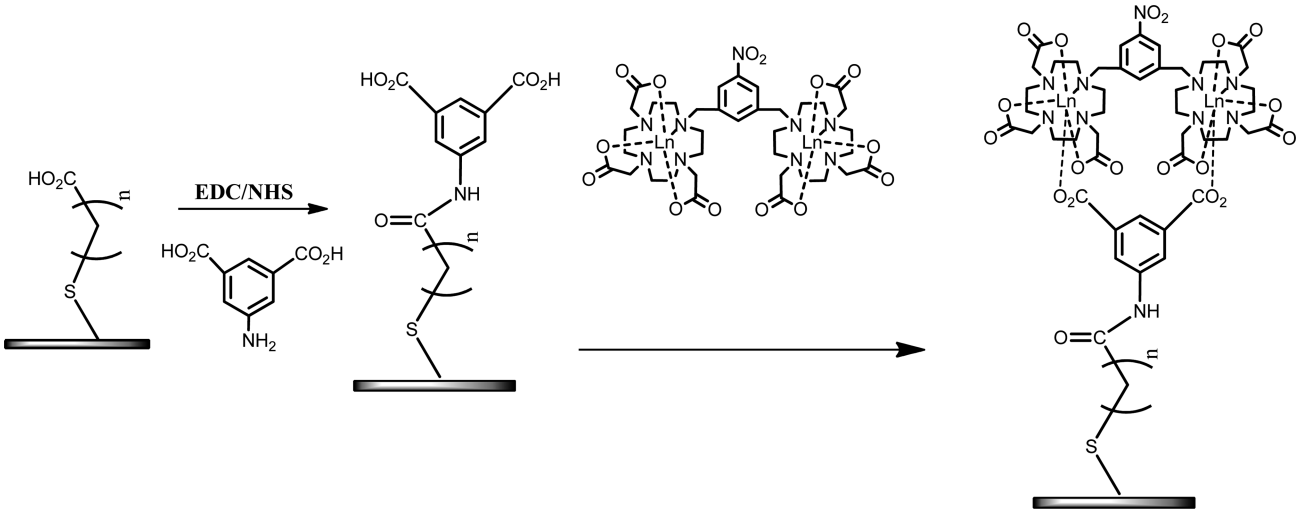
The functionalization of surfaces with well-defined monolayers of carefully designed molecular architectures has received significant attention in recent years. Possible application of these systems in chemical sensing,[1] data storage,[2] molecular electronics,[3] and the development of molecular machines[4] has driven much of this research.[5] The incorporation of luminescent species into such systems provides a convenient means of monitoring binding events and triggered motion within the surface bound molecular assemblies.[6,7] Lanthanides have photophysical characteristics that are attractive in this context, exhibiting long lifetimes and sharp, well-defined, emission bands. Terbium and europium exhibit low absorption coefficients, due to the quasi-atomic nature of f−f transitions. However, this "limitation" can be turned to an advantage by using sensitizer groups (otherwise referred to as antennae) to promote formation of the lanthanide emissive state following energy transfer from a chromophore.[8] Excitation of the sensitizer from its ground state to a singlet excited state is followed by intersystem crossing to the triplet state and intramolecular energy transfer to the excited state of the lanthanide, leading to emission. The sensitizer itself is generally an organic chromophore or transition metal complex with a triplet state that is significantly higher in energy than the emissive state of the lanthanide.[9] The quantum yields of lanthanide emissions are highly dependent on the distance separating the lanthanide and the sensitizer, with the efficiency of the Förster energy transfer following r^6 distance dependence.[10] Direct coordination of the sensitizer to the lanthanide is accordingly highly beneficial if one seeks strong emission.[8] Chemical or electrochemical control of the nature or proximity of the sensitizer to the lanthanide ion has allowed several groups to modulate lanthanide emission in a manner that has significant potential applications in the reporting of molecular conformation, sensing, or display technologies.[11−13] In addition, lanthanide-containing architectures have been incorporated into organic light emitting diodes.[14]

Despite the potential benefits of lanthanide luminescence across a number of applications, very few architectures containing lanthanide ions have been reported at solid interfaces. Gulino, Condorelli, and co-workers have reported the immobilization of presensitized luminescent (5-amino-1,10-phenanthroline) tris (dibenzoylmethane)europium(III) on fused silica[15] and Si (100)[16] substrates. The work of Huskins and co-workers describes the coimmobilization of a europium complex and a carboxylate containing naphthalene-based sensitizer on a β-cyclodextrin molecular print-board on glass.[17] In a further example, Gunnlaugsson and co-workers have reported the attachment of a europium complex to gold by standard thiol-based chemistry; subsequent binding of a naphthalene-based ligand from solution "switches on" lanthanide emission.[18] Lanthanide immobilization has not been restricted to planar surfaces, with the groups of Gunnlaugsson[19−22] and Pikramenou[23,24] reporting a number of examples of lanthanide-functionalized gold nanoparticles. Gadolinium-based chelates have been extensively immobilized on a range of nanoparticle scaffolds for MRI purposes.[25−27] To the best of our knowledge, the ligating recruitment and simultaneous sensitization of lanthanide complexes at molecular films is unprecedented.

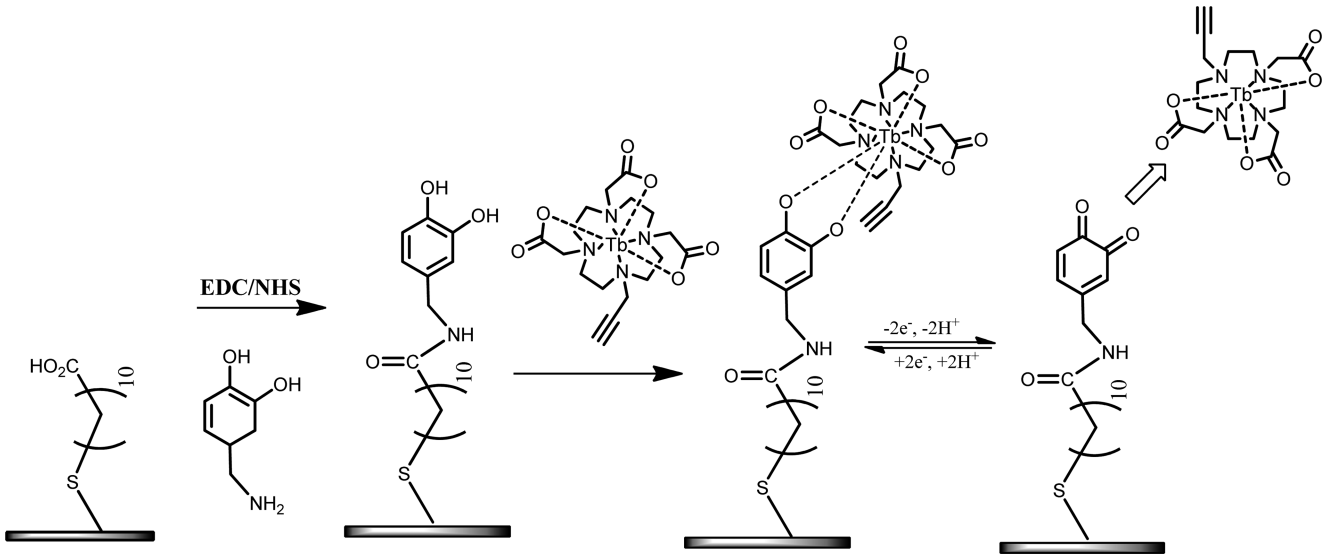
Received: November 25, 2012
Revised: January 12, 2013
Published: January 15, 2013

 © 2013 American Chemical Society dx.doi.org/10.1021/la3046725 | *Langmuir* 2013, 29, 1475−1482

Scheme 1. Immobilization of ISPA on Gold Surface and Subsequent Recruitment of *m*-Xylyl Binuclear Lanthanide Complexes (Where n = 5, 10, and 15)



Scheme 2. Formation of Catechol Films and Electrochemical Control of Mononuclear Terbium DO3A Complex (Tb.P-DO3A) Recruitment



Faulkner and co-workers have recently described the formation of a stable adduct between isophthalic acid (ISPA) and binuclear lanthanide complexes comprising a *m*-xylyl bridging unit linking two lanthanide binding domains, with $K_a > 20 \times 10^6$ M^{-1} for the bis-europium complex.[28,29] In the present work, we exploit the behavior of coordinatively unsaturated lanthanide complexes in recruiting stable lanthanide complexes to surface films, and compare the effectiveness of two approaches to achieving this goal. In the first, we explore the ISPA functionalization of planar gold substrates, and the subsequent recruitment and luminescence of terbium (Tb_2*m*-xyl(DO3A)$_2$) and europium (Eu_2*m*-xyl(DO3A)$_2$) containing *m*-xylyl binuclear lanthanide complexes (Scheme 1). We compare these results with those of the recruitment of a mononuclear propargyl DO3A terbium complex (Tb.P-DO3A).

In a second approach, we investigate the recruitment of Tb.P-DO3A onto catechol-modified gold films. Catechols exhibit a two electron reversible electrochemical switch at mild potentials (Scheme 2). At both molecular films, complex recruitment is specific and predictably pH or oxidation state dependent.

EXPERIMENTAL SECTION

Ln_2*m*-xyl(DO3A)$_2$[30] and Ln.P-DO3A[31] complexes were prepared as previously described. All other chemicals and solvents, with the exception of ethyl(dimethylaminopropyl) carbodiimide (EDC, Alfa Aesar), were purchased from Sigma Aldrich. All aqueous solutions were prepared from 18.2 Ω Millipore water. Gold substrates for ellipsometry and fluorescence were prepared by vapor deposition of 10 nm of chromium, followed by 100 nm of gold, onto Si (100) substrates (Silicon Materials). Gold substrates for infrared reflection absorption spectroscopy (IRRAS) were prepared in the same manner, using glass microscope slides as a support.

The formation of ligating SAMs was achieved by immersion of gold substrates (cleaned by immersion in piranha solution (a 3:1 by volume mixture of 18 M sulfuric acid and 30% hydrogen peroxide) for 5 s), and subsequent washing with H_2O prior to incubation in a 2 mM solution of either 16-mercapohexadecanoic (MHDA), 11-mercaptoundecanoic acid (MUA), or 6-mercapohexanoic acid (MHA), in ethanol

dx.doi.org/10.1021/la3046725 | *Langmuir* 2013, 29, 1475−1482

(HPLC grade) for >10 h. After being rinsed with ethanol and drying with a stream N_2 (g), the gold samples were immersed in a solution consisting of 0.4 M EDC and 0.1 M *N*-hydroxysuccinimide (NHS) in H_2O for 40 min. The substrates were washed with H_2O and dried with a stream of N_2(g), prior to being transferred to a 2 M solution of either 4-amino-isophthalic acid (AISPA)/dimethyl sulfoxide (DMSO), in the preparation of films bearing the ISPA functionality, or 3,4-dihydroxybenzylamine (DHBA)/H_2O, to prepare catechol films. Control films, not containing recruiting ligands, were prepared by immersing the activated NHS ester surface in aniline. All films were washed thoroughly with DMSO and water prior to subsequent experiments.

Recruitment of lanthanide complexes was achieved by immersion of the ISPA or catechol-modified substrates in an approximately 1 mM solution of either Ln_2*m*-xyl(DO3A)$_2$ or Ln(P-DO3A) in a 3:1 mixture of MeOH:H_2O, adjusted to pH 11.0 by addition of KOH, for >8 h, unless stated otherwise. Solution pH was adjusted as required with KOH. After recruitment, and prior to analysis, the surfaces were rinsed for 5 s with pH 11.0 MeOH:H_2O. Alkylated derivatives such as *p*-DO3A form stable complexes with lanthanide ions: the replacement of the cyclen N−H with a noncoordinating substituent can reduce solvation at the metal center, stabilizing the complex through its hydrophobicity and steric bulk.[31]

Ellipsometry measurements were performed on a Beaglehole Instruments Picometer ellipsometer assuming a refractive index of 1.45 for the monolayer over the gold layer (with pseudo optical constants of approximately $n + ik = 0.52 + i \times 3.570$ determined from a fit to each individual gold sample prior to modification).[32] Reported film thicknesses are those determined from, and averaged over, two separately prepared samples, with two measurements per sample.

IRRAS spectra were recorded on a Varian Digilab FTS 6000 series FTIR spectrometer, using a liquid nitrogen cooled MCT detector and a Pike Veemax Specular reflectance accessory. An 80° angle of incidence of was used for all IRRAS measurements. The instrument and the reflectance accessory were purged with N_2 (g) prior to measurements using a FTIR Purge Gas Generator (Whatman). Background scans were recorded using a clean, bare gold substrate, taking an average of 1024 scans. Sample data were collected and averaged over 512 scans using a resolution of 4 cm^{-1} for each measurement.

All luminescence measurements were performed using a Cary Eclipse fluorescence spectrophotometer. Excitation and emission spectra of lanthanide luminescence were obtained using a delay time of 0.2 ms and a gate time of 0.5 ms. Slit widths of 5 nm were used for spectra of solutions and 10 nm for solid substrates. Lifetimes were determined by fitting a single exponential decay function; no statistically significant improvement in fit was observed when multiexponential models were applied.

Electrochemistry of catechol films was carried out on an Autolab PGSTAT-12 system and analyzed using General Purpose Electrochemical Software (GPES) version 4.9. All voltammograms were recorded at 100 mV s^{-1} unless otherwise stated. A platinum wire auxiliary electrode was used in anhydrous acetonitrile (ACN)/0.1 M $TBAPF_6$ with a silver nitrate reference electrode. Polycrystalline gold disk electrodes (diameter = 1.6 mm) purchased from BASi were used as working electrodes. After mechanical polishing (0.1 μm diamond spray), electrodes were immersed in fresh piranha solution for 15 min, prior to electrochemical polishing (200 cycles at 1 V s^{-1}, in the 0 and 1.3 V potential window) in 0.5 M H_2SO_4. The surface area of the electrodes was determined from the gold oxide reduction peak in a final scan at 100 mV s^{-1}.[33]

RESULTS AND DISCUSSION

Part I: Recruitment of Binuclear Lanthanide Complexes at ISPA Surfaces. *Generation of ISPA Films.* Carboxyl-terminated monolayers were initially prepared on freshly cleaned gold substrates prior to carbodiimide driven coupling of 5-aminoisophthalic acid (AISPA), a procedure monitored with IRRAS and ellipsometry. After immersion of the gold substrates in MHDA, the CH_2 asym, CH_2 sym, and CH_2 def bands were observed at 2919, 2850, and 1466 cm^{-1}, respectively, consistent with previous results obtained for MHDA SAMs on gold.[34] The broad peak at ~1720 cm^{-1} is assigned to the presence of cyclic dimer, acyclic dimer, and monomeric carboxylic acid C═O stretch, which have been reported at 1699, 1718, and 1743 cm^{-1}, respectively.[34] ISPA coupling was accompanied by the emergence of the amide I and amide II peaks at 1651 and 1545 cm^{-1},[35] and a strong C═O stretch at 1751 cm^{-1}, indicative of a high concentration of monomeric aryl carboxylic acid functionalities[34] associated with the bound ISPA (Figure 1).

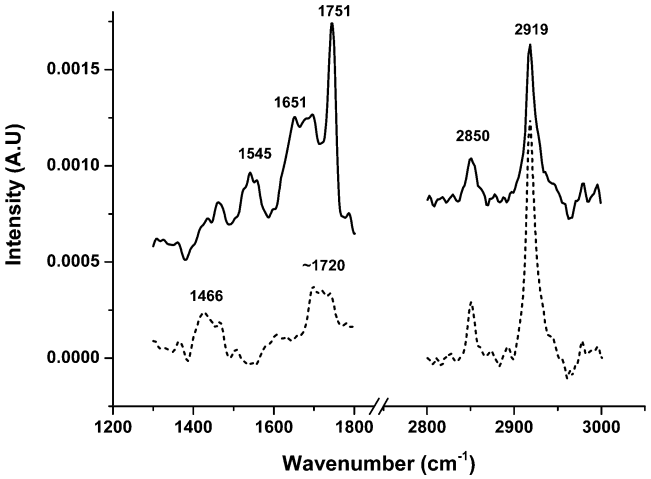


Figure 1. Typical IRRAS spectra of $HS(CH_2)_{15}CO_2H$ (- - -) and ISPA-derived film (−) on gold. Note the emergence of amide I and II in the latter.

The ellipsometric changes associated with this construction, at three different film thicknesses, are summarized in Table 1. MHA, MUA, and MHDA initially generated film thicknesses of 0.5 ± 0.1, 1.4 ± 0.2, and 2.1 ± 0.2 nm, respectively.[36] Subsequent coupling of AISPA uniformly resulted in a 0.7 ± 0.2 nm increase in film thickness.

Recruitment and Luminescence of DO3A-Based Lanthanide Complexes. The association, in solution, of ISPA with binuclear (Ln_2.*m*-xyl(DO3A)$_2$) and mononuclear (Ln.P-DO3A) lanthanide complexes has been previously reported.[28] Recruitment of these complexes at ISPA films was initially investigated by immersion of Au-MHDA-ISPA substrates in Tb_2.*m*-xyl(DO3A)$_2$ and Tb.P-DO3A solutions. Control samples, where aniline rather than AISPA was coupled to the MHDA layers, were also immersed. Figure 2a shows emission spectra (λ_{ex} = 230 nm) of Au-MHDA-ISPA substrates after immersion in Tb_2*m*-xyl(DO3A)$_2$ (−) and Tb.P-DO3A (− − −) solutions. The spectra for the Au-MHDA-ISPA substrates show the characteristic terbium $^5D_4 \rightarrow {}^4F_J$, J = 6, 5, 4, 3, transitions at 490, 546, 585, and 617 nm, respectively, after immersion, and correspond well to that of the solution spectrum of Tb_2*m*-xyl(DO3A)$_2$ (· · ·). In contrast, the Au-MHDA-aniline control samples (not shown) showed virtually no (I_{max} = 6, < 5% of that of the Au-MHDA-ISPA-Tb_2*m*-xyl(DO3A)$_2$ sample) terbium emission after immersion in Tb_2*m*-xyl(DO3A)$_2$, consistent with the central role of ISPA carboxylate ligation. We assign the notably higher emission intensity observed with dimeric Tb_2*m*-xyl(DO3A)$_2$, than the corresponding Tb.P-DO3A surfaces, to a combination of both its markedly higher

dx.doi.org/10.1021/la3046725 | *Langmuir* 2013, 29, 1475−1482

Table 1. Ellipsometeric Film Thicknesses

			film thickness (nm)		
n in S-$(CH_2)n$$CO_2$H	amine	complex	prior to coupling	after coupling	after recruitment
5 (MHA)	AISPA	Tb_2*m*-xyl$(DO3A)_2$	0.5 ± 0.1	1.2 ± 0.1	2.8 ± 0.1
10 (MUA)	AISPA	Tb_2*m*-xyl$(DO3A)_2$	1.4 ± 0.2	2.0 ± 0.2	3.9 ± 0.2
	DHBA	Tb.P-DO3A	1.4 ± 0.2	2.1 ± 0.3	3.1 ± 0.2
15 (MHDA)	AISPA	Tb_2*m*-xyl$(DO3A)_2$	2.1 ± 0.2	2.9 ± 0.3	4.7 ± 0.4
	aniline	Tb_2*m*-xyl$(DO3A)_2$	2.2 ± 0.2	2.8 ± 0.1	2.7 ± 0.2
	AISPA	Tb.P-DO3A	2.3 ± 0.2	2.8 ± 0.1	3.9 ± 0.2

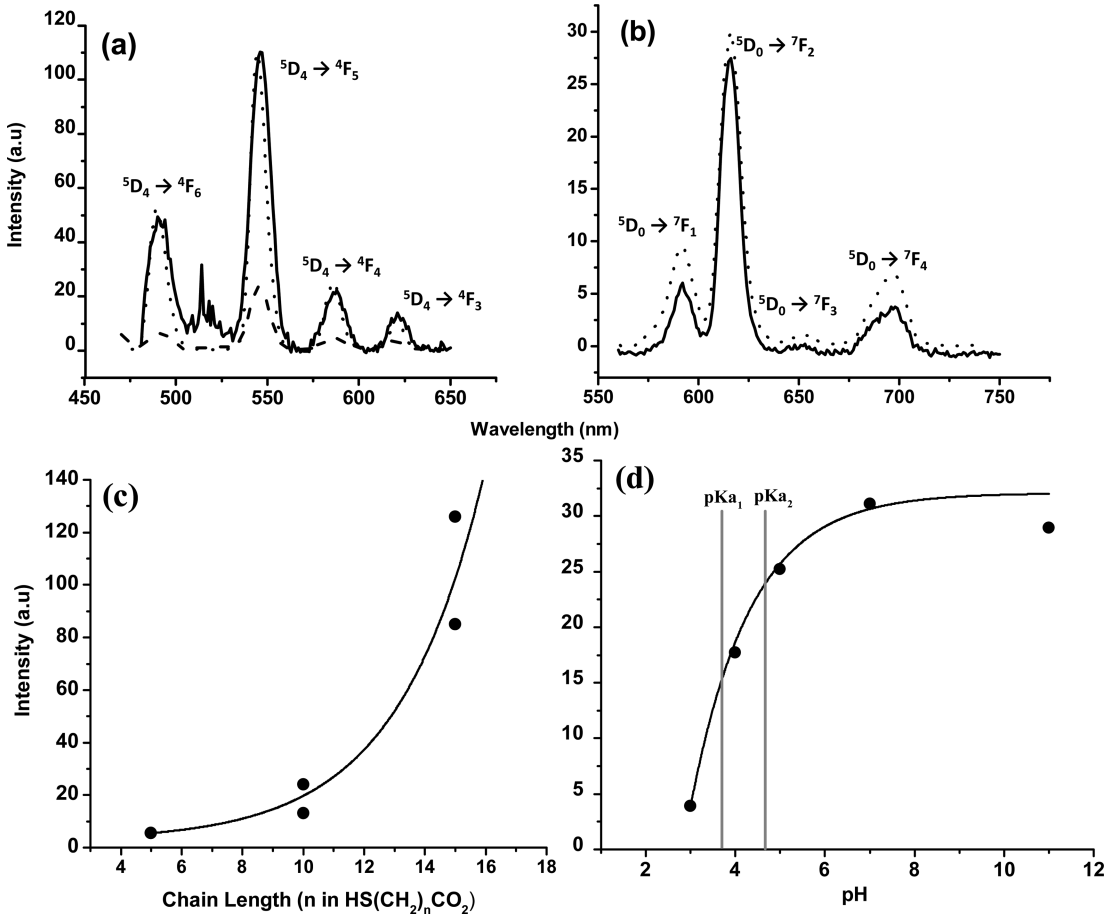


Figure 2. (a) Emission spectra (λ_{ex} = 230 nm) of Tb_2*m*-xyl$(DO3A)_2$ in solution (···) and of Au-MHDA-ISPA substrate after immersion in Tb_2*m*-xyl$(DO3A)_2$ (−) and Tb.P-DO3A (− − −) solution. (b) Emission (λ_{ex} = 230 nm) spectra of Au-MHDA-ISPA-Eu_2*m*-xyl$(DO3A)_2$ substrates (−) and Eu_2*m*-xyl$(DO3A)_2$ in solution (···). Solution spectra recorded at 0.5 mM and normalized by dividing the solution phase intensity as required to enable plotting on the same scale. (c) Plot of thiol chain length versus emission intensity at 546 nm for ISPA films after immersion in Tb_2*m*-xyl$(DO3A)_2$ (d) Emission intensity at 546 nm of Au-MHDA-ISPA substrate after immersion in Tb.P-DO3A solutions of selected pH. Exponential (c) and logarithmic (d) lines of best fit carried out using Origin Pro 8.1, to guide the eye.

association with ISPA (K_a > 20 × 10^6 M^{-1} for binuclear binding, as compared to ∼1.2 × 10^4 M^{-1} for mononuclear binding for Eu DO3A-based complexes[28]) and the potential of additional sensitization through the nitrophenyl moiety.

Recruitment of the *m*-xylyl bieuropium analogue (Eu_2*m*-xyl$(DO3A)_2$) to ISPA films, by immersion of Au-MHDA-ISPA substrates in Eu_2*m*-xyl$(DO3A)_2$, generated films with characteristic europium $^5D_0 \rightarrow {}^7F_J$ emission fingerprints, where J = 1, 2, 3, and 4, observed at 590, 616, 655, and 680 nm, respectively, as seen in Figure 2b (−). The relative intensities of the $^5D_0 \rightarrow {}^7F_1$ and $^5D_0 \rightarrow {}^7F_2$ transition are similar to those of Eu_2*m*-xyl$(DO3A)_2$ in solution (···) confirming that (in light of the hypersensitivity of europium[9]) the emission observed at the surface arises from europium in the Eu_2*m*-xyl$(DO3A)_2$ environment, and hence that binding to ISPA has a negligible effect on the I_{590}/I_{616} ratio, in accordance with previous results in solution.[28]

Ellipsometry confirmed the recruitment of lanthanide complexes to the Au-MHDA-ISPA-modified surfaces, with film thickness changes of ∼1.8 and ∼1.1 nm (indicative of the binding of a single layer of lanthanide complex to the surface; the diameter of the DO3A moiety is 0.9 nm)[37] observed upon immersion of the ISPA-modified gold substrates in Tb_2*m*-xyl$(DO3A)_2$ and Tb.P-DO3A, respectively. No change in film thickness was observed after immersion of the Au-MHDA-aniline control interfaces. The larger (∼1.8 nm) increase in film

dx.doi.org/10.1021/la3046725 | *Langmuir* 2013, 29, 1475−1482

thickness associated with Tb_2*m*-xylyl(DO3A)$_2$ is attributed to the increased steric bulk of this unit relative to that of Tb.P-DO3A. The relatively uniform (~15% variation) thickness increase across the differing chain length films, upon recruitment of the Tb_2*m*-xyl(DO3A)$_2$ complex, is indicative of comparable surface loadings of bound complex across these films.

The expected highly pH-dependent Tb_2*m*-xyl(DO3A)$_2$ or Tb.P-DO3A surface association was demonstrated initially by confirming total emission loss after a 10 s film incubation in 0.1 M H_2SO_4, a loss not observed with an equivalent pH 11.0 ($MeOH/H_2O$) wash. Emission loss was also accompanied by a return (to within 2−3 Å) of film thickness to that observed prior to recruitment. The pH dependence of surface association was further investigated (and confirmed) by immersion of the Au-MHDA-ISPA in Tb.P-DO3A solutions of varying pH prior to spectral analysis at the resulting surfaces, Figure 2d. Note ISPA's carboxylate functionalities solution pK_{a1} = 3.7, pK_{a2} = 4.6.[38]

Energy Loss. Metallic, and in particular gold, substrates are known to quench luminescence, including that from lanthanides, with an efficiency that is expected to be sensitively dependent on the spatial separation between the flourophore and the substrate.[10,39,40] Figure 2c shows a plot of emission intensity at 546 nm versus chain length, for ISPA-terminated films of varying thicknesses (controlled by the length of the precursor carboxylate film) after immersion in Tb_2*m*-xyl-(DO3A)$_2$. As expected, the emission intensity is seen to increase with increasing film thickness from ~3.0 to ~5.0 nm. Luminescence quenching can take place via two distinct mechanisms: Förster resonance energy transfer (FRET) and surface energy transfer (SET), with distance dependencies of $1/d^6$ and $1/d^4$, respectively. The scatter in the data presented here precludes a reliable mechanistic differentiation, although SET would generally be expected to occur in proximity to a gold surface.[10] Substrate luminescence quenching was further assessed by lifetime measurements resolved as 1.22 ± 0.01, 0.85 ± 0.05, and 0.17 ± 0.03 ms for Tb_2*m*-xyl(DO3A)$_2$ in solution, Au-MHDA-ISPA-Tb_2*m*-xyl(DO3A)$_2$ interfaces, and Au-MUA-ISPA-Tb_2*m*-xyl(DO3A)$_2$ interfaces, respectively. (A lifetime for Au-MUA-ISPA-Tb_2*m*-xyl(DO3A)$_2$ could not be determined due to of low S/N ratio observed, arising from low emission intensity.) A decreased lifetime of emissive lanthanide complexes on gold nanoparticle immobilization has previously been noted.[23]

Part II: Redox-Dependent Recruitment of DO3A at Catechol Films. *Modification of Gold with Catechol Films.* Figure 3 shows IRRAS spectra of an MUA film before (- - -) and after (−) attachment of a catechol moiety by carbodiimide coupling of 3,4-dihydroxybenzylamine (DHBA). As with the MHDA film described in the previous section, the CH_2 asym, CH_2 sym, and CH_2 def bands were observed at 2919, 2850, and 1466 cm^{-1}, respectively. The peak at ~1720 cm^{-1} is assigned to the C═O stretches, as described above. The emergence of the amide I and amide II bands at 1660 and 1545 cm^{-1}, respectively, indicates amide bond formation via the coupling of the 4-dihydroxybenzyl moiety after formation of the activated NHS ester. Accompanying film thickness increases are from 1.3 ± 0.1 to 2.1 ± 0.2 nm, consistent with the attachment of 3,4-dihydroxybenzyl moiety after reaction.

The typical voltammetric characteristics of catechol-modified electrodes are represented by Figure 4, where the quasi-reversible and asymmetric redox wave at 0.05 V vs Ag/Ag$^+$ is

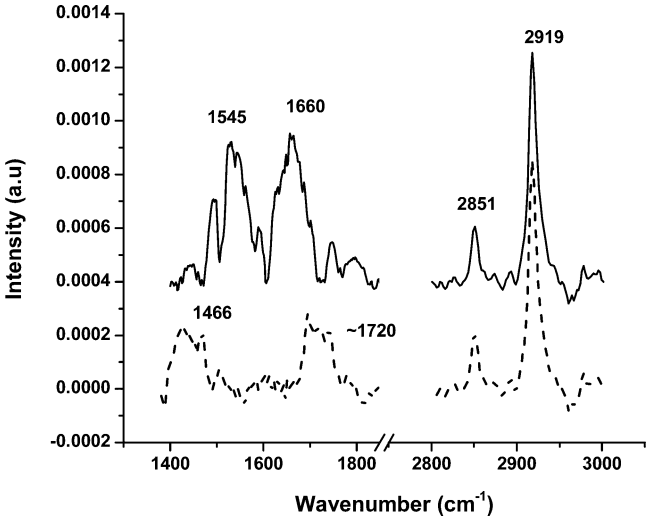


Figure 3. IRRAS spectra of $HS(CH_2)_{10}CO_2H$ film (- - -) and ISPA films (−) on gold, with the expected emergence of amide I and II signals upon coupling.

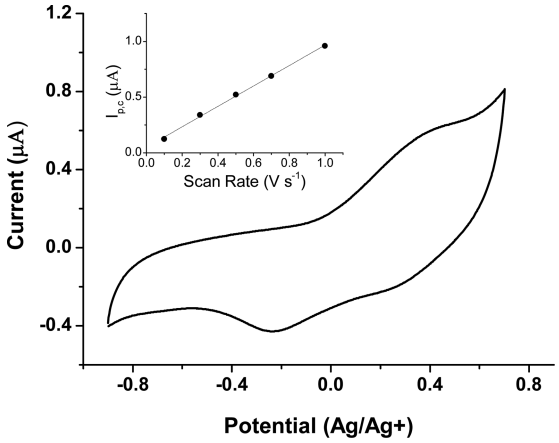


Figure 4. Cyclic voltammogram of MUA-catechol-modified gold in 0.1 M $TBAPF_6$/ACN. Scan rate = 100 mV s^{-1}, scanning in positive direction, second scan shown. Inset: Cathodic peak current versus scan rate.

assigned to the two electron catechol/quinone redox couple (Scheme 2). Although somewhat less well-defined than electrochemical signatures reported for films of spontaneously surface assembling catechols (likely to be more crystalline),[41,42] this response, the associated linear relationship between the scan rate and peak current (figure inset), and catechol surface density (1.6 × 10^{-10} mol cm^{-2}) are broadly in line with expectations.

Recruitment and Luminescence of Terbium DO3A to Catechol Films. Figure 5a shows an emission spectrum of an Au-MHDA-catechol surface after immersion in propargyl terbium DO3A (Tb.P-DO3A) solution. The characteristic terbium $^5D_4 \rightarrow {}^4F_J$, J = 6, 5, 4, 3, transitions are observed at 490, 546, 585, and 617 nm. As stated in the previous section, immersion of Au-MHDA-aniline substrates in Tb.P-DO3A produced negligible lanthanide emission, an observation consistent with hydroxyl-based recruitment in the Au-MHDA-catechol system. Ellipsometry confirms an increase of film thickness of 1.0 ± 0.5 nm, close to the theoretical diameter

dx.doi.org/10.1021/la3046725 | *Langmuir* 2013, 29, 1475−1482

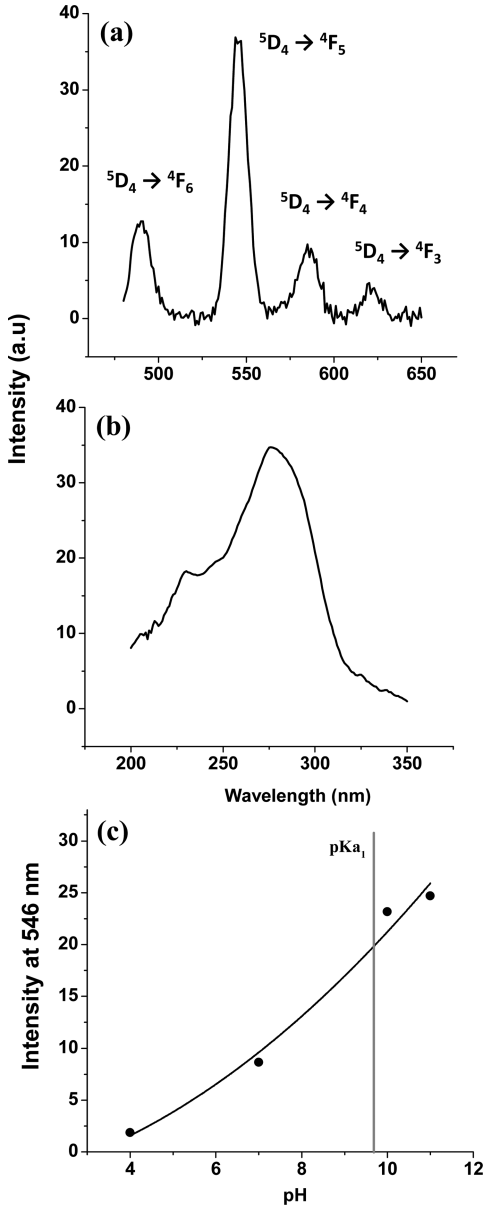


Figure 5. (a) Emission spectrum (λ_{ex} = 290 nm) and (b) excitation spectrum (λ_{em} = 546 nm) for Au-MHDA-catechol surface after immersion in Tb.P-DO3A. (c) Emission intensity at 546 nm (λ_{ex} = 290 nm) after immersion in Tb.P-DO3A at selected pH's. Solution phase: catechol pK_{a1} = 9.7. Polynomial fit carried out using Origin pro 8.1; line added to guide the eye.

of DOTA, suggesting a monolayer of Tb.P-DO3A bound to the catechol film.[37]

Figure 5b shows the excitation spectrum (λ_{em} = 546 nm) of the Au-MHDA-catechol after immersion in Tb.P-DO3A solution. The maximum at ~290 nm indicates excitation of the terbium through the surface bound catechol (π–π* transition centered at ~290 nm; there is only negligible absorption observed at ~290 nm by the propargyl chromophore; see the Supporting Information)[43] and supports specific association of the lanthanide complex via the catechol's hydroxyl groups (Scheme 2). This conclusion was further supported by the pH dependence of recruited emission intensity (Figure 5c) on the deprotonation of the first hydroxyl group (Catechol solution pK_{a1} = 9.7 and pK_{a2} = 13.7).[44]

Electrochemical Controlled Dissociation of Recruited Tb.P-DO3A. Because binding of the Tb.P-DO3A to the surface occurs via the catechol oxygen atoms, electrochemical oxidation of the catechol would be expected to bring about a cessation of binding and a releasing of bound Tb.P-DO3A from the surface.

In initially examining the robustness of Tb.P-DO3A association, we first confirmed emission from the recruited catechol-Tb.P-DO3A substrates to be constant on 10 m surface immersion in stirred ACN/TBAPF$_6$ at open circuit potential (~ −0.3 V vs Ag/Ag$^+$). The emission intensity was then recorded after application of selected potentials between −0.2 and 0.5 V vs Ag/Ag$^+$ in 0.1 M TBAPF$_6$ (stirred) for 60 s, starting at −0.2 V and finishing at +0.5 V (Figure 6). The

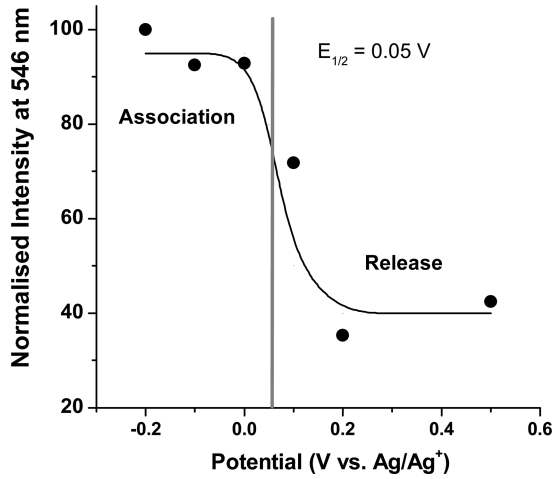


Figure 6. Emission intensity at 546 nm (λ_{ex} = 290 nm) versus potential applied to the substrate (in TBAPF$_6$/ACN) with stirring for 60 s at each potential; $E_{1/2}$ of surface bound catechol is given by vertical line. Second-order polynomial fit carried out using Origin pro 8.1 (line added to guide the eye).

significant (~50%) loss in emission intensity in the potential region of the catechol half wave potential is consistent with the loss of Tb.P-DO3A from the interface upon oxidation of the surface bound catechol, and indicates electrochemical control of DO3A recruitment. The emission remaining after oxidation can be ascribed to catechol groups that are not electronically accessible, or a nonzero association of DO3A with the oxidized form of the catechol. The rate dependence of this redox triggered release remains the subject of further investigation.

■ CONCLUSION

We have demonstrated the ligating recruitment of mononuclear and binuclear DO3A-based lanthanide complexes at isophthalic acid and catechol-modified electrodes. Surface association is predictably pH dependent and accompanied by clearly resolved emission fingerprints that are sensitively dependent on electronic coupling to the supporting electrode. The weak ligation offered by catechol films was utilized in electrochemically triggering release of the lanthanide unit from the surface with accompanying loss of emission. We believe the work reported herein is of considerable value in enhancing progress and understanding the generation of lanthanide-containing surface confined supramolecular architectures.

dx.doi.org/10.1021/la3046725 | *Langmuir* 2013, 29, 1475−1482

■ ASSOCIATED CONTENT

Supporting Information

Solution and molecular film excitation spectra. This material is available free of charge via the Internet at http://pubs.acs.org.

■ AUTHOR INFORMATION

Corresponding Author

*E-mail: jason.davis@chem.ox.ac.uk.

Notes

The authors declare no competing financial interest.

■ ACKNOWLEDGMENTS

We would like to thank the European Research Council under the European Union's seventh Framework Programme (FP7/2007-2013) for funding this research council (EU seventh framework, ERC Advanced Grant Agreement Number 267426). We would also like to thank Dr. Robert M. J. Jacobs for assistance with surface analysis.

■ REFERENCES

(1) Evans, N. H.; Rahman, H.; Davis, J. J.; Beer, P. D. Surface-attached sensors for cation and anion recognition. *Anal. Bioanal. Chem.* **2012**, *402*, 1739−1748.

(2) Cavallini, M.; Biscarini, F.; Leon, S.; Zerbetto, F.; Bottari, G.; Leigh, D. A. Information storage using supramolecular surface patterns. *Science* **2003**, *299*, 531−531.

(3) Collier, C. P.; Wong, E. W.; Belohradsky, M.; Raymo, F. M.; Stoddart, J. F.; Kuekes, P. J.; Williams, R. S.; Heath, J. R. Electronically configurable molecular-based logic gates. *Science* **1999**, *285*, 391−394.

(4) Balzani, V.; Credi, A.; Venturi, M. Molecular machines working on surfaces and at interfaces. *ChemPhysChem* **2008**, *9*, 202−220.

(5) Davis, J. J.; Orlowski, G. A.; Rahman, H.; Beer, P. D. Mechanically interlocked and switchable molecules at surfaces. *Chem. Commun.* **2010**, *46*, 54−63.

(6) Zhang, T.; Mu, L.; She, G.; Shi, W. Light-driven molecular shuttles modified on silicon nanowires. *Chem. Commun.* **2012**, *48*, 452−454.

(7) Chmielewski, M. J.; Davis, J. J.; Beer, P. D. Interlocked host rotaxane and catenane structures for sensing charged guest species via optical and electrochemical methodologies. *Org. Biomol. Chem.* **2009**, *7*, 415−424.

(8) Faulkner, S.; Natrajan, L. S.; Perry, W. S.; Sykes, D. Sensitised luminescence in lanthanide containing arrays and d-f hybrids. *Dalton Trans.* **2009**, 3890−3899.

(9) Richardson, F. S. Terbium(III) and europium(III) ions as luminescent probes and stains for biomolecular systems. *Chem. Rev.* **1982**, *82*, 541−552.

(10) Yun, C. S.; Javier, A.; Jennings, T.; Fisher, M.; Hira, S.; Peterson, S.; Hopkins, B.; Reich, N. O.; Strouse, G. F. Nanometal surface energy transfer in optical rulers, breaking the FRET barrier. *J. Am. Chem. Soc.* **2005**, *127*, 3115−3119.

(11) Lee, K.; Dzubeck, V.; Latshaw, L.; Schneider, J. P. De novo designed peptidic redox potential probe: Linking sensitized emission to disulfide bond formation. *J. Am. Chem. Soc.* **2004**, *126*, 13616−13617.

(12) Tropiano, M.; Kilah, N. L.; Morten, M.; Rahman, H.; Davis, J. J.; Beer, P. D.; Faulkner, S. Reversible luminescence switching of a redox-active ferrocene-europium dyad. *J. Am. Chem. Soc.* **2011**, *133*, 11847−11849.

(13) Butler, S. J.; Parker, D. Anion binding in water at lanthanide centres: from structure and selectivity to signalling and sensing. *Chem. Soc. Rev.* **2012**, DOI: 10.1039/c1032cs35144g.

(14) Binnemans, K. Lanthanide-based luminescent hybrid materials. *Chem. Rev.* **2009**, *109*, 4283−4374.

(15) Gulino, A.; Lupo, F.; Condorelli, G. G.; Motta, A.; Fragala, I. L. Tunable luminescent properties of a europium complex monolayer. *J. Mater. Chem.* **2009**, *19*, 3507−3511.

(16) Condorelli, G. G.; Tudisco, C.; Motta, A.; Di Mauro, A.; Lupo, F.; Gulino, A.; Fragala, I. L. Multistep anchoring route of luminescent (5-amino-1,10-phenanthroline)tris(dibenzoylmethane)europium(III) on Si(100). *Eur. J. Inorg. Chem.* **2010**, 4121−4129.

(17) Hsu, S.-H.; Yilmaz, M. D.; Blum, C.; Subramaniam, V.; Reinhoudt, D. N.; Velders, A. H.; Huskens, J. Expression of sensitized Eu3+ luminescence at a multivalent interface. *J. Am. Chem. Soc.* **2009**, *131*, 12567−12569.

(18) Murray, N. S.; Jarvis, S. P.; Gunnlaugsson, T. Luminescent self-assembly formation on a gold surface observed by reversible "off-on" switching of Eu(III) emission. *Chem. Commun.* **2009**, 4959−4961.

(19) Massue, J.; Quinn, S. J.; Gunnlaugsson, T. Lanthanide luminescent displacement assays: The sensing of phosphate anions using Eu(III)-cyclen-conjugated gold nanoparticles in aqueous solution. *J. Am. Chem. Soc.* **2008**, *130*, 6900−6901.

(20) Bonnet, C. S.; Massue, J.; Quinn, S. J.; Gunnlaugsson, T. Lanthanide luminescent gold nanoparticles: pH-driven self-assembly formation between Eu(III)-cyclen conjugated AuNPs and sensitising beta-diketonate antenna in water. *Org. Biomol. Chem.* **2009**, *7*, 3074−3078.

(21) Comby, S.; Gunnlaugsson, T. Luminescent lanthanide-functionalized gold nanoparticles: Exploiting the interaction with bovine serum albumin for potential sensing applications. *ACS Nano* **2011**, *5*, 7184−7197.

(22) Truman, L. K.; Comby, S.; Gunnlaugsson, T. pH-responsive luminescent lanthanide-functionalized gold nanoparticles with "on-off" ytterbium switchable near-infrared emission. *Angew. Chem., Int. Ed.* **2012**, *51*, 9624−9627.

(23) Lewis, D. J.; Day, T. M.; MacPherson, J. V.; Pikramenou, Z. Luminescent nanobeads: attachment of surface reactive Eu(III) complexes to gold nanoparticles. *Chem. Commun.* **2006**, 1433−1435.

(24) Davies, A.; Lewis, D. J.; Watson, S. P.; Thomas, S. G.; Pikramenou, Z. pH-controlled delivery of luminescent europium coated nanoparticles into platelets. *Proc. Natl. Acad. Sci. U.S.A.* **2012**, *109*, 1862−1867.

(25) Davis, J. J.; Huang, W. Y.; Davies, G.-L. Location-tuned relaxivity in Gd-doped mesoporous silica nanoparticles. *J. Mater. Chem.* **2012**, *22*, 22848−22850.

(26) Huang, W. Y.; Davies, G.-L.; Davis, J. J. High signal contrast gating with biomodified Gd doped mesoporous nanoparticles. *Chem. Commun.* **2013**, *49*, 60−62.

(27) Huang, W. Y.; Davis, J. J. Multimodality and nanoparticles in medical imaging. *Dalton Trans.* **2011**, *40*, 6087−6103.

(28) Tilney, J. A.; Sorensen, T. J.; Burton-Pye, B. P.; Faulkner, S. Self-assembly between dicarboxylate ions and a binuclear europium complex: formation of stable adducts and heterometallic lanthanide complexes. *Dalton Trans.* **2011**, *40*, 12063−12066.

(29) Hill, L. R.; Sørensen, T. J.; Blackburn, O. A.; Brown, A.; Beer, P. D.; Faulkner, S. Self-assembly between dicarboxylate ions and binuclear europium complexes: moving to water−pH dependence and effects of buffers. *Dalton Trans.* **2012**, *42*, 67−70.

(30) Placidi, M. P.; Natrajan, L. S.; Sykes, D.; Kenwright, A. M.; Faulkner, S. Bimetallic lanthanide complexes derived from macrocycle-appended m-xylyl derivatives: Synthesis and spectroscopic properties. *Helv. Chim. Acta* **2009**, *92*, 2427−2438.

(31) Jauregui, M.; Perry, W. S.; Allain, C.; Vidler, L. R.; Willis, M. C.; Kenwright, A. M.; Snaith, J. S.; Stasiuk, G. J.; Lowe, M. P.; Faulkner, S. Changing the local coordination environment in mono- and bi-nuclear lanthanide complexes through "click" chemistry. *Dalton Trans.* **2009**, 6283−6285.

(32) Basabe-Desmonts, L.; Beld, J.; Zimmerman, R. S.; Hernando, J.; Mela, P.; Garcia-Parajo, M. F.; van Hulst, N. F.; van den Berg, A.; Reinhoudt, D. N.; Crego-Calama, M. A simple approach to sensor discovery and fabrication on self-assembled monolayers on glass. *J. Am. Chem. Soc.* **2004**, *126*, 7293−7299.

(33) Tkac, J.; Davis, J. J. An optimized electrode pre-treatment for SAM formation on polycrystalline gold. *J. Electroanal. Chem.* **2008**, *621*, 117−120.
(34) Arnold, R.; Azzam, W.; Terfort, A.; Woll, C. Preparation, modification, and crystallinity of aliphatic and aromatic carboxylic acid terminated self-assembled monolayers. *Langmuir* **2002**, *18*, 3980−3992.
(35) Frey, B. L.; Corn, R. M. Covalent attachment and derivatization of poly(L-lysine) monolayers on gold surfaces as characterized by polarization-modulation FT-IR spectroscopy. *Anal. Chem.* **1996**, *68*, 3187−3193.
(36) Mendoza, S. M.; Arfaoui, I.; Zanarini, S.; Paolucci, F.; Rudolf, P. Improvements in the characterization of the crystalline structure of acid-terminated alkanethiol self-assembled monolayers on Au(111). *Langmuir* **2007**, *23*, 582−588.
(37) Corot, C.; Port, M.; Raynal, I.; Dencausse, A.; Schaefer, M.; Rousseaux, O.; Simonot, C.; Devoldere, L.; Lin, J.; Foulon, M.; Bourrinet, P.; Bonnemain, B.; Meyer, D. Physical, chemical, and biological evaluations of P760: A new gadolinium complex characterized by a low bate of interstitial diffusion. *J. Magn. Reson.* **2000**, *11*, 182−191.
(38) Dabek-Zlotorzynska, E.; Piechowski, M. Application of CE with novel dynamic coatings and field-amplified sample injection to the sensitive determination of isomeric benzoic acids in atmospheric aerosols and vehicular emission. *Electrophoresis* **2007**, *28*, 3526−3534.
(39) Persson, B. N. J.; Lang, N. D. Electron-hole-pair quenching of exited-states near a metal. *Phys. Rev. B* **1982**, *26*, 5409−5415.
(40) Lakowicz, J. R. Radiative decay engineering: Biophysical and biomedical applications. *Anal. Biochem.* **2001**, *298*, 1−24.
(41) Nguyen, N. H.; Esnault, C.; Gohier, F.; Belanger, D.; Cougnon, C. Electrochemistry and reactivity of surface-confined catechol groups derived from diazonium reduction. Bias-assisted Michael addition at the solid/liquid interface. *Langmuir* **2009**, *25*, 3504−3508.
(42) Brooksby, P. A.; Schiel, D. R.; Abell, A. D. Electrochemistry of catechol terminated monolayers with Cu(II), Ni(II) and, Fe(III) cations: A model for the marine adhesive interface. *Langmuir* **2008**, *24*, 9074−9081.
(43) Vaillancourt, F. H.; Barbosa, C. J.; Spiro, T. G.; Bolin, J. T.; Blades, M. W.; Turner, R. F. B.; Eltis, L. D. Definitive evidence for monoanionic binding of 2,3-dihydroxybiphenyl to 2,3-dihydroxybiphenyl 1,2-dioxygenase from UV resonance Raman spectroscopy, UV/Vis absorption spectroscopy, and crystallography. *J. Am. Chem. Soc.* **2002**, *124*, 2485−2496.
(44) Matocha, C. J.; Sparks, D. L.; Amonette, J. E.; Kukkadapu, R. K. Kinetics and mechanism of birnessite reduction by catechol. *Soil Sci. Soc. Am. J.* **2001**, *65*, 58−66.

Chemical Science

RSC Publishing

EDGE ARTICLE

View Article Online
View Journal | View Issue

Lanthanide appended rotaxanes respond to changing chloride concentration†

Cite this: *Chem. Sci.*, 2013, 4, 489

Clémence Allain,[a] Paul D. Beer,*[a] Stephen Faulkner,*[a] Michael W. Jones,[a] Alan M. Kenwright,[b] Nathan L. Kilah,[a] Richard C. Knighton,[a] Thomas Just Sørensen[a] and Manuel Tropiano[a]

Received 27th September 2012
Accepted 22nd October 2012

DOI: 10.1039/c2sc21614k

www.rsc.org/chemicalscience

Published on 22 October 2012 on http://pubs.rsc.org | doi:10.1039/C2SC21614K
Downloaded on 25 February 2013

Lanthanide appended rotaxanes have been prepared by the CuAAC 'click' reaction between an azide appended rotaxane and lanthanide complexes of propargyl DO3A. The resulting complexes are luminescent, and exhibit chloride responsive luminescence behavior consistent with the existence of two independent halide binding pockets, one in the rotaxane cavity and one on the ninth (axial) coordination site of the lanthanide. Strong halide binding to europium gives rise to changes in the relative intensity of the hypersensitive $\Delta J = 2$ transition compared to the rest of the europium emission spectrum, combined with quenching of the overall intensity of emission as a consequence of non-radiative quenching by the bound halide. The weaker interaction with the rotaxane pocket mediates a subsequent recovery of intensity of the europium centered luminescence despite the considerable separation between the lanthanide and the rotaxane binding pocket.

Luminescence from lanthanide ions has been widely studied for more than a quarter of a century, partly as a consequence of the usefulness of luminescent lanthanide complexes in imaging and assay.[1,2] The long-lived luminescence from lanthanides can be exploited in combination with time-gating methodologies to give very low detection limits and eliminate background fluorescence from organic chromophores and biological molecules.[3,4] The low extinction coefficients associated with lanthanide absorption spectra can be overcome by incorporating chromophores into the ligand structure; these act as antennae and mediate formation of the lanthanide emissive state,[5] usually *via* the chromophore triplet state, though charge transfer mediated energy transfer is common for ytterbium complexes.[6] Energy transfer can occur by both Dexter exchange and Förster energy transfer depending upon the structure of the complex.[7]

Studies of luminescence from lanthanide containing systems have, understandably, tended to focus upon the local environment at the metal centre, and upon the sensitizing chromophore. Considerable effort has focused in recent years upon the development of new organic and d-block transition metal chromophores as sensitizers of lanthanide emission.[8] Furthermore, the energy transfer cascade in such systems has been exploited in the development of a range of responsive complexes for which the luminescence is modulated by perturbations to intermediate states (*e.g.* non-radiative quenching of the excited aryl singlet state by chloride, or quenching of the triplet state by molecular oxygen),[9] by chemical or electrochemical modification of the chromophore,[10] or by coordination to the lanthanide with concomitant displacement of solvent.[11]

While lanthanide containing assemblies, particularly helicates and coordination polymers, are now becoming commonplace,[12] the incorporation of lanthanide complexes into mechanically interlocked structures has been largely neglected. In 2006 we reported the synthesis and properties of a d–f hybrid pseudorotaxane that was assembled through anion templation in non-competitive solvent media,[13] but which dissociates in competitive solvents. Stable, interlocked, mechanically bonded rotaxanes appended with lanthanides have proved elusive until now. We have utilised anion templation to construct a range of mechanically interlocked host molecules which, upon removal of the templating anion, bind anions selectively in competitive water-containing solvent mixtures.[14] We reasoned that coupling of the interlocked architecture to a lanthanide containing luminescent reporter would allow us to explore the possibility of time-gated luminescence detection of anions in the rotaxane cavity, while also permitting us to evaluate the anion coordination chemistry of both the rotaxane binding site and the ninth (axial) coordination site on the lanthanide. Here we report the synthesis of a lanthanide containing rotaxane and the rationalization of its luminescence response in the presence of

[a]*Chemistry Research Laboratory, University of Oxford, 12 Mansfield Road, Oxford OX1 3TA, UK. E-mail: stephen.faulkner@chem.ox.ac.uk*

[b]*Department of Chemistry, University of Durham, South Road, Durham DH1 3LE, UK*

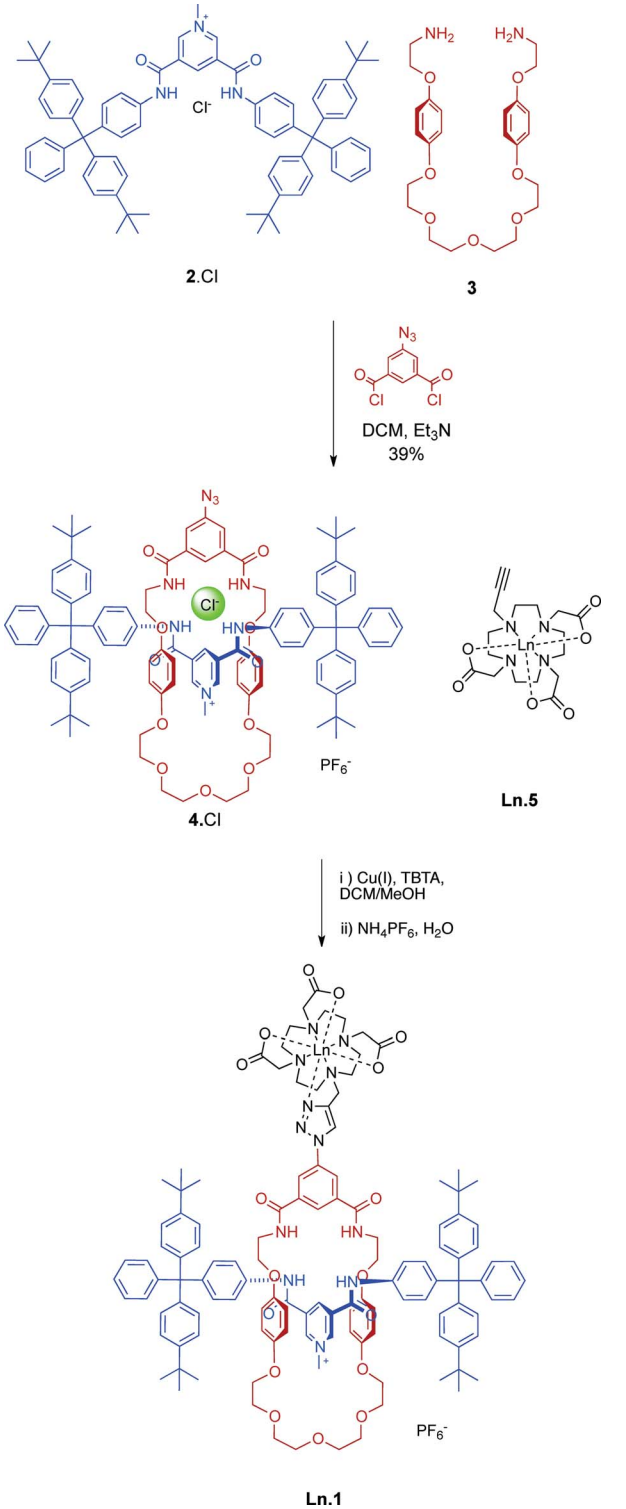
† Electronic supplementary information (ESI) available: Experimental details for synthetic and spectroscopic procedures, including the synthesis of **4**·Cl: characterisation and structural data; binding studies and photophysical measurements, including detailed analysis of binding models. CCDC 903824 and 903825. For ESI and crystallographic data in CIF or other electronic format see DOI: 10.1039/c2sc21614k

Published on 22 October 2012 on http://pubs.rsc.org | doi:10.1039/C2SC21614K
Downloaded on 25 February 2013

chloride and other anions. The use of a kinetically and thermodynamically stable luminescent tag is shown to greatly lower the chloride detection limit thanks to the use of superior sensitivity of luminescence detection over NMR. Furthermore, the effect of changes remote from the lanthanide site is shown to influence the photophysical properties of the lanthanide, suggesting that it is always necessary to consider the system as a whole.

The synthetic approach used to prepare the target lanthanide containing rotaxanes involved the initial assembly of an appropriately functionalized rotaxane, which was then coupled to a kinetically stable lanthanide complex. A chloride anion templated condensation clipping reaction between a pyridinium chloride axle (**2**·Cl), diamine macrocycle precursor (**3**) and 5-azidoisophthaloyl chloride afforded the azide functionalized rotaxane **4**·Cl (Scheme 1).

4·Cl formed crystals that were suitable for X-ray crystallography. The structure confirms the interlocked nature of the system with the templating chloride anion located in the rotaxane cavity encapsulated by the orthogonal hydrogen-bonding array, with a mean N–Cl distance of 3.37 Å. The complexes Ln·**5** (Ln = Eu, Lu) were prepared by the literature procedure.[10,15] We were fortunate that Lu·**5** also gave crystals suitable for crystallographic study; these are the first crystals of such a system to be studied, and give a direct insight into the precursor structure in such systems. The structure of Lu·**5** is unusual in that two complexes are bridged by a carbonate, while the structure is stabilized by two sodium ions in the asymmetric



Scheme 1 Preparation of Ln·**1** [Ln = Lu and Eu].

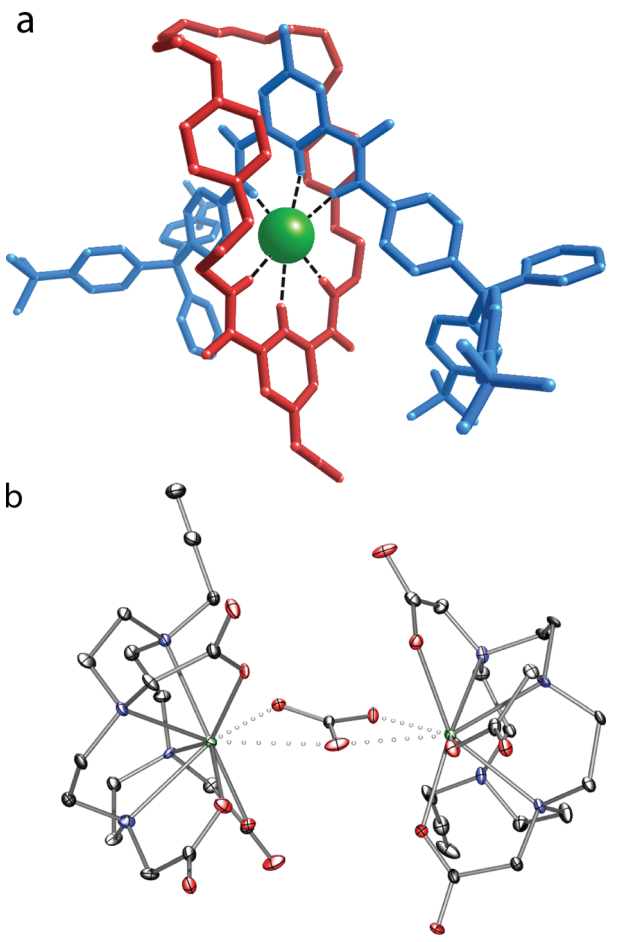


Fig. 1 Representation of the solid state structure of (a) **4**·Cl (Mercury capped stick depiction showing the components of the rotaxane) and (b) Lu·**5** (ORTEP depiction) with thermal ellipsoids of Lu·**5** displayed at 30% probability and the water, sodium, and hydrogen atoms omitted for clarity.

This journal is © The Royal Society of Chemistry 2013

Published on 22 October 2012 on http://pubs.rsc.org | doi:10.1039/C2SC21614K
Downloaded on 25 February 2013

unit and multiple water molecules in an extensive, complex 3-dimensional hydrogen-bonding network. The crystal was found to be a non-merohedral twin by rotation about the *c*-axis with a twin ratio of *ca.* 70 : 30. The structures are illustrated in Fig. 1, and further details are tabulated in the ESI.†

CuAAC 'click' reaction between **4**·Cl and Ln·**5** yielded Ln·**1** as its chloride complex, which upon halide anion removal from the rotaxane host cavity *via* washing with aqueous ammonium hexafluorophosphate was then converted to the non-coordinating hexafluorophosphate salt.

The rotaxane systems Ln·**1** were characterized by mass spectrometry and NMR spectroscopy (further details are available in the ESI†). For Eu·**1**, the shifted regions of the spectra provide clear evidence for successful CuAAC 'click' reaction. Comparison of the ^{1}H spectra for Ln·**1** with published data for other related systems[15a] clearly indicates an octadentate ligand bound to the metal centre (as opposed to the heptadentate ligand in Ln·**5**), with a square antiprismatic geometry predominating at the lanthanide centre. This is in accordance with previous observations on the triazoloDO3A system.[10,15] Though the protons on the rotaxane are too far from the paramagnetic lanthanide centre to be shifted significantly as a consequence of the presence of the lanthanide, the NMR spectrum of the Lu·**1** complex is entirely consistent with the structure of the rotaxane domain being closely related to **4**·Cl. Luminescence spectroscopy was used to probe the association of Ln·**1** with chloride, dihydrogen phosphate and acetate in dichloromethane solution. There are two possible binding pockets for anions, since binding can occur on the ninth (axial) coordination site of the lanthanide metal as well as in the rotaxane binding pocket. Indeed, in dichloromethane solution binding to both is to be expected.

[Eu·**1**]·PF_6 exhibits sensitized emission following excitation of the aryl chromophore, and the modulation of this sensitised emission upon titration with anions was used to probe the binding of these. Titration of a dichloromethane solution of [Eu·**1**]·PF_6 with tetrabutylammonium chloride produced clear changes in the luminescence spectra. As the titration progressed, the luminescence intensity initially decreased sharply, before recovering as additional equivalents of chloride were added (Fig. 2), indicating that two binding events occur. Initially, increasing concentrations of chloride ions gave rise to a rapid decrease in lanthanide-centered emission accompanied by a change in the general band structure of the peaks arising from the $\Delta J = 2$ and the $\Delta J = 4$ transitions. Further increasing the concentration of chloride is followed by a more gradual increase in intensity without any change in appearance of the peaks in the spectrum. The initial binding process clearly

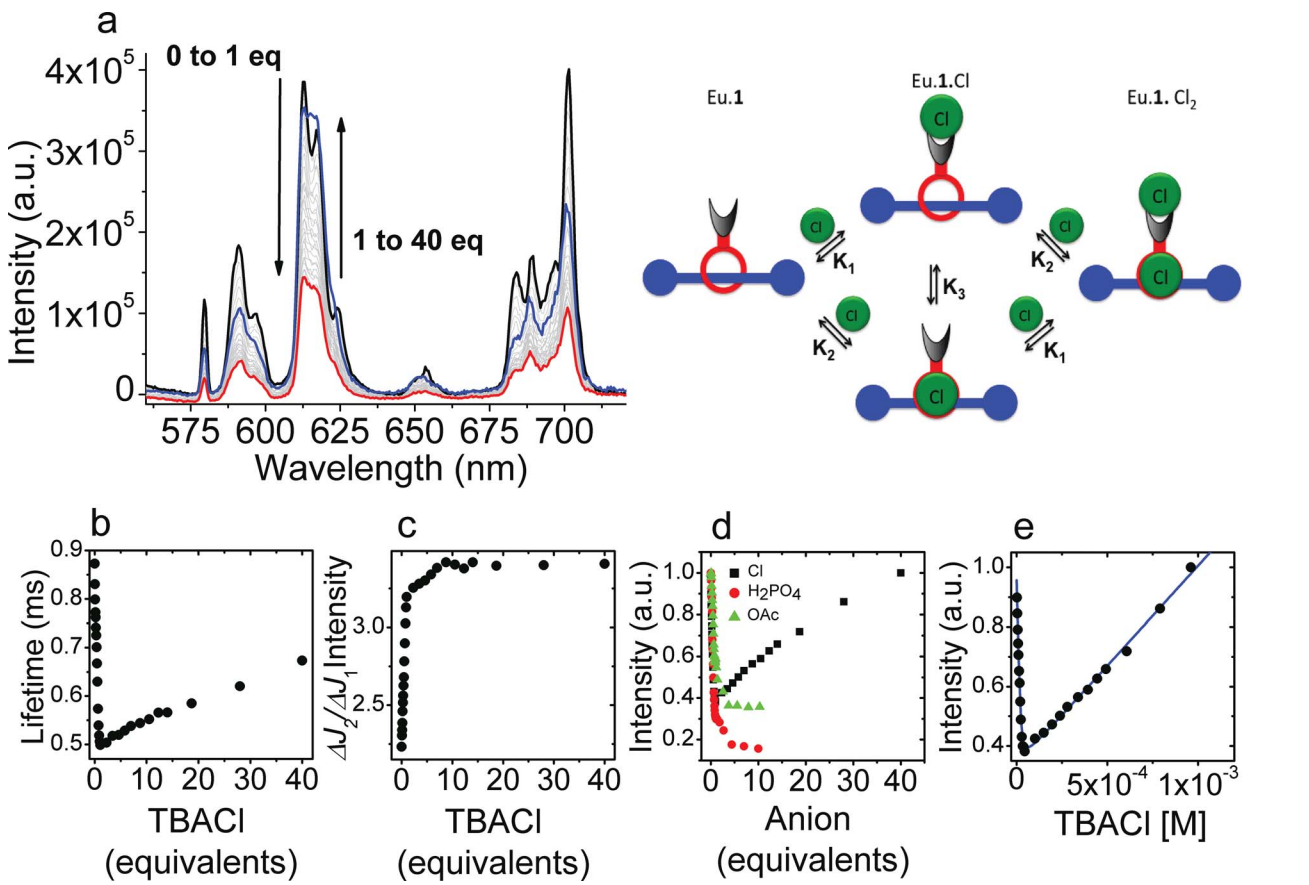


Fig. 2 (a) Variation in the luminescence spectrum of Eu·**1** upon titration with chloride ($\lambda_{ex} = 270$ nm) in dichloromethane; (b) variation in luminescence lifetime of the europium centered emission arising from $^5D_0$ as the titration progresses; (c) variation in the ratio of the intensities of the $^5D_0$–$^7F_2$ and $^5D_0$–$^7F_1$ transitions with increasing halide concentration; (d) variation in the luminescence intensity observed upon titration of Eu·**1** with TBA·Cl, TBA·H_2PO_4 and TBA·OAc; (e) fitting the observed changes in luminescence intensity upon titration of Eu·**1** with chloride in dichloromethane using an independent binding sites model as shown in the picture above.

Published on 22 October 2012 on http://pubs.rsc.org | doi:10.1039/C2SC21614K
Downloaded on 25 February 2013

involves a substantial change in the intensity of the hypersensitive $\Delta J = 2$ transition at 617 nm relative to the other europium centered transitions. This is clear evidence for binding of chloride to the ninth (axial) donor site on the lanthanide complex.[16] For the first strong binding event, the association constant could be determined from the luminescence titration data. Fitting the observed data using Dynafit[17] to a 1 : 1 model gave a binding constant for the association of chloride to $[Eu\cdot\mathbf{1}]\cdot PF_6$ in dichloromethane of 504 000 M^{-1}. The data did not allow for a determination of the association constant for the second binding event. Modelling the data shown in Fig. 2 allowed us to study the binding in depth and demonstrate that completely independent binding events[18] have to be used to emulate the observed data; the representation was modelled using an association constant for the axial coordination site on the lanthanide (K_1) of 750 000 M^{-1} and an association constant (K_2) for binding in the rotaxane pocket of 1360 M^{-1}.

Time-resolved data casts further light upon the processes involved. The luminescence lifetimes of the europium centered emission initially falls off rapidly, as a consequence of intramolecular non-radiative quenching of the excited state of the lanthanide by a photo-electron transfer process involving the bound chloride. There is a subsequent recovery in lanthanide luminescence lifetime as a consequence of rigidification and changes in solvation following chloride binding in the rotaxane pocket. Importantly, the europium-centered emission acts as a sensor of the relatively remote structural changes that occur upon binding a chloride anion in the rotaxane cavity.

By contrast, when the binding of acetate and dihydrogenphosphate anions was studied in dichloromethane, we observed only one binding event, also accompanied by changes in the $\Delta J = 2$ transition, indicating that binding to the lanthanide center is completely predominant; no structural changes in the rotaxane was observed for these anions. In the case of acetate and dihydrogenphosphate titrants, the affinity of the axial donor site for the anion was reduced relative to the affinity for chloride (K_1 = 58 000 M^{-1} and 304 000 M^{-1} for acetate and dihydrogenphosphate respectively). The absence of a second binding event in the rotaxane cavity is to be expected given the known selectivity of response to chloride for related rotaxane hosts.[14] In more competitive solvent media comprising 1 : 1 dichloromethane–methanol mixtures, the affinity of anions for both lanthanide center and the rotaxane cavity was found to be diminished (see Table 1), and only binding to the former was observed in the luminescence titrations.

The assignment of binding sites was further supported by additional titrations of a model system containing only the lanthanide binding pocket in 1 : 1 DCM–MeOH (see ESI† for further details), which exhibited an association constant of 65 000 M^{-1}, similar to the association constant of the lanthanide site in $Eu\cdot\mathbf{1}$ with chloride in the same system. NMR studies on $\mathbf{4}\cdot PF_6$ were used to probe the affinity of the rotaxane for anions, revealing that the association constant with chloride (K_1 = 1460 M^{-1}) ($CDCl_3$, MeOD, D_2O, 45 : 45 : 10) was significantly greater than that for dihydrogenphosphate or acetate (K_1 = 188 M^{-1} and K_1 = 115 M^{-1} respectively). These observations lend further credence to the observation of two binding events in the titration of $Eu\cdot\mathbf{1}$ with chloride.

Table 1 Association constants of $Eu\cdot\mathbf{1}$ with chloride, dihydrogenphosphate and acetate at the europium center, determined from the changes to the europium luminescence spectra upon titration with tetrabutylammonium salts

Solvent	Added salt	K_1[a] (M^{-1})	
DCM	TBA·Cl	504 000[b]	[298 900–1 014 000][c]
	TBA·H_2PO_4	304 000	[264 200–354 600][c]
	TBA·OAc	58 000	[52 520–64 300][c]
DCM–MeOH 1 : 1	TBA·Cl	95 000	[87 554–102 540][c]
	TBA·H_2PO_4	70 000	[54 780–86 250][c]
	TBA·OAc	23 000	[20 290–26 310][c]

[a] Obtained from ΔJ ratios binding plots. [b] Modelling the observed data to an independent binding model for the two binding sites gave two association constants (K_1 = 750 000 M^{-1} and 1360 M^{-1}) that can be assigned to binding at the lanthanide and in the rotaxane cavity. [c] Confidence intervals determined as the values of K that are possible while keeping χ^2 with 99% of the minimum value.

Conclusions

These results show that lanthanide containing rotaxanes can be constructed *via* a modular approach, where an appropriately functionalized rotaxane can be coupled to a lanthanide centre. Furthermore, the lanthanide ion is an effective component in anion responsive behaviour, both in the binding event directly and when acting as a sensor for remote changes of rotaxane host molecular structure due to specific anion binding. In the systems described in this manuscript, it is clear that two binding domains exist, and that binding of chloride ions can take place both through axial ligation to the lanthanide center and through binding in the rotaxane cavity. In this system, the two binding sites operate separately. However, the results reveal that lanthanides can act as efficient luminescent reporters and receptors in anion binding systems. Furthermore, the long-lived luminescence from lanthanide ions can be time-gated to remove background fluorescence and scatter, meaning that this work sets a clear precedent for the development of lanthanide-containing supramolecular sensing systems. The exploitation of changes to distant parts of the molecule in other fields is also possible, since the effects of rigidification and changes to energy transfer and non-radiative quenching pathways can clearly be exploited in a much greater range of systems than that described here.

It is also clear from these results that axial anion coordination by lanthanides can be very effective in mediating a response, even in the case of simple mono-dentate anions such as halides. We are currently engaged in the preparation of a second generation of lanthanide containing mechanically bonded arrays, in which the lanthanide is incorporated into the rotaxane cavity.

Acknowledgements

The research leading to these results has received funding from the European Research Council under the European Union's 7th Framework Programme (FP7/2007-2013)/ERC-Advanced Grant

 This journal is © The Royal Society of Chemistry 2013

Agreement Number 267426) and a Marie-Curie Fellowship for CA. We also thank the University of Oxford, EPSRC and Helmore for support (studentships for MT and RK), The Danish Council for Independent Research, Technology and Production Sciences (grant 10-093546) for financial support for TJS, and the Royal Commission for the Exhibition of 1851 (research fellowship for NLK). We thank Diamond Light Source for an award of beam time on I19 (MT1858) and the University of Oxford Crystallography Service for instrument use and helpful discussions.

Notes and references

1 (*a*) S. Faulkner and J. L. Matthews, *Fluorescent Complexes for Biomedical Applications in Comprehensive Coordination Chemistry II*, ed. M. D. Ward, Pergamon, Oxford, 2004, vol. 9, pp. 913–944; (*b*) J.-C. G. Bünzli and C. Piguet, *Chem. Soc. Rev.*, 2005, **34**, 1048–1077.

2 (*a*) I. A. Hemmilä, *Applications of Fluorescence in Immunoassays*, Wiley, New York, Chichester, 1991; (*b*) J.-C. G. Bünzli, S. Comby, A. S. Chauvin and C. D. B. Vandevyver, *J. Rare Earths*, 2007, **25**, 257–274.

3 P. Hanninen and H. Härmä, *Lanthanide Luminescence*, Springer Series on Fluorescence, Springer, Heidelberg, 2011, vol. 7.

4 A. Beeby, S. W. Botchway, I. M. Clarkson, S. Faulkner, A. W. Parker, D. Parker and J. Williams, *J. Photochem. Photobiol., B*, 2000, **57**, 83–89.

5 For reviews, see (*a*) S. Faulkner, B. P. Burton-Pye and S. J. A. Pope, *Appl. Spectrosc. Rev.*, 2005, **40**, 1–31; (*b*) S. Faulkner, L. S. Natrajan, W. S. Perry and D. Sykes, *Dalton Trans.*, 2009, 3890–3899.

6 A. Beeby, S. Faulkner and J. A. G. Williams, *Dalton Trans.*, 2002, 1918–1922.

7 T. Lazarides, D. Sykes, S. Faulkner, A. Barbieri and M. D. Ward, *Chem.–Eur. J.*, 2008, **14**, 9389–9399.

8 For a review see: M. D. Ward, *Coord. Chem. Rev.*, 2007, **251**, 1663–1677.

9 (*a*) D. Parker, R. S. Dickins, H. Puschmann, C. Crossland and J. A. K. Howard, *Chem. Rev.*, 2002, **102**, 1977–2010; (*b*) T. Gunnlaugsson and J. P. Leonard, *Chem. Commun.*, 2005, 3114–3131; (*c*) C. Allain and S. Faulkner, *Future Med. Chem.*, 2010, **2**, 339–350.

10 M. Tropiano, N. L. Kilah, M. Morten, H. Rahman, J. J. Davis, P. D. Beer and S. Faulkner, *J. Am. Chem. Soc.*, 2011, **133**, 11847–11849.

11 C. P. Montgomery, B. S. Murray, E. J. New, R. Pal and D. Parker, *Acc. Chem. Res.*, 2009, **42**, 925–937.

12 (*a*) C. Piguet, M. Borkovec, J. Hamacek and K. Zeckert, *Coord. Chem. Rev.*, 2005, **249**, 705–726; (*b*) K. Zeckert, J. Hamacek, J.-M. Senegas, N. Dalla-Favera, S. Floquet, G. Bernardinelli and C. Piguet, *Angew. Chem., Int. Ed.*, 2005, **44**, 7954–7958; (*c*) L. Aboshyan-Sorgho, H. Nozary, A. Aebischer, J.-C. G. Bünzli, P.-Y. Morgantini, K. R. Kittilstved, A. Hauser, S. V. Eliseeva, S. Petoud and C. Piguet, *J. Am. Chem. Soc.*, 2012, **134**, 12675–12684; (*d*) C. Lincheneau, F. Stomeo, S. Comby and T. Gunnlaugsson, *Aust. J. Chem.*, 2011, **64**, 1315–1326.

13 M. R. Sambrook, D. Curiel, E. J. Hayes, P. D. Beer, S. J. A. Pope and S. Faulkner, *New J. Chem.*, 2006, **30**, 1133–1136.

14 (*a*) M. D. Lankshear and P. D. Beer, *Acc. Chem. Res.*, 2007, **40**, 657–668; (*b*) L. M. Hancock and P. D. Beer, *Chem.–Eur. J.*, 2009, **15**, 42–44; (*c*) L. M. Hancock, L. C. Gilday, S. Carvalho, P. J. Costa, V. Felix, C. J. Serpell, N. L. Kilah and P. D. Beer, *Chem.–Eur. J.*, 2010, **16**, 13082–13094; (*d*) L. M. Hancock, L. C. Gilday, N. L. Kilah, C. J. Serpell and P. D. Beer, *Chem. Commun.*, 2011, **47**, 1725–1727; (*e*) N. H. Evans, C. J. Serpell and P. D. Beer, *Chem. Commun.*, 2011, **47**, 8775–8777.

15 (*a*) M. Jauregui, W. S. Perry, C. Allain, L. R. Vidler, M. C. Willis, A. M. Kenwright, J. S. Snaith, G. J. Stasiuk, M. P. Lowe and S. Faulkner, *Dalton Trans.*, 2009, 6283–6285; (*b*) G. J. Stasiuk and M. P. Lowe, *Dalton Trans.*, 2009, 9725–9727.

16 R. S. Dickins, J. I. Bruce, D. J. Tozer and D. Parker, *Dalton Trans.*, 2003, 1264–1271.

17 P. Kuzmic, *Anal. Biochem.*, 1996, **237**, 260–273.

18 M. Borkevec, G. J. M. Koper and C. Piguet, *Curr. Opin. Colloid Interface Sci.*, 2006, **11**, 280–289.

Published on 22 October 2012 on http://pubs.rsc.org | doi:10.1039/C2SC21614K
Downloaded on 25 February 2013

View Article Online / Journal Homepage / Table of Contents for this issue
Dynamic Article Links

PCCP

Cite this: *Phys. Chem. Chem. Phys.*, 2012, **14**, 13378–13384

www.rsc.org/pccp

PAPER

Luminescence and upconversion from thulium(III) species in solution†

Octavia A. Blackburn,[a] Manuel Tropiano,[a] Thomas Just Sørensen,*[ab] James Thom,[a] Andrew Beeby,*[c] Lisa M. Bushby,[c] David Parker,[c] Louise S. Natrajan[d] and Stephen Faulkner*[a]

Received 2nd July 2012, Accepted 14th August 2012
DOI: 10.1039/c2cp42228j

Published on 14 August 2012 on http://pubs.rsc.org | doi:10.1039/C2CP42228J
Downloaded by University of Oxford on 25 February 2013

Thulium salts and complexes are shown to be emissive from three states in the excited state manifold of Tm^{3+}. Formation of the $^1D_2$ state can result in luminescence, or in energy transfer to the lower energy $^1G_4$ and $^3H_4$ emissive states. Where chromophores are present in the ligand structure, emission is restricted to thulium centred emissive states that are lower in energy than the chromophore centred donor state. We have also observed direct multi-photon excitation of the thulium excited state manifold. Furthermore, additional transitions are observed in the multi-photon excitation spectra that are consistent with upconversion as a consequence of sequential single photon absorption and relaxation processes within the thulium excited state manifold.

Introduction

Lanthanide luminescence has become a vital tool in assay, imaging and telecommunications over the course of the last quarter of a century.[1] The luminescence from highly emissive lanthanide ions such as europium and terbium has been well-known for even longer than that, and the long luminescence lifetimes arising from *f–f* transitions have been shown to lend themselves to applications in time-gated imaging.[2] More recently, we and others have devoted considerable effort to establishing the solution state luminescence properties of lanthanide ions that are emissive in the near IR,[3] particularly, neodymium[4] and ytterbium.[5] We have reached the point where the solution state luminescence spectroscopy of nearly all the open shell lanthanide ions has been well-characterized. The remaining exceptions for which very little published data exists are cerium(III), for which the $^2F_{5/2} \rightarrow {}^2F_{7/2}$ transition is comparable in energy to typical IR vibrations of organic compounds,[1] promethium(III) which is highly radioactive and self-luminescent as a consequence of its radioactivity, and thulium(III), which we will discuss further in this manuscript. In the case of thulium, reports of the solution photophysics are restricted to steady state studies of the near IR emission from the $^3H_4$ state,[6] and to emission from the $^1G_4$ state in β-diketonate complexes.[7] However, a study of the energy level diagram for thulium, combined with consideration of the energy gap law,[8] suggested that visible emission should also be readily detected in complexes with appropriate ligands.

The solid-state luminescence properties of thulium(III) are already relatively well-understood.[9] Thulium compounds have been used in a variety of photophysical applications, but interest has focused chiefly on two-photon processes that can occur through the thulium manifold. Güdel and co-workers have established that thulium doped compounds can exhibit up-conversion properties through absorption of red or near IR light,[10] followed by relaxation to an intermediate excited state and a second absorption event that leads to the formation of a high energy emissive state. Such phenomena can be observed through intermediate states that are localized on thulium, or through states that are localized on other lanthanide ions: ytterbium-thulium co-doped systems have proved particularly popular in this regard.[11]

The nature of the thulium excited state manifold, in which changes in the *f*-electron configuration (and consequent changes in L, S and J) fortuitously give rise to several excited states with comparable energy gaps to the next lowest state, led us to believe that there might be a number of different emissive states in the system. This is not entirely unprecedented: indeed we and others have previously observed such behaviour in praseodymium and europium complexes.[12,13] The existence of several emissive states raises the prospect of tuning the colour of the luminescence observed from a complex by tuning the ligand structure.

[a] *Chemistry Research Laboratory, University of Oxford, Mansfield Road, Oxford, OX1 3TA, UK. E-mail: Stephen.Faulkner@chem.ox.ac.uk; Fax: +44 (0)186 528 5148; Tel: +44 (0)186 528 5005*
[b] *Nano-Science Center & Department of Chemistry, University of Copenhagen, Universitetsparken 5, DK-2100 København Ø, Denmark. E-mail: TJS@chem.ku.dk; Fax: +45 35320214; Tel: +45 35320213*
[c] *Department of Chemistry, University of Durham, South Road, Durham, DH1 3LE, UK. E-mail: Andrew.Beeby@dur.ac.uk; Fax: +44 (0)191 334 2051; Tel: +44 (0)191 334 2023*
[d] *School of Chemistry, University of Manchester, Oxford Road, Manchester, M13 9PL, UK*
† Electronic supplementary information (ESI) available: Absorption spectra, TCSPC traces and fits and emission spectra. See DOI: 10.1039/c2cp42228j

This journal is © the Owner Societies 2012

Published on 14 August 2012 on http://pubs.rsc.org | doi:10.1039/C2CP42228J
Downloaded by University of Oxford on 25 February 2013

We now report the results of a study of the photophysics of a range of thulium salts and complexes, identifying the effect of solvent on emission lifetime, probing the effect of structure on luminescence and establishing the nature of one- and two-photon excitation pathways in thulium containing systems.

Experimental section

Chemicals were used as received. Thulium triflate (trifluoromethanesulfonate, OTf) was obtained from Strem chemicals and DMSO from Sigma-Aldrich. One photon excitation and emission spectra were recorded from a >10 mM solution of $Ln(OTf)_3$ in d_6-DMSO in a 1 cm HELLMA QS cuvette using a Horiba Fluorolog 3. Two-photon excitation and emission spectra were recorded from a solution of $Tm(OTf)_3$ in d_6-DMSO in a 1 cm cuvette using the double grating emission monochromator and detector on a Horiba Fluorolog 3. Excitation was achieved using a Coherent Chameleon APE-OPO tuneable femtosecond laser, the wavelength was monitored using the internal spectrometer of the Chameleon and the OPO. The range available was from 680 to 1080 nm (9260 to 14 705 cm^{-1}), and excitation wavelengths down to 340 nm were achieved through frequency doubling of the Ti : Sa and the OPO. A 5 cm focal length lens fixed in front of the cuvette was used to focus the excitation pulse onto the sample and achieve two-photon excitation. In all cases no signal was recorded when the lens was removed. Laser power was measured at each excitation wavelength with a standard wavelength dependent power meter. The excitation spectra were recorded by measuring the total emission spectrum at each excitation wavelength. The excitation spectrum was then created by integration of all emission bands and dividing by the laser power squared.

All spectra and fitted temporal profiles are available as ESI.†

Complexes were synthesized as previously reported,[14] DOTA was used as its H_3O^+ salt. In the case of thulium DO3A-P, the literature procedure used for the preparation of Tb·DO3A-P[14c] was modified by using thulium(III) trifluoromethanesulfonate in lieu of the terbium salt; the product was characterized by NMR spectroscopy: ^{1}H-NMR (500 MHz; D_2O): δ 181.06 (s, 1H), 132.79 (s, 1H), 113.26 (s, 1H), 94.47 (s, 1H), 58.68 (s, 1H), 43.63 (s, 1H), 26.10 (s, 1H), 20.08 (s, 1H), −6.47 (s, in solvent peak), −9.61 (s, in solvent peak), −16.05 (s, 1H), −42.67 (s, 1H), −50.40 (s, 1H), −52.02 (s, 1H), −69.72, −72.18, −73.12, −77.80, −78.31 (4H).

Results and discussion

Fundamental photophysics

There has been some debate about the ordering of the excited states of thulium, with a variety of published energy level diagrams giving different term symbols for some of the intermediate excited states. For the purpose of this report, we have used the energy level diagram published by Carnell and co-workers in 1983.[9a] We intially checked the correlation of the published energy level diagram with the high resolution absorption spectra of thulium trifluoromethanesulfonate in D_2O and d_6-DMSO (Fig. S1, ESI†). The excited state energies relative to the ground state are collated in Table 1, and show good correlation with Carnell's published energy levels for all transitions below 4×10^4 cm^{-1},[9a] as shown in Fig. 1. The *f–d* transitions in the UV region of the spectrum ($E >$ 33 000 cm^{-1}) are formally allowed and dramatically more intense than the *f–f* transitions that underpin the emissive photophysics that we observed. As would be expected for *f–f* transitions in a lanthanide ion, the observed absorption bands are sharp, with low absorption coefficients. Small changes in energy levels are observed as a consequence of weak ligand field effects owing to changes in the solvation sphere, with no splittings greater than a few hundred wavenumbers.

Table 1 Absorption and emission maxima of $Tm(O_3SCF_3)_3$ in d_6-DMSO

Excited state	Absorption maxima ν/cm^{-1}	Emission from $^1D_2$		Emission from $^1G_4$	
		ν/cm^{-1}	ΔE^a	ν/cm^{-1}	ΔE^a
$^3H_6$				20 870	21 200
				21 480	21 490
$^3F_4$	5650	21 990	21 790	15 420	15 540
	5950	22 120	22 090		
$^3H_5$	8220 (sh)	19 400	19 270	12 760	13 020
	8260	19 560	19 480		
	8470	19 620	19 520		
$^3H_4$	12 650 (sh)	15 180	14 950		
	12 790				
	12 860				
$^3F_3$	14 300 (sh)	13 320	13 160		
	14 580				
$^3F_2$	15 130	12 760	12 610		
$^1G_4$	21 200 (sh)				
	21 490				
$^1D_2$	27 740				
	27 890 (sh)				
$^1I_6$	34 660 (sh)				
$^3P_0$	35 000				
$^3P_1$	36 170 (sh)				
	36 360				
$^3P_2$	38 020				

[a] Energy gap calculated from the absorption spectrum.

Luminescence

Thulium(III) trifluoromethanesulfonate was dissolved in a variety of solvents, and the thulium centred luminescence properties were initially studied following single-photon excitation of the $^3H_6 \rightarrow {}^1D_2$ transition around 28 000 cm^{-1}. A typical emission spectrum (for thulium(III) trifluoromethanesulfonate in d_6-DMSO) is shown in Fig. 2, while the peaks in the emission spectrum are given in Table 1. The steady state absorption and emission spectra both correlate well with the energy level diagram, as can be seen from Fig. 1, though it is clear on cursory inspection that the emission spectrum can only be explained by the presence of more than one emissive state. Furthermore, it is apparent that the spectrum is dominated by emission from the $^1D_2$ and $^1G_4$ states. In many ways, this is unsurprising, in that the energy gap between $^1D_2$ and $^1G_4$ is similar to that between $^1G_4$ and $^3F_2$ (6400 cm^{-1} and 5900 cm^{-1} respectively). Further study of the energy level diagram reveals that other states might also be expected to be emissive on the basis of substantial energy gaps (ΔE) to the next lowest state.

Published on 14 August 2012 on http://pubs.rsc.org | doi:10.1039/C2CP42228J
Downloaded by University of Oxford on 25 February 2013

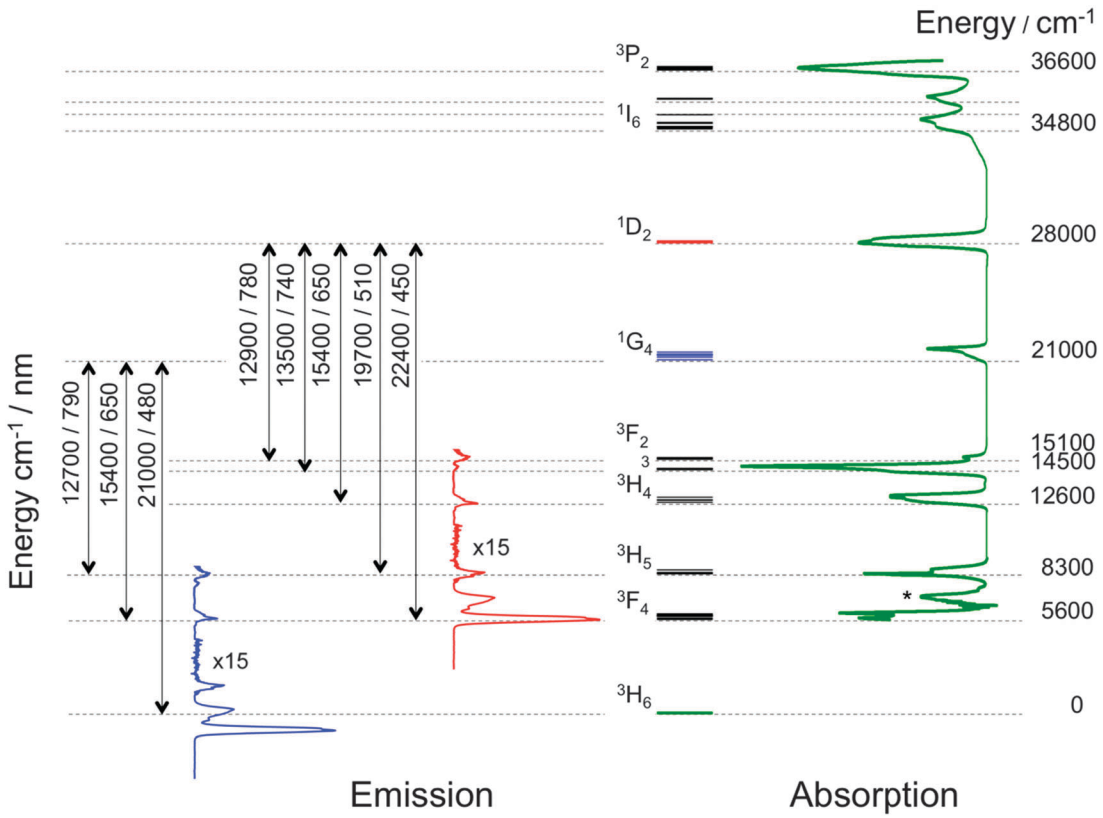


Fig. 1 Energy level diagram for Tm^{III} (taken from Carnell *et al.* 1983[9a]) with states aligned with absorption maxima in d_6-DMSO; and the emission spectrum in d_6-DMSO, given twice to indicate emission from $^1D_2$ (right) and $^1G_4$ (left), with the signal intensity multiplied by 15 at 500–600 nm. *Indicates features corresponding to trifluoromethanesulfonate.

Specifically, these would be the $^3F_4$ state (for which ΔE is 5600 cm^{-1}), which would be expected to be emissive at around 5600 cm^{-1}, and the $^3H_4$ state (for which ΔE is 4300 cm^{-1}), which would be expected to be emissive at around 12 600 cm^{-1}. Of these, study of the $^3F_4$ state is beyond the capabilities of our instrumentation, since the emission wavelength is too great to fall within the range of available detectors. However, the emission bands from $^3H_4$ could fall within our capabilities, though other emissive transitions (namely $^1D_2 \rightarrow {}^3F_{2,3}$ and $^1G_4 \rightarrow {}^3H_5$) are likely to overlap with $^3H_4 \rightarrow {}^3H_6$. Time-resolved studies are essential if we are to deconvolute these overlapping transitions and understand the photophysics of the thulium(III) ion more fully.

The temporal variation in luminescence intensity following the excitation pulse was examined by time-correlated single photon counting methods, using tail fitting to establish luminescence lifetimes significantly longer than the detector response, and iterative reconvolution methods to establish lifetimes for shorter-lived species. Table 2 shows the lifetimes of the principal transitions in the luminescence spectrum of

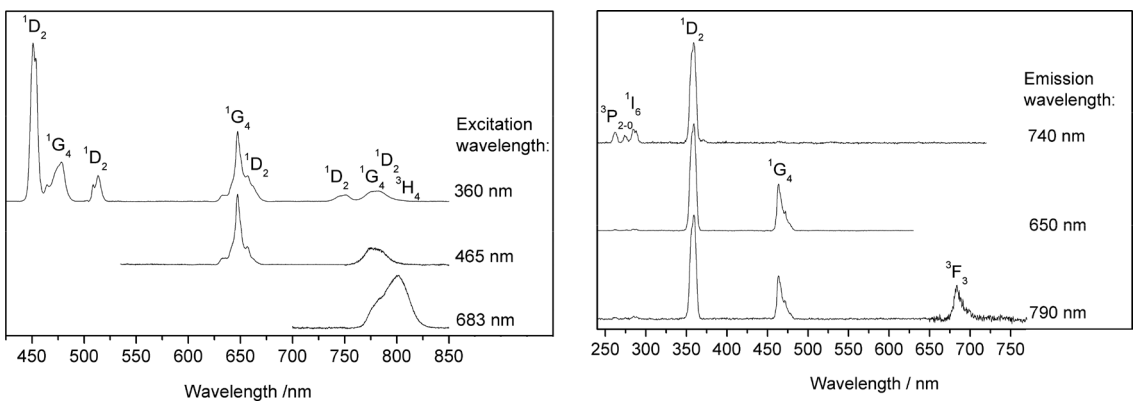


Fig. 2 Top: Emission spectra of $Tm(O_3SCF_3)_3$ in d_6-DMSO exciting at 360, 465 and 683 nm. (The signal has been multiplied by 20 at 500–700 nm and by 50 at 700–850 nm with 360 nm excitation; by 5 at 750–850 nm with 465 nm excitation.) Bottom: Excitation spectra of $Tm(O_3SCF_3)_3$ in d_6-DMSO monitoring at 740, 650 and 790 nm. (The signal has been multiplied by 5 at 650–770 nm when monitoring at 790 nm.)

 This journal is © the Owner Societies 2012

Table 2 Luminescence lifetimes and assignments of observed emission bands (λ_{em}) of $Tm(O_3SCF_3)_3$ in various solvents exciting at 360 nm

	τ/ns[a]						
	452	479	515	648	657	751	783
λ_{em}/nm	$^1D_2 \rightarrow {}^3F_4$	$^1G_4 \rightarrow {}^3H_6$	$^1D_2 \rightarrow {}^3H_5$	$^1G_4 \rightarrow {}^3F_4$	$^1D_2 \rightarrow {}^3H_4$ $^1G_4 \rightarrow {}^3F_4$	$^1D_2 \rightarrow {}^3F_3$	$^1D_2 \rightarrow {}^3F_2$ $^1G_4 \rightarrow {}^3H_5$ $^3H_4 \rightarrow {}^3H_6$
d_6-DMSO	224	193[b]	215	183	170	183	177
		1200[c]		1215[c]	1209		1256
DMSO	152	152[b,d]	149	152[b,d]	147	145	133
		302[c]		296[c]	289		309
D_2O	89	89[b,d]	86	89[b,d]	98	92	285
		311[c]		308[c]	332		
CD_3OD	124	135[b,d]	117	140[b]	109	125	334
		427[c]		429[c]	383		
CH_3OD	89	166[c]	—[e]	—[e]	—[e]	—[e]	—[e]

[a] All lifetimes have errors of ±10%. [b] Positive or rise component in the fit of the time resolved emission profile. [c] Negative or decay component in the fit of the time resolved emission profile. [d] Rise fixed at lifetime determined at 452 nm. [e] Signal too weak.

Published on 14 August 2012 on http://pubs.rsc.org | doi:10.1039/C2CP42228J
Downloaded by University of Oxford on 25 February 2013

thulium(III) in a variety of solvents. It is clear from the data that our hypothesis of more than one emissive state is valid, since groups of transitions share similar temporal profiles for a given solvent. Assignments of the transitions within each band are based upon the energy level diagram in Fig. 1.

Each transition from the $^1D_2$ state demonstrates single exponential decay kinetics consistent with a rise-time that is within the envelope of the laser pulse (as might be expected for an experiment in which this state is excited directly). However, transitions involving the $^1G_4$ emissive state exhibit more complicated kinetics, with the temporal profile of the emission fitting well to a rise-time and a decay component. In every case, the rise-time obtained is within experimental error of the lifetime of the $^1D_2$ excited state. Fig. 3 shows the temporal profile of the observed emission at 479 nm in d_6-DMSO, fitted to a rise-time component coupled to a decay component while allowing a floating population of the $^1G_4$ state at time zero. This fit is of demonstrably better quality than a simpler model which merely allows for a rise-time and decay. This is clear evidence that $^1G_4$ is populated by decay of $^1D_2$, but also suggests that rapid population of $^1G_4$ occurs by a different pathway. Such behaviour is not entirely without precedent. In 2001, we observed similar kinetics for population of the $^5D_0$ state of europium in an antenna bearing complex.[13a] The temporal profile of the transition addressed at 657 nm is much more complicated, and consists of a mixture of two excited state emission bands, $^1D_2 \rightarrow {}^3H_4$ and $^1G_4 \rightarrow {}^3F_4$: however, the rise-time of the $^1G_4$ emission is masked by the decay of the $^1D_2$ emission at this wavelength. A similar situation exists when the emission is observed at 783 nm, though this is more complicated, as there should be three overlapping transitions at this wavelength, namely $^1D_2 \rightarrow {}^3F_2$, $^1G_4 \rightarrow {}^3H_5$ and $^3H_4 \rightarrow {}^3H_6$. The transitions from $^1D_2$ and $^1G_4$ dominate the observed data, and the profiles observed are very similar to those observed at 657 nm. In the simple salt systems, it is impossible to make any observation of the relatively allowed $^3H_4 \rightarrow {}^3H_6$ transition, which would be expected to have a greatly reduced lifetime compared to the other transitions at this wavelength.

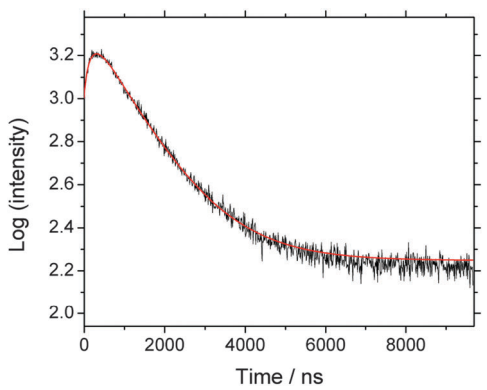


Fig. 3 Time resolved emission profile of $Tm(O_3SCF_3)_3$ in d_6-DMSO with λ_{ex} = 360 nm and λ_{em} = 479 nm with biexponential fit.

Table 3 Observed rate constants ($k_{obs} = 1/\tau$) for the Tm(III) ion in various solvents comparing the effects of C–H and C–D oscillators

	k_{obs}/s^{-1}			
	DMSO		Methanol-OD	
	d_6	h_6	d_3	h_3
$^1D_2$	4.5×10^6	6.6×10^6	8.1×10^6	1.1×10^7
$^1G_4$	8×10^5	3.3×10^6	2.3×10^6	6.0×10^6

Quoted rate constants have errors of ±10%.

The variation in luminescence lifetime with solvent is also worthy of comment. It is clear from Table 3 that replacing C–D oscillators with C–H oscillators has a slightly greater effect upon the luminescence from $^1G_4$ than the luminescence from $^1D_2$. O–H oscillators are remarkably effective at bringing about non-radiative quenching of every emissive state and good spectra or data could not be obtained in protic solvents.‡

Luminescent thulium complexes

To probe the luminescence from thulium further, we studied the emissive behaviour of a range of amino-carboxylate complexes derived from azamacrocyclic ligand systems, using the complexes

‡ Solvents were used as received and no special precautions were taken to avoid water absorption of the sample solution. To investigate the effect of water 10 v/v% of water was added to a D_2O solution of thulium triflate, the addition resulted in total quenching of all thulium emission.

Published on 14 August 2012 on http://pubs.rsc.org | doi:10.1039/C2CP42228J
Downloaded by University of Oxford on 25 February 2013

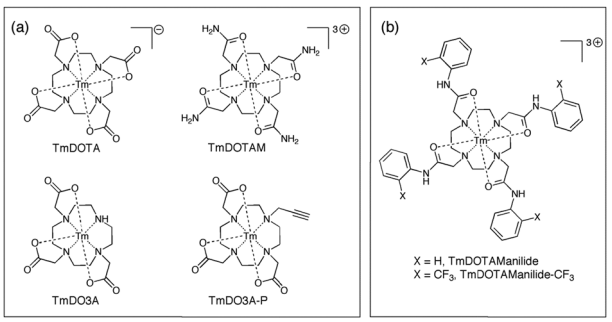


Fig. 4 Molecular structures of the complexes studied (a) complexes exhibiting a full set of peaks and (b) complexes exhibiting only the 790 nm peak.

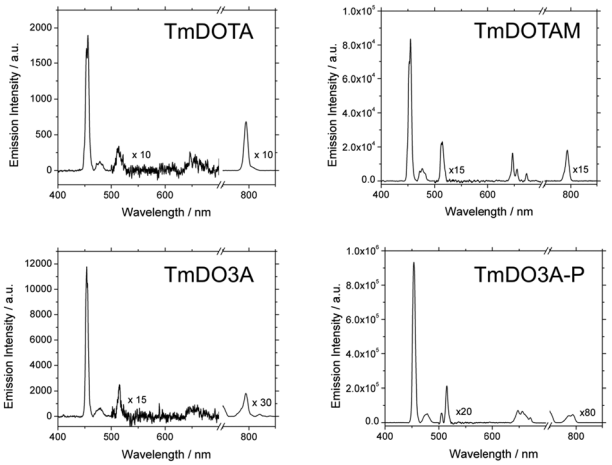


Fig. 5 Emission spectra of thulium complexes in D_2O exciting at 360 nm. The intensities of the two data sets are corrected for differing slit widths. The intensities at 500–750 nm and 750–850 nm are multiplied by the factors indicated. The spectra have been smoothed and baseline corrected. Emission slit widths of 0.2–0.5 nm were used at 400–700 nm, and 0.5–1 nm were used in the 750–850 nm region.

shown in Fig. 4.[14] In these complexes, approach of solvent to the metal centre is restricted by the multi-dentate ligand architectures. The complexes exhibit broadly similar emission spectra shown in Fig. 5, though the variations in fine structure within each emission band are clearly indicative of differences in the local coordination environment at the lanthanide (Fig. S12, ESI†). Furthermore, such complexes are known to have high kinetic stability while the octadentate ligands exhibit slow exchange between diastereomeric forms. However, these ligand architectures incorporate a multitude of C–H oscillators close to the metal centre. In these systems, the lifetime of the emission from $^1D_2$ is longer than that observed for thulium trifluoromethanesulfonate dissolved in D_2O though not dramatically so (see Table 4), suggesting that the reduced quenching by solvent oscillators is almost entirely offset by C–H oscillator quenching. The picture is different for the $^1G_4$ state, in that all the complexes exhibit very similar lifetimes for the decay component. At first, this seems at odds with our observations of increased C–H oscillator quenching for the solvated salts. In fact, it suggests that the non-radiative quenching of the $^1D_2$ state by O–D oscillators is significantly

Table 4 Lifetimes and observed rate constants of the $^1D_2$ (at 452 nm) and $^1G_4$ (at 479 nm) states of complexes in D_2O exciting at 360 nm

	$^1D_2$		$^1G_4$	
	τ/ns[a]	k_{obs}/s^{-1}	τ/ns[a]	k_{obs}/s^{-1}
Tm(III)	89	1.1×10^7	311	3.2×10^6
TmDOTA	136	7.4×10^6	136[b,d]	7.4×10^6
			333[c]	3.0×10^6
TmDOTAM	150	6.7×10^6	150[b,d]	6.7×10^6
			339[c]	2.9×10^6
TmDO3A	119	8.4×10^6	—[e]	—[e]
TmDO3A-P	156	6.4×10^6	156[b,d]	6.4×10^6
			340[c]	2.9×10^6

[a] All lifetimes have errors of ±10%. [b] Positive or rise component in the fit of the time resolved emission profile. [c] Negative or decay component in the fit of the time resolved emission profile. [d] Rise fixed at lifetime determined at 452 nm. [e] Signal too weak.

reduced upon ligand coordination, but that this effect is offset for $^1G_4$ by the increasing number of local C–H oscillators.

$^1D_2$ and $^1G_4$ luminescence was not observed in systems in which an aryl chromophore has been incorporated into the ligand structure. Both TmDOTAManilide and TmDOTAM-anilide-CF_3 exhibited no lanthanide centred emission in the visible part of the spectrum. However, a weak band was observed at 790 nm with a lifetime comparable to the detector response (*ca.* 2 ns). This can be assigned to a $^3H_4 \rightarrow {}^3H_6$ transition, which is swamped in the simpler ligands by the overlapping bands arising from $^1G_4$ and $^1D_2$ emission. This behaviour can be ascribed to the high energy of the $^1D_2$ state (28 000 cm^{-1}), which cannot readily be populated even by simple aryl chromophores, as even simple phenyl chromophores would be expected to have comparable triplet energies to the $^1D_2$ state. Indeed, this also explains the observations of low energy emissive states in the literature,[6,7] since the published emission spectra are of complexes containing complex aryl chromophores. Even the acetanilide chromophores in the systems studied here will act to quench these excited states once formed.

Two photon excitation

Multi-photon direct excitation of lanthanide ions in the solid phase has been studied in depth, but solution state multi-photon excitation has only recently been characterised.[15] For d_6-DMSO solutions of thulium trifluoromethanesulfonate and $[TmDOTA]^-$, excitation at 728 nm using a focused excitation beam resulted in the observation of an emission spectrum (Fig. S14, ESI†) corresponding to that observed following single photon direct excitation of $^1D_2$. When the focusing lens was removed, no emission spectrum was observed. This concurs with our earlier observations on different lanthanide systems,[15] and confirms that two photon excitation of thulium in solution is possible.

For thulium trifluoromethanesulfonate, multi-photon excitation spectra were obtained by observing the emission from $^1D_2$ (450 nm) and $^1G_4$ (480 nm); these are shown in Fig. 6. In the case of emission from $^1D_2$, the observed spectrum shows bands that correspond to two photon excitation to $^1D_2$ and three photon excitation to the upper excited state manifold followed by relaxation to the emissive $^1D_2$ state. The excitation

 This journal is © the Owner Societies 2012

Published on 14 August 2012 on http://pubs.rsc.org | doi:10.1039/C2CP42228J
Downloaded by University of Oxford on 25 February 2013

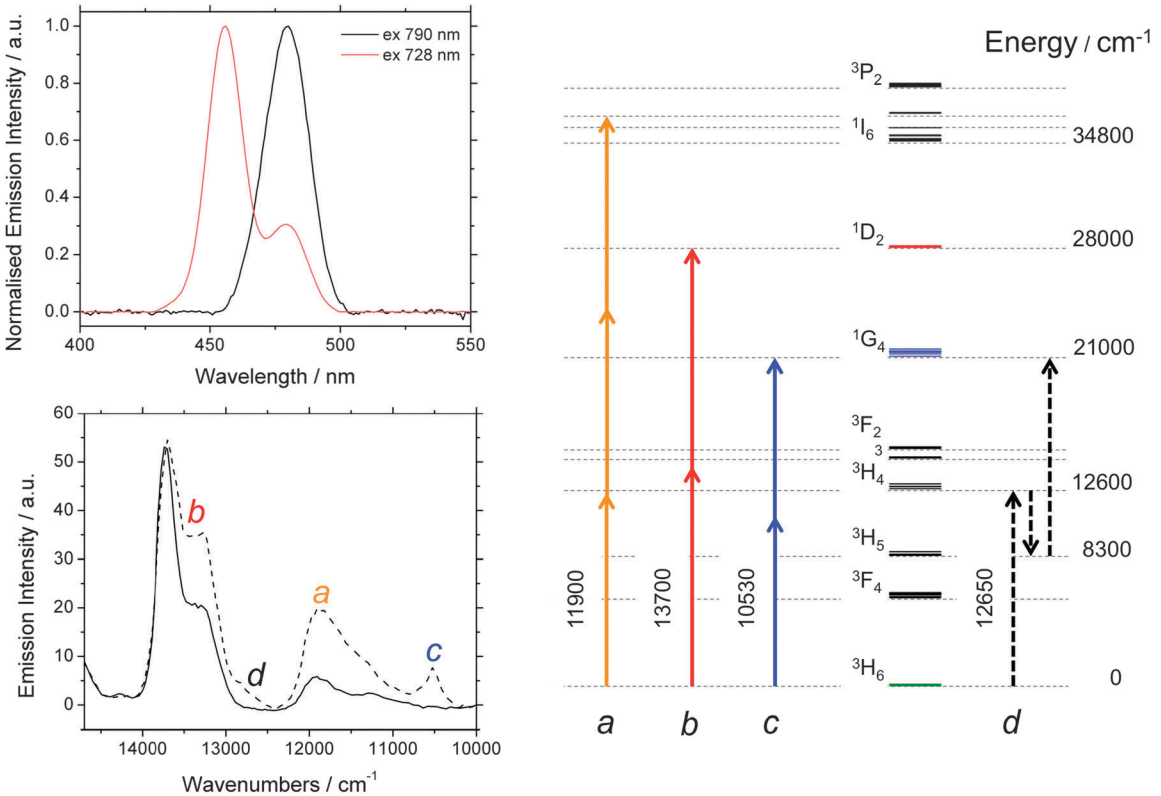


Fig. 6 Top left: Emission spectra observed upon two photon excitation into $^1D_2$ at 728 nm, and upconversion *via* $^3H_4$ and $^3H_5$ to $^1G_4$ at 790 nm of $Tm(O_3SCF_3)_3$ in d_6-DMSO. Bottom left: Two photon excitation spectra of $Tm(O_3SCF_3)_3$ in d_6-DMSO monitoring at 450 nm (solid) and 480 nm (dashed) bands. The italicised letters *a–d* assign each of the observed transitions. Right: Accounting for the observed transitions in the multi-photon excitation spectrum. All processes are reflected in the emission from the $^1G_4$ state, while only *a* and *b* result in observed emission from the $^1D_2$ state.

spectrum obtained when observing emission from $^1G_4$ is much more complicated. It clearly contains all the bands observed in the excitation spectrum of $^1D_2$, together with a band for direct two-photon excitation to $^1G_4$. These processes are shown as *a*, *b* and *c* in Fig. 6. However, there is also an additional band in the spectrum, which does not correspond directly to overlap with any of the excited states of thulium. We investigated this further, and it is clear from Fig. 6 that the emission spectrum corresponds to emission from $^1G_4$. Excitation at 12 650 cm^{-1} (790 nm) corresponds to the $^3H_6 \rightarrow {}^3H_4$ transition, and our observations can be explained in the context of such a single photon absorption event being followed by relaxation to $^3H_5$, and subsequent absorption of a second photon giving rise to a $^3H_5 \rightarrow {}^1G_4$ transition. The bands corresponding to processes *a–d* are indicated in the multi-photon excitation spectra in Fig. 6. Such sequential upconversion has been observed in solid state structures,[10,11] but we are not aware of previous reports of solution state upconversion events following this pathway. Clearly such a pathway requires that the $^1G_4$ state is not itself quenched by non-radiative decay, and is likely to be precluded in systems containing organic chromophores.

Conclusions

Thulium(III) exhibits rich and diverse solution state photophysics. Multiple emissive states give rise to a variety of (often overlapping) transitions in the visible and near-IR regions of the spectrum, and the different emissive states are quenched to differing degrees by solvent and ligand vibrations. Furthermore, energy transfer from one emissive state to another can give rise to multiple pathways by which the lower energy emissive states can be populated.

Perhaps our most interesting observations relate to multi-photon excitation. The fortuitous spacing of the excited states in the thulium manifold means that both "conventional" two photon absorption mechanisms (involving virtual intermediate states) and upconversion processes involving states within the thulium manifold are observed. This observation requires further investigation, and we will continue to study the multi-photon excitation of thulium in mono- and bi-metallic systems. This study opens up the possibility of using molecular systems and polymer based upconverters in lieu of the current generation of solid state lanthanide based optical amplifiers.

Acknowledgements

The authors thank the Universities of Oxford and Durham for support, and the Danish Council for Independent Research, Technology and Production Sciences (grant 10-093546) for financial support for TJS, and the European Research Council ((FP7/2007-2013)/ERC-Grant Agreement Number 267426) for support for OAB, and EPSRC for studentships for LMB, JT and MT. We thank the EPSRC Laser Loan Pool for the loan of the Coherent Chameleon Ultra II and the Compact OPO.

References

1 For recent reviews see: (*a*) S. Faulkner, L. S. Natrajan, W. S. Perry and D. Sykes, *Dalton Trans*., 2009, 3890; (*b*) *Lanthanide Luminescence*, ed. P. Hänninen and H. Härmä, *Springer Series on Fluorescence*, Series Editor O. S. Wolfbeis, Springer, Berlin, 2009, vol. 7; (*c*) L. S. Natrajan, *Curr. Inorg. Chem*., 2011, **1**, 61; (*d*) A. Polman, *MRS. Online Proc. Libr*. 1999, **597**, 3; (*e*) K. Kuriki, Y. Koike and Y. Okamata, *Chem. Rev*., 2002, **102**, 2347; (*f*) F. Wang and X. Liu, *Chem. Soc. Rev*., 2009, **38**, 976.

2 (*a*) A. Beeby, I. M. Clarkson, S. Faulkner, S. Botchway, D. Parker, J. A. G. Williams and A. W. Parker, *J. Photochem. Photobiol., B*, 2000, **57**, 83; (*b*) L. Charbonnière, R. Ziessel, M. Guardigli, A. Roda, N. Sabbatini and M. Cesario, *J. Am. Chem. Soc*., 2001, **13**, 2436.

3 S. Faulkner, S. J. A. Pope and B. P. Burton-Pye, *Appl. Spectrosc. Rev*., 2005, **40**, 1.

4 (*a*) A. Beeby and S. Faulkner, *Chem. Phys. Lett*., 1997, **266**, 116; (*b*) Y. Hasegawa, T. Ohkubo, K. Sogabe, Y. Kawamura, Y. Wada, N. Nakashima and S. Yanagida, *Angew. Chem., Int. Ed*., 2000, **39**, 357.

5 (*a*) A. Beeby, R. S. Dickins, S. Faulkner, D. Parker and J. A. G. Williams, *Chem. Commun*., 1997, 1401; (*b*) W. D. Horrocks, J. P. Bolender, W. D. Smith and R. M. Supkowski, *J. Am. Chem. Soc*., 1997, **119**, 5972; (*c*) M. H. V. Werts, J. W. Hofstraat, F. A. J. Geurts and J. W. Verhoeven, *Chem. Phys. Lett*., 1997, **276**, 196; (*d*) N. M. Shavaleev, S. J. A. Pope, Z. R. Bell. S. Faulkner and M. D. Ward, *J. Chem. Soc., Dalton Trans*., 2003, 808.

6 (*a*) J. Zhang and S. Petoud, *Chem.–Eur. J*., 2008, **14**, 1264; (*b*) J. Zhang, P. D. Badger, S. J. Geib and S. Petoud, *Angew. Chem., Int. Ed*., 2005, **44**, 2508.

7 (*a*) O. A. Serra, E. J. Nassov, P. S. Celfi and I. L. V. Rosa, *J. Alloys. Compd*., 1998, **275**, 838; (*b*) P. K. Sharma, A. R. van Doorn and A. G. J. Staring, *J. Lumin*., 1994, **62**, 219.

8 G. Stein and E. Wurzberg, *J. Chem. Phys*., 1975, **62**, 208.

9 (*a*) W. T. Carnall and H. Crosswhite, *J. Less–Common Met*., 1983, **93**, 127; (*b*) W. T. Carnall, G. L. Goodman, K. Rajnak and R. S. Rana, *J. Chem. Phys*., 1989, **90**, 3443.

10 J. Grimm, E. Beurer, P. Gerner and H. U. Güdel, *Chem.–Eur. J*., 2007, **13**, 1152.

11 J. F. Suyver, A. Aebischer, D. Biner, P. Gerner, J. Grimm, S. Heer, K. W. Krämer, C. Reinhard and H. U. Güdel, *Opt. Mater. (Amsterdam)*, 2005, **27**, 1111.

12 G. M. Davies, R. J. Aarons, G. R. Motson, J. C. Jeffery, H. Adams, S. Faulkner and M. D. Ward, *Dalton Trans*., 2004, 1136.

13 (*a*) A. Beeby, S. Faulkner, D. Parker and J. A. G. Williams, *J. Chem. Soc., Perkin Trans. 2*, 2001, 1268; (*b*) A. I. Voloshin, N. M. Shavaleev and V. P. Kazakov, *J. Lumin*., 2001, **93**, 199.

14 (*a*) C. C. Bryden, C. N. Reilley and J. F. Desreux, *Anal. Chem*., 1981, **53**, 1418; (*b*) S. Amin, J. R. Morrow, C. H. Lake and M. R. Churchill, *Angew. Chem., Int. Ed. Engl*., 1994, **33**, 773; (*c*) M. Jauregui, C. Allain, M. C. Willis, A. M. Kenwright, J. S. Snaith and S. Faulkner, *Dalton Trans*., 2009, 6283; (*d*) D. Parker, H. Puschmann, A. S. Batsanov and K. Senanayake, *Inorg. Chem*., 2003, **42**, 8646; (*e*) K. H. Chalmers, E. de Luca, N. H. M. Hogg, A. M. Kenwright, I. Kuprov, D. Parker, M. Botta, J. I. Wilson and A. M. Blamire, *Chem.–Eur. J*., 2010, **16**, 134; (*f*) G. Zucchi, R. Scopelliti and J. C. G. Bunzli, *J. Chem. Soc., Dalton Trans*., 2001, 1975.

15 T. J. Sørensen, O. A. Blackburn, M. Tropiano and S. Faulkner, *Chem. Phys. Lett*., 2012, **541**, 16.

Published on 14 August 2012 on http://pubs.rsc.org | doi:10.1039/C2CP42228J
Downloaded by University of Oxford on 25 February 2013

 This journal is © the Owner Societies 2012

ORGANOMETALLICS

Communication

pubs.acs.org/Organometallics

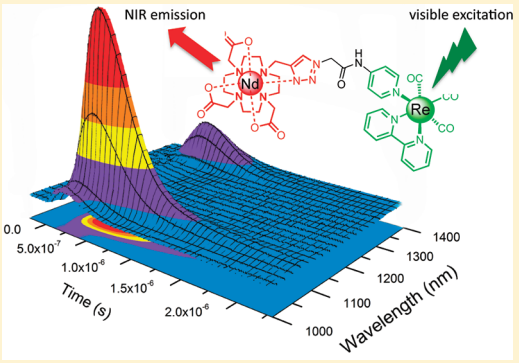
Synthesis and Spectroscopic Study of d–f Hybrid Lanthanide Complexes Derived from triazolylDO3A

Manuel Tropiano, Christopher J. Record, Eleanor Morris, Hardeep S. Rai, Clémence Allain, and Stephen Faulkner*

Chemistry Research Laboratory, University of Oxford, 12 Mansfield Road, Oxford OX1 3TA

Supporting Information

ABSTRACT: Lanthanide complexes of triazolylDO3A have been used to prepare bimetallic d–f hybrid complexes in which the triazolyl pendant arm coordinates to both the lanthanide and a transition-metal ion, and their properties have been compared with those of analogous systems in which the lanthanide triazoloDO3A domain is separated from the rhenium chromophore by an alkyl spacer. The triazole-bridged system has been shown to facilitate energy transfer from the chromophore to the lanthanide but also exhibits reduced affinity of the triazole nitrogen for the lanthanide center. In contrast, the system in which the two domains are separated by a spacer shows phosphate-independent relaxometric properties and has potential as a bimodal contrast agent for MRI luminescence.



The use of luminescent lanthanide complexes in bioassay and time-gated imaging is now well established.[1] Owing to the low molar absorption coefficients associated with f–f transitions in lanthanide ions, chromophores with much larger absorption cross sections are often used as antennas to sensitize the formation of the lanthanide emissive state. The mechanism of this sensitization process has been the focus of considerable interest and can occur by two pathways.[2] In the majority of cases, absorption by the chromophore results in formation of an excited singlet state which undergoes intersystem crossing to populate a triplet state before energy transfer to the lanthanide ion.[3] Ytterbium complexes represent a special case, and an alternative energy transfer mechanism can occur when it is thermodynamically feasible.[4] In this alternative mechanism, the formation of the lanthanide excited state is mediated by a ligand to metal charge transfer state involving the ytterbium center.

Since solution state luminescence from the near-IR emissive lanthanides was first studied in detail more than a decade ago,[5] considerable interest has focused on the use of luminescent d-block complexes as sensitizing antennas.[6] A wide range of such complexes have very large molar absorption coefficients in the visible part of the spectrum combined with high yields for intersystem crossing to the triplet metal to ligand charge transfer state (^{3}MLCT), making them ideal as sensitizers for lanthanide ions with suitable emissive states. Our own studies on the mechanism of energy transfer have shown that energy transfer in such systems generally occurs by a Dexter exchange mechanism, where such a mechanism is permitted by the ligand structure,[7] and that superexchange mediated energy transfer can occur over very long distances indeed (up to 2 nm). We have also recently shown that energy transfer in d–f hybrids can be modulated by electrochemical means when ferrocene is used as the d-block chromophore.[8]

We recently observed that, in a number of systems containing ytterbium as the luminescent lanthanide, electron transfer from the chromophore to the lanthanide also dominates energy transfer and competes with formation of the ^{3}MLCT state of the transition-metal chromophore.[9] Surprisingly, such systems show negligible sensitization via the ^{3}MLCT state.

We now report the results of a study in which a bridging group coordinates to a lanthanide ion and a rhenium(I) ion. Lowe and Stasiuk recently reported the synthesis of Eu.**1**.H from Eu.**2** (see Scheme 1) and demonstrated that deprotonation to form [Eu.**1**]$^-$ occurs readily in aqueous media.[10] We reasoned that complexes of the form [Ln.**1**]$^-$ would be ideal as building blocks for d–f hybrids such as [Ln.**1**.ReBpy(CO)$_3$], since the triazolyl bridging group should also be suitable for mediating Dexter exchange, particularly in systems containing near-IR luminescent lanthanides. We resolved to compare these complexes with analogues of the form [Ln.**3**.ReBpy(CO)$_3$]$^+$, in which the chromophore is separated from the lanthanide by an alkyl spacer. Furthermore, gadolinium-containing analogues have the potential to be effective single-molecule dual-mode contrast agents in cases where the luminescence from the rhenium ^{3}MLCT state is relatively long-lived.

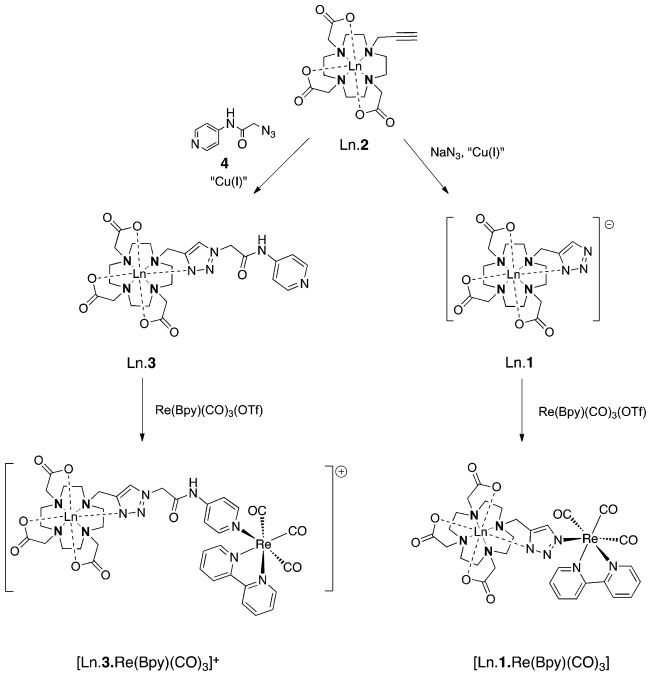
Our synthetic approach is shown in Scheme 1. The tris-*tert*-butyl ester of DO3A[11] was used to prepare Ln.**2** as previously

Special Issue: Organometallics in Biology and Medicine

Received: April 29, 2012
Published: June 19, 2012

 © 2012 American Chemical Society dx.doi.org/10.1021/om3003569 | *Organometallics* 2012, 31, 5673–5676

Scheme 1. Synthesis of Ligands and Complexes Used in This Study



described.[8,12] In addition to the literature variants (Ln = Gd, Yb), we also prepared Nd.**2** by the same method. These complexes were then used as substrates for Click chemistry. Lowe's methodology for the synthesis of Eu.**1** from Eu.**2**[10] was extended to the synthesis of complexes of **1** with gadolinium, ytterbium, and neodymium from Ln.**2**.

fac-$Re(CO)_3(Bpy)Cl$ was prepared according to literature procedures[13] and activated by reaction with silver triflate. Upon addition of $[Ln.\mathbf{1}]^-$, the heterobimetallic complexes Ln.**1**.$Re(Bpy)(CO)_3$ were formed. These were purified by trituration and recrystallization. Conversion of Ln.**1** to Ln.**1**.$Re(Bpy)(CO)_3$ was confirmed by NMR spectroscopy and accurate mass spectrometry (ES-MS). The ^1H NMR spectra of Ln.**1** are all pD dependent, consistent with the observations by Lowe et al.[10] However, coordination of the triazole to rhenium means that the ^1H NMR spectra of Ln.**1**.$Re(Bpy)(CO)_3$ are essentially independent of pD over the range pD 2−11. Figure 1a,b shows the ^1H NMR spectra of $[Yb.\mathbf{1}]^-$ and Yb.**1**.$Re(Bpy)(CO)_3$, respectively, while Figure 1c shows the change in shift of the axial ring protons on the azamacrocycle in Yb.**1** with changing pD.

The Ln.**2** complexes were also used as substrates for click reactions with *N*-(4-pyridyl)-2-azidoacetamide (**4**) to yield Ln.**3**, and $[Ln.\mathbf{3}.ReBpy(CO)_3]^+$. In contrast with the case for Ln.**1**, the ^1H NMR spectra of Ln.**3** are independent of pD in the shift region corresponding to aza macrocycle resonances. The dominant square-antiprismatic geometry at the lanthanide center is in equilibrium with a twisted-square-antiprismatic form only at pD 12 (see Figure S1 in the Supporting Information). The ^1H NMR spectra of $[Ln.\mathbf{3}.ReBpy(CO)_3]^+$ are remarkably similar to those of Ln.**3**, though splitting of the resonances is observed, corresponding to the existence of diastereomeric pairs. Indeed, coupling of two chiral centers around each metal results in the formation of two diastereoisomers that give rise to two different, although very similar, sets of resonances in the complex structure that are in

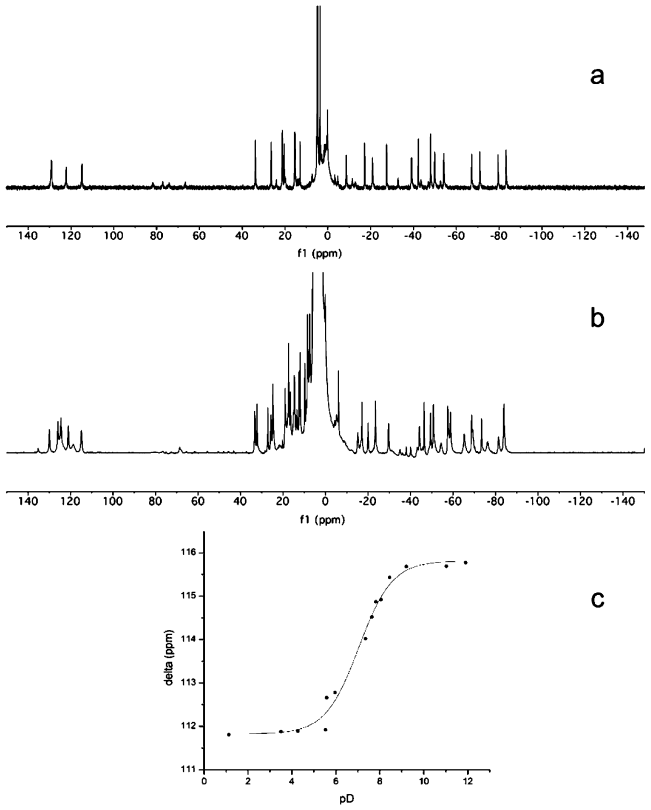


Figure 1. ^1H NMR spectra (300 MHz, 296 K) of (a) Yb.**1** (pD **9**) and (b) Yb.**1**.$Re(Bpy)(CO)_3$ (pD 7). (c) pD dependence of the axial ring proton shift of Yb.**1**.

slow exchange on the NMR time scale, owing to the bulk of the triazole substituent. This can be seen in Figure 2, in which the NMR spectrum for Yb.**3** is shown in Figure 2a while the spectrum of $[Yb.\mathbf{3}.ReBpy(CO)_3]^+$ is shown in Figure 2b. Comparison with Figure 1 reveals that a similar splitting of the ring protons is also observed in $[Yb.\mathbf{1}.ReBpy(CO)_3]$.

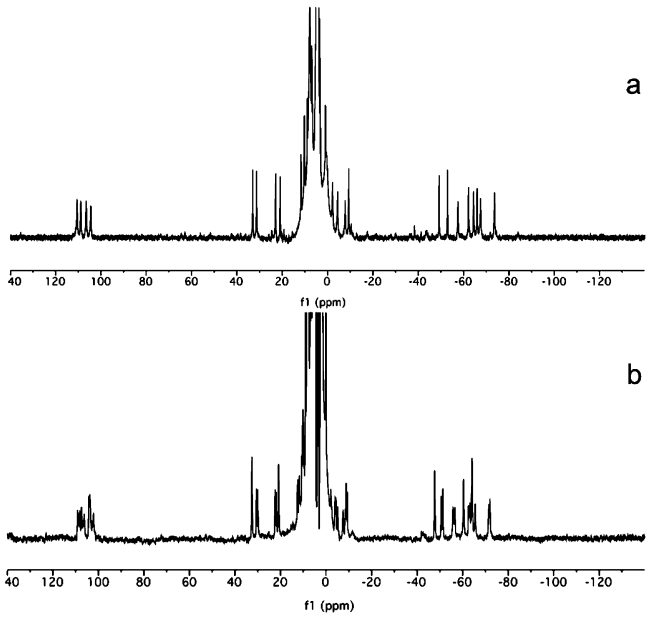


Figure 2. ^1H NMR spectra (300 MHz, 296 K) of (a) Yb.**3** (pD 7) and (b) $[Yb.\mathbf{3}.Re(Bpy)(CO)_3]^+$ (pD 7).

dx.doi.org/10.1021/om3003569 | *Organometallics* 2012, 31, 5673−5676

Luminescence measurements were used to probe the complex structures further. The luminescence lifetimes of the complexes are summarized in Table 1, which also shows

Table 1. Luminescence Lifetimes of the Complexes Following Excitation at 337 nm[a]

	λ_{em}/nm	τ_{H_2O}/ns	τ_{D_2O}/ns	q_{Yb}
Nd.**1**	1064	70	320	
Yb.**1**	980	990	5660	0.7
Nd.**3**	1064	105	338	
Yb.**3**	980	1700	3500	0.2
[Nd.**1**.ReBpy(CO)$_3$]	1064	64	296	
	600	17 (^{3}MLCT)	23 (^{3}MLCT)	
[Gd.**1**.ReBpy(CO)$_3$]	600	109 (^{3}MLCT)	119 (^{3}MLCT)	
[Yb.**1**.ReBpy(CO)$_3$]	980	910	6470	0.8
		78 (^{3}MLCT)	94 (^{3}MLCT)	
[Nd.**3**.ReBpy(CO)$_3$]$^+$	1064	191	342	
		76 (^{3}MLCT)	112 (^{3}MLCT)	
[Gd.**3**.ReBpy(CO)$_3$]$^+$	600	115 (^{3}MLCT)	129 (^{3}MLCT)	
[Yb.**3**.ReBpy(CO)$_3$]$^+$	980	729	6160	1.1
		66 (^{3}MLCT)	79 (^{3}MLCT)	

[a]Lifetimes are quoted with errors of ±10%; this represents the error for the weakest emission decays, and all represent a minimization over 2500 data points. No values of q_{Nd} are reported, since the lifetimes of neodymium complexes are highly dependent on ligand structure, and such calculations can be misleading. Similarly, no luminescence lifetimes are reported for Gd.**1** and Gd.**3**, since the emissive state of Gd^{3+} is too high in energy to be populated by the aryl chromophores.

calculated values for q_{Yb}, the number of inner-sphere water molecules bound to the ytterbium(III) ions. These were calculated using the equation

$$q_{Yb} = k_{H_2O} - k_{D_2O} - 0.1 \qquad ([1])$$

where k_{H_2O} and k_{D_2O} are the observed rate constants (in μs^{-1}) for luminescence from the ytterbium center.[14] The lifetimes of the ytterbium and neodymium complexes reveal that the triazolyl group in Ln.**1** coordinates to the lanthanide center regardless of whether it is also coordinated to the rhenium center. Only very small changes in lanthanide solvation are observed between [Ln.**1**.ReBpy(CO)$_3$] and [Ln.**3**.ReBpy(CO)$_3$]$^+$.

The rhenium chromophore acts as an effective sensitizer for both neodymium and ytterbium. However, while the structures are very similar, the photophysical behavior of Nd.**1**.Re(Bpy)(CO)$_3$ is clearly very different from that of Yb.**1**.Re(Bpy)(CO)$_3$; while the latter exhibits double exponential decay kinetics when the emission is observed at 980 nm, the former is undoubtedly single exponential. This is emphasized by the time-resolved emission spectra shown in Figure 3. While Nd.**1**.Re(Bpy)(CO)$_3$ has a time-resolved spectrum containing only bands corresponding to luminescence from neodymium and shows no evidence for emission from the rhenium ^{3}MLCT state in the near-IR part of the spectrum, Yb.**1**.Re(Bpy)(CO)$_3$ shows a broad short-lived emission band (corresponding to the tail of the rhenium ^{3}MLCT emission) superimposed upon the long-lived emission spectrum associated with the lanthanide ion. This partial quenching suggests that sensitization of the neodymium ion is much more efficient than that of ytterbium, suggesting that the increased spectral overlap with the high energy excited states in the neodymium manifold plays a

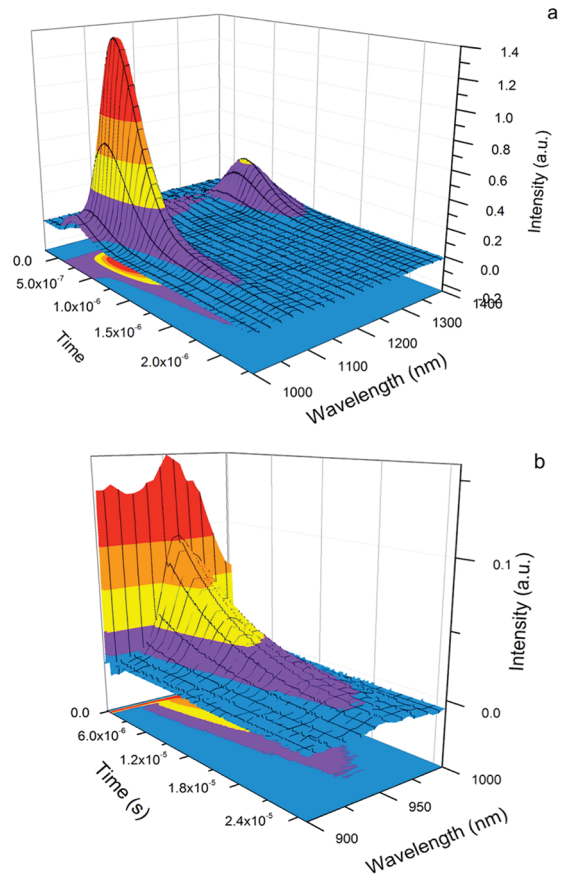


Figure 3. Time-resolved emission spectra of (a) [Nd.**1**.Re(Bpy)(CO)$_3$]$^+$ and (b) [Yb.**1**.Re(Bpy)(CO)$_3$]$^+$ following excitation at 337 nm.

significant role in energy transfer, as also confirmed by the total emission spectra in Figure 4. This is borne out by the

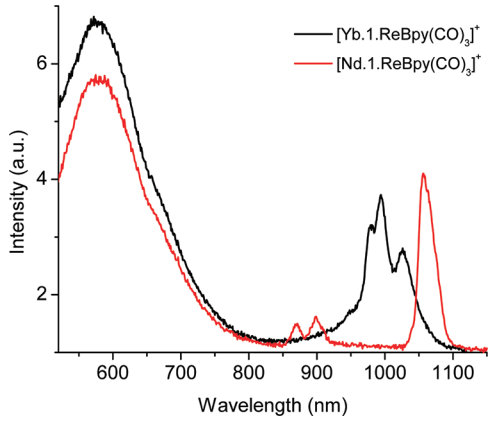


Figure 4. Total emission spectra of [Yb.**1**.Re(Bpy)(CO)$_3$]$^+$ and [Nd.**1**.Re(Bpy)(CO)$_3$]$^+$ following excitation at 360 nm.

luminescence from the rhenium chromophore, in which nonradiative quenching processes are clearly more efficient for the ytterbium complex than for the gadolinium complex and are still more efficient for the neodymium complex.

Relaxometric studies on the gadolinium complexes were used to establish the relaxivity at physiological pH in water and phosphate-buffered saline solution (PBS) at 37 °C and 7 T. The results are shown in Table 2. It is clear from these results

dx.doi.org/10.1021/om3003569 | *Organometallics* 2012, 31, 5673−5676

Table 2. Relaxometric Properties of the Complexes[a]

	r1(H_2O)/(mmol of Gd)$^{-1}$ s^{-1}	r1(PBS)/(mmol of Gd)$^{-1}$ s^{-1}
Gd.**2**	4.1 ± 0.4	2.5 ± 0.3
Gd.**1**	3.4 ± 0.3	2.6 ± 0.3
Gd.**3**	4.4 ± 0.4	4.1 ± 0.4
Gd.**1**.ReBpy$(CO)_3$	5.3 ± 0.5	3.2 ± 0.3
[Gd.**3**.ReBpy$(CO)_3$]$^+$	4.2 ± 0.4	4.1 ± 0.4

[a]All measurements were made at pH 7.4, 37 °C, and 7 T.

that Gd.**3** shows no significant effect of phosphate binding, as the two values are within error of one another. The same is true of [Gd.**3**.ReBpy$(CO)_3$]$^+$, suggesting that the coordinated rhenium does not influence coordination at the lanthanide. Gd.**1** shows similar behavior, though there is a greater variation between the values in water and PBS. However, there is a dramatic change in relaxivity between the values obtained for [Gd.**1**.ReBpy$(CO)_3$] in water and PBS. The former approaches the value that would be expected for a q = 2 complex,[15] while the latter is much lower. This implies that there is an equilibrium between gadolinium coordinated and uncoordinated triazole. This is clearly a consequence of the coordination of the rhenium reducing the donor ability of the other nitrogen atoms on the triazole ring. In the gadolinium complex, the weighted average will overemphasize the q = 2 gadolinium form, since this will contribute most to the relaxivity. In contrast, the luminescence discussed early will favor the octadentate ligand, making q appear lower than it actually is. The "true" coordination equilibrium will lie somewhere between these extremes.

Click reactions offer an effective route to access d−f hybrids. In the course of this study, we have established that simple triazolyl-DO3A complexes can be used as building blocks for d−f hybrids in which the triazole bridges the d- and f- metal centers. Alternatively, extended architectures can be prepared by click methods to incorporate related chromophores in which the metal centers are removed from one another and are more effectively "insulated". Superficially, these two types of assemblies have similar properties. However, there are important differences. Energy transfer is mediated most effectively when the metal centers are held in close proximity to one another. Nevertheless, the d−f hybrid systems with bridging donors are much more likely to exist in conformations where the triazole is not coordinated to the ring system. In the case of the gadolinium rhenium dyads, this is reflected in the high dependence of the relaxivity on the concentration of phosphate. These observations suggest that bimodal imaging systems should preserve separate chromophoric and MRI-active components within a single assembly. While the synthesis of [Ln.**1**.ReBpy$(CO)_3$] is simple, effective, and attractive, its key use is likely to be in the preparation of luminescent assemblies in which the transition-metal chromophore acts as an antenna. In contrast, the synthesis of [Ln.**3**.ReBpy$(CO)_3$]$^+$ is more demanding, but the long lifetime of the rhenium chromophore (when Ln = Gd) and the phosphate-independent relaxometric behavior suggest that these systems have real promise as contrast media. Further studies are ongoing.

■ ASSOCIATED CONTENT

Supporting Information

Text and figures giving further experimental details and spectroscopic information. This material is available free of charge via the Internet at http://pubs.acs.org.

■ AUTHOR INFORMATION

Author Contributions

The manuscript was written through contributions of all authors. All authors have given approval to the final version of the manuscript.

Notes

The authors declare no competing financial interest.

■ ACKNOWLEDGMENTS

We thank the University of Oxford and EPSRC for support (Studentship for M.T.) and the European Commission for a Marie Curie Intra-European fellowship (to C.A., Grant PIEF-GA-2008-221281).

■ REFERENCES

(1) Hemilla, I. A. *Applications of Fluorescence in Immunoassays*; Wiley-Interscience: New York, 1991. Bunzli, J. C. G.; Comby, S.; Chauvin, A. S.; Vandevyer, C. D. *J. Rare Earths* **2007**, *25*, 257. Montgomery, C. P.; Murray, B. S.; New, E. J.; Pal, R; Parker, D. *Acc. Chem. Res.* **2009**, *42*, 925.

(2) Faulkner, S; Natrajan, L. S.; Perry, W. S.; Sykes, D. *Dalton Trans.* **2009**, 3890.

(3) Beeby, A.; Faulkner, S.; Parker, D; Williams, J. A. G. *J. Chem. Soc., Perkin Trans 2* **2001**, 1268.

(4) Beeby, A.; Faulkner, S.; Williams, J. A. G. *Dalton Trans.* **2002**, 1918.

(5) Beeby, A.; Faulkner, S. *Chem. Phys. Lett.* **1997**, *266*, 116−122. Hasegawa, Y.; Ohkubo, T.; Sogabe, K.; Kawamura, Y.; Wada, Y.; Nakashima, N.; Yanagida, S. *Angew. Chem., Int. Ed.* **2000**, *39*, 357. Beeby, A.; Dickins, R. S.; Faulkner, S.; Parker, D.; Williams, J. A. G. *Chem. Commun.* **1997**, 1401−1402. Werts, M. H. V.; Woudenberge, R. H.; Emmerink, P. G.; van Gassel, R.; Hofstraat, J. W.; Verhoeven, J. W. *Angew. Chem., Int. Ed.* **2000**, *39*, 4542. Shavaleev, N. M.; Pope, S. J. A.; Bell., Z. R.; Faulkner, S.; Ward., M. D. *Dalton Trans.* **2003**, 808.

(6) Ward, M. D. *Coord. Chem. Rev.* **2007**, *251*, 1663. Klink, S. I.; Keizer, H.; Hofstraat, H. W.; van Veggel, F. C. J. M. *Synth. Met.* **2002**, *127*, 213. Nonat, A. M.; Quinn, S. J.; Gunnlaugsson, T. *Inorg. Chem.* **2009**, *48*, 4646.

(7) Lazarides, T.; Sykes, D.; Faulkner, S.; Barbieri, A.; Ward, M. D. *Chem. Eur. J.* **2008**, *14*, 9389.

(8) Tropiano, M; Kilah, N. L.; Morten, M; Rahman, H; Davis, J. J.; Beer, P. D.; Faulkner, S. *J. Am. Chem. Soc.* **2011**, *133*, 11847.

(9) Perry, W. S.; Pope, S. J. A.; Allain, C; Coe, B. J.; Kenwright, A. M.; Faulkner, S. *Dalton Trans.* **2010**, *39*, 10974.

(10) Stasiuk, G. J.; Lowe, M. P. *Dalton Trans.* **2009**, 9725−9727.

(11) Dadabhoy, A.; Faulkner, S.; Sammes, P. G. *J. Chem. Soc., Perkin Trans 2.* **2002**, 348. Dadabhoy, A.; Faulkner, S.; Sammes, P. G . *J. Chem. Soc., Perkin Trans. 2* **2000**, 2359−2360.

(12) Jauregui, M.; Perry, W. S.; Allain, C.; Vidler, L. R.; Willis, M. C.; Kenwright, A. M.; Snaith, J. S.; Stasiuk, G. J.; Lowe, M. P.; Faulkner, S. *Dalton Trans.* **2009**, 6283.

(13) Wrighton, M.; Morse, D. L. *J. Am. Chem. Soc.* **1974**, *96*, 998.

(14) Beeby, A.; Clarkson, I. M.; Dickins, R. S.; Faulkner, S.; Parker, D.; de Sousa., A. S.; Williams, J. A. G. *J. Chem. Soc., Perkin Trans. 2* **1999**, 493.

(15) Murray, B. S.; New, E. J.; Pal, R.; Parker, D. *Org. Biomol. Chem.* **2008**, *6*, 2085. Koullourou, T.; Natrajan, L. S.; Bhavsar, H.; Pope, S. J. A.; Feng, J.; Narvainen, J.; Shaw, R.; Scales, E.; Kauppinen, R.; Kenwright, A. M.; Faulkner, S. *J. Am. Chem. Soc.* **2008**, *130*, 2178.

Chemical Physics Letters 541 (2012) 16–20

Contents lists available at SciVerse ScienceDirect

Chemical Physics Letters

journal homepage: www.elsevier.com/locate/cplett

Direct two-photon excitation of Sm^{3+}, Eu^{3+}, Tb^{3+}, $Tb.DOTA^{-}$, and Tb.propargylDO3A in solution

Thomas Just Sørensen [a,b,*], Octavia A. Blackburn [a], Manuel Tropiano [a], Stephen Faulkner [a,*]

[a] University of Oxford, Chemistry Research Laboratory, Mansfield Road, Oxford OX1 3TA, UK
[b] Nano-Science Center and Department of Chemistry, University of Copenhagen, Universitetsparken 5, DK-2100 København Ø, Denmark

ARTICLE INFO

Article history:
Received 28 March 2012
In final form 23 May 2012
Available online 30 May 2012

ABSTRACT

We have observed direct two-photon excitation of samarium, europium and terbium ions in solution upon near IR excitation using a tuneable pulsed light source, and have also studied two-photon processes in a pair of related terbium complexes, namely $[Tb.DOTA]^{-}$ and Tb.propargylDO3A. Direct two-photon excitation of lanthanides is observed in simple systems in the absence of sensitizing chromophores. Where even simple chromophores such as a triple bond are present in the complex, then single and two-photon excitation of chromophore excited states competes with direct two-photon excitation of the ions and is the dominant pathway for sensitizing formation of the lanthanide excited state.

© 2012 Elsevier B.V. All rights reserved.

1. Introduction

Luminescence from lanthanide ions in solution is well-established as a tool in bio-assay and is becoming established in time-resolved imaging [1]. Two-photon excitation microscopy has been established for deep tissue imaging using organic dyes to provide image contrast [2]. Even though two-photon excitation of organic chromophores has been used extensively to sensitize lanthanide luminescence [3], direct two-photon excitation of lanthanide ions is much less well understood. Two-photon excitation spectroscopy has been used to study lanthanide emission in solid matrices [4], but up until now no solution phase two-photon excitation of lanthanides has been reported. While two-photon processes would be formally Laporte allowed for *f–f* transitions in a centrosymmetric system [1a], the nature of the solution state makes selection rules of limited utility since solvated ions adopt fluxional geometries while the vast majority of lanthanide complexes do not adopt centrosymmetric solution state geometries around the lanthanide center, despite having stable speciation on the luminescence timescale [1]. It is also possible that absorption transitions that can occur as a consequence of ligand centered processes are of comparable intensity to two-photon transitions. With these points in mind, we have been investigating the two-photon excitation of lanthanide salts and some simple complexes.

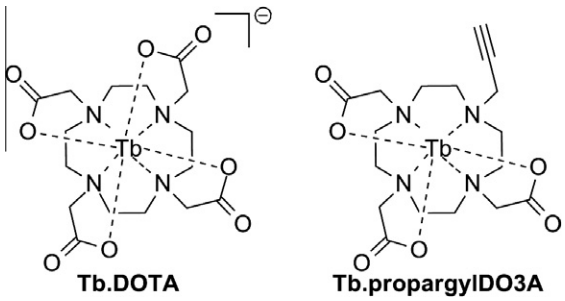
In this Letter we report the observation of lanthanide luminescence following direct two-photon excitation of samarium, europium, and terbium trifluoromethanesulfonate salts in deuterated dimethylsulfoxide ($dmso\text{-}d_6$) solution, and describe the two-photon excitation spectra of terbium and europium ions in solution. In the case of terbium, we also report the two-photon excitation of $[Tb.DOTA]^{-}$ (the terbium complex of 1,4,7,10-tetraazacyclododecane-1,4,7,10-tetraacetate) and Tb.propargylDO3A (the complex of 10-propargyl-1,4,7,10-tetraazacyclododecane-1,4,7-triacetate) (Scheme 1).

2. Experimental

Chemicals were used as received. Lanthanide triflates (trifluoromethanesulfonates) were obtained from Strem chemicals and $dmso\text{-}d_6$ from Sigma–Aldrich. One photon excitation and emission spectra were recorded from a 10 mM solution of $Ln(OTf)_3$ in $dmso\text{-}d_6$ in a 1 cm HELLMA QS cuvette using a Horiba Fluorolog 3. Two-photon excitation and emission spectra were recorded from a 10 mM solution of $Ln(OTf)_3$ in $dmso\text{-}d_6$ in a 1 cm HELLMA QS cuvette using the double grating emission monochromator and detector on a Horiba Fluorolog 3. Excitation was achieved using a Coherent Chameleon APE-OPO tuneable femtosecond laser, and the wavelength was monitored using the internal spectrometer of the Chameleon and the OPO. The range available was from 680 to 1080 nm (9260 to 14705 cm^{-1}). A 5 cm focal length lens fixed in front of the cuvette was used to focus the excitation pulse onto the sample and achieve two-photon excitation. In all cases no signal was recorded when the lens was removed. Laser power was measured at each excitation wavelength with a standard wavelength dependent power meter. The excitation spectra were recorded by

* Corresponding authors. Address: University of Oxford, Chemistry Research Laboratory, Mansfield Road, Oxford OX1 3TA, UK. Fax: +45 35320214 (T.J. Sørensen).
E-mail addresses: TJS@chem.ku.dk (T.J. Sørensen), Stephen.Faulkner@chem.ox.ac.uk (S. Faulkner).

0009-2614/$ - see front matter © 2012 Elsevier B.V. All rights reserved.
http://dx.doi.org/10.1016/j.cplett.2012.05.053



Scheme 1. Structures of the complexes used in this study.

measuring the total emission spectrum at each excitation wavelength. The excitation spectrum was then created by integration of all emission bands and dividing by the square of the laser power.

[Tb.DOTA]$^-$ and Tb.propargylDO3A were synthesized as previously reported [5,6], and the former was used as its H_3O^+ salt.

3. Results and discussion

Initially, we studied the 0.25 nm resolution excitation spectra of the chosen lanthanides and compared our results to the transition energies reported by Carnall [7]. The single photon excitation transitions in the range achievable by the excitation source used in this work are listed in Table 1. Samarium, europium and terbium excitation and emission spectra were recorded. It is worth noting that, in the case of the europium complex, with the benefit of modern high-resolution spectroscopy, we observed a significantly greater number of discrete absorption maxima than have been reported in the literature.

Table 1
Transition energies in the range 33 500–15 500 cm^{-1} as measured in 10 mM solutions in dmso-d_6 and from Carnall et al. in water.

Sm^{3+}		Eu^{3+}		Tb^{3+}	
H_2O[a]	dmso-d_6	H_2O[b]	dmso-d_6	H_2O[c]	dmso-d_6
ν/cm^{-1}					
30 200	30 722	33 190	33 113	33 000	33 003
–	30 098	31 520	31 447	31 600	31 447
29 100	29 007	31 250	–	30 650	30 581
28 250	28 229	–	30 581	29 450	–
27 700	27 624	–	28 653	29 300	29 240
26 750	26 649	27 670	27 624	28 400	28 490
25 650	25 575	–	27 322	27 800	27 933
24 950	24 829	26 700	26 596	27 100	27 100
24 570	–	26 300	26 247	26 500	26 525
24 050	24 024	–	26 042	–	21 459
22 700	22 740	25 400	25 381	20 500	20 534
22 200	22 210	24 408	24 038		
21 600	21 563	–	23 310		
21 100	–	–	22 989		
20 800	20 877	–	22 831		
20 050	20 030	–	22 523		
–	19 569	–	22 222		
18 900	18 966	–	21 930		
–	18 349	21 499	21 552		
–	18 100	–	21 142		
17 900	17 913	–	20 576		
–	17 629	–	19 646		
–	17 483	19 028	19 048		
–	17 414	–	18 727		
		–	18 116		
		–	17 953		
		–	17 606		
		–	17 422		
		17 277	17 301		
		–	16 978		

[a] Ref. [7a].
[b] Ref. [7b].
[c] Ref. [7c].

Having established the energies of the accessible lanthanide states, we studied the two-photon excitation properties of these three lanthanides in solution in deuterated dimethylsulfoxide. Our initial efforts focused on two-photon excitation of the $^6H_{5/2}$ $^4G_{7/2}$ transition for Sm^{3+} (20 030 cm^{-1} in dmso-d_6) [7], and on the $^7F_0 \rightarrow {}^5L_6$ and $^7F_6 \rightarrow {}^5G_6$ transitions for Eu^{3+} and Tb^{3+}, respectively (25 381 cm^{-1} and 27 933 cm^{-1}, respectively) [7]. In each case, excitation at a frequency corresponding to half the transition energy resulted in observation of emission spectra clearly originating from the corresponding metal when the excitation source was focused on the sample using a 5 cm focal length lens. When the lens was removed from the excitation path or if the laser power was lowered by a factor of 100, no lanthanide-centred emission could be observed. These results clearly indicate that two-photon direct excitation is likely to be responsible for the observed spectra, since a hundred fold decrease in emission intensity would still result in an emission spectrum considerably more intense than the background. Figure 1 shows the emission spectra obtained following two-photon excitation for each of these lanthanide ions in dmso-d_6; these are superimposed upon spectra obtained using single photon excitation of the same transitions.

The emission intensity from a dmso-d_6 solution of Eu^{3+} following two-photon excitation was sufficient to record a two-photon excitation spectrum. The normalized spectrum is shown superimposed on the single photon excitation spectrum in Figure 2. Upon even the most cursory examination, it is clear that, while transitions are observed at comparable energies, there are marked differences between the relative intensities of the transitions. While most transitions have similar one and two-photon cross sections, the peaks corresponding to the $^7F_0 \rightarrow {}^5L_6$ and $^7F_0 \rightarrow {}^5D_4/{}^5L_3$ transitions are markedly less pronounced in the two-photon excitation spectrum. In this case, variations in local symmetry at the metal centre in solution make it difficult to state with certainty why these transitions are relatively disallowed for two-photon excitation. It is, however, important to note that more intense emission is observed upon exciting transitions with much lower single-photon extinction coefficients.

The Tb^{3+} luminescence upon two-photon excitation was more than three times more intense than the Eu^{3+} centred emission. Thus two-photon excitation spectra could be recorded, for dmso-d_6 solutions of Tb^{3+}, [Tb.DOTA]$^-$ and Tb.propargylDO3A, the spectra are shown in Figure 3. In all three systems, two-photon excitation resulted in the observation of terbium centred emission, with sharp lines corresponding to *f–f* transitions (as opposed to the broad lines that are commonly associated with ligand centred emission). Furthermore, the $^7F_6 \rightarrow {}^5G_6$ two-photon cross-section is markedly more pronounced than any other transition studied in the simple systems. The local symmetry is well defined in both DOTA [8] and propargylDO3A [6] complexes of lanthanides. While the coordination geometry of solvated lanthanide ions is generally discussed in terms of di- or tri-capped trigonal prismatic geometry, and DOTA complexes adopt fourfold symmetric square-antiprismatic or twisted-square-antiprismatic geometries about the lanthanide, propargylDO3A complexes have broken symmetry at the metal centre. Indeed, we have shown that small changes to the local geometry in such systems are often reflected in large variations in the observed emission spectra following single photon excitation [6]. However, in this case, the local coordination sphere does not seem to influence the two-photon cross-section of the metal, and in all cases the dominant two-photon absorption by the metal centre occurs through the $^7F_6 \rightarrow {}^5G_6$ transition. In all cases, the ratio of the two-photon cross-section of the $^7F_6 \rightarrow {}^5G_6$ transition to that of the $^7F_6 \rightarrow {}^5D_4$ transition is comparable.

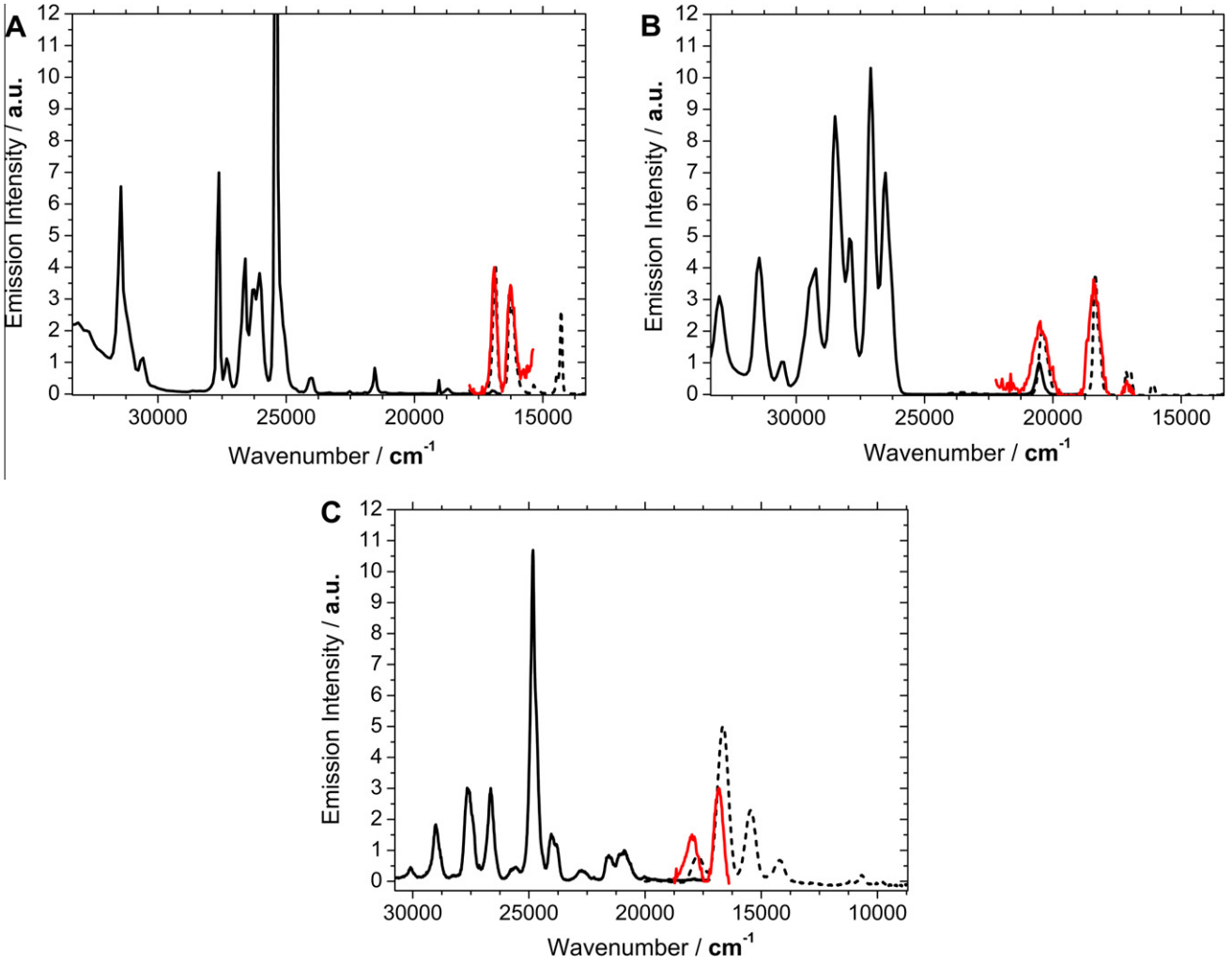


Figure 1. Excitation (single photon – black line) and emission spectra (dotted black line – following single photon excitation; red line – following two-photon excitation) of Eu (A), Tb (B) and Sm (C) in dmso-d_6. Excitation was achieved in the most intense single photon absorption bands (397 nm (Eu), 352 nm (Tb), and 400 nm (Sm) and twice these wavelengths, respectively) and emission was monitored at the most intense emission band (617 nm (Eu), 545 nm (Tb), and 600 nm (Sm)). (For interpretation of the references to colour in this figure legend, the reader is referred to the web version of this article.)

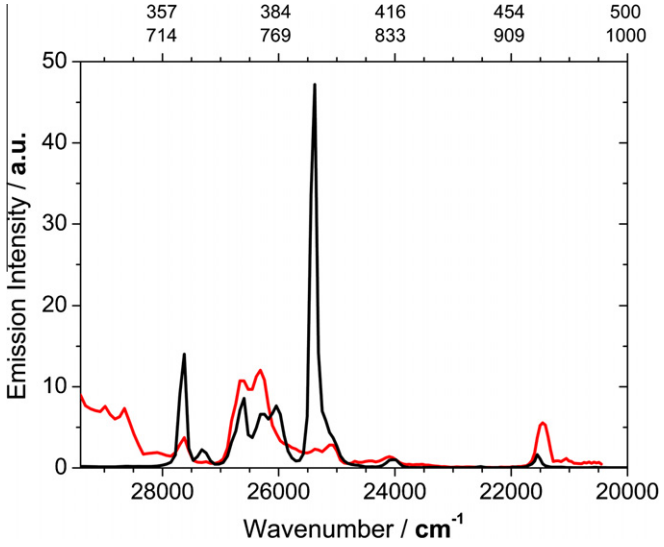


Figure 2. Excitation spectra of Eu^{3+} in dmso-d_6 monitored following single photon excitation (black line), and following two-photon excitation (red line). (For interpretation of the references to colour in this figure legend, the reader is referred to the web version of this article.)

It must be noted that any organic chromophore present will be able to dominate the two-photon excitation spectrum. Even the simple propargyl chromophore in propargylDO3A (for which λ_{max} = 265 nm and $E_T \sim 28\,800\ cm^{-1}$) significantly alters the two-photon absorption spectrum in Figure 3C, where the edge of the propargyl absorption almost swamps the spectrum. Excitation studies with more complicated chromophores (including phenyl and naphthyl sensitizers) revealed that two-photon absorption by the lanthanide is completely swamped by aryl absorption events, indicating that two-photon sensitized emission is dramatically more effective at generating lanthanide excited states.

The intense Tb^{3+} emission also made it possible to study the variation in emission intensity from Tb^{3+} in solution with laser power. The output power from the excitation source was varied using a rotating half-wave plate and a Glan–Thompson prism and the emission intensity was determined by integrating the terbium emission spectrum from 450 to 600 nm. The variation in emission intensity with the square of the laser power is shown in Figure 4. This clearly shows a linear relationship between intensity and the square of the power. In combination with the fact that no emission is observed when the laser is not focused, we consider this to be proof that the emission observed arises from two-photon excitation.

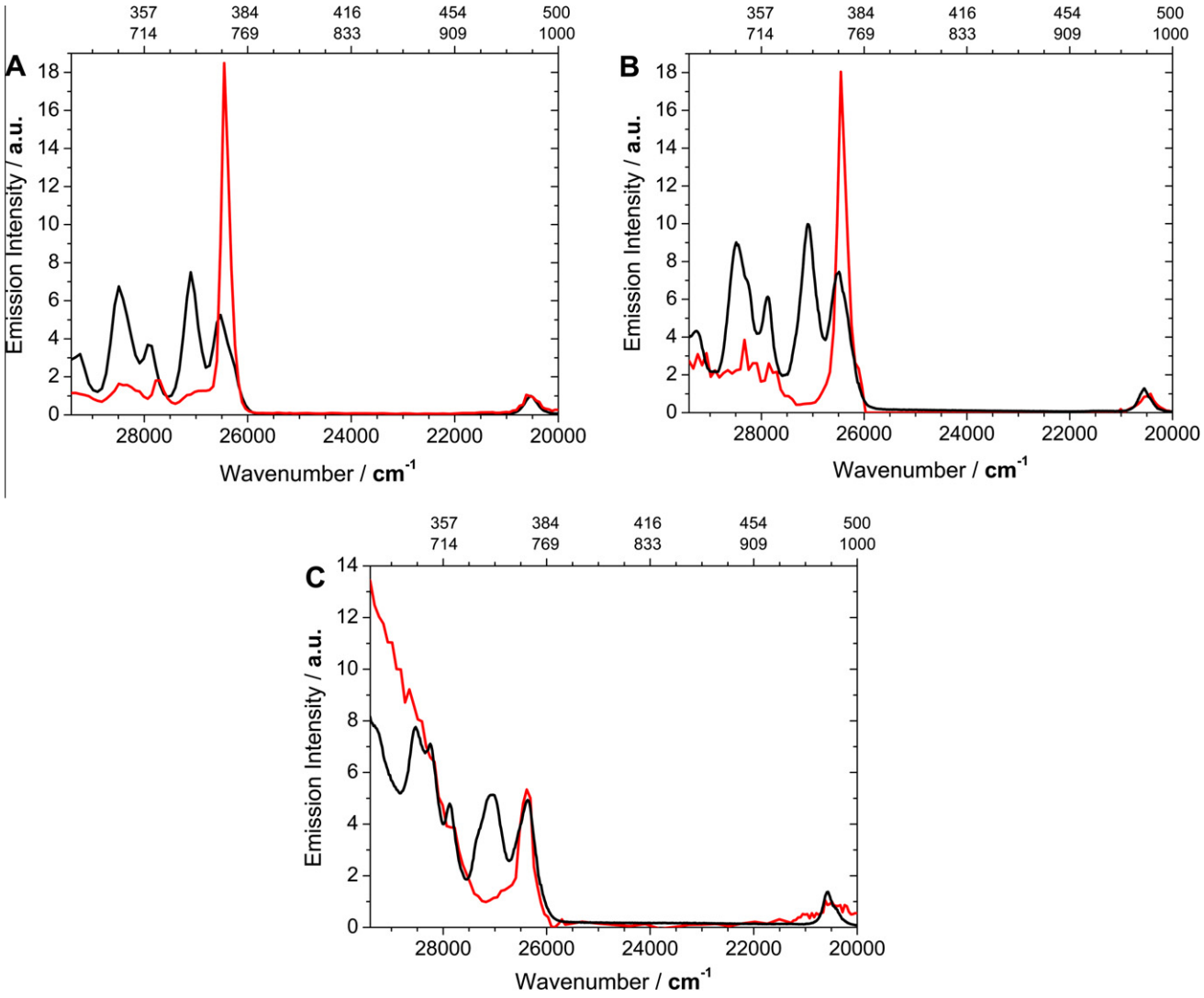


Figure 3. Excitation spectra of Tb^{3+} (A), $[Tb.DOTA]^{-}$ (B), Tb.propargylDO3A (C) in dmso-d_6 monitored following single photon excitation (black line), and following two-photon excitation (red line). (For interpretation of the references to colour in this figure legend, the reader is referred to the web version of this article.)

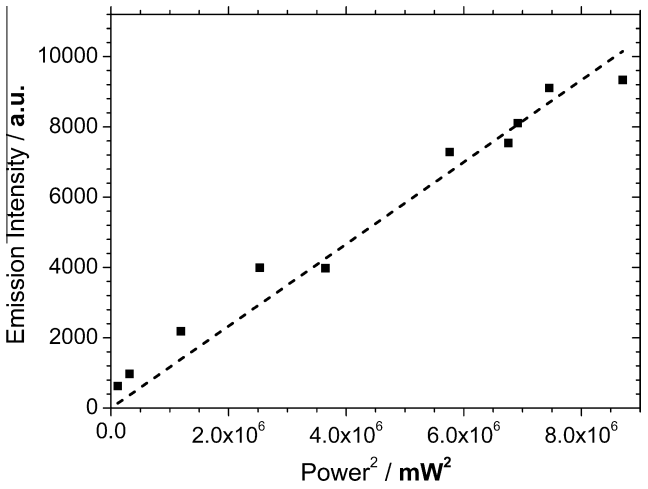


Figure 4. Excitation power squared at 755 nm as a function of observed emission intensity for Tb^{3+} in dmso-d_6 (■) and a linear fit to the data (dashed line).

4. Conclusion

We have demonstrated that direct two-photon excitation of samarium (III), europium (III) and terbium (III) ions and their complexes is possible in solution. For europium and terbium it proved possible to obtain two-photon excitation spectra. These measurements showed that the two- and one-photon absorption cross-sections vary, so that it cannot be assumed that a strongly one-photon absorbing transition has a high two-photon cross-section. We must conclude that even though it is possible to two-photon excite lanthanides, the presence of any organic chromophore will completely dominate the behaviour if two-photon excitation is applied.

Acknowledgement

The authors thank the University of Oxford for support, and the Danish Council for Independent Research|Technology and Production Sciences (Grant 10-093546) for financial support for TJS. We thank the EPSRC Laser Loan Pool for the loan of the Coherent Chameleon Ultra II and the Compact OPO.

References

[1] (a) S. Faulkner, L.S. Natrajan, W.S. Perry, D. Sykes, Dalton Trans. (2009) 3890;
(b) P. Hanninen, H. Härmä, Lanthanide Luminescence, Springer Series on Fluorescence, vol. 7, Springer, Heidelberg, 2011.

[2] (a) D.R. Larson, W.R. Zipfel, R.M. Williams, S.W. Clark, M.P. Bruchez, F.W. Wise, W.W. Webb, Science 300 (2003) 1434;
(b) F. Helmchen, W. Denk, Nat. Methods 2 (2005) 932;
(c) M. Pawlicki, H.A. Collins, R.G. Denning, H.L. Anderson, Angew. Chem. Inter. Ed. 48 (2009) 3244.

[3] (a) L.-O. Palsson, R. Pal, B.S. Murray, D. Parker, A. Beeby, Dalton Trans. (2007) 5726;
(b) A. d'Aleo et al., Chem. Phys. Chem. 8 (2007) 2125;
(c) S.V. Eliseeva, G. Aubock, F. van Mourik, A. Cannizzo, B. Song, E. Deiters, A.-S. Chauvin, M. Chergui, J.-C.G. Bunzli, J. Phys. Chem. B 114 (2010) 2932.

[4] (a) R.G. Denning, Eur. J. Solid State Inorg. Chem. 28 (1991) 33;
(b) C.S. McCaw, K.M. Murdoch, R.G. Denning, Mol. Phys. 101 (2003) 427;
(c) J.R.G. Thorne, M. Jones, C.S. McCaw, K.M. Murdoch, R.G. Denning, N.M. Khaidukov, J. Phys. Condensed 11 (1999) 7851;
(d) J.R.G. Thorne, A. Karunathilake, H. Choi, R.G. Denning, T. Luxbacher, J. Phys. Condensed 11 (1999) 7867;
(e) A.J. Berry, I.D. Morrison, R.G. Denning, Mol. Phys. 93 (1998) 1;
(f) A.J. Berry, R.G. Denning, I.D. Morrison, Chem. Phys. Lett. 266 (1997) 195.

[5] J.F. Desreux, Inorg. Chem. 19 (1980) 1319.

[6] M. Jauregui, C. Allain, M.C. Willis, A.M. Kenwright, J.S. Snaith, S. Faulkner, Dalton Trans. (2009) 6283.

[7] (a) W.T. Carnall, P.R. Fields, K. Rajank, J. Chem. Phys. 49 (1968) 4424;
(b) W.T. Carnall, P.R. Fields, K. Rajank, J. Chem. Phys. 49 (1968) 4450;
(c) W.T. Carnall, P.R. Fields, K. Rajank, J. Chem. Phys. 49 (1968) 4447.

[8] S. Aime, M. Botta, G. Ermondi, Inorg. Chem. 31 (1992) 4291.

View Article Online / Journal Homepage / Table of Contents for this issue
Dynamic Article Links

Dalton Transactions

Cite this: *Dalton Trans.*, 2011, **40**, 11451

www.rsc.org/dalton

PAPER

Lanthanide complexes of DOTA monoamide derivatives bearing an isophthalate pendent arm†

Emma J Shiells,[a] Louise S. Natrajan,[a] Daniel Sykes,[a,b] Manuel Tropiano,[b] Paul Cooper,[a] Alan M. Kenwright[c] and Stephen Faulkner*[a,b]

Received 1st June 2011, Accepted 18th August 2011
DOI: 10.1039/c1dt11029b

Published on 26 September 2011 on http://pubs.rsc.org | doi:10.1039/C1DT11029B
Downloaded by University of Oxford on 25 February 2013

An isophthalate-bearing DOTA monoamide derivative has been synthesised and used to prepare a family of lanthanide complexes. Luminescence and NMR studies in solution show that the predominant form of the complexes in solution is a mono-capped square antiprism about the lanthanide centre, in which a solvent molecule occupies the ninth coordination site. The crystal structure of the terbium complex is presented and is in close agreement with the solution state data.

Introduction

Kinetically stable lanthanide complexes are already being widely used as imaging agents in both whole body MRI and luminescence microscopy.[1,2] In recent years, the use of gadolinium complexes as MRI contrast agents has become almost ubiquitous in MRI blood pool imaging,[3] and the strategy has been extended using complexes that respond to changes in their environment,[4] and to bioconjugates with peptides that are internalised by specific cell types.[5] Luminescent lanthanide complexes have become a keystone of bioassay,[6] and are beginning to be exploited as tags[7] and responsive probes[8] for time-gated luminescence microscopy, where the long luminescence lifetimes associated with lanthanide centred transitions lend themselves to such applications.

Over the last few years, we and others have devoted considerable effort to developing strategies that can be used to link lanthanide complexes together through carrying out chemical modifications to stable complexes, using Ugi[9] and click[10] reactions, and developing orthogonal protection strategies that can be used to control the position of lanthanide complexation.[11] Related strategies have also been used to incorporate aromatic and transition metal complexes into lanthanide containing systems.[12,13]

We now report the synthesis of a family of DOTA-monoamide complexes bearing an isophthalate group which is suitable for further functionalisation with a pair of targeting vectors.

Results and discussion

Our synthetic strategy is shown in Scheme 1. Reaction of dimethyl 3-aminoisophthalate (**1**) with chloroacetyl chloride in the presence of sodium hydrogencarbonate yielded 2-chloro-*N*-(3,5-di(methoxycarbonyl)phenyl)acetamide (**2**). Reaction of the well-known triester[14] (**3**) with compound **2** yielded the orthogonally protected DOTA-monoamide derivative (**4**). Cleavage of the *tert*-butyl ester groups using trifluoroacetic acid yielded H_3·**5**, which was used to form the Ln·**5** complexes. Base hydrolysis of H_3·**5** and subsequent work up and complexation with the appropriate lanthanide triflate yielded H_5·**6** and Ln·**6** respectively. We elected to use this approach in the light of previous experience of lability of lanthanide coordinated amide bonds:[11] indeed, attempts at base hydrolysis of Ln·**5** proved capricious, with evidence of Ln·DOTA contaminants being observed in NMR spectra of the crude mixtures that were obtained. This lends further weight to the supposition that treatment of aqueous solutions of such complexes with strong base should be avoided wherever possible.

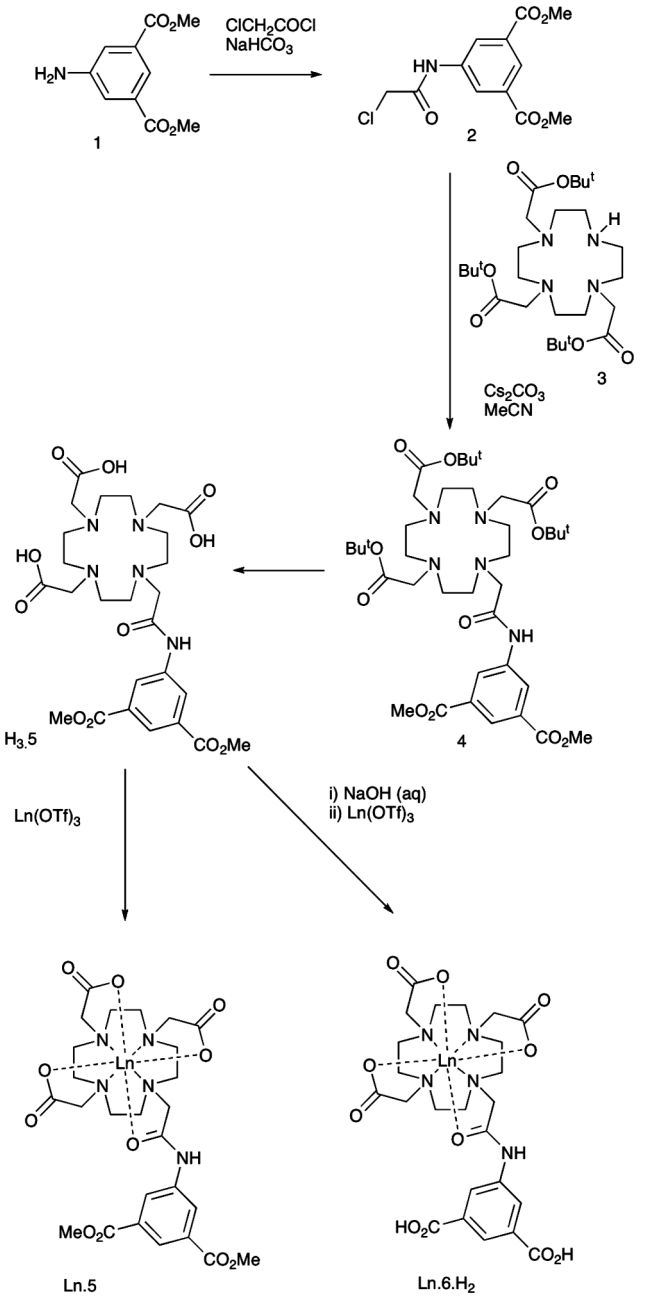
Structures of the complexes in solution

Initially, NMR spectroscopy was used to probe the structures of the complexes in solution. The NMR spectra of the complexes are shown in Fig. 1 and 2. All bear a clear resemblance to the NMR spectra of other DOTA-monoamide complexes,[9,11] and the chemical shifts observed are similar to the analogous complexes of DOTA itself,[15] with the obvious difference that the broken symmetry in these structures gives rise to a much greater number of peaks in the spectra of the monoamide complexes (since all the protons in the structure are now inequivalent). For the neodymium complexes, this inequivalence is much less obvious than it is in the other complexes, since exchange broadening gives rise to broad and relatively featureless spectra. The other complexes all give rise to clearly defined spectra, and in all cases comparison of the chemical shifts observed for the most shifted protons with those corresponding to the same protons in literature

[a]*School of Chemistry, University of Manchester, Oxford Road, Manchester, UK, M13 9PL*
[b]*University of Oxford, Chemistry Research Laboratory, Mansfield Road, Oxford, UK, OX1 3TA. E-mail: Stephen.Faulkner@chem.ox.ac.uk; Tel: +44 1865 285148*
[c]*University of Durham, Department of Chemistry, South Road, Durham, UK, DH1 3LE. E-mail: A.M.Kenwright@dur.ac.uk; Tel: +44 191 334 2095*

† Electronic supplementary information (ESI) available: Crystallographic Information File (CIF) of Tb·**5**. CCDC reference number 828726. See DOI: 10.1039/c1dt11029b

Published on 26 September 2011 on http://pubs.rsc.org | doi:10.1039/C1DT11029B
Downloaded by University of Oxford on 25 February 2013



Scheme 1

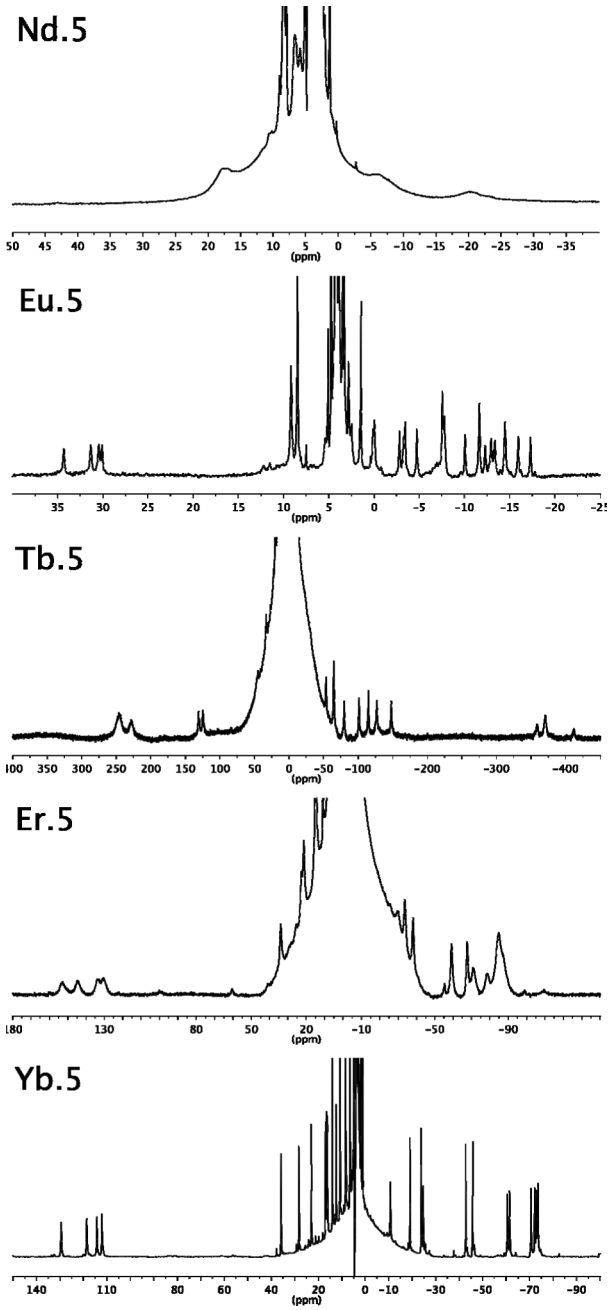


Fig. 1 ^{1}H NMR spectra (500 MHz, D_2O, 295 K) of the lanthanide complexes of **5**.

reports[9,11,15,16] suggest that the dominant isomer in solution is a hydrated square antiprismatic structure. Tb·**5**, Tb·**6**, Yb·**5** and Yb·**6** are all dominated by a single set of resonances, with only traces of the diastereomeric twisted square antiprismatic form being observed in solution at 295 K (*e.g.* around 80 ppm in the case of Yb·**6**). In the case of the europium complexes, there is much clearer evidence for a minor isomer in which the metal adopts a twisted square antiprismatic geometry.

Furthermore, it is clear that the spectra of the complexes of **5** and **6** with the same lanthanide are very similar to one another, implying that remote substituents have little effect on the local environment close to the lanthanide.

Luminescence spectroscopy was used to probe the structures further. All the complexes were found to be luminescent, though facile quenching by O–H oscillators ensured that only weak emission was observed from the erbium complexes. Key aspects of their properties are shown in Table 1.

Time-resolved data was used to assess the inner sphere hydration of the complexes. The lifetimes of lanthanide-centred emission in water and deuterium oxide can be used to calculate q_{Ln}, the number of inner-sphere water molecules bound to the lanthanide ion, using the equation

$$q_{Ln} = A(1/\tau_{H_2O} - 1/\tau_{D_2O} - B) \quad (1)$$

 This journal is © The Royal Society of Chemistry 2011

Published on 26 September 2011 on http://pubs.rsc.org | doi:10.1039/C1DT11029B
Downloaded by University of Oxford on 25 February 2013

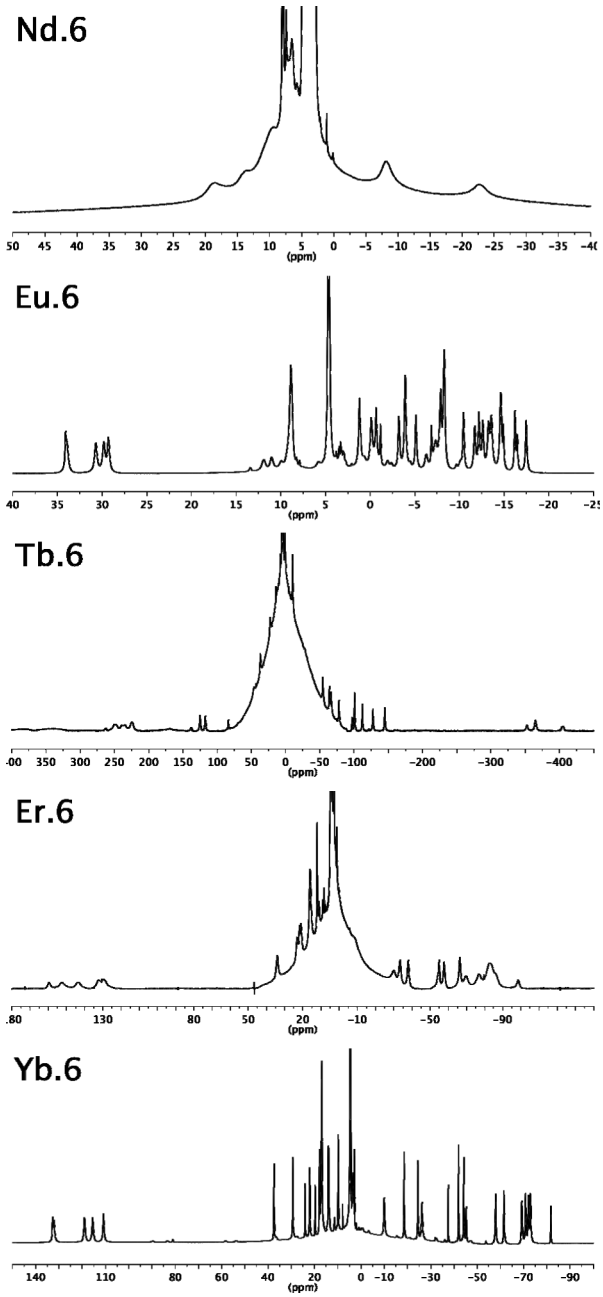


Fig. 2 ^{1}H NMR spectra (500 MHz, D_2O, 295 K) of the lanthanide complexes of **6**.

where A and B are constants for a given lanthanide ion. For europium A_{Eu} = 1.2 ms and B_{Eu} = (0.25 − 0.075x) ms^{-1}, where x is the number of exchangeable N–H oscillators (*i.e.* x = 1, in this case). Effective calculations of q are also possible for terbium and ytterbium complexes (A_{Tb} = 5 ms, B_{Tb} = 0.06 ms^{-1}, A_{Yb} = 1 μs and B_{Yb} = 0.1 μs^{-1}), but the facility of C–H quenching in neodymium and erbium complexes means that this approach cannot be applied to calculate q_{Nd} and q_{Er}.[18] In the cases for which q can be calculated effectively, it is clear that the data from luminescence spectroscopy bears out the NMR study. In all cases, calculated values of q are close to 1, implying that a hydrated square antiprismatic structure dominates in solution.

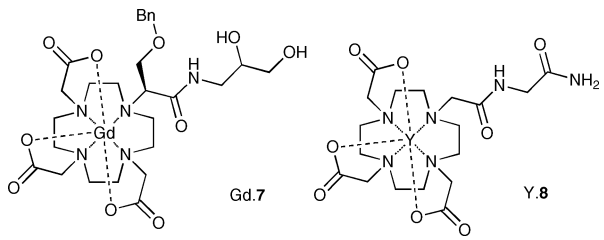
Table 1 Photophysical properties of the complexes[a]

Complex	λ_{ex}/nm	λ_{em}/nm	τ_{H_2O}/μs	τ_{D_2O}/μs	q_{calc}
Nd·**5**	337	1055	0.14	0.38	
Eu·**5**	260	617	550	1850	1.1
Tb·**5**	260	545	1630	2730	0.9
Er·**5**	337	1530	—	0.81	
Yb·**5**	337	980	0.78	5.21	0.9
[Eu·**6**]$^{2-}$	260	617	570	2180	1.0
[Tb·**6**]$^{2-}$	260	545	1690	3030	1.0
[Er·**6**]$^{2-}$	337	1530	—	0.94	
[Yb·**6**]$^{2-}$	337	980	0.79	7.74	1.0
[Nd·**6**]$^{2-}$	337	1055	0.11	0.34	

[a] q_{Ln} was calculated using eqn (1), and the A and B parameters in ref. 17.

Crystal structure of Tb·5

Suitable colourless needles of Tb·**5** for structural analysis were obtained by slow evaporation of a saturated aqueous solution at room temperature. To the best of our knowledge, there is only one previous structural report of a DOTA monoamide complex and one group 3 derivative; these are Gd·**7**[19] and Y·**8**.[20]



The complex crystallises as a racemate and both $\Lambda(\delta\delta\delta\delta)$ and $\Delta(\lambda\lambda\lambda\lambda)$ configurations are observed in the asymmetric unit cell. Average cyclen N–C–C–N and N–C–C–O torsion angles are respectively measured as +58.7° and −28.6° for the $\Lambda(\delta\delta\delta\delta)$ diastereomer and −58.9° and +28.2° for the $\Delta(\lambda\lambda\lambda\lambda)$ configuration.

The solid state structure of Tb·**5** (Fig. 3) shows that the terbium(III) ion is 9 coordinate and the resultant coordination geometry is best described as a distorted mono capped square antiprism (SAP). The basal plane is described by the four cyclen N atoms (N(1)–N(4)) and the orthogonal plane occupied by the three acetate O atoms (O(2), O(4), O(6)) and the amide O atom (O(8)). The displacements of these atoms from their respective mean planes are 0.006 and 0.019 Å respectively. The two planes lie almost parallel to one another; the angle between them being 1.8° and the Tb^{3+} ion lies 1.611 Å from the centre of the N_4 plane and 0.709 Å from the O_4 plane. The dihedral or twist angle between the cyclen N_4 donor set and that of the acetate/amide donor set is 39° (±1°) and is characteristic of distorted SAP coordination polyhedra observed in mono, bis, tri and tetraamide DOTA derivatives.[21]

The average N_{cyclen}–Tb distance is 2.641(4) Å, the mean $O_{acetate}$–Tb distance is 2.341(3) Å and the O_{amide}–Tb distance is longer at 2.409(3) Å. These values are again consistent with those reported for mid-lanthanide DOTA and amide derivatives.[21] The axial position is occupied by a water molecule; the interatomic distance between the oxygen atom and the terbium ion is 2.415(4) Å. This value is comparable to that measured for the Gd·**7** (2.429(5) Å), and to [Gd·DOTA(OH_2)]$^-$ (2.463 Å), [Gd·DOTAM(OH_2)]$^{3+}$ (2.395 Å) and related terbium triamide complexes.[22]

Published on 26 September 2011 on http://pubs.rsc.org | doi:10.1039/C1DT11029B
Downloaded by University of Oxford on 25 February 2013

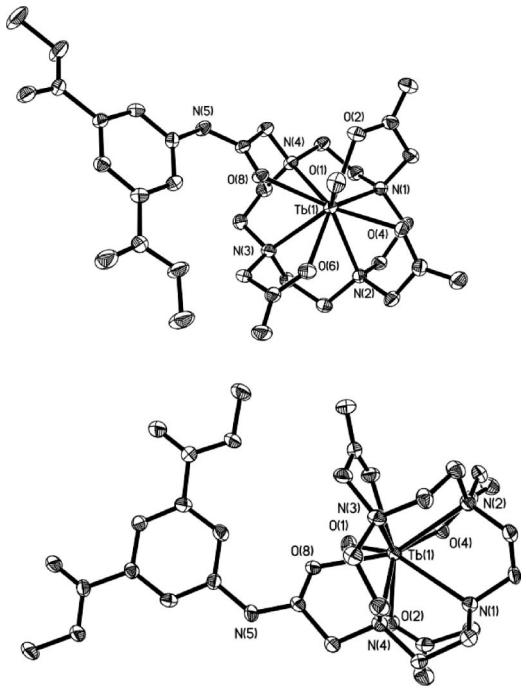


Fig. 3 Thermal ellipsoid drawings of Tb·**5** at the 50% probability level, H atoms and lattice water molecules removed for clarity. Top: perspective above the plane of the aza macrocycle. Bottom: perspective in the mean plane of the isophthalate ring. Selected distances (Å) and angles (°): Tb(1)–O(1) 2.415(4), Tb(1)–O(2) 2.364(3), Tb(1)–O(4) 2.295(3), Tb(1)–O(6) 2.365(3), Tb(1)–O(8) 2.409(3), Tb(1)–N(1) 2.612(4), Tb(1)–N(2) 2.659(4), Tb(1)–N(4) 2.654(4); O(4)–Tb(1)–O(2) 87.57(12), O(2)–Tb(1)–O(6) 146.11(13), O(6)–Tb(1)–O(8) 83.67(11), O(8)–Tb(1)–O(1) 69.56(12), O(6)–Tb(1)–N(1) 140.41(12), N(1)–Tb(1)–N(3) 104.00(13), N(1)–Tb(1)–N(4) 69.08(13), N(4)–Tb(1)–N(2) 105.65(12), N(1)–Tb(1)–N(2) 67.81(12).

The solid state structure clearly correlates closely with the structure in solution in this case. Though attempts to crystallise Ln·**6** complexes proved unsuccessful, the similarities between solution state data for Ln·**5** and Ln·**6** suggest that this structural motif persists in the fully deprotected form.

Conclusions

Isophthalate appended DOTA-monoamide derivatives form stable and well-defined complexes in solution and in the solid phase. The dominant form is a nine-coordinate square antiprismatic diastereoisomer with a single water molecule bound to the metal ion. This structural motif is well suited to applications in luminescence spectroscopy and contrast imaging. Furthermore, the two carboxylic acid groups lend themselves to further functionalisation with chromophores or targeting vectors. In the latter case, this complex offers the potential for functionalisation with more than one vector, raising the possibility of chelating interactions that can enhance specificity. We are currently investigating these possibilities.

Experimental

General methods

Cyclen was purchased from Strem Chemicals, and other reagents, solvents and starting materials were obtained from the Aldrich Chemical Company. All chemicals were used as supplied.

Mass spectra were obtained using positive electrospray in acetonitrile or methanol solutions on a Micromass Platform II spectrometer, or by MALDI using methanol solutions with an ALPHA matrix on a Micromass TOF Spec 2E spectrometer.

Elemental analyses were performed using a Carlo ERBA Instruments CHNS-O EA1108 elemental analyzer (C, H, N and S analysis) and a Fisons Horizon Elemental Analysis ICP-OED spectrometer for metals and halogens.

Absorption spectra were recorded in H_2O on a T60U spectrometer (PG Instruments Ltd.) using fused silica cells with a path length of 1 cm.

NMR spectra of the complexes were recorded at 500 MHz and 295 K unless otherwise stated, using millimolar solutions of the complex and referencing spectra to the water peak at 4.7 ppm. Spectra were acquired over 5000 repetitions using an acquisition time of 0.1 s, relaxation delay of 0.1 s, and appropriate spectral widths of up to 500 kHz.

Preparation of ligands and complexes

1,3-Dimethyl-5-aminoisophthalate acetylchloride, (2). Dimethyl-5-aminoisophthalate (1.02 g, 4.79 mmol) was dissolved in dichloromethane (50 cm^3), and then $NaHCO_3$ (5.08 g, 47.9 mmol) was added to the stirring mixture. Chloroacetyl chloride (0.53 g, 0.37 cm^3, 4.79 mmol) was added drop-wise to the solution, and then the mixture was stirred at room temperature for 24 h. Dichloromethane (200 cm^3) was added to the mixture, which was then filtered. The filtrate was evaporated under reduced pressure, to produce a creamy beige/white solid. The crude product was then recrystallised using minimum hot DCM (~75 cm^3) to leave the product as a white solid, (1.29 g, 93%). ES^- MS (MeCN): m/z 284 $\{M - H\}^+$; ES^+ MS (MeCN): m/z 308 $\{M + Na\}^+$; ^1H NMR (400 MHz, $CDCl_3$, 300 K) δ_H (ppm) 3.8 (6H, s, 2C$\underline{H}_3$), 4.2 (2H, s, C$\underline{H}_2$-Cl), 8.4 (3H, s, Ar-$\underline{H}$), 8.5 (1H, s, N$\underline{H}$); $^{13}C\{^1H\}$ NMR (400 MHz, MeOD, 300 K) δ_C (ppm) 42.8 ($CO_2\underline{C}H_3$), 52.6 ($CO\underline{C}H_2Cl$), 125.1, 127.3, 131.7, 137.2 (Ar-$\underline{C}$), 164.1 ($\underline{C}ONH$), 165.7 (Ar-$\underline{C}O_2CH_3$); IR(ATR): ν (C═O) 1716 cm^{-1}, (C═O) 1683 cm^{-1}, (N–H) 1547 cm^{-1}; CHN expected for $C_{12}H_{12}NO_5Cl$: C, 50.45; H, 4.23; N, 4.90; found: C, 50.21; H, 4.15; N, 4.86.

Tris-*tert*-butyl 1,4,7,10-tetraazacyclododecane-1,4,7-triacetate hydrobromide salt (3). Prepared as described in ref. 14.

1,4,7-Tris-(*tert*-butoxycarbonylmethyl)-10-acetyldimethyl-5-aminoisophthalate-1,4,7,10-tetraazacyclododecane, (4). Triester **3** (1.02 g, 1.98 mmol) was dissolved in acetonitrile (30 cm^3), then caesium carbonate (3.18 g, 9.78 mmol) was added to the stirring solution. Dimethyl-5-aminoisophthalate acetylchloride **2** (0.55 g, 1.98 mmol) was dissolved in acetonitrile (10 cm^3), and added drop-wise to the triester mixture. The mixture was stirred at room temperature for 5 d, and was monitored by TLC. The solution was filtered and the filtrate was evaporated under reduced pressure to yield a yellow solid. The yellow solid was dissolved in minimum hot methanol (~10 cm^3), from which the product crystallised out as a white powder overnight in the fridge (0.51 g, 34%). λ_{max} ($\pi \rightarrow \pi^*$) = 263 nm (ε 11 588 M^{-1} cm^{-1}); ES^+ MS (MeCN): m/z 764 $\{M + H\}^+$, 785 $\{M + Na\}^+$; ^1H NMR (400 MHz, $CDCl_3$, 300 K) δ_H 1.3 (81H, m, CC$\underline{H}_3$), 2.6, 2.8, 2.9, 3.0, 3.1, 3.2, 3.3, 3.4 (24H, m,

 This journal is © The Royal Society of Chemistry 2011

Published on 26 September 2011 on http://pubs.rsc.org | doi:10.1039/C1DT11029B
Downloaded by University of Oxford on 25 February 2013

N-C$\underline{H}_2$ and NC$\underline{H}_2$CO), 8.3 (1H, s, Ar$\underline{H}$), 8.5 (2H, s, Ar$\underline{H}$); $^{13}C\{^1H\}$ NMR (400 MHz, $CDCl_3$, 300 K) δ_C 28.2 (C$\underline{C}H_3$), 50.8, 51.9, 52.3, 52.9, 55.2, 56.0, 56.9, 59.0 ($CO_2\underline{C}H_3$, N-$\underline{C}H_2$CONH, N-$\underline{C}H_2$ and N-$\underline{C}H_2$COO), 80.8, 81.1 ($\underline{C}CH_3$), 124.7, 125.8, 131.1, 139.2 (Ar-$\underline{C}$), 166.2 ($\underline{C}$ONH), 170.5, 170.7, 171.2 ($\underline{C}O_2CH_3$ and $\underline{C}O_2CCH_3$); IR(ATR): ν (C═O) 1720 cm^{-1}, (C═O) 1682 cm^{-1}; CHN expected for $C_{38}H_{61}N_5O_{11}$: C, 59.75; H, 8.05; N, 9.17. Found: C, 59.46; H, 8.21; N, 8.99.

10-Acetyldimethyl-5-aminoisophthalate-1,4,7,10-tetraazacyclododecane-1,4,7-triacetate (H_3·5). 1,4,7-Tris-(*tert*-butoxycarbonylmethyl)-10-acetyldimethyl-5-aminoisophthalate-1,4,7,10-tetraazacyclododecane **4** (0.6 g, 7.9×10^{-4} mol) was dissolved in dichloromethane (10 cm^3) and trifluoroacetic acid (10 cm^3) was added drop-wise to the stirring solution. The reaction mixture was stirred at room temperature for 24 h. The solvents were then removed *in vacuo* and the residue was washed repeatedly with dichloromethane (3×10 cm^3) and methanol (5×10 cm^3). This yielded a hygroscopic yellow solid (0.43 g, 91%). λ_{max} ($\pi \rightarrow \pi^*$) = 261 nm (ε 79 250 M^{-1} cm^{-1}); Maldi MS (α-MeOH): *m/z* 596 $\{M+H\}^+$; ^1H NMR (400 MHz, D_2O, 300 K) δ_H 3.0–3.6 (24H, broad signal, N-C$\underline{H}_2$ and NC$\underline{H}_2$CO), 3.9 (6H, s, $CO_2C\underline{H}_3$), 8.15 (2H, s, ar$\underline{H}$), 8.25 (1H, s, Ar$\underline{H}$); $^{13}C\{^1H\}$ NMR (400 MHz, D_2O, 300 K) δ_C 50.9, 54.9 (broad signal, $CO_2\underline{C}H_3$, N-$\underline{C}H_2$CONH, N-$\underline{C}H_2$ and N-$\underline{C}H_2$COO), 114.9, 117.6, 125.2, 126.2, 130.9 (Ar-$\underline{C}$), 162.3, 163.4, 167.5 ($\underline{C}$ONH, $\underline{C}O_2CH_3$ and $\underline{C}$OOH); IR(ATR): ν (C═O) 1718 cm^{-1}, (C═O) 1664 cm^{-1}, (N–H) 1574 cm^{-1}; CHN expected for $C_{26}H_{37}N_5O_{11}(CF_3COOH)(H_2O)_2$: C, 45.10; H, 5.68; N, 9.39. Found: C, 45.69; H, 5.95; N, 9.19.

10-Acetyldicarboxylic acid-5-aminoisophthalate-1,4,7,10-tetraazacyclododecane-1,4,7-triacetate sodium salt, (Na_5·6). H_3·5 (0.2 g, 3.36×10^{-4} mol) was dissolved in distilled water (2 cm^3), then 5 molar equivalents of NaOH (1.67 cm^3, 1 M) were added drop-wise to the stirring solution. The solution was stirred at room temperature for 5 h. Any precipitate was filtered off, before adding an excess of acetone to the filtrate, until the solution went cloudy. The solution was kept in the fridge overnight, where an orange oil formed at the bottom of the flask. The solution was carefully decanted off, to leave behind the orange oil product, which was dried overnight under vacuum, to yield the product (0.13 g, 68%). Maldi MS (α-MeOH): *m/z* 568 $\{M+H\}^+$, 590 $\{M+Na\}^+$, 612 $\{M-H+2Na\}^+$, 634 $\{M-2H+3Na\}^+$, 656 $\{M-3H+4Na\}^+$; ^1H NMR (400 MHz, D_2O, 300 K) δ_H 2.2, 2.4, 2.6, 2.9, 3.2, 3.3 (24H, br m, N-C$\underline{H}_2$ and N-C$\underline{H}_2$CO), 7.8 (2H, s, Ar-$\underline{H}$), 7.9 (1H, s, Ar-$\underline{H}$); ^{13}C $\{^1H\}$ NMR (400 MHz, D_2O, 300 K) δ_C 56.9, 58.6, 58.7, 59.3 (broad signal, N-$\underline{C}H_2$CONH, N-$\underline{C}H_2$ and N-$\underline{C}H_2$COO), 123.9, 124.1, 125.6, 136.9, 137.4 (Ar-$\underline{C}$), 172.2, 173.5, 174.3, 180.2, 180.3, 180.4 ($\underline{C}$ONH, Ar-$\underline{C}O_2$H and $\underline{C}$OOH); IR(ATR): ν (O–H) 3319 cm^{-1}, (C═O) 1695 cm^{-1}, (N–H) 1590 cm^{-1}; CHN expected for $C_{24}H_{27}N_5O_{11}Na_6(NaOH)_6 \cdot 6H_2O$: C, 27.52; H, 4.33; N, 6.69; Na, 26.34. Found: C, 27.91; H, 4.24; N, 6.57; Na, 26.78.

General procedure for the preparation of Ln·5

5 (0.13 g, 1.4×10^{-4} mol) was dissolved in the minimum volume of methanol (3 cm^3), and mixed with a solution of the lanthanide triflate salt (1.0 eq, 1.4×10^{-4} mol) in methanol (3 cm^3). The solution was stirred at room temperature for 7 d. The solution was filtered, and the filtrate was evaporated under reduced pressure to yield a colourless oil. To the residue minimum ethanol (3 cm^3) was added, followed by the addition of diethyl ether until precipitate formed. The white precipitate was filtered, washed with diethyl ether and dried under vacuum to give the product.

Nd·5 (0.09 g, 88%). λ_{max} ($\pi \rightarrow \pi^*$) = 260 nm (ε 2102 M^{-1} cm^{-1}); Maldi MS (α-MeOH) *m/z*: 596 $\{M\text{-}Nd + H\}^+$, 737 $\{M + 3H\}^+$; NMR (500 MHz, D_2O, 295 K) δ_H –20.0, –7.7, –6.1, 10.2, 16.9, Only major resolved peaks outside the range +10 to –5 ppm reported; IR (ATR): ν (C═O) 1722 cm^{-1}, (C═O) 1581 cm^{-1}; Luminescence: λ_{em} = 1055 nm, λ_{ex} = 337 nm, $\tau_{(H_2O)}$ = 144 ns, $\tau_{(D_2O)}$ = 376 ns.

Eu·5 (0.10 g, 96%). λ_{max} ($\pi \rightarrow \pi^*$) = 260 nm (ε 1547 M^{-1} cm^{-1}); Maldi MS (α-MeOH) *m/z*: 598 $\{M\text{-}Eu + 3H\}^+$, 748 $\{M+3H\}^+$, 768 $\{M+Na+2H\}^+$, 1492 $\{Mx2+2H\}^+$; NMR (500 MHz, D_2O, 295 K) δ_H –17.3, –15.9, –14.5, –13.4, –10.1, –7.8, –7.6, –4.7, –3.4, –2.8, –0.01, 1.5, 7.5, 8.5, 9.1, 9.2, 30.1, 30.5, 31.4, 34.4 (only major resolved peaks outside the range +2 to +6 ppm reported); IR (ATR): ν (C═O) 1721 cm^{-1}, (C═O) 1582 cm^{-1}; Luminescence: λ_{em} = 617 nm, λ_{ex} = 260 nm, $\tau_{(H_2O)}$ = 0.55 ms, $\tau_{(D_2O)}$ = 1.83 ms, q = 1.1.

Gd·5 (0.05 g, 45%). λ_{max} ($\pi \rightarrow \pi^*$) = 260 nm (ε 33 100 M^{-1} cm^{-1}); Maldi MS (α-MeOH) *m/z*: 595 $\{M\text{-}Gd\}^+$, 751 $\{M+H\}^+$, 1500 $\{Mx2\}^+$; IR (ATR): ν (C═O) 1718 cm^{-1}, (C═O) 1583 cm^{-1}; CHN expected for $C_{26}H_{34}N_5O_{11}(H_2O)_4$: C, 38.00; H, 5.15; N, 8.52; Gd, 19.13. Found: C, 38.00; H, 4.69; N, 8.48; 19.37.

Tb·5 (0.10 g, 90%). λ_{max} ($\pi \rightarrow \pi^*$) = 260 nm (ε 2832 M^{-1} cm^{-1}); Maldi MS (α-MeOH) *m/z*: 596 $\{M\text{-}Tb + H\}^+$, 752 $\{M+H\}^+$; NMR (500 MHz, D_2O, 295 K) δ_H –411.6, –370.8, –359.1, –147.8, –142.4, –126.6, –114.4, –100.7, –95.9, –88.9, –79.4, –63.9, –52.9, 84.2, 125.8, 131,9, 181.0, 189.1, 230.8, 246.7 (only major peaks outside the range +60 to – 45 ppm reported); IR (ATR): ν (C═O) 1721 cm^{-1}, (C═O) 1582 cm^{-1}; CHN expected for $C_{26}H_{34}N_5O_{11}Tb \cdot (CF_3COOH)_3(H_2O)_3$: C,33.49; H, 3.78; N, 6.10; Tb, 13.84. Found: C, 29.39; H, 3.61; N, 6.02; Tb, 14.32. Luminescence: λ_{em} = 545 nm, λ_{ex} = 260 nm, $\tau_{(H_2O)}$ = 1.63 ms, $\tau_{(D_2O)}$ = 2.73 ms, q = 0.9.

Er·5 (0.07 g, 66%). λ_{max} ($\pi \rightarrow \pi^*$) = 260 nm (ε 1984 M^{-1} cm^{-1}); Maldi MS (α-MeOH) *m/z*: 597 $\{M\text{-}Er + H\}^+$, 760 $\{M\}^+$, 1520 $\{Mx2\}^+$; NMR (500 MHz, D_2O, 295 K) δ_H –84.4, –77.9, –70.7, –67.6, –59.0, –55.2, –37.9, –33.5, –30.0, 14.9, 21.4, 22.7, 25.5, 33.9, 130.2, 133.4, 144.6, 152.7 (only major peaks outside the range +10 to –20 ppm reported); IR (ATR): ν (C═O) 1722 cm^{-1}, (C═O) 1582 cm^{-1}; Luminescence: λ_{em} = 1530 nm, λ_{ex} = 337 nm, $\tau_{(D_2O)}$ = 805 ns.

Yb·5 (0.09 g, 84%). λ_{max} ($\pi \rightarrow \pi^*$) = 260 nm (ε 967 M^{-1} cm^{-1}); Maldi MS (α-MeOH) *m/z*: 596 $\{M\text{-}Yb + H\}^+$, 767 $\{M+H\}^+$, 1534 $\{Mx2 + 2H\}^+$; NMR (500 MHz, D_2O, 295 K) δ_H –73.5, –72.9, –72.1, –70.5, –61.4, –60.4, –45.6, –42.7, –24.6, –23.8, –18.9, –10.7, 10.8, 12.5, 14.1, 16.2, 16.5, 17.0, 23.1, 28.3, 35.9, 112.0, 114.2, 118.5, 129.5 (only major peaks outside the range +10 to –4 ppm reported); IR (ATR): ν (C═O) 1719 cm^{-1}, (C═O) 1584 cm^{-1}; Luminescence: λ_{em} = 980 nm, λ_{ex} = 337 nm, $\tau_{(H_2O)}$ = 0.78 μs, $\tau_{(D_2O)}$ = 5.21 μs, q = 0.9.

General procedure for the preparation of $[Ln \cdot 6]^{2-}$

Na_5·6 (0.05 g, 4.8×10^{-5} mol) was dissolved in distilled water (1 cm^3), and the pH was adjusted from pH 11 to pH 5 by

Published on 26 September 2011 on http://pubs.rsc.org | doi:10.1039/C1DT11029B
Downloaded by University of Oxford on 25 February 2013

adding dilute HCl (~3 cm^3, 1 M) to the solution. A solution of the lanthanide triflate salt dissolved distilled water (1 cm^3) was then added drop-wise to the mixture. The solution was heated at 60 °C for 18 h. The solvent was then evaporated under reduced pressure to yield a white solid. Minimum ethanol (3 cm^3) was added to dissolve the white residue, followed by the addition of excess diethyl ether until the white product precipitated out. The solution was filtered using a filter stick under vacuum, and the hygroscopic white product was then washed with diethyl ether and dried under vacuum to give the product.

[Nd·6]$^{2-}$ (0.02 g, 67%). Maldi MS (α-MeOH) *m/z*: 710 {M+4H}$^+$, 1418 {Mx2 + 6H}; IR (KBr): *ν* (O–H) 3449 cm^{-1}, (C═O) 1702 cm^{-1}, (N–H) 1614 cm^{-1}. Luminescence: λ_{em} = 1055 nm, λ_{ex} = 337 nm, $\tau_{(H_2O)}$ = 110 ns, $\tau_{(D_2O)}$ = 340 ns.

[Eu·6]$^{2-}$ (0.03 g, 81%). λ_{max} ($\pi \rightarrow \pi^*$) = 260 nm (ε 4700 M^{-1} cm^{-1}); Maldi MS (no matrix) *m/z*: 718 {M+H}$^+$; ^{1}H NMR (500 MHz, D_2O, 300 K) δ_H (ppm) –17.5, –16.5, –16.2, –14.9, –14.6, –13.6, –13.2, –12.6, –12.2, –11.7, –10.5, –8.3, –7.9, –7.3, –6.9, –5.1, –3.9, –3.2, –1.2, –0.7, –0.1, +1.0, +1.2, +8.9, +11, +12, +13.5, +29.3, +29.8, +30.7, +34.1 (only major resolved peaks outside the range +3 to +5 ppm reported); IR (ATR): *ν* (O–H) 3427 cm^{-1}, (C═O) 1708 cm^{-1}, (N–H) 1582 cm^{-1}; Luminescence: λ_{em} = 617 nm, λ_{ex} = 260 nm, $\tau_{(H_2O)}$ = 0.57 ms, $\tau_{(D_2O)}$ = 2.18 ms, *q* = 1.2.

[Tb·6]$^{2-}$ (0.03 g, 87%). λ_{max} ($\pi \rightarrow \pi^*$) = 260 nm (ε 3840 M^{-1} cm^{-1}); Maldi MS (α-MeOH) *m/z*: 746 {M+Na}$^+$, 768 {M+2Na – H}$^+$, 790 {M+3Na – 2H}$^+$, 1447 {Mx2 + H}$^+$, 1470 {Mx2+Na + H}$^+$, 1491 {Mx2 + 2Na – H}$^+$, 1513 {Mx2 + 3Na – 2H}$^+$, 1535 {Mx2 + 4Na – 3H}$^+$, 1557 {Mx2 + 5Na – 4H}$^+$, 1578 {Mx2 + 6Na – 6H}$^+$; ^{1}H NMR (500 MHz, D_2O, 300 K) δ_H (ppm) –405.4, –364.6, –352.4, –144.7, –127.3, –121.3, –111.9, –100.6, –96.8, –77.9, –73.7, –66.3, –63.9, –54.2, +83.9, +117.4, +125.2, +138.0, +169.5, +224.2, +234.3, +238.7, +247.8, +262.7 (only major resolved peaks outside the range –40 to +100 ppm reported), IR (KBr): *ν* (O–H) 3446 cm^{-1}, (C═O) 1700 cm^{-1}, (N–H) 1617 cm^{-1}; Luminescence: λ_{em} = 545 nm, λ_{ex} = 260 nm, $\tau_{(H_2O)}$ = 1.69 ms, $\tau_{(D_2O)}$ = 3.03 ms, *q* = 1.0.

[Er·6]$^{2-}$ (0.03 g, 81%). λ_{max} ($\pi \rightarrow \pi^*$) = 260 nm (ε 4660 M^{-1} cm^{-1}); Maldi MS (α-MeOH) *m/z*: 755 {M+Na}$^+$, 778 {M+2Na}$^+$, 800 {M+3Na – 1H}$^+$, 1468 {Mx2 – 4H}$^+$, 1486 {Mx2+Na – 1H}$^+$, 1508 {Mx2 + 2Na – 2H}$^+$, 1530 {Mx2 + 3Na – 3H}$^+$, 1551 {Mx2 + 4Na – 5H}$^+$, 1572 {Mx2 + 5Na – 7H}$^+$; ^{1}H NMR (500 MHz, D_2O, 300 K) δ_H (ppm) –98.5, –82.9, –76.6, –69.5, –66.2, –57.6, –54.9, –37.9, –37.4, –33.4, –29.9, +21.0, +21.9, +34.0, +129.4, +132.2, +143.8, +152.5, +159.7 (only major resolved peaks outside the range –20 to +20 ppm reported); IR (KBr): *ν* (O–H) 3437 cm^{-1}, (C═O) 1697 cm^{-1}, (N–H) 1631, 1608 and 1586 cm^{-1}.

[Yb·6]$^{2-}$ (0.03 g, 89%). λ_{max} ($\pi \rightarrow \pi^*$) = 260 nm (ε 6120 M^{-1} cm^{-1}); Maldi MS (α-MeOH) *m/z*: 761 {M+Na}$^+$, 783 {(M+6H + K}$^+$, 1498 {Mx2 – H + Na}$^+$; ^{1}H NMR (500 MHz, D_2O, 300 K) δ_H (ppm) –81.6, –72.9, –72.0, –70.8, –69.2, –61.6, –57.9, –45.2, –44.1, –41.9, –37.5, –26.2, –24.4, –18.5, –9.9, +19.8, +22.1, +24.1, +29.4, +37.4, +110.9, +115.5, +119.0, +132.1, +132.8 (only major resolved peaks outside the range –5 to +19 ppm reported); IR (KBr): *ν* (O–H) 3488 cm^{-1}, (C═O) 1694 cm^{-1}, (N–H) 1633, 1614 and 1588 cm^{-1}.

Photophysical measurements

Steady state and time-resolved luminescence properties of the terbium and europium complexes were determined using a Perkin-Elmer LS55 fluorimeter operating in phosphorescence mode counting. In the case of the erbium, ytterbium and neodymium complexes, the sample was excited using a pulsed nitrogen laser (337 nm) operating at 10 Hz. Light emitted at right angles to the excitation beam was focused onto the slits of a monochromator, which was used to select the appropriate wavelength. The growth and decay of the luminescence at selected wavelengths was detected using a germanium photodiode (Edinburgh Instruments, EI-P) and recorded using a digital oscilloscope (Tektronix TDS220) before being transferred to a PC for analysis. Luminescence lifetimes were obtained by iterative reconvolution of the detector response (obtained by using a scatterer) with exponential components for growth and decay of the metal centred luminescence, using a spreadsheet running in Microsoft Excel. The details of this approach have been discussed elsewhere.[23] Unless otherwise stated, fitting to a double exponential decay yielded no improvement in fit as judged by minimisation of residual squared and reduced chi squared.

X-Ray crystallography

X-Ray diffraction data for Tb·**5** were collected at 150 K using a Bruker APEX II CCD diffractometer on station 9.8 of the Synchrotron Radiation Source at CCLRC Daresbury Laboratory, at 0.69040 Å, from a silicon 111 monochromator using ω scans. The structure was solved by direct methods using SHELXS-97.[24] The structure was completed by iterative cycles of Δ*F*-syntheses and a full matrix least squares refinement. All non-H atoms were refined anisotropically and difference Fourier syntheses were employed in positioning idealised hydrogen atoms and were allowed to ride on their parent C or N-atoms. All refinements were against F^2 and used SHEL-XL-97.[25]

Notes and references

1 P. Caravan, *Chem. Soc. Rev.*, 2006, **35**, 512; D. Parker, R. S. Dickins, H. Puschmann, C. Crossland and J. A. K. Howard, *Chem. Rev.*, 2002, **102**, 1977.
2 For recent reviews, see: S. Faulkner, L. S. Natrajan, W. S. Perry and D. Sykes, *Dalton Trans.*, 2009, 3890; C. M. G. dos Santos, A. J. Harte, S. J. Quinn and T. Gunnlaugsson, *Coord. Chem. Rev.*, 2008, **252**, 2512; J. C. G. Bunzli, S. Comby, A. S. Chauvin and C. D. B. Vandevyer, *J. Rare Earths*, 2007, **25**, 257.
3 P. Caravan, J. J. Ellison, T. J. Mc Murry and R. B. Lauffer, *Chem. Rev.*, 1999, **99**, 2293.
4 E. L. Que and C. J. Chang, *Chem. Soc. Rev.*, 2010, **39**, 51; G. L. Law, R. Pal, L. O. Palsson, D. Parker and K.-L. Wong, *Chem. Commun.*, 2009, 7321; S. Pandya, J. Yu and D. Parker, *Dalton Trans.*, 2006, 2757.
5 R. J. Aarons, J. Notta, M. M. Meloni, J. Feng, S. Allan, N. Spencer, R. A. Kauppinen, J. S. Snaith and S. Faulkner, *Chem. Commun.*, 2006, 909.
6 I. A. Hemilla, *Applications of fluorescence in immunoassays*, Wiley Interscience, 1991; S. Faulkner and J. L. Matthews, *Fluorescent and Luminescent complexes for Biomedical Applications*, chapter in volume 9 of Comprehensive Coordination Chemistry 2nd Edition, Applications of Coordination Chemistry (ed. M. D. Ward), Elsevier, 2004.
7 A. Beeby, I. M. Clarkson, S. Faulkner, S. Botchway, D. Parker, J. A. G. Williams and A. W. Parker, *J. Photochem. Photobiol., B*, 2000, **57**, 83; L. Charbonniere, R. Ziessel, M. Guardigli, A. Roda, N. Sabbatini and M. Cesario, *J. Am. Chem. Soc.*, 2001, **123**, 2436; N. Weibel, L. J. Charbonniere, M. Guardigli, A. Roda and R. Ziessel, *J. Am. Chem. Soc.*, 2004, **126**, 4888.
8 For a recent review, see: C. Allain and S. Faulkner, *Future Med. Chem.*, 2010, **2**, 339.

 This journal is © The Royal Society of Chemistry 2011

View Article Online

9 M. Main, J. S. Snaith, M. M. Meloni, M. Jauregui, D. Sykes, S. Faulkner, A. M. Kenwright and J. S. Snaith, *Chem. Commun.*, 2008, 5212.
10 M. Jauregui, C. Allain, M. C. Willis, A. M. Kenwright, J. S. Snaith and S. Faulkner, *Dalton Trans.*, 2009, 6283.
11 L. S. Natrajan, A-J. L. Villaraza, A. M. Kenwright and S. Faulkner, *Chem. Commun.*, 2009, 6020.
12 M. P. Placidi, A-J. L. Villaraza, L. S. Natrajan, D. Sykes, A. M. Kenwright and S. Faulkner, *J. Am. Chem. Soc.*, 2009, **131**, 9916.
13 T. Koullourou, L. S. Natrajan, H. Bhavsar, S. J. A. Pope, J. Feng, J. Narvainen, R. Shaw, E. Scales, R. Kauppinen, A. M. Kenwright and S. Faulkner, *J. Am. Chem. Soc.*, 2008, **130**, 2178; S. I. Klink, H. Keizer and F. C. J. M van Veggel, *Angew. Chem., Int. Ed.*, 2000, **39**, 4319; A. Beeby, R. S. Dickins, S. Fitzgerald, L. J. Govenlock, C. L. Maupin, D. Parker, J. P. Riehl, G. Siligardi and J. A. G. Williams, *Chem. Commun.*, 2000, 1183; D. Imbert, M. Cantuel, J.-C. G. Bünzli, G. Bernardinelli and C. Piguet, *J. Am. Chem. Soc.*, 2003, **125**, 15698; S. Torelli, D. Imbert, M. Cantuel, G. Bernardinelli, S. Delahaye, A. Hauser, J.-C. G. Bünzli and C. Piguet, *Chem.–Eur. J.*, 2005, **11**, 3228; S. J. A. Pope, B. J. Coe and S. Faulkner, *Chem. Commun.*, 2004, 1550; D. Guo, C.-Y. Duan, F. Lu, Y. Hasegawa, Q.-J. Meng and S. Yanagida, *Chem. Commun.*, 2004, 1486; P. B. Glover, P. R. Ashton, L. J. Childs, A. Rodger, M. Kercher, R. M. Williams, L. De Cola and Z. Pikramenou, *J. Am. Chem. Soc.*, 2003, **125**, 9918; K. Senechal-David, S. J. A. Pope, S. Quinn, S. Faulkner and T. Gunnlaugsson, *Inorg. Chem.*, 2006, **45**, 10040.
14 A. Dadabhoy, S. Faulkner and P. G. Sammes, *J. Chem. Soc., Perkin Trans. 2*, 2002, 348; A. Dadabhoy, S. Faulkner and P. G. Sammes, *J. Chem. Soc., Perkin Trans. 2*, 2000, 2359–2360.
15 S. Aime, M. Botta and G. Ermondi, *Inorg. Chem.*, 1992, **31**, 4291; S. Aime, M. Botta, M. Fasano, M. P. M. Marques, C. F. G. C. Geraldes, D. Pubanz and A. E. Merbach, *Inorg. Chem.*, 1997, **36**, 2059.
16 R. S. Dickins, J. I. Bruce, D. Parker and D. J. Tozer, *Dalton Trans.*, 2003, 1264.
17 A. Beeby, I. M. Clarkson, R. S. Dickins, S. Faulkner, D. Parker, A. S. de Sousa and J. A. G. Williams, *J. Chem. Soc., Perkin Trans. 2*, 1999, 493.
18 S. Faulkner, B. P. Burton-Pye and S. J. A. Pope, *Appl. Spectrosc. Rev.*, 2005, **40**, 1.
19 S. Aime, P. L. Anelli, M. Botta, F. Fedeli, M. Grandi, P. Paoli and F. Uggeri, *Inorg. Chem.*, 1992, **31**, 2422.
20 A. Heppeler, S. Froidevaux, H. R. Mäcke, E. Jermann, M. Béhé, P. Powell and M. Hennig, *Chem.–Eur. J.*, 1999, **5**, 1974.
21 F. Benetollo, G. Bombieri, L. Calabi, S. Aime and M. Botta, *Inorg. Chem.*, 2003, **42**, 148; M. R. Spirlet, J. Rebizant, J. F. Desreux and M.-F. Loncin, *Inorg. Chem.*, 1984, **23**, 359; K. O. Aileen, J. R. Morrow, C. H. Lake and M. R. Churchill, *Inorg. Chem.*, 1994, **33**, 656; S. Aime, A. Barge, J. I. Bruce, M. Botta, J. A. K. Howard, J. M. Moloney, D. Parker, A. S. de Sousa and M. Woods, *J. Am. Chem. Soc.*, 1999, **121**, 5762; R. S. Dickins, D. Parker, J. I. Bruce and D. J. Tozer, *Dalton Trans.*, 2003, 1264; S. Zhang, L. Michaudet, S. Burgess and A. D. Sherry, *Angew. Chem., Int. Ed.*, 2002, **41**, 1919; A. L. Thompson, D. Parker, D. A. Fulton, J. A. K. Howard, S. U. Pandya, H. Puschmann, P. K. Senanayake, P. A. Stenson, A. Badari, M. Botta, S. Avedano and S. Aime, *Dalton Trans.*, 2006, 5605; T. Gunnlaugsson, A. P. Harte, J. P. Leonard and M. Nieuwenhuyzen, *Chem. Commun.*, 2002, 2134.
22 G. Zucchi, A.-C. Ferrand, R. Scopelliti and J.-C. G. Bünzli, *Inorg. Chem.*, 2002, **41**, 2459; T. Gunnlaugsson, A. P. Harte, J. P. Leonard and M. Nieuwenhuyzen, *Supramol. Chem.*, 2003, **15**, 505.
23 A. Beeby and S. Faulkner, *Chem. Phys. Lett.*, 1997, **266**, 116.
24 G. M. Sheldrick, *SHELX-97*, University of Göttingen, Göttingen, Germany, 1998.
25 *SHELXL-PC Package*, Bruker Analytical X-ray Systems, Madison, WI, 1998.

Published on 26 September 2011 on http://pubs.rsc.org | doi:10.1039/C1DT11029B
Downloaded by University of Oxford on 25 February 2013

JACS
JOURNAL OF THE AMERICAN CHEMICAL SOCIETY

COMMUNICATION

pubs.acs.org/JACS

Reversible Luminescence Switching of a Redox-Active Ferrocene−Europium Dyad

Manuel Tropiano, Nathan L. Kilah, Michael Morten, Habibur Rahman, Jason J. Davis, Paul D. Beer, and Stephen Faulkner*

Chemistry Research Laboratory, University of Oxford, Mansfield Road, Oxford OX1 3TA, U.K.

Supporting Information

ABSTRACT: The copper-catalyzed cycloaddition reaction between a propargyl-appended europium complex and azidomethylferrocene yields a d−f dyad whose photophysical properties can be reversibly switched by varying the oxidation state of the ferrocene chromophore.

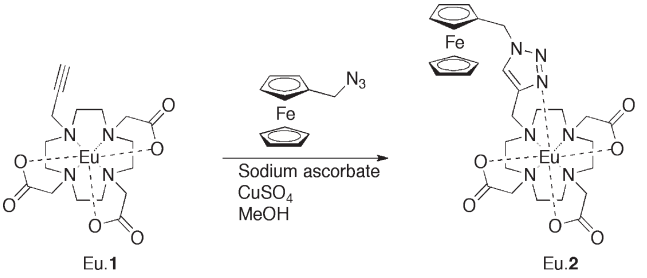
Sensitized luminescence from lanthanide complexes has been of interest for many years[1] and has begun to be widely applied in bioassays and microscopy.[2,3] The long-lived luminescence associated with luminescent lanthanide ions is readily separated from fluorescence and scattered light using time-gated techniques, meaning that very low concentrations of lanthanide probes can be observed in biological media.[4] Within the past decade or so, a number of important breakthroughs have been made in the development of lanthanide complexes that respond to changes in the concentration of a range of analytes:[5] these have been developed into ratiometric probes of ionic concentration,[6] and some show considerable promise as clinical agents for the early-stage diagnosis of tumor markers.[7]

Early studies on luminescent lanthanide complexes focused on the development and utilization of europium and terbium complexes, which emit visible light, but over the past decade or so the approach has been extended to exploit the long-wavelength emission from lanthanides such as neodymium, ytterbium, and erbium.[8−10] The low-lying emissive states of these ions can be populated using a much wider range of chromophores,[11] and much has been made of the use of transition metal complexes as antennae.[12]

We recently demonstrated that lanthanide complexes of propargyl DO3A (Ln.**1**) could be used as substrates for the copper-catalyzed 'click' reaction. We now report the use of this methodology to prepare a ferrocene-appended europium complex (Eu.**2**). Our synthetic strategy is shown in Scheme 1. Eu.**1** was prepared as described in the literature.[14] Reaction with azidomethylferrocene[15] (**3**) in the presence of copper(I) yielded Eu.**2**. We subsequently demonstrate that the redox characteristics of the antennae can be utilized in the reversible, high-fidelity switching of luminescence from the lanthanide center (Figure 1). While ferrocene has been used as a sensitizer for lanthanides in the past,[13] we believe that this is the first example in which its electrochemistry has been exploited as an emission switch.

The ^{1}H NMR spectrum of Eu.**2** (Figure S4) shows sharp, well-resolved signals for the ligand protons close to the lanthanide center. This can be contrasted with the broad signals observed in the NMR spectrum of Eu.**1** (Figure S5) and provides clear evidence for the rigidification of the complex by coordination of one of the triazole nitrogen atoms to the europium center.

Scheme 1. Synthesis of Eu.2



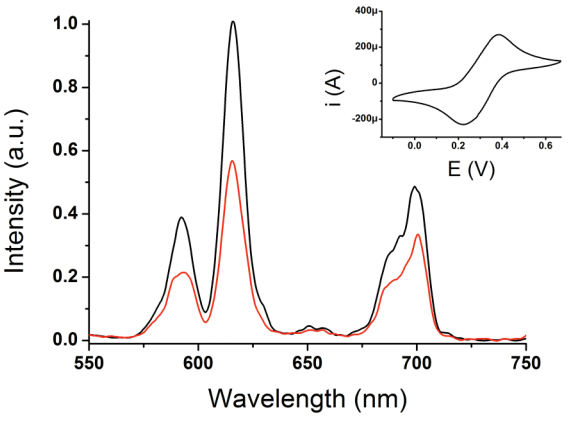


Figure 1. Emission spectrum of Eu.**2** in its reduced state (black line) and after oxidation (red line). Inset: diffusive cyclic voltammogram of Eu.**2** (2 mM in 100 mM $NaClO_4$, 100 mVs^{-1} at a Pt guaze working electrode).

Figure S4 shows that the aqueous speciation of Eu.**2** is dominated by a single isomer, though close inspection of the baseline reveals peaks corresponding to a minor isomer present in <5% abundance. For the major form, the shifts of the axial ring protons on the macrocycle are consistent with the adoption of monocapped square-antiprismatic geometry around the lanthanide center and are comparable with data in the literature for other europium complexes with similar geometries.[16]

Received: April 4, 2011
Published: July 15, 2011

ACS Publications © 2011 American Chemical Society

Having established that this process provided an effective method for preparing a ferrocene-containing d−f hybrid complex, we also used the same methodology to prepare Yb.**2** from Yb.**1**. The ^{1}H NMR spectra of Yb.**2** and Yb.**1** (Figures S6 and S7, respectively) revealed that these complexes behave very similarly to their europium-containing analogues.

Time-resolved luminescence measurements were used to define the inner-sphere solvation of the complexed lanthanide, using the equation

$$q_{Eu} = A_{Ln}(\tau_{H_2O}{}^{-1} - \tau_{D_2O}{}^{-1} - B_{Ln}) \quad (1)$$

to define q, the number of bound water molecules, from the luminescence lifetimes in H_2O and D_2O (τ_{H_2O} and τ_{D_2O}) measured in milliseconds (A_{Eu} = 1.2 ms, B_{Eu} = 0.25 ms^{-1}; A_{Yb} = 1.0 μs, B_{Yb} = 0.1 μs^{-1}).[17] The observed temporal profiles of the luminescence of Eu.**2** were fitted by iterative reconvolution with the detector response, to give lifetimes of 0.38 and 0.82 ms in H_2O and D_2O, respectively, following excitation at 340 nm. Applying eq 1 to these lifetimes gives q_{Eu} = 1.4, suggesting that the monocapped square-antiprismatic form does indeed predominate. For the ytterbium complex, the observed lifetimes, 1.0 and 5.9 μs in H_2O and D_2O, respectively, give q_{Yb} = 0.7. This smaller value is consistent with the lanthanide contraction and the change in structure across the lanthanide series commonly observed as a consequence of decreasing ionic radius.

Though ferrocene is known to act as an efficient triplet and lanthanide excited-state quencher,[18] this is likely to be efficient only at intermetallic separations where electron transfer is effective,[19] and ferrocene derivatives have also been shown to sensitize emission from europium complexes.[13a] Ferrocene also displays a well-known ligand-to-metal charge-transfer transition where the extinction coefficient is highly sensitive to the metal redox state.[20] We accordingly reasoned that this could be exploited to tune the luminescence from the lanthanide center.

Initial analyses with a 1:1 aqueous solution of ferrocene monocarboxylic acid and Eu.**1** in 100 mM sodium perchlorate confirmed not only the ability of ferrocene illumination to sensitize Eu emission but also the ability of ferrocene-centered electrochemistry to reversibly switch the process (see Supporting Information). Since this assembly is not kinetically inert, analogous experiments with the dyad Eu.**2** (Figure 1) were then carried out in a 10 mm path length quartz fluorimeter electrochemical cell (total solution volume ~140 μL). Chronoamperometry was employed to cycle a Pt gauze working electrode between oxidative (0.6 V) and reductive (0 V) potentials for 30 and 40 min, respectively. Simultaneous luminescence analyses confirm an on/off switching with high fidelity (Figure 2).

Similarly reversible switching was observed in the case of Yb.**2** (Figure 3). Oxidation of the sample in D_2O was found to be accompanied by a change in luminescence lifetime from 5.9 μs for the reduced form to 4.4 μs for the oxidized form. This suggests that the oxidized form of ferrocene sensitizes the formation of the ytterbium $^2F_{5/2}$ excited state, but that low-lying excited states of ferrocenium can act to quench this excited state once it has formed. The efficiency of such quenching (ϕ_{quench}) is given by

$$\phi_{quench} = 1 - \tau_{red}/\tau_{ox} \quad (2)$$

In this case, ϕ_{quench} = 0.25. This is borne out closely by the ratio of the observed intensities of ytterbium-sensitized emission (Figure 3), suggesting that nonradiative quenching of the ytterbium excited state is the dominant pathway for modulating the intensity of emission.

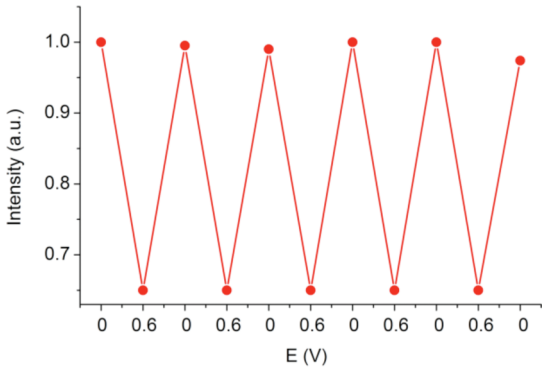


Figure 2. Reversible electrolytic switching of Eu.**2** emission (2 mM solution) at a fine Pt mesh working electrode (Pt wire counter electrode, Ag/AgCl reference electrode, in 0.1 $NaClO_4$ electrolyte).[21]

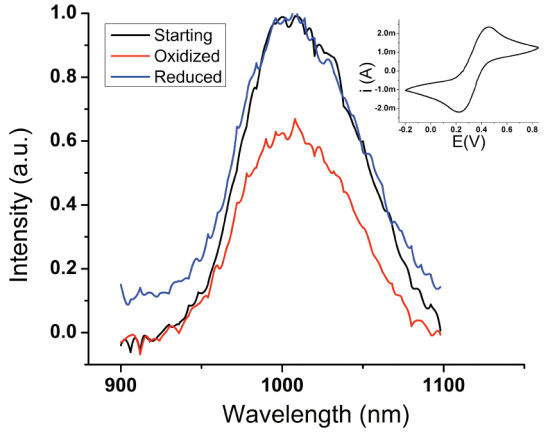


Figure 3. Emission spectrum of Yb.**2** after sequential oxidation and reduction under a 425 nm excitation light. Inset: diffusive cyclic voltammogram of Yb.**2** (2 mM in 0.1 M $NaClO_4$, 100 mV s^{-1}, Pt gauze working electrode).

It is clear that electrolytic oxidation of the ferrocene chromophore results in a significant reduction of the intensity of the lanthanide-centered emission in both cases. Triplet energy measurements on Gd.**2** at 77 K revealed that the phosphorescence spectrum of the ligand is dominated by a triazole-centered triplet state at high energy (~23 000 cm^{-1}), while no ferrocene-centered phosphorescence could be detected.

While energy transfer in most lanthanide-containing systems has been shown to proceed via a triplet-mediated mechanism,[1a] an alternative mechanism involving the generation of an intermediate chromophore-to-lanthanide charge transfer state has been shown to provide the dominant pathway for sensitization of ytterbium where it is feasible.[22] In this case, inhibition of such a sequential double charge transfer mediated pathway upon oxidation might initially appear plausible for Yb.**2**. However, this pathway would not be expected to influence the behavior of Eu.**2** in its oxidized form, since the intermediate state in such a system would be expected to be lower in energy than $^5D_0$. Thus, it is reasonable to conclude that, in both cases, quenching of the lanthanide by ferrocenium excited states is responsible for the observed switching; such a pathway is available to all lanthanide

ions (provided that the quencher state is lower in energy than the lanthanide emissive state), suggesting that redox switching can be applied to modulating lanthanide luminescence in a wide variety of applications. This area clearly merits further investigation using a wider variety of redox-active chromophores and transient absorption studies.

In summary, the click reaction offers a facile synthetic route to access d−f hybrid complexes containing ferrocene, while the incorporation of a redox-active chromophore provides the means for highly reversible electrochemical switching of lanthanide emission. We are currently working on refining these systems so that they may be exploited as devices.

■ ASSOCIATED CONTENT

Supporting Information. Experimental procedures and ^{1}H NMR spectra of the lanthanide complexes. This material is available free of charge via the Internet at http://pubs.acs.org.

■ AUTHOR INFORMATION

Corresponding Author
Stephen.Faulkner@chem.ox.ac.uk

■ ACKNOWLEDGMENT

The research leading to these results has received funding from the European Research Council under the European Union's seventh Framework Programme (FP7/2007−2013)/ERC-Grant Agreement Number 267426. We also thank the University of Oxford and EPSRC for support (studentships for M.T. and H. R.), and the Royal Commission for the Exhibition of 1851 (research fellowship for N.L.K.).

■ REFERENCES

(1) (a) Faulkner, S.; Natrajan, L. S.; Perry, W. S.; Sykes, D. *Dalton Trans.* **2009**, 3890. (b) Bünzli, J.-C. G.; Piguet, C. *Chem. Soc. Rev.* **2005**, *34*, 1048.

(2) (a) Hemmilä, I. A. *Applications of fluorescence in immunoassays*; Wiley: New York/Chichester, 1991. (b) Bünzli, J.-C. G.; Comby, S.; Chauvin, A.-S.; Vandevyver, C. D. B. *J Rare Earth* **2007**, *25*, 257.

(3) Beeby, A.; Botchway, S.; Clarkson, I. M.; Faulkner, S.; Parker, A. W.; Parker, D.; Williams, J. *J. Photochem. Photobiol. B* **2000**, *57*, 83.

(4) Hemmila, I.; Mukkala, V. M. *Crit. Rev. Clin. Lab. Sci.* **2001**, *38*, 441.

(5) (a) Parker, D.; Dickins, R.; Puschmann, H.; Crossland, C.; Howard, J. *Chem. Rev.* **2002**, *102*, 1977. (b) Gunnlaugsson, T.; Leonard, J. P. *Chem. Commun.* **2005**, 3114. (c) Allain, C.; Faulkner, S. *Future Med. Chem.* **2010**, *2*, 339.

(6) Montgomery, C. P.; Murray, B. S.; New, E. J.; Pal, R.; Parker, D. *Acc. Chem. Res.* **2009**, *42*, 925.

(7) Pal, R.; Parker, D.; Costello, L. C. *Org. Biomol. Chem.* **2009**, *7*, 1525.

(8) (a) Beeby, A.; Faulkner, S. *Chem. Phys. Lett.* **1997**, *266*, 116. (b) Hasegawa, Y.; Ohkubo, T.; Sogabe, K.; Kawamura, Y.; Wada, Y.; Nakashima, N.; Yanagida, S. *Angew. Chem., Int. Ed.* **2000**, *39*, 357.

(9) (a) Beeby, A.; Dickins, R. S.; Faulkner, S.; Parker, D.; Williams, J. A. G. *Chem. Commun.* **1997**, 1401. (b) Horrocks, W. D., Jr.; Bolender, J. P.; Smith, W. D.; Supkowski, R. M. *J. Am. Chem. Soc.* **1997**, *119*, 5972. (c) Werts, M. H. V.; Woudenberg, R. H.; Emmerink, P. G.; van Gassel, R.; Hofstraat, J. W.; Verhoeven, J. W. *Angew. Chem., Int. Ed.* **2000**, *39*, 4542.

(10) (a) Werts, M. H. V.; Hofstraat, J. W.; Geurts, F. A. J.; Verhoeven, J. W. *Chem. Phys. Lett.* **1997**, *276*, 196. (b) Shavaleev, N. M.; Pope, S. J. A.; Bell, Z. R.; Faulkner, S.; Ward, M. D. *Dalton Trans.* **2003**, 808.

(11) Placidi, M. P.; Villaraza, A. J. L.; Natrajan, L. S.; Sykes, D.; Kenwright, A. M.; Faulkner, S. *J. Am. Chem. Soc.* **2009**, *131*, 9916.

(12) Ward, M. D. *Coord. Chem. Rev.* **2007**, *251*, 1663.

(13) (a) Yuan, Y.-F.; Cardinaels, T.; Lunstroot, K.; Van Hecke, K.; Van Meervelt, L.; Görller-Walrand, C.; Binnemans, K.; Nockemann, P. *Inorg. Chem.* **2007**, *46*, 5302. (b) Klink, S. I.; Keizer, H.; van Veggel, F. C. J. M. *Angew. Chem., Int. Ed.* **2000**, *39*, 4319.

(14) Jauregui, M.; Perry, W. S.; Allain, C.; Vidler, L. R.; Willis, M. C.; Kenwright, A. M.; Snaith, J. S.; Stasiuk, G. J.; Lowe, M. P.; Faulkner, S. *Dalton Trans.* **2009**, 6283.

(15) Casas-Solvas, J. M.; Ortiz-Salmerón, E.; Giménez-Martínez, J. J.; García-Fuentes, L.; Capitán-Vallvey, L. F.; Santoyo-González, F.; Vargas-Berenguel, A. *Chem.—Eur. J.* **2009**, *15*, 710.

(16) Dickins, R. S.; Parker, D.; Bruce, J. I.; Tozer, D. J. *Dalton Trans.* **2003**, *2003*, 1264.

(17) Beeby, A.; Clarkson, I. M.; Dickins, R. S.; Faulkner, S.; Parker, D.; Royle, L.; Sousa, A. S.; Williams, J. A. G.; Woods, M. *J. Chem. Soc., Perkin Trans. 2* **1999**, *1999*, 493.

(18) Christensen, K. M.; Bakac, A.; Espenson, J. H. *Chem. Phys.* **1993**, *176*, 359.

(19) Hall, C. D.; Sharpe, N. W. *J. Photochem. Photobiol., A* **1991**, *56*, 255.

(20) Gray, H. B.; Sohn, Y. S.; Hendrickson, N. *J. Am. Chem. Soc.* **1971**, *93*, 3603.

(21) The emission was measured at 616 nm. The cycle number is limited only by solution evaporation.

(22) Beeby, A.; Faulkner, S.; Williams, J. A. G. *J. Chem. Soc., Dalton Trans.* **2002**, 1918.